

AFRL-AFOSR-UK-TR-2023-0052

Application of Wire+ Arc Additive Manufacture to primary metallic elements

SUPRIYO GANGULY
CRANFIELD UNIVERSITY
COLLEGE ROAD
BEDFORD, , MK43 0AL
GBR

12/11/2023
Final Technical Report

DISTRIBUTION A: Distribution approved for public release.

Air Force Research Laboratory
Air Force Office of Scientific Research
European Office of Aerospace Research and Development
Unit 4515 Box 14, APO AE 09421

REPORT DOCUMENTATION PAGE

PLEASE DO NOT RETURN YOUR FORM TO THE ABOVE ORGANIZATION.

1. REPORT DATE	2. REPORT TYPE	3. DATES COVERED	
20231211	Final	START DATE 20190815	END DATE 20210814

4. TITLE AND SUBTITLE
Application of Wire+ Arc Additive Manufacture to primary metallic elements

5a. CONTRACT NUMBER	5b. GRANT NUMBER	5c. PROGRAM ELEMENT NUMBER
	FA9550-19-1-7037	
5d. PROJECT NUMBER	**5e. TASK NUMBER**	**5f. WORK UNIT NUMBER**

6. AUTHOR(S)
Supriyo Ganguly

7. PERFORMING ORGANIZATION NAME(S) AND ADDRESS(ES)
CRANFIELD UNIVERSITY
COLLEGE ROAD
BEDFORD MK43 0AL
GBR

8. PERFORMING ORGANIZATION REPORT NUMBER

9. SPONSORING/MONITORING AGENCY NAME(S) AND ADDRESS(ES)	10. SPONSOR/MONITOR'S ACRONYM(S)	11. SPONSOR/MONITOR'S REPORT NUMBER(S)
EOARD UNIT 4515 APO AE 09421-4515	AFRL/AFOSR IOE	AFRL-AFOSR-UK-TR-2023-0052

12. DISTRIBUTION/AVAILABILITY STATEMENT
A Distribution Unlimited: PB Public Release

13. SUPPLEMENTARY NOTES

14. ABSTRACT
Within this program, The PI and team have reviewed 3 nickel based and 1 cobalt based alloy for high strength, high temperature and corrosion resistant applications.

They have prepared this report with five pieces of completed work presented as appendices describing the additive manufacture of IN625, IN718, Rene41 and H188. The impact of inter-pass cold working and different solutionizing treatment during post deposition heat treatment were also studied.

They were planning to synthesize the findings and compare the strengthening response to different treatments between these different alloys but unfortunately in this report they could not include it as some more work needs to be done, however, the report contains all the data pertaining to the different WAAM deposition of these 4 alloys and in particular Rene41 and IN718 was experimented in significant depth to understand their response to cold working during deposition.

15. SUBJECT TERMS

16. SECURITY CLASSIFICATION OF:			17. LIMITATION OF ABSTRACT	18. NUMBER OF PAGES
a. REPORT U	b. ABSTRACT U	c. THIS PAGE U	SAR	195

19a. NAME OF RESPONSIBLE PERSON	19b. PHONE NUMBER *(Include area code)*
DAVID SWANSON	785-6565

Standard Form 298 (Rev.5/2020)
Prescribed by ANSI Std. Z39.18

DISTRIBUTION A: Distribution approved for public release.

Project: Application of Wire+ Arc Additive Manufacture to primary metallic elements

Synopsis:

Primarily high strength nickel and cobalt-based alloys for high temperature application and manufactured by wire plus arc additive manufacturing (WAAM) route were studied in this project. The main premise of the study is to understand the manufacturability of such high strength alloys using the WAAM route and to understand how the microstructural conditions of alloys manufactured through this route would respond to post processing heat treatment for strength development. The benchmark used to measure the performance is the wrought variant of such alloys. Four different alloys studied were reported as given below:

- IN718
- IN625
- Rene 41
- H188

The importance of interpass cold working, in the form of robotic machine hammer peening, was also reported for IN718 and Rene 41

The report is compiled in the form of four different piece of works as given below

Appendix I: Microstructure and mechanical properties of Inconel 718 and Inconel 625 produced through the wire + arc additive manufacturing process – paper published in NATO conference - https://www.sto.nato.int/publications/STO Meeting Proceedings/STO-MP-AVT-356/MP-AVT-356-21.pdf
Appendix II: In-process mechanical working of additive manufactured Rene 41 – published in Proceedings of the 2022, International Additive Manufacturing Conference, IAM2022, October 19-20, 2022, Lisbon, Portugal, IAM2022-94060
http://asmedigitalcollection.asme.org/MSEC/proceedings-pdf/IAM2022/86601/V001T02A008/6975586/v001t02a008-iam2022-94060.pdf

Appendix III: Individual research project, Masters thesis on “Effect of Peening and Heat Treatment processes on Inconel 718 (nickel alloy) manufactured by WAAM for creep resistant application” – within this thesis the hardness response and microstructural characteristics were evaluated for IN718, in as-deposited and after interpass mechanical working, in

Appendix IV: Individual research project, Master’s thesis on “Additive Manufacturing of a Heat Resistant Nickel-Based Superalloy” - Impact of solutionising cycle on as-deposited Rene 41 was studied in this thesis.

Appendix V: Individual research project, Master’s thesis on “Additive Manufacture of a heat-resistant Cobalt-based superalloy” – Impact of solutionising cycle on H188 was reported in this thesis.

The methodology followed in all these work are similar where a plasma arc power source was used to deposit single pass straight length wall structure.

DISTRIBUTION A: Distribution approved for public release.

Appendix I: Inconel 718 and Inconel 625

DISTRIBUTION A: Distribution approved for public release.

Microstructure and mechanical properties of Inconel 718 and Inconel 625 produced through the wire + arc additive manufacturing process

William Sean James, Supriyo Ganguly, Goncalo Pardal
Welding Engineering and Laser Processing Centre, Cranfield University
Cranfield, Bedfordshire, MK43 0AL
UNITED KINGDOM

w.james@cranfield.ac.uk

Keywords: Additive manufacture, characterisation, mechanical properties, Inconel 718, Inconel 625

ABSTRACT

In developing the wire + arc additive manufacturing (WAAM) process for heat and creep resistant alloys, structures were built from nickel-based superalloys Inconel 718 (IN718) and Inconel 625 (IN625). In this paper, wall structures were deposited in both superalloys, using a plasma transferred arc process. The microstructure was analysed optically and under SEM; both alloys revealed typical dendritic structure with long columnar grains, with little variation between the alloys. The findings suggest that the structures included significant segregation of alloying elements, with potential intermetallic phases e.g. Laves phases and δ-phases also found across the alloys, which showed significantly more segregation of Nb and Mo at the grain boundaries and inter-dendritic regions. The alloys also underwent room temperature mechanical testing, in addition to this IN625 specimens were tested after a solutionising and ageing treatment. Hardness measurements indicated that in general the WAAM process has the effect of increasing material hardness by approximately 10 %, when compared to wrought alloy in a solutionised state. In IN625 the heat-treated specimens showed an increase in hardness of around 6 %, when compared with its as-deposited condition. Elongation in IN625 showed much greater values. Overall, IN718 showed a greater strength with less elongation than IN625. A comparison between both alloys and their stated maximum UTS and YS values from literature revealed that WAAM built IN718 and IN625 in its as-deposited condition can achieve just over half the maximum achievable UTS, with no post-process treatment. The heat-treatment process tested in IN625 marginally reduced the gap in UTS performance by 3.5 %.

1.0 INTRODUCTION

Wire + Arc Additive Manufacturing (WAAM) has been undergoing development since the 1990's. WAAM is "the combination of an electric arc as heat source and wire as feedstock" (Williams et al., 2016). WAAM is not dissimilar to more traditional manual welding technologies such as TIG/MIG welding (Kou, 2003), with the exception that WAAM uses traditional arc welding technologies with a motion control system, such as a robotic system or retrofitted onto a computer numerical control (CNC) system (Williams et al., 2016). The main difference in automated welding systems and the WAAM system is the thermal profile of as-deposited WAAM components. To build shapes and subsequent components WAAM deposits the wire feedstock in a layer-by-layer manner (Xu et al., 2018a). Unlike other more well established additive manufacturing (AM) methods WAAM is often not used to manufacture a finished product, instead WAAM is used to deposit a net-shape product (Baufeld et al., 2010), which can then be further processed, if required, to achieve a finished product.

As a method to rapid prototype metal structures WAAM is often advantageous over more traditional methods such as machining. As WAAM only deposits the net shape of the product, compared with

DISTRIBUTION A: Distribution approved for public release.

machining WAAM is capable of reducing: the waste material, cost, and lead time. (Baufeld et al., 2010).

Superalloys are defined as “a group of nickel-, iron-nickel-, and cobalt-base materials that are used at temperatures of 540 °C and above” (Davis, 1997). Superalloys were initially developed for use in superchargers in aircraft piston engines, however much of their later development was in components for gas-turbines. Nickel-based superalloys can be found in gas-turbines for a variety of applications from aerospace to power generation. Newer gas-turbines operate at higher temperatures than has been seen historically, due to increasing demand for more efficient engines, the nickel superalloys in these environments experience operating temperatures of between 650-700+ °C (Akca and Gürsel, 2015).

The use of WAAM to manufacture components from heat resistant alloys is a relatively new area of study with a relatively low volume of research published in this area. The impact of the WAAM process on the high temperature material properties of heat resistant alloys is largely unknown. Alloys that have been investigated in this study include those suitable for high temperature applications, including largely nickel based super-alloys, this is due to the high temperature performance of these alloys.

Another type of AM process that has been considered as less appropriate for the high-speed flight application include the powder-bed laser AM process. The powder bed process is also a process by which shapes are produced by a layer-by-layer process, however metallic powder particles are used as the feedstock which is then melted to form the part via laser. Benefits that the powder bed AM process shares with the WAAM process includes the ability to produce complex shapes that would be difficult to produce by traditional machining methods (Wang et al., 2017), as well as greater efficiency brought by the minimal waste that is produced by most AM processes. There are, however, some limitations of powder-bed over WAAM which makes WAAM more appropriate for this application. WAAM is more suited to the production of larger scale parts as well as being capable of a higher deposition rate of material. The metallic powder used in powder-bed is more expensive to produce than wire-feedstock, which being coupled with powder loss (which can be as high as 25 % even for more advanced versions of the technology), makes powder-bed produced parts less economical (Tanvir et al., 2020). Larger powder-bed produced components can include pores in the structure which reduces the mechanical performance. In terms of loss of material, WAAM can operate with near to no loss of raw material and can produce pore free structures (Tanvir et al., 2020). After post-processing heat-treatment Wang et al. found that powder-bed produced IN718 was comparable in room temperature tensile strength as the wrought alloy (Wang et al., 2017). For IN625, Tanvir et al. found that WAAM built parts needed further research to achieve the same strength level as powder-bed produced parts, and recommended that a solutionising treatment for IN625 might further increase the performance (Tanvir et al., 2020).

High temperature metals that have been deposited by WAAM at Cranfield University so far include:
Nickel alloys:

- Inconel 625 (Xu, 2018)
- Inconel 718 (Xu, 2018)

Refractory metals:

- Tungsten; WAAM is capable of depositing high purity tungsten and other refractory metals (Marinelli et al., 2019).
- Molybdenum (Martina et al., 2016)
- Tantalum (Martina et al., 2016)
- Ti–6Al–4V (Martina et al., 2012) + other less heat resistant alloys (Welding Engineering and Laser Processing Centre Cranfield University, 2019).

In this paper, research performed towards deposition and wall building of IN625 and IN718 using a plasma transferred arc WAAM process are discussed. A comparison of the two WAAM built alloys was completed and their suitability for high-speed flight applications was discussed.

DISTRIBUTION A: Distribution approved for public release.

2.0 MATERIALS AND METHODS

2.1 Overview of Design Parameters

There is interest in developing AM alloys specifically for use as structural components in high-speed missiles with short flight times (< 1 hour). In service temperatures could reach 1000 K for external structural components, or even 1200+ K for components in the propulsion flow path. These components will be highly stressed to minimise structural mass. The desired aim is for the WAAM built alloys to achieve properties similar to currently available wrought materials, such as IN718 (standard) or Haynes 282 (best case), and ideally have low thermal expansion. Creep is not considered to be a major issue due to the short flight time, but there is a lack of data in this regime (high stress, high temperature and short duration). With a focus on very good short-term properties and a particular importance on high temperature performance of these alloys, the room temperature data shown in this paper is a precursor to further high temperature investigations.

2.2 Deposition Process

2.2.1 Inconel 625

IN625 was deposited via a WAAM system consisting of a Kuka six-axis robot, a plasma power source, a water-cooled plasma welding torch mounted to the robot, an external wire feeder, and a part rotator – allowing for symmetrical layer-by-layer WAAM wall building. Also attached to the robot head was a trailing shield (shown in Figure 1) which surrounded the welding torch and extended behind the torch, this provided an argon environment during the WAAM process to prevent excessive oxidisation. The experimental set-up is shown in Figure 2.

The process used for IN625 was a symmetrical wall building process, where two wall structures were built simultaneously on opposite sides of the substrate plate and the part rotator is utilised to alternate between the two sides of the substrate plate. The benefits of this process over a single sided operation is intended to reduce residual stresses on the structure as the warping of the substrate is effectively 'cancelled out' when welded on both sides (Williams et al., 2016). It also has the effect of increasing productivity as inter-pass cooling can partially take place on one side when the process is ongoing on the opposite side, minimising the time the system remains inactive while cooling takes place.

Directly below the trailing shield at a torch-to-work distance of 8 mm, argon shielding was provided to keep the level of oxygen below 800 ppm, with an argon flow of approx. 80 l/min.

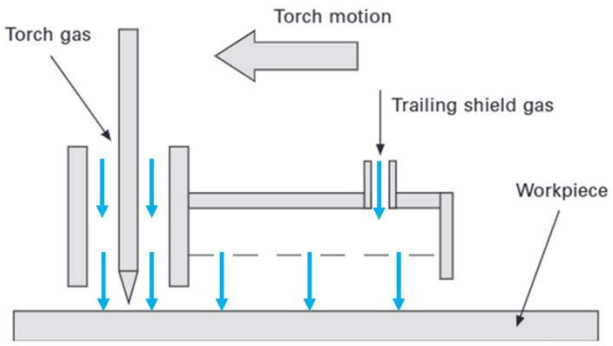


Figure 1: Trailing shield device used during deposition of IN625 (Norrish, 2006), blue arrows

DISTRIBUTION A: Distribution approved for public release.

indicate gas flow direction.

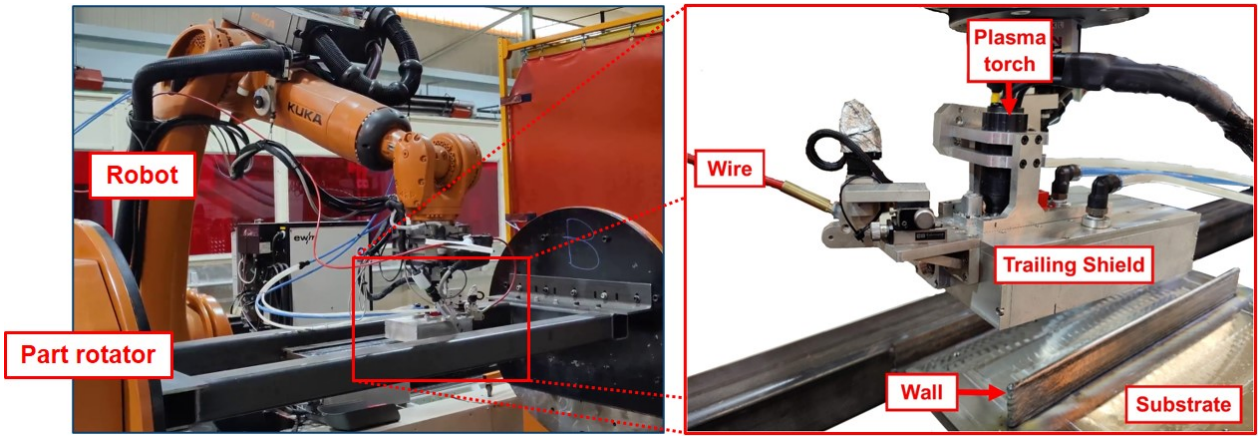


Figure 2: Experimental set-up used to deposit IN625. Boxed area in the LH image is shown in further detail in RH image.

2.2.2 Inconel 718

For the Inconel 718 (IN718) alloy, a WAAM system consisting of three-axis linear CNC system, a Tecarc 320 A AC/DC plasma power source, a water-cooled plasma torch mounted to an adjustable jig on the CNC system, an external wire feeder and a glove box filled with Pureshield argon, controlled below 800 ppm controlled as in section **Error! Reference source not found.**.

The process used for the deposition was a linear wall building system where the layers were deposited in a single direction on a single side of the substrate, due to the limitations of the system used. The experimental set-up used to deposit IN718 is shown in Figure 3.

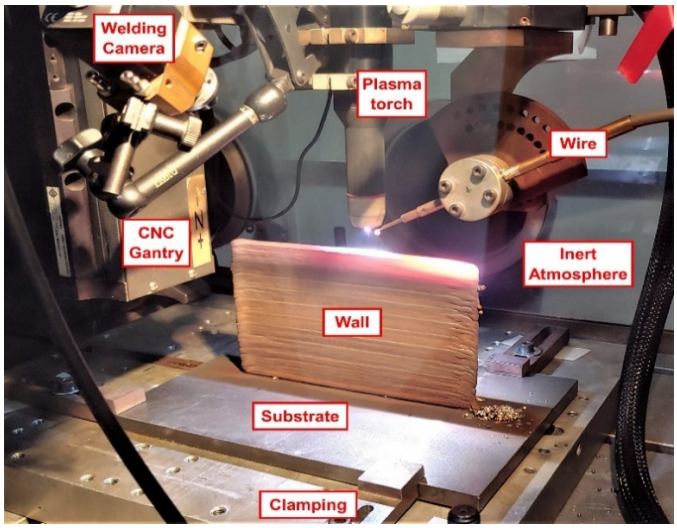


Figure 3: Experimental set-up used to deposit IN718.

2.2.3 Materials

The dimension of the nickel wires used and the welding parameters for each alloy are shown in Table 1 and the chemical composition of these wires is shown in Table 2. For both alloys a 10 mm thick mild steel plate

DISTRIBUTION A: Distribution approved for public release.

was used as the substrate. Large linear wall structures were deposited in each alloy measuring approx. 500×110×8 mm for IN625 and 315×110×8 mm for IN718, Figure 4 shows directional axes and orientation of extracted tensile specimens. The welding parameters were kept constant, with the exception of the initial welding layers, where a slower travel speed and reduced wire feed speed were used to better the wetting of the deposit onto the substrate plate.

Table 1: Wire and welding parameters.

	IN718	IN625
Wire Diameter (mm)	1.2	1.2
Torch to work distance (mm)	8	8
Current (A)	180	180
Wire feed speed (m/min)	1.8	2
Travel speed (mm/sec)	5	6
Inter-pass cooling time (min)	3	3

Table 2: Elemental composition of IN718 and IN625 filler wires, %wt. (Elements <0.01% omitted)

	C	Ni	Cr	Mo	Fe	Al	Ti	Nb	Mn	Si	Cu
IN718	0.04	53.57	18.56	2.87	17.8	0.60	0.97	5.01	0.10	0.08	0.07
IN625	0.01	64.75	22.16	8.79	0.24	0.17	0.19	3.60	0.02	0.04	0.02

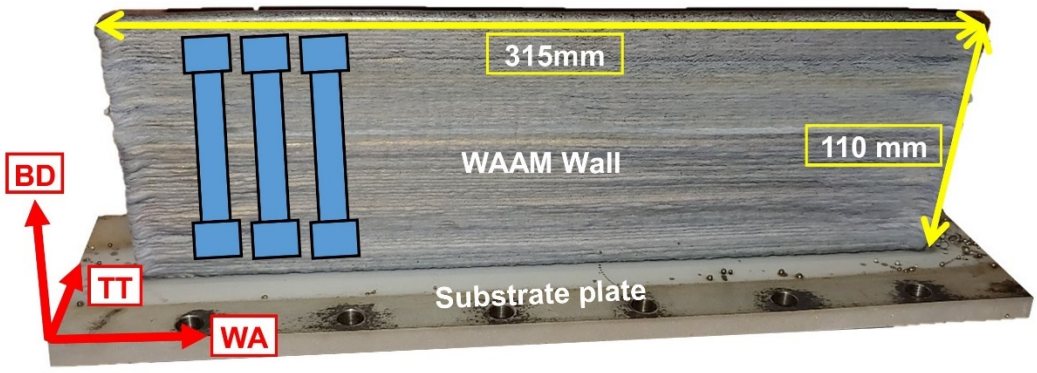


Figure 4 WAAM wall labelled with build dimensions and directional axes. Build direction (BD), through thickness (TT), wall axis (WA).

2.3 Analytical Methods & Mechanical Testing

In IN718 and IN625 alloys, WAAM walls of 226, and 130 layers respectively were built. Once completed the walls were cut from the substrate plates and samples were extracted both along the wall height and length. Cross-sections were extracted and prepared for metallographic analysis following a procedure consisting of mounting, grinding, polishing, and etching. IN718 samples were etched in Kalling's 2 while IN625 was etched in aqua regia. The microhardness was measured using a Zwick/Roell hardness tester under

DISTRIBUTION A: Distribution approved for public release.

a load of 500 g and holding time of 15 s, welding filler wire samples of the alloys also underwent a similar process as above to obtain comparative results for the hardening effect of the WAAM process. The microstructure was also analysed, using a Tescan VEGA 3 scanning electron microscope, and optically using a Leica DM 2700M Microscope. To determine composition an Oxford Instruments X-Max 20 mm was used in combination with the SEM for the EDS analyses.

For room temperature mechanical testing an Instron 5500R Electro-mechanical testing machine was used with a load cell of 100 kN and a crosshead speed of 1 mm/min. Elongation was measured using a laser extensometer over a gauge length of 25 mm. At least three samples were tested for each condition (orientation, as-deposited and heat-treated variants), and samples conformed to ASTM E8/E8M subsize specimen standard. A schematic drawing of the tensile specimens used is shown in Figure 5.

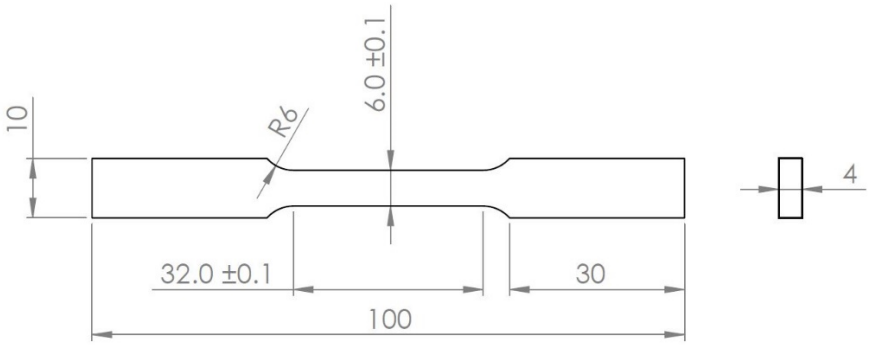


Figure 5: Dimensions (in mm) of the tensile specimens used for RT tensile testing, conforming to ASTM E8/E8M subsize standard.

2.3.1 Post-process Treatment of Inconel 625

A heat-treatment was conducted on several IN625 tensile specimens. The heat treatment made use of a Carbolite Gero CWF 11/13 furnace and consisted of a two-stage heating process, a solutionising and heat-treating process. The first stage included heating the samples in the furnace to 1100 °C holding at this temperature for 15 mins, with the aim to dissolve Laves and secondary phases. After this process the specimens were water quenched to room temperature. The specimens then underwent an ageing process at 750 °C for 8 hours, followed by air cooling to room temperature. The aim of the second stage was to increase the mechanical strength through the precipitation of γ″ Ni_3Nb in the inter-dendritic regions (Kasravi et al., 2021). This treatment was used in a previous study on IN625 by Cortial et al (Cortial et al., 1995).

3.0 RESULTS

3.1 Macrostructure

The macrostructure seen in the samples of the as-deposited IN718 WAAM wall, i.e. without any additional heat or solution treatment to the material are shown in Figure 6 with an enlarged image at higher magnification shown in Figure 7. In the macrostructure large cracks can be seen extending through the layers. IN718 exhibits a typical solidified dendritic structure made up of large columnar grains which appear to extend along the height of the wall in the build direction (BD seen in Figure 6), this structure was expected and has been seen in previous studies namely by Xu et al (Xu et al., 2018b).

IN625 exhibits a similar structure to IN718 as can be seen in Figure 8. Nearest the substrate in both alloys, it can be seen that the structure has much finer cellular grains, whereas in later layers extending though the

DISTRIBUTION A: Distribution approved for public release.

build direction grains get steadily longer exhibiting a more columnar dendritic structure. Overall, more cracking was seen in IN718.

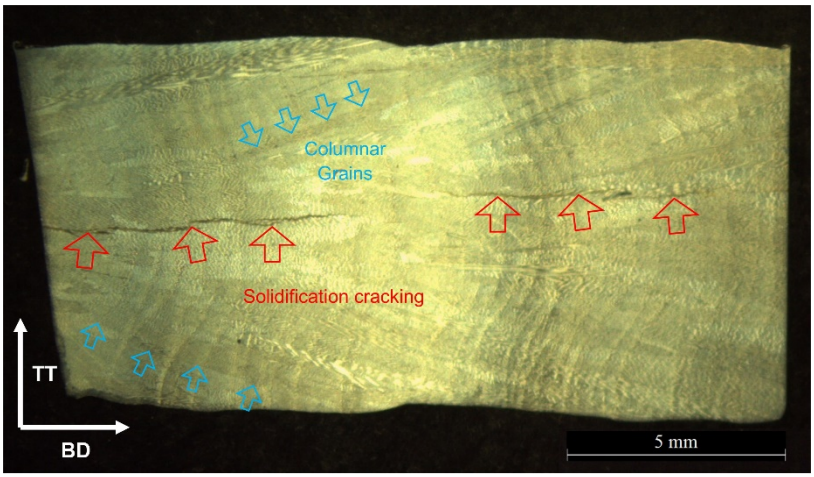


Figure 6: Macrograph cross-section of as-deposited IN718. This is a sample near to the top of the wall. From bottom to top of the build direction is shown from left to right. Red arrows indicating solidification cracking, blue arrows show columar grains.

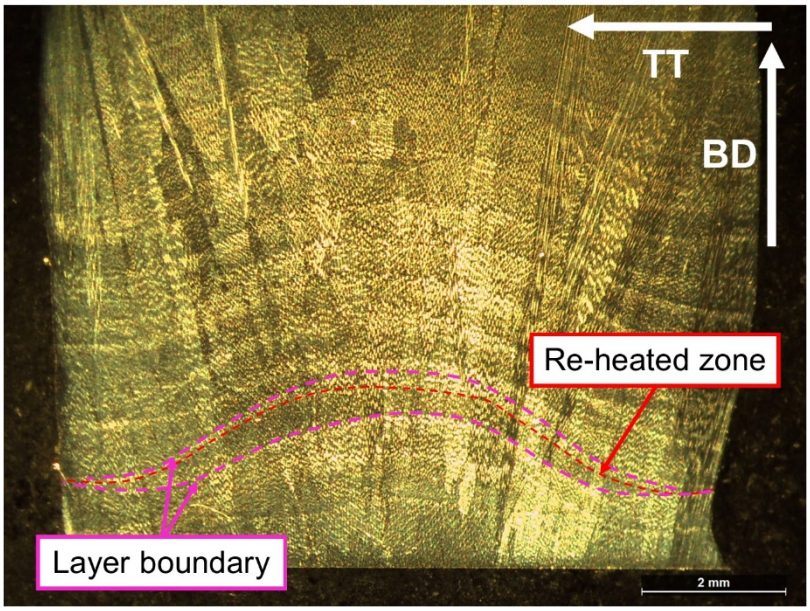


Figure 7: Macrograph cross-section of as-deposited IN718, showing layer boundary and re-heated zone Pink dotted line and arrows showing boundary between layers and red dotted line shows re-heated zone.

DISTRIBUTION A: Distribution approved for public release.

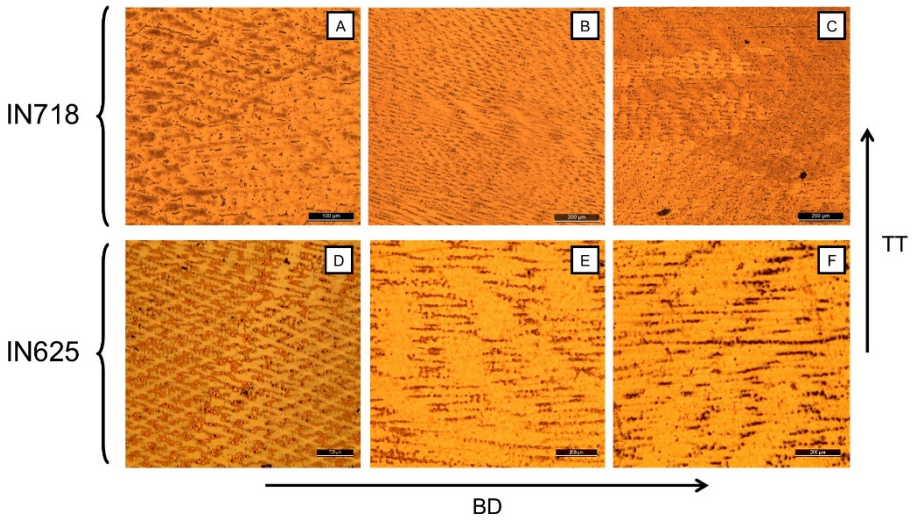


Figure 8: Optical micrograph of as-deposited macrostructure of IN718 and IN625 samples. Top three images show IN718, bottom three images show IN625.

3.2 Microstructure

The microstructure seen in IN718 at the grain boundary is shown in Figure 9. The as-deposited WAAM structure shows significant amounts of segregation of Nb and Mo at the grain boundaries, an EDS analysis of the area revealed the lighter coloured phases to be Ni_2Nb (green arrows), purely based on the similarity in the composition and closeness to the atomic percentages of the A_2B type Ni_2Nb Laves phase seen in literature (Xu et al., 2018b). This phase can also clearly be seen on the elemental map (Figure 10), which shows the segregation of Nb as well as the depletion of heavier metals such as Nb and Mo in the surrounding regions.

The red arrows in Figure 9 are indicating Ti rich phases, which appears as smaller darker precipitates. These precipitates have been identified as a possible MC type carbide TiC based on appearance seen in literature and composition of approximately 50 % Ti (Mitchell, 2010).

An analysis into the composition of the above precipitates seen in IN718 was carried out, the composition is shown in Table 3. The composition of area B, highlighted in yellow in Figure 9, shows a significant increase over base values of Nb while the amount of Ni has decreased significantly. Comparing the values in terms of atomic percentage, suggests that the composition is very close to that of Ni_2Nb. While area D shows a significant increase in both Ti, Nb and Al without any indicated elements.

The solidification cracks seen in IN718 were also analysed based on composition and found to contain Ni_2Nb Laves phase at the crack edge, as seen in Figure 11 the lighter coloured phases along the crack also form the root of the crack.

The microstructure of heat-treated IN625 is shown in Figure 12, although this image is not of a grain boundary location, the phases seen appear smaller and more evenly distributed. The purpose of the post-deposition heat-treatment was to dissolve Laves phase and allow for the formation of more useful γ'' strengthening phase. It does appear that a significant amount of potential Laves phases have been dissolved compared to as-deposited IN718, although some that remains are similar in appearance however smaller in size than was seen in IN718. In IN625 the darker Ti rich zones (shown as area F in Figure 12, with composition in Table 3) also appear and typically vary in size and are seen at a greater frequency than those seen in IN718.

DISTRIBUTION A: Distribution approved for public release.

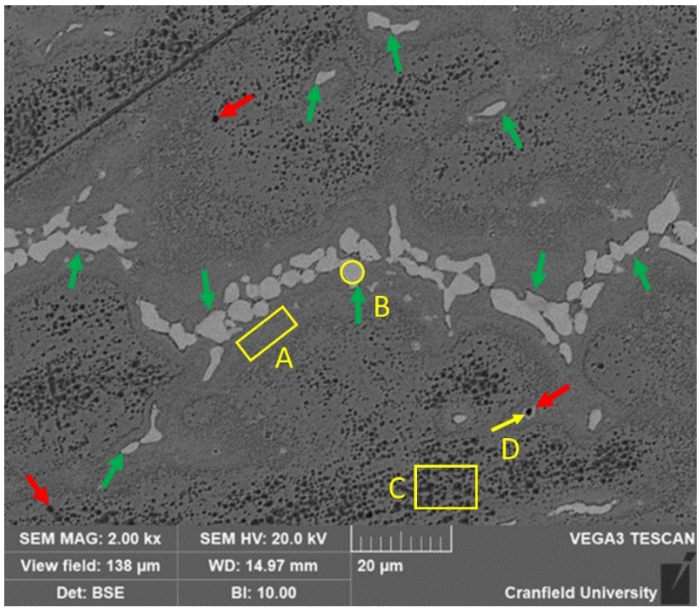


Figure 9: Microstructure in IN718 showing grain boundary and segregated zones, in the through thickness (TT) and wall axis (WA) cross-section. This sample is located mid-height in the build direction. Green arrows showing lighter coloured segregated Ni2Nb, red arrows indicating Ti rich carbides. In yellow are areas where the composition was analysed (Table 3).

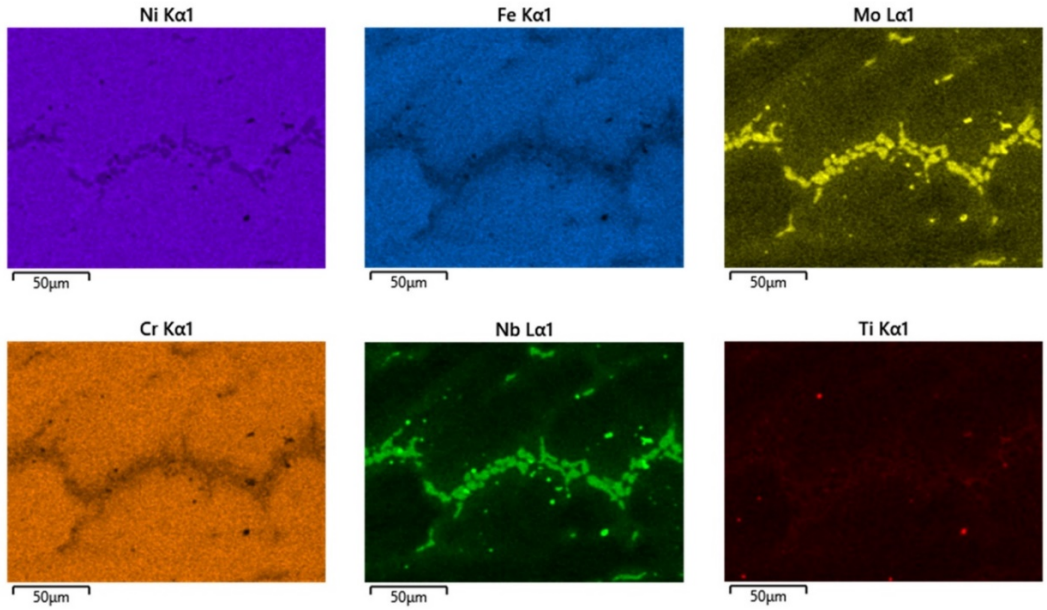


Figure 10: EDS Elemental map of IN718 segregated zone.

DISTRIBUTION A: Distribution approved for public release.

Table 3: EDS composition of alloys, labelled A – D on IN718 SEM image (Figure 9), E – F on IN625 SEM image (Figure 12). Values proceeded by a green (+) represent a significant increase over base values, values with a red (–) represent significantly less and a purple (*) represent anomalous elements.

Spectrum Label	% At.						
	IN718				IN625		
	A	B	C	D	E	F	G
C	(+)12.04	(–)0	(+)10.02	(–)0	(+)18.35	(+)12.82	(+)9.73
F	(*)6.95						
Al	1.11	(–)0	1.25	(+)15.20	(–)0.22	0.31	0.38
Si					(*)0.73	(*)0.18	(*)0.12
Ti	1.50	1.95	0.63	(+)51.85	0.25	(+)1.52	0.17
Cr	16.64	(–)17.67	19.97	(–)0	(–)17.24	20.32	23.64
Fe	13.77	(–)12.96	18.30	(–)0		(–)0.17	(–)0.21
Ni	42.51	(–)46.26	46.92	(–)0	(–)35.18	(–)50.61	60.36
Nb	3.91	(+)21.15	(–)1.39	(+)32.95	(+)16.46	(+)7.81	(–)1.00
Mo	1.58	(–)0	1.53	(–)0	(+)11.58	6.25	4.39

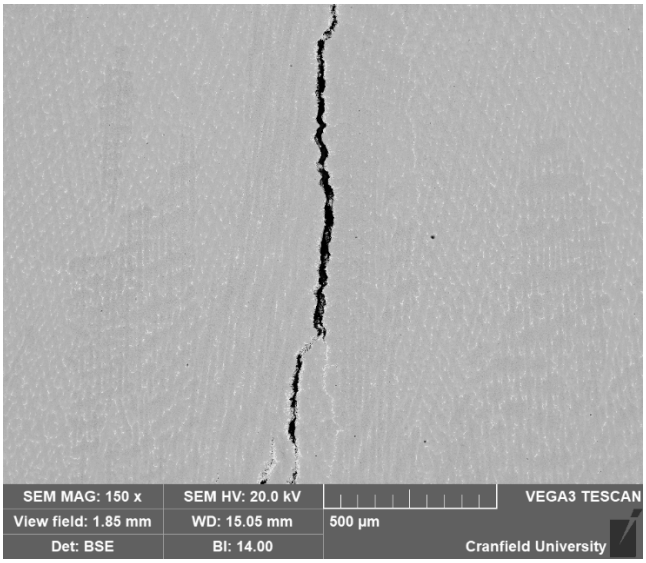


Figure 11: Solidification crack seen in IN718, showing lighter coloured Laves phases in crack root. Through thickness (TT) and build direction (BD) cross-section.

DISTRIBUTION A: Distribution approved for public release.

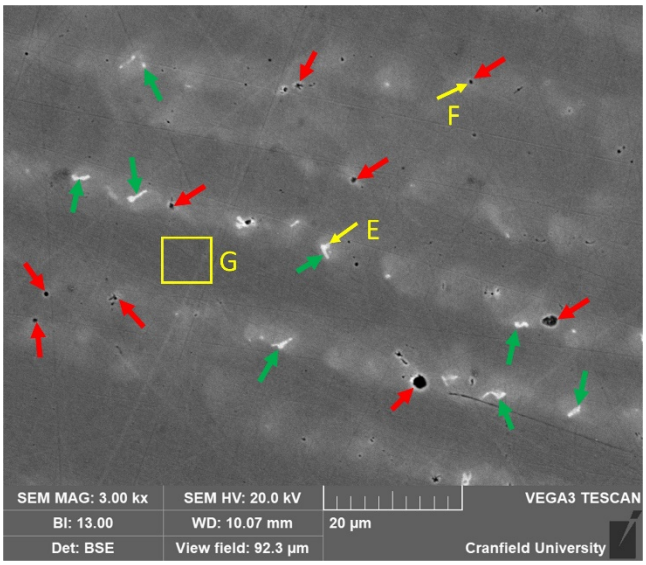


Figure 12: Microstructure of post-deposition heat-treated IN625 showing segregated zones, in the through thickness (TT) and wall axis (WA) cross-section. This sample is located mid-height in the build direction. Green arrows showing lighter coloured segregated Ni2Nb, red arrows indicating Ti rich zones possible Ti rich carbides. In yellow are areas where the composition was analysed (Error! Reference source not found.**).**

3.3 Hardness Comparison

Hardness between both alloys, in their as-deposited condition was compared. As-deposited IN625 was also compared with its heat-treated variant. The hardness was tested at 1 mm increments along the surface of the samples. Micro hardness results were obtained using a Zwick/Roell hardness tester under a load of 500 g and holding time of 15 s, results are displayed as Vickers Hardness in Table 4. A comparison of the data revealed that IN718 is harder than IN625, with average values for both alloys at 293.9 HV and 248.5 HV respectively. The heat-treatment that IN625 underwent showed a marginal increase in the average micro hardness with a value of 262.75 HV, representing a 5.7 % increase over the as-deposited average.

Table 4: Vickers hardness values. [a](Xu et al., 2018b), [b](Special Metals, 2007), [c] (Kasravi et al., 2021), [d] (Special Metals, 2013)

Alloy	Condition		Hardness (HV)
IN718	WAAM	as-dep	293.9
		Heat treated	388 [a]
	Wrought		354 [b]
IN625	WAAM	as-dep	248.5 [c]
		Heat treated	262.8 [c]
	Wrought		238 [d]

3.4 Room Temperature Tensile Comparison of Inconel 718 & 625

Room temperature tensile test comparison between as-deposited IN718 and IN625 revealed that IN718 had an average UTS of 841.7 MPa compared with an average of 622.2 MPa for IN625. YS for both IN718 and

DISTRIBUTION A: Distribution approved for public release.

IN625 was calculated to be 528.8 MPa and 396.7 MPa respectively. Elongation on average was substantially higher in IN625 than was seen in IN718, with the IN625 specimens breaking on average at +57 % of their original length and IN718 specimens breaking at an average of +30.5 % of their original length. Overall IN718 showed greater strength with less elongation than IN625. The alloys were then compared against their stated maximum UTS and YS values from literature, which revealed that WAAM built IN718 and IN625 in its as-deposited condition can achieve approximately 62 % of the maximum achievable UTS (64.5 % for IN625, 58.7 % for IN718), with no post-process treatment. With heat-treatment however, IN625 was able to reduce the gap slightly in UTS performance compared to literature to 68 % of maximum performance. Heat treated IN625 also resulted in a reduction in elongation compared with as-deposited material, bringing it below the value given for the wrought alloy. Tensile testing results compared with wrought alloy are shown in Table 5. A stress/strain graph of the best and worst performing sample in each category is shown in Figure 13, where the suffix (A) is the best performance and (B) the worst. As IN718 is more age-hardenable than IN625, IN718 did not undergo a heat-treatment. A comparison between the alloys in their partially aged (as-dep) condition is more prudent.

Table 5: Mechanical tensile testing results for IN718 and IN625, with wrought data (Donachie, 2002).

Alloy	Condition		UTS (MPa)	0.2 % YS (MPa)	Elongation (%)
IN718	WAAM	as-dep	841.70	528.84	30.47%
	Wrought		1435	1185	21%
IN625	WAAM	as-dep	622.21	396.67	57.26%
		Heat treated	659.70	328.36	41.88%
	Wrought		965	490	50%

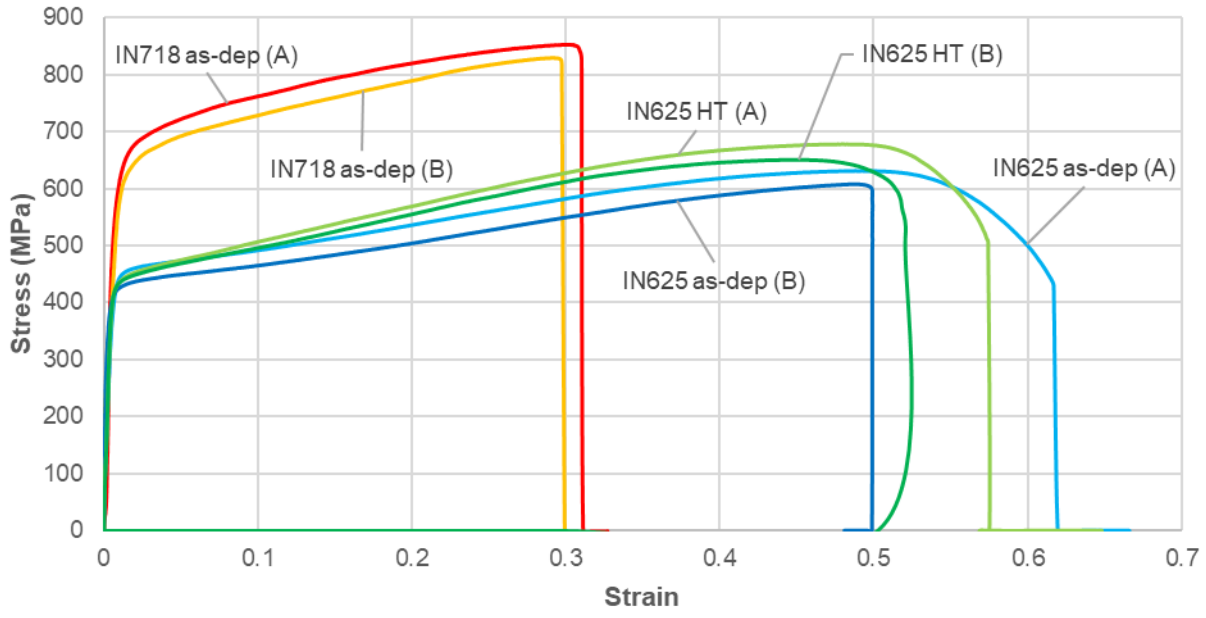


Figure 13: RT Stress vs. Strain for as-deposited IN718, IN625 & Heat-treated (HT) IN625. Best (A) and worst (B) performing samples are shown in each category.

DISTRIBUTION A: Distribution approved for public release.

4.0 DISCUSSION

4.1 Macro and Microstructure

The macrostructure of both alloys are very similar in appearance, and exhibit the same characteristics in relation to the earlier and later built layers as shown in Figure 8. In IN718 much more cracking was observed compared to IN625, it is possible that the different building process is the cause with slightly different equipment and parameters used to deposit the alloys, even though conditions inside the enclosure should have been more optimum for oxidisation induced cracks. It is also possible that as IN625 was built in a more open environment and onto larger equipment that the rate of cooling for IN625 was faster than IN718, meaning IN718 was effectively aged more as part of its WAAM process than IN625 experienced. The data for hardness would also suggest that IN718 was harder in its as deposited condition that IN625 which could suggest that IN718 was more brittle and hence more prone to cracking, this would also explain the large difference between the elongation of the alloys during tensile testing, with IN718 relativity restrained compared with IN625.

The columnar grains (seen to grow through the layers and across the height of the walls in both alloys), are similar to what has been seen in previous studies on as-deposited material, where the columnar dendrites are not precisely vertical but extend at an angle of approx. 70 ° to the substrate. This was also seen in a study by Wang et al, in which the reason for this was related to heat flux direction, where dendrite growth follows the maximum temperature gradient, which is opposite to the unidirectional heat flux direction (Wang et al., 2016).

The potential Ni_2Nb Laves phase seen at the edge of the crack in Figure 11 suggest that the heavier metals in the alloy, such as Nb, which has a higher melting point than the other elements, are segregating from the rest of alloy during solidification. The root of the cracks also appears to be filled with the same compound suggesting that the formation of these Laves phase are the cause of the cracking seen in the alloy. The size however of the columnar grains seen, especially in the as-deposited material, of both alloys may suggest that there is in fact less grain boundary area for these precipitates to form and consequently they have less of a reducing effect on the strength.

Laves phase formation in alloys are known to be detrimental to the performance as it depletes the elements that would otherwise form more useful substances such as precipitation hardening carbides (Donachie, 2002), or strengthening phases. The solution treatment that IN625 underwent was performed to homogenise the microstructure and by dissolving Laves phases into the matrix which could then form the γ″ strengthening phase, which is shown under SEM to have reduced the size and frequency of Laves phases. Generally, the results from the SEM and EDS analysis of the microstructure give a good indication of the presence of the Laves phases described, such as Ni_2Nb in IN625 and IN718. For example, looking at Table 3 a simple calculation of multiplying the value for Nb by two to get a rough value for Ni, seems to confirm the presence of Ni_2Nb for both spectrum B and E within 2-4 % At.

However, further work to confirm the presence of Laves phases would help to eliminate any doubt that remains. Another point for further investigation is the appearance of Ti rich zones in both alloys, but specifically the appearance of the Ti rich zones in IN625 which appeared in a greater frequency in heat-treated IN625 than those seen in as-dep IN718 despite the matrix containing significantly less Ti than IN718.

The heat treatment process that IN625 underwent which was based on a previous study on the alloy by Cortial et al. In the study, Cortial et al found that the treatment resulted in increased mechanical strength due to the precipitation of γ″ Ni_3Nb phase in the inter-dendritic spaces, which is a strengthening phase in IN625 (Cortial et al., 1995). Longer aging time tends to provide a more uniform distribution of these precipitates. γ″ Ni_3Nb and aging of IN625 produces a more carbides in the alloy. Carbides that have been observed in a study by Shaikh et al included carbides rich in Ti, Nb and Si (Shaikh et al., 2000). The fact that Ti rich

DISTRIBUTION A: Distribution approved for public release.

carbides have been observed in the literature in the IN625, suggests that the Ti rich zones that exist in the alloys with no other significant increase are Ti carbide. The potential Ti carbides found in IN625 and IN718 were observed to be smaller in size, dark in colour as well as more sparsely distributed, compared to potential Laves phases. Area D of Figure 9 suggest with the significant increase in the percentage of Nb, Ti and Al (over the base values), without the presence of the other elements, that perhaps this is indicative of a complexed carbide where any Carbon has been removed by the etching process, although the presence of Carbon in EDM results is often unreliable.

4.2 Mechanical Properties

The increase in material hardness of IN625 in the as-deposited condition suggests that the cyclic heating of the WAAM process has at least a partial ageing effect on the alloy. This was also seen when IN625 underwent a post-process aging treatment which resulted in an approximate 5.7 % increase in hardness vs. as-deposited material. In the case IN718, the as-deposited hardness was shown to be significantly less than manufacturer's data for the wrought alloy. This is probably due to the more extensive ageing process that IN718 typically undergoes to achieve the best mechanical properties, with proper aging treatment it is anticipated that hardness would further increase. In a study on heat treating WAAM built IN718 Xu et al. found that heat treated material showed an increase in hardness of 158 HV compared with as-deposited material. This represents an approx. 69 % increase (Xu et al., 2018b), highlighting the difference between the aging processes of the two alloys and why a comparison between the aged material is less useful than a comparison between the partially aged as-deposited material.

Overall, the improvement in performance by heat-treating IN625 specimens was disappointing, with only a marginal increase in UTS performance compared to the wrought values given by Donachie in the Superalloys technical guide (Donachie, 2002); which provided data in suitably comparable format. WAAM built IN625 and IN718 has some improvements to be made before it can achieve the performance of the wrought alloys. Xu et al in a paper based on IN718 found that interpass rolling was able to increase the UTS performance of the WAAM built material up to and above what was achievable in wrought alloy, and meet the wrought standard for YS and elongation (Xu et al., 2018b).

In evaluating these two WAAM built alloys for a high-speed flight application, IN718 and IN625 show promise, however further work is required to understand their high temperature performance at a temperature range of RT to 1000 °C, and what effect the heat-treatment process will have on the performance at elevated temperatures. An investigation into the interpass rolling process described by Xu et al would also be desirable to understand the performance of the rolled WAAM alloys. Finally, IN718 at least at RT would appear to be preferable over IN625 for its higher strength performance, however IN718 does appear to be a harder more brittle alloy and the results of the RT study do correlate to what the data suggested for the wrought alloys. Further study into the high temperature performance of both these WAAM built alloys will help to understand their performance for high-speed flight.

5.0 CONCLUSIONS

1. WAAM built material of IN718 at room temperature had a higher UTS and YS performance, however IN625 had a much greater elongation under testing. Perhaps, although a high frequency of Nb rich segregated compounds were found along the grain boundary in IN718, the larger columnar grains provided less grain boundary area for the precipitation of segregated compounds to form. This difference may also be due to IN718 potentially being partially aged to a larger extent during the deposition process than IN625.

2. A heat-treatment consisting of solutionising and heat-treatment had the effect of increasing the performance of IN625 by approx. 6 %, which was less than anticipated but may have been due to

DISTRIBUTION A: Distribution approved for public release.

cracking seen in the alloy which potentially reduced its performance.

3. Refractory elements Nb, Mo segregate and contribute to formation of Laves phases, specifically Ni_2Nb, which were indicated in both alloys with precipitation seen at the grain boundaries and interdendritic regions.

4. The heat treatment process was found to increase hardness of IN625 by an average of 5.7 % compared with as-deposited WAAM material, and when compared with manufacturer's data on the wrought alloy an increase of 10.4 %.

ACKNOWLEDGEMENTS

The authors wish to acknowledge the UK Ministry of Defence for their financial support, and the industrial supervisors from DSTL Porton Down, for their ongoing advice and guidance: Mr Graham Simpson, Dr Sarah Baker and Dr Matthew Lunt.

The authors would also like to acknowledge the expert help from welding technicians Mr Flemming Nielsen, Mr Nisar Shah, and Lab manager Mr John Thrower, without whom this work would not have been possible. The technical assistance of Mr Steve Pope and Mr Kristopher Bramley for their help with imaging during the Coronavirus lockdowns. As well as the Cranfield MSc students whose group project contributed to the experimental data presented in this paper.

REFERENCES

Akca, E., Gürsel, A., 2015. A Review on Superalloys and IN718 Nickel-Based INCONEL Superalloy. Period. Eng. Nat. Sci. 3. https://doi.org/10.21533/pen.v3i1.43

Baufeld, B., Biest, O. Van der, Gault, R., 2010. Additive manufacturing of Ti-6Al-4V components by shaped metal deposition: Microstructure and mechanical properties. Mater. Des. 31, S106–S111. https://doi.org/10.1016/j.matdes.2009.11.032

Cortial, F., Corrieu, J.M., Vernot-Loier, C., 1995. Influence of heat treatments on microstructure, mechanical properties, and corrosion resistance of weld alloy 625. Metall. Mater. Trans. A 26, 1273–1286. https://doi.org/10.1007/BF02670621

Davis, J.R., 1997. ASM Specialty Handbook: Heat-Resistant Materials, in: ASM Specialty Handbook: Heat-Resistant Materials, ASM Specialty Handbook. ASM International, p. 36.

Donachie, M.J., 2002. Superalloys: A Technical Guide, 2nd Edition. America (NY). https://doi.org/10.1361

Kasravi, N., Hidayat, R., Tuncer, C., Themistokleous, M., Sambo, A.M., 2021. Additive manufacture of alloys for high temperature application. Cranfield University.

Kou, S., 2003. Welding Metallurgy, 2nd ed. ed. Hoboken, N.J. : Wiley-Interscience.

Marinelli, G., Martina, F., Ganguly, S., Williams, S., 2019. Development of Wire + Arc additive manufacture for the production of large-scale unalloyed tungsten components. Int. J. Refract. Met. Hard Mater. 82, 329–335. https://doi.org/10.1016/j.ijrmhm.2019.05.009

Martina, F., Marinelli, G., Ganguly, S., Williams, S.W., 2016. Wire + Arc Additive Manufacturing of

DISTRIBUTION A: Distribution approved for public release.

Refractory Metals.

Martina, F., Mehnen, J., Williams, S.W., Colegrove, P., Wang, F., 2012. Investigation of the benefits of plasma deposition for the additive layer manufacture of Ti-6Al-4V. J. Mater. Process. Technol. 212, 1377–1386. https://doi.org/10.1016/j.jmatprotec.2012.02.002

Mitchell, A., 2010. Primary Carbides in Alloy 718, in: 7th International Symposium on Superalloy 718 and Derivatives 2010. The Minerals, Metals & Materials Society, pp. 161–167.

Norrish, J., 2006. Advanced welding processes : technologies and process control, [New editi. ed.

Shaikh, M.A., Ahmad, M., Shoaib, K.A., Akhter, J.I., Iqbal, M., 2000. Precipitation hardening in Inconel 625. Mater. Sci. Technol. 16, 129–132. https://doi.org/10.1179/026708300101507613

Special Metals, 2013. INCONEL® alloy 625 [WWW Document]. URL https://www.specialmetals.com/assets/smc/documents/alloys/inconel/inconel-alloy-625.pdf (accessed 6.4.20).

Special Metals, 2007. INCONEL® alloy 718 [WWW Document]. URL https://www.specialmetals.com/assets/smc/documents/inconel_alloy_718.pdf (accessed 5.8.20).

Tanvir, A.N.M., Ahsan, M.R.U., Seo, G., Kim, J. duk, Ji, C., Bates, B., Lee, Y., Kim, D.B., 2020. Heat treatment effects on Inconel 625 components fabricated by wire + arc additively manufacturing (WAAM)—part 2: mechanical properties. Int. J. Adv. Manuf. Technol. 110, 1709–1721. https://doi.org/10.1007/s00170-020-05980-w

Wang, J.F., Sun, Q.J., Wang, H., Liu, J.P., Feng, J.C., 2016. Effect of location on microstructure and mechanical properties of additive layer manufactured Inconel 625 using gas tungsten arc welding. Mater. Sci. Eng. A 676, 395–405. https://doi.org/10.1016/j.msea.2016.09.015

Wang, X., Gong, X., Chou, K., 2017. Review on powder-bed laser additive manufacturing of Inconel 718 parts. Proc. Inst. Mech. Eng. Part B J. Eng. Manuf. 231, 1890–1903. https://doi.org/10.1177/0954405415619883

Welding Engineering and Laser Processing Centre Cranfield University, 2019. MATERIALS AND PROPERTIES [WWW Document]. URL https://waammat.com/about/materials-and-properties (accessed 11.8.19).

Williams, S.W., Martina, F., Addison, A.C., Ding, J., Pardal, G., Colegrove, P., 2016. Wire + Arc additive manufacturing. Mater. Sci. Technol. (United Kingdom) 32, 641–647. https://doi.org/10.1179/1743284715Y.0000000073

Xu, X., 2018. Wire + Arc Additive Manufacture of New and Multiple Materials. Cranfield University.

Xu, X., Ganguly, S., Ding, J., Guo, S., Williams, S., Martina, F., 2018a. Microstructural evolution and mechanical properties of maraging steel produced by wire + arc additive manufacture process. Mater. Charact. 143, 152–162. https://doi.org/10.1016/j.matchar.2017.12.002

Xu, X., Ganguly, S., Ding, J., Seow, C.E., Williams, S., 2018b. Enhancing mechanical properties of wire + arc additively manufactured INCONEL 718 superalloy through in-process thermomechanical processing. Mater. Des. 160, 1042–1051. https://doi.org/10.1016/j.matdes.2018.10.038

DISTRIBUTION A: Distribution approved for public release.

Appendix II: Rene41 + Cold work

DISTRIBUTION A: Distribution approved for public release.

Check for updates

Proceedings of the 2022
International Additive Manufacturing Conference
IAM2022
October 19-20, 2022, Lisbon, Portugal

IAM2022-94060

Downloaded from http://asmedigitalcollection.asme.org/MSEC/proceedings-pdf/IAM2022/86601/V001T02A008/6975586/v001t02a008-iam2022-94060.pdf by Cranfield University user on 13 February 2023

IN-PROCESS MECHANICAL WORKING OF ADDITIVE MANUFACTURED RENE 41

William Sean James, Supriyo Ganguly, Goncalo Pardal

Welding Engineering and Laser Processing Centre, Cranfield University, UK

ABSTRACT

In developing the wire + arc additive manufacturing (WAAM) process for creep resistant alloys for defence applications, structures were built from nickel-based superalloy Rene 41 (RE41). The performance of the additive manufactured alloy was analysed for applications including components used in high-speed flight environments, where external structures could reach service temperatures of up to 1000 K. As a single use system with relatively short flight times of < 1 hour, components will be highly stressed to minimise structural mass. In this paper, three wall structures were deposited using a plasma transferred arc process, in a layer-by-layer manner where each layer was mechanically worked by machine hammer peening directly after deposition. With a constant impact frequency, three different travel speeds for the peening tool were used for each wall structure. To understand the most effective cold working parameters, samples were tested and analysed for their mechanical properties and microstructural characteristics after aging treatment. Samples were tested at room temperature and compared with results of both non-worked heat-treated AM material and wrought data obtained from literature review.

Heat-treated only material showed a typical dendritic structure with large columnar grains, and peened material showed a significantly different grain structure. No noticeable difference was observed in the formed phases between the two conditions. Mechanical testing showed promising results with a significant improvement over the non-worked strength. Intermediate and slow peening speeds were very effective, achieving UTS and YS results close to that of the wrought alloy, with a similar increase in the elastic modulus compared to non-worked material. However, faster peening speeds were less effective at returning the material to wrought strength.

NOMENCLATURE

WAAM	Wire + Arc Additive Manufacturing
DED	Directed energy deposition
RE41	Rene 41
AD	As deposited
HT	Heat-treated
RT	Room-temperature
SEM	Scanning Electron Microscope
EDS	Energy-dispersive Spectrometry
BD	Build direction
TT	Through-thickness

1. INTRODUCTION

Wire + arc additive manufacturing (WAAM) is a directed energy deposition (DED) metal AM process whereby a wire feedstock is deposited using an electrical arc as a heat source [1]. In previous studies using WAAM to deposit nickel-based superalloys, as deposited (AD) material has been unable to match the performance of the fully heat-treated (HT) wrought alloy strength, and heat-treating WAAM material does not result in a sufficient increase to match wrought strength [2]. When deposited via WAAM and tested for mechanical performance nickel-based superalloy Rene 41 (RE41), achieved just 59 % of the wrought UTS in AD condition and 61 % when the same material was HT post-deposition [3].

Highlighting the need for additional processing to meet the wrought performance, a previous study by Xu et al found that inter-pass cold rolling of WAAM Inconel 718 was able to increase the UTS of the material to where the rolled WAAM material outperformed the wrought material in both the vertical and horizontal orientations when tested [2]. In developing the WAAM process for maximising the performance of components built using RE41, a series of trials using inter-pass peening was investigated and tested to establish the most suitable peening parameters.

Large columnar grains are typically observed in WAAM built nickel-superalloy microstructure with associated segregation, which can have undesirable effects on the material properties, such as reduced strength, if large grains were not originally desired. In most cases this is due to the nickel-superalloy being precipitation strengthened or age hardened, meaning that the strength is derived mainly from the precipitation of secondary phases, such as γ', within the matrix and at the grain boundaries which inhibit dislocation motion. An elongated dendritic structure with associated segregation makes the solutionising process difficult compared to a wrought

Copyright © 2022 by ASME

DISTRIBUTION A: Distribution approved for public release.

structure where smaller grains with high angle grain boundaries facilitate the diffusion process, as such most of the wrought structures are dynamically recrystallised during rolling or other high temperature deformation processes. The large dendritic grains which make up the microstructure in WAAM material make the formation of these secondary precipitates less likely to occur as the process of diffusion is hindered due to lack of grains with large angle boundary area and segregation owing to solidification from a molten state. Xu et al also examined the effect of heat-treating WAAM built Inconel 718 and found that unless the material underwent a process to produce a more favourable microstructure the mechanical strength is unlikely to meet the wrought performance through an age hardening heat-treatment alone [4]. It should be noted that there are cases where large grains are benefitable to the performance of nickel superalloys, such as in gas turbine blades, where a single crystal is specially formed in the correct orientation to primarily improve fatigue performance [5].

RE41 shares some similarities with the strengthening mechanism of Inconel 718, however the composition varies. RE41 is a nickel-based precipitation strengthened alloy which is alloyed significantly with Cr, Co and Mo. RE41 has a face-centred-cubic austenitic matrix, and is mainly strengthened through the formation of γ' particles $Ni_3(Al,Ti)$ [6].

The benefits of WAAM over other metal AM processes such as powder bed processes, is the ability to build larger components with little adjustment or expensive equipment set-ups. WAAM is also capable of higher deposition rates when compared with power bed, which increases productivity for larger components. The metal wire feedstock used in WAAM is often less expensive than metallic powder and is easier to change for a different alloy without the need for extensive cleaning. Material loss in WAAM is also much reduced compared to powder bed which can be as much as 25 % [7]. Powder-bed does however have some advantages over WAAM, which includes the ability to create more intricate and complex lattice structures and net shape parts, whereas WAAM is a near net shape process. Parts produced using powder bed also more closely match the wrought strength of alloys [8], compared with WAAM where the need for post-processing and/or in-process working is more extensive.

The ability to manufacture larger components makes WAAM ideal for defence applications and the production of high-speed flight components. The application of such components will be in the external structure of a single use system subjected to service temperature of 1000 K for a short flight time of < 1 hour. As such components for use in this system will be highly stressed to minimise structural mass, these components will be optimised for maximum strength at maximum temperature. It is therefore the aim of this research to maximise the performance of WAAM built RE41 for this purpose.

2. MATERIALS AND METHODS

2.1 WAAM Process

A commercially available 1 mm diameter RE41 wire was used as the feedstock in a WAAM system (Figure 1) consisting of: a Kuka six-axis robotic arm, a plasma water-cooled welding torch mounted to the robotic arm, a local shielding device surrounding the plasma torch, and a wire feeder. To facilitate the inter-pass mechanical working, an Atlas Copco RRH06P riveting hammer was also mounted to the robotic arm and configured to allow for semi-automatic operation.

The composition of the RE41 wire was tested as part of a previous study using inductively coupled plasma - optical emission spectroscopy (ICP-OES), the composition is given in Table 1 [3].

A short wall approach was adopted in-order to build just enough material to extract specimens for metallographic and tensile analysis. Four walls measuring approx. 360 × 20 × 8 mm were built on an Inconel 718 substrate plate, using an arc current of 180 A, a wire feed speed of 2.4 m/min, a torch travel speed of 0.36 m/min, a torch to work distance of 8 mm, and an inter-pass temperature of 170 °C after an approx. cooling time of 3 mins. Shielding via a local shielding device, as shown in Figure 1, was provided at 30 L/min of Argon. To establish the best peening parameters one wall was built AD, without any inter-pass peening to provide a baseline. Three further walls were built using a constant impact frequency of 2160 impacts per min with a load of 30 kg, where the tool travel speed was varied for each wall. Three different travel speed of 18, 36, and 112.5 mm/s were trialled during manufacture of the walls. The use of these peening parameters provided an input energy of approx. 4.85, 2.43, 0.776 J/mm^2 for the 18, 36, and 112.5 mm/s travel speed respectively.

After the walls were manufactured, specimens for tensile, microhardness and metallographic analysis were extracted. All specimens underwent an aging heat-treatment to maximise tensile performance based on historic research by Weisenberg and Morris. The treatment consisted of: solutionising at 1065 °C for four hours followed by air quenching to room-temperature (RT) followed by a further 16 hours aging at 760 °C after which the material was again air quenched [9].

Downloaded from http://asmedigitalcollection.asme.org/MSEC/proceedings-pdf/IAM2022/86601/V001T02A008/6975586/v001t02a008-iam2022-94060.pdf by Cranfield University user on 13 February 2023

Copyright © 2022 by ASME

DISTRIBUTION A: Distribution approved for public release.

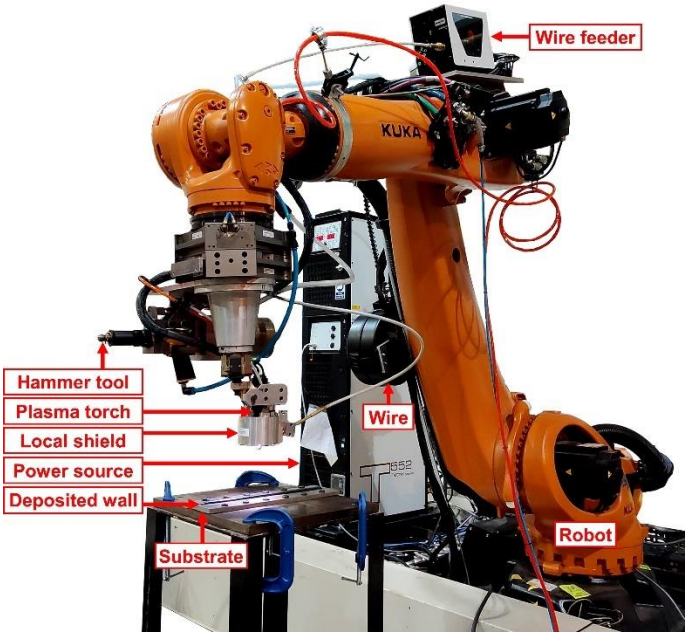


FIGURE 1: WAAM EXPERIMENTAL SETUP.

TABLE 1: COMPOSITION OF RE41 WIRE.

Ni	Cr	Co	Mo	Fe	Ti	Al	Nb	V
53.7	18.9	10.2	9.08	2.72	3.20	1.64	0.12	0.12

Si	C	Cu	Mn	B	S
0.09	0.07	0.04	0.03	0.004	<0.003

2.2 Mechanical Testing

Three tensile specimens in each condition were tested at RT to failure using an Instron 8801 Servo Hydraulic Universal Testing System. A strain rate of 0.005 mm/min was adopted until plastic deformation whereafter a rate of 1.6 mm/min was used. Testing was conducted according to the ASTM specification E8/E8M, a standard test method for tension testing of metallic materials. The specimen dimensions conformed to the sub-size category, a drawing of which is given in Figure 2.

Microhardness was measured using a Zwick/Roell hardness tester under a load of 0.5 kg and a holding time of 15 sec. Measurements were taken at 1 mm increments through the cross-section of the wall height and thickness.

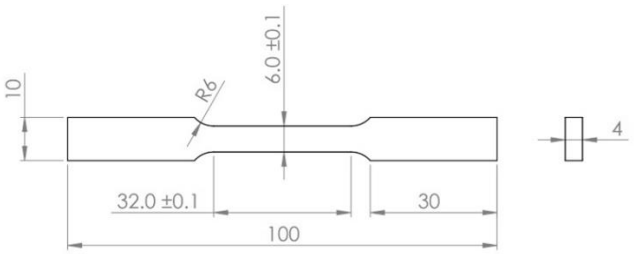


FIGURE 2: TENSILE TESTING SPECIMEN.

2.3 Metallographic Preparation and Analysis

Cross-sections in the build direction (BD) and through-thickness (TT) plane were extracted and prepared for metallographic analysis to reveal the microstructure. Following a procedure of successive grinding and polishing, samples were swab etched for 30 sec using a solution containing 3 g $CuSO_4$, 80 ml HCl, and 20 ml Ethanol.

Samples were viewed optically using a Leica DM 2700M Microscope. The microstructure was also examined using a Tescan VEGA 3 scanning electron microscope (SEM). Composition was determined by energy-dispersive spectrometry (EDS), as such the SEM was fitted with an Oxford Instruments X-Max 20 mm EDS detector.

3. RESULTS AND DISCUSSION

3.1 Mechanical

When tested at RT, tensile specimens extracted from material mechanically worked using 4.85, 2.43, and 0.776 J/mm^2, achieved an average UTS of 1284.5, 1299.4, and 1048.3 MPa and a YS of 1048.7, 1054.0, and 906.1 MPa respectively. The full set of results is presented in Table 2, where the working energies are abbreviated as W High, W Med, and W Low for 4.85, 2.43, and 0.776 J/mm^2, respectively. Figure 3 presents the stress-strain variations of material in the AD [3] and HT condition together with the worked HT material. It can be seen that with the application of higher impact energy per unit area, the elastic modulus of the material increases with the tensile strength and almost meets the performance of a wrought variant. In comparing the UTS and YS results the best performance was achieved through peening at 2.43 J/mm^2. However, when the variation in results is accounted for, it can be assumed that between the 4.85 and 2.43 J/mm^2 impacting energies, the maximum performance increase possible had been achieved by working at just 2.43 J/mm^2, due to the negligible difference in performance. Subsequently in future studies on inter-pass peening of RE41, there would be little advantage to peening beyond 2.43 J/mm^2.

In comparing the hardness of RE41 in each condition presented in Table 2, the hardness is seen to increase with impacts per area and is significantly higher that the wrought minimum. The hardness of the material affects the machinability, and difficulties were encountered during the manufacture of the tensile coupons. It is noted by Weisenberg and Morris that the rate at which RE41 work hardens makes it particularly difficult to machine, and they recommend the use of carbide tools and sulphurated oils [9]. Silicon carbide cutting disks were utilised for cutting the deposited walls from the substrate plates which worked comparatively well.

The elastic modulus (E) is also shown to vary in the results, although there is not a great deal of correlation between the working energy. Peening at room temperature hydrostatically deforms the alloy and generates dislocations and other associated metal defects which strain hardens the alloy. Subsequent transitory thermal cycles, during deposition of successive layers, would annihilate some of these dislocations but some hardening

Downloaded from http://asmedigitalcollection.asme.org/MSEC/proceedings-pdf/IAM2022/86601/V001T02A008/6975586/v001t02a008-iam2022-94060.pdf by Cranfield University user on 13 February 2023

Copyright © 2022 by ASME

DISTRIBUTION A: Distribution approved for public release.

effects will remain which would work to make the deposit stiffer when compared to the non-worked variant. It should also be noted this difference could be due to E being calculated from tensile data which can be error prone. Further investigation is required to fully discuss this observation.

TABLE 2: MECHANICAL PERFORMANCE AT RT.

Condition	UTS (MPa)	YS (MPa)	E (GPa)	HV
Wrought [10]	1420	1060	220	363 (min)
HT	880.8	829.4	161.4	406.3
HT + W Low	1048.3	906.1	156.7	437.2
HT + W Med	1299.4	1054.0	194.4	442.9
HT + W High	1284.5	1048.7	186.3	459.0

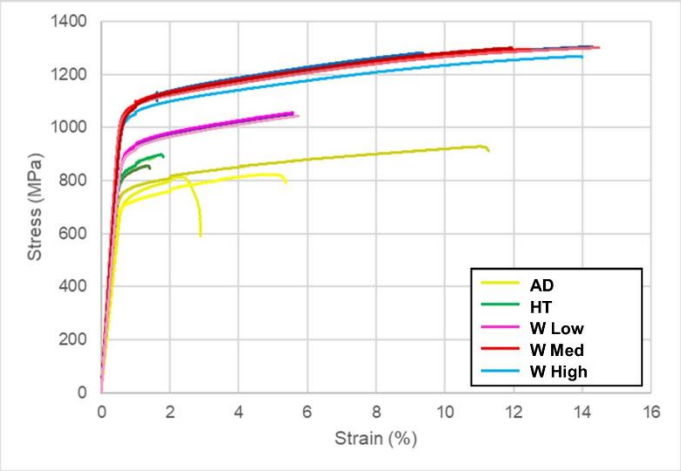


FIGURE 3: STRESS-STRAIN OF RT MECHANICAL PERFORMANCE.

3.2 Microstructural Observations

Of the examined specimens there is observable differences in the macrostructure of the HT and worked material, seen in Figure 4. The main differences are in the granular structure, where the dendritic structure of the worked material has been disrupted by the peening process, leading to the disruption of the long columnar grain structure which is so typically observed in alloys deposited via wire-arc DED processes. This affect is best observed when comparing HT material in Figure 5 and the worked material Figure 6.

No cracking was observed in worked material; however, several large solidification cracks were observed in the HT material (Figure 4), note that of these cracks only the largest is visible in Figure 4. Solidification cracks were identified based on orientation along the BD axis owing to lateral stresses and segregation at the crack edge. The crack edge segregation can be seen in Figure 7. It is thought that the stress input into the material due to peening has allowed for relaxation of the strain created during the deposition process, which has subsequently resulted in the elimination of cracking. Cracking has been known to occur in DED built superalloys, notably in WAAM built Inconel 718 [11]. Atabay et al found that RE41 did not experience cracking when used in laser powder bed fusion (LPBF), and attributed this to the fine microstructure produced when using LPBF [12], it is possible that the disruption of the typically larger grain structure seen in WAAM components has resulted in the both an increased strength and a reduction in susceptibility to cracking.

When the microstructure is examined at greater magnification using a SEM the difference between HT only (Figure 8) and worked material (Figure 9) is negligible, with the same phases observed in both specimens, indicating that the in-process working has no impact on the formed phases. An EDS mapping (Figure 10) and composition table (Table 3) is provided for the phases observed in the worked material. Lighter coloured areas are indicative of Mo rich phases, likely a complex intermetallic known as σ phase (CrNiMo) which is known to occur in nickel superalloys [13], these phases were analysed using EDS and the results are presented in Table 3. The darker grey coloured phases however are indicative of Ti rich precipitates, suggesting the presents of Ti rich carbides.

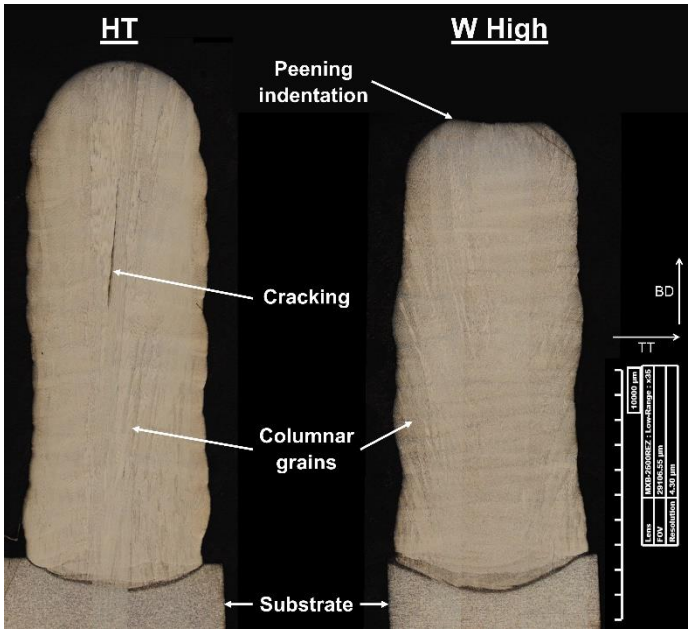


FIGURE 4: MACROSRUCTURE OF HT AND WORKED (W HIGH) MATERIAL.

Downloaded from http://asmedigitalcollection.asme.org/MSEC/proceedings-pdf/IAM2022/86601/V001T02A008/6975586/v001t02a008-iam2022-94060.pdf by Cranfield University user on 13 February 2023

Copyright © 2022 by ASME

DISTRIBUTION A: Distribution approved for public release.

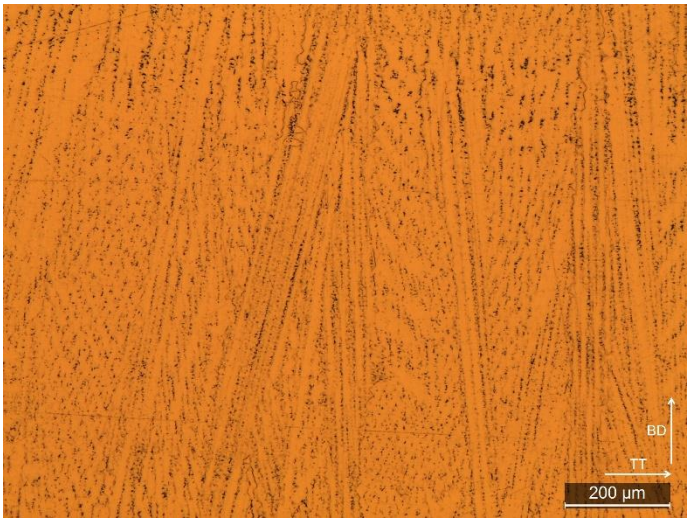


FIGURE 5: MICROGRAPH OF HT MATERIAL DISPLAYING LONG COLUMNAR GRAIN STRUCTURE.

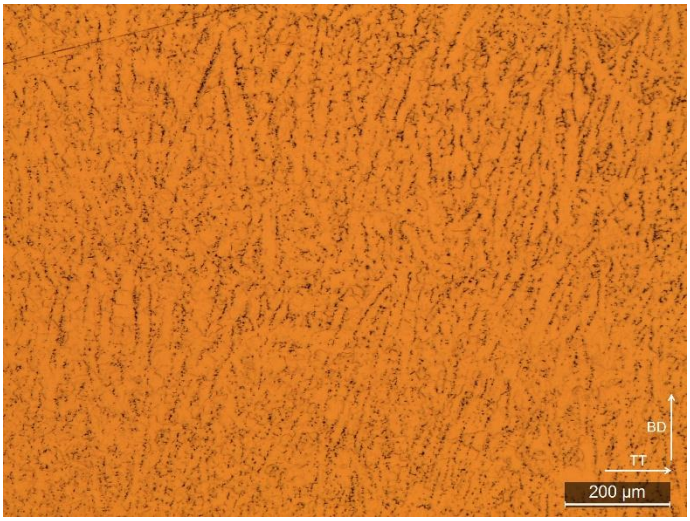


FIGURE 6: MICROGRAPH OF WORKED (W HIGH) SHOWING DISTRUPTED DENDRITIC STRUCTURE.

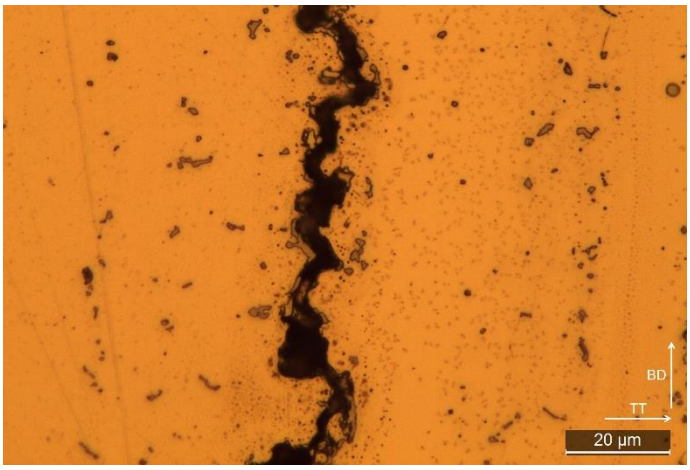


FIGURE 7: SOLIDIFICATION CRACK OBSERVED IN HT SAMPLE SEEN IN FIGURE 4.

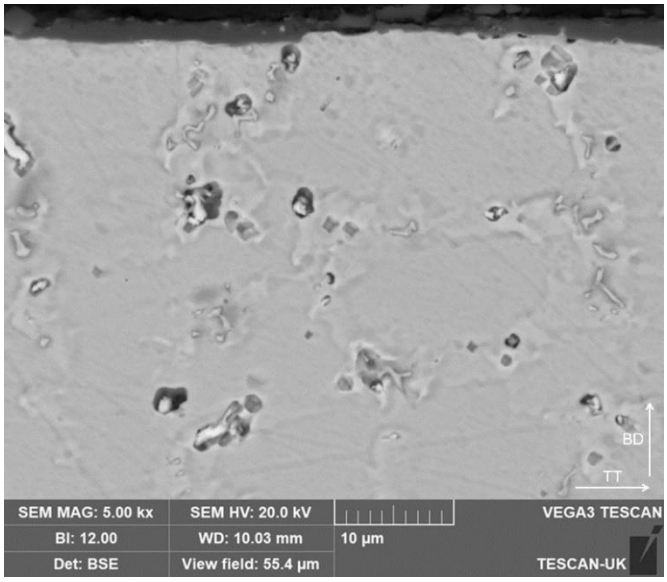


FIGURE 8: SEM BSE IMAGE OF HT MATERIAL.

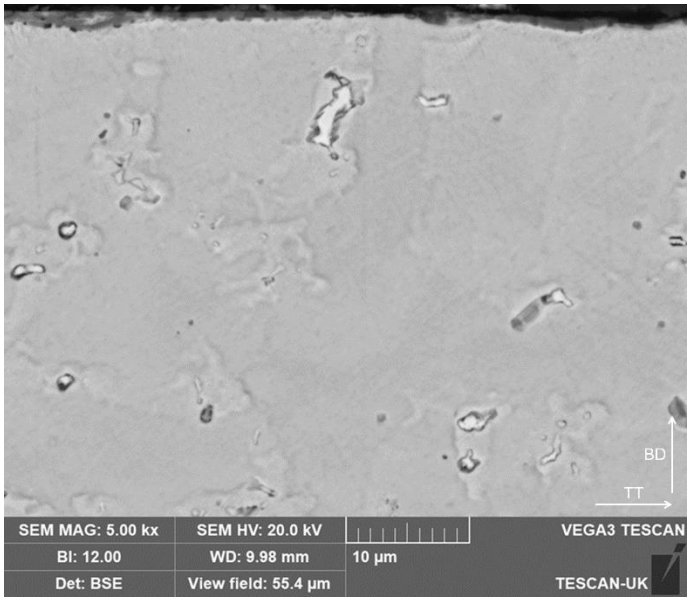


FIGURE 9: SEM BSE IMAGE OF WORKED (W HIGH) MATERIAL.

Downloaded from http://asmedigitalcollection.asme.org/MSEC/proceedings-pdf/IAM2022/86601/V001T02A008/6975586/v001t02a008-iam2022-94060.pdf by Cranfield University user on 13 February 2023

Copyright © 2022 by ASME

DISTRIBUTION A: Distribution approved for public release.

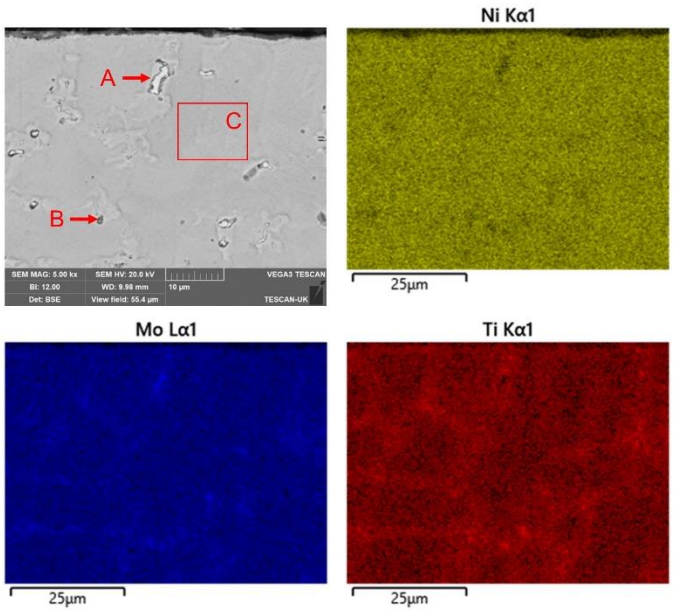


FIGURE 10: EDS ELEMENTAL MAPPING OF WORKED (W HIGH) MATERIAL.

TABLE 3: EDS COMPOSITION OF AREAS MARKED IN FIGURE 10 (% AT.).

Element	Spectrum A	Spectrum B	Spectrum C
Al	1.48	2.37	3.72
Ti	3.35	12.24	3.22
V	0.15		0.12
Cr	31.40	20.08	21.39
Fe	2.35	2.51	3.00
Co	9.70	8.94	10.44
Ni	30.73	46.64	52.67
Mo	20.84	7.22	5.44

4. CONCLUSION

- In-process working during WAAM deposition can increase the performance of RE41 by up to 48 % over HT only material.
- Use of a peening energy density of more than 2.43 J/mm^2 does not result in any additional benefit.
- RE41 work hardens quickly, and microhardness increases with work done.
- In-process working of RE41 disrupts the long columnar grain structure typically observed in wire-arc DED built material.
- In-process working of RE41 results in a decreased susceptibility to cracking.

ACKNOWLEDGEMENTS

The authors wish to acknowledge the Ministry of Defence (UK) for their financial support, and the industrial supervisors from DSTL Porton Down, for their ongoing advice and guidance: Graham Simpson and Dr Matthew Lunt.

REFERENCES

[1] S. W. Williams, F. Martina, A. C. Addison, J. Ding, G. Pardal, and P. Colegrove, “Wire + Arc additive manufacturing,” *Mater. Sci. Technol.*, vol. 32, no. 7, pp. 641–647, 2016.

[2] X. Xu, S. Ganguly, J. Ding, C. E. Seow, and S. Williams, “Enhancing mechanical properties of wire + arc additively manufactured INCONEL 718 superalloy through in-process thermomechanical processing,” *Mater. Des.*, vol. 160, pp. 1042–1051, 2018.

[3] W. S. James, S. Ganguly, and G. Pardal, “[Manuscript submitted for publication] High Temperature Failure and Microstructural Investigation of Additive Manufactured Rene 41,” *Mater. Sci. Eng. A*, 2022.

[4] X. Xu, J. Ding, S. Ganguly, and S. Williams, “Investigation of process factors affecting mechanical properties of INCONEL 718 superalloy in wire + arc additive manufacture process,” *J. Mater. Process. Technol.*, vol. 265, no. September 2018, pp. 201–209, 2019.

[5] N. K. Arakere and G. Swanson, “Effect of crystal orientation on fatigue failure of single crystal nickel base turbine blade superalloys,” *J. Eng. Gas Turbines Power*, vol. 124, no. 1, pp. 161–176, 2002.

[6] M. Schwartz, R. Ciocoiu, D. Gheorghe, G. Jula, and I. Ciucă, “Preliminary research for using Rene 41 in confectioning extrusion dies,” *Mater. Characterisation VII*, vol. 1, pp. 95–106, 2015.

[7] A. N. M. Tanvir *et al.*, “Heat treatment effects on Inconel 625 components fabricated by wire + arc additively manufacturing (WAAM)—part 2: mechanical properties,” *Int. J. Adv. Manuf. Technol.*, vol. 110, no. 7–8, pp. 1709–1721, 2020.

[8] X. Wang, X. Gong, and K. Chou, “Review on powder-bed laser additive manufacturing of Inconel 718 parts,” *Proc. Inst. Mech. Eng. Part B J. Eng. Manuf.*, vol. 231, no. 11, pp. 1890–1903, 2017.

[9] L. A. Weisenberg and R. J. Morris, “How to Fabricate Rene 41,” *Met. Prog.*, vol. 78, pp. 70–74, 1960.

[10] M. J. Donachie and S. J. Donachie, “Selection of Superalloys,” in *Superalloys - A Technical Guide*, 2nd ed., ASM International, 2002, pp. 11–24.

[11] W. S. James, S. Ganguly, and G. Pardal, “[Manuscript submitted for publication] Microstructure and Mechanical Properties of Inconel 718 and Inconel 625 Produced Through the Wire + Arc Additive Manufacturing Process,” in *AVT-356 Physics of Failure for Military Platform Critical Subsystems*, 2021.

Downloaded from http://asmedigitalcollection.asme.org/MSEC/proceedings-pdf/IAM2022/86601/V001T02A008/6975586/v001t02a008-iam2022-94060.pdf by Cranfield University user on 13 February 2023

Copyright © 2022 by ASME

DISTRIBUTION A: Distribution approved for public release.

[12] S. E. Atabay, O. Sanchez-Mata, J. A. Muñiz-Lerma, R. Gauvin, and M. Brochu, "Microstructure and mechanical properties of rene 41 alloy manufactured by laser powder bed fusion," *Mater. Sci. Eng. A*, vol. 773, no. October 2019, 2020.

[13] H. E. Collins, "Relative Stability of Carbide and Intermetallic Phases in Nickel-Base Superalloys," in *International Symposium on Structural Stability in Superalloys*, 1968, pp. 171–198.

Downloaded from http://asmedigitalcollection.asme.org/MSEC/proceedings-pdf/IAM2022/86601/V001T02A008/6975586/v001t02a008-iam2022-94060.pdf by Cranfield University user on 13 February 2023

Copyright © 2022 by ASME

DISTRIBUTION A: Distribution approved for public release.

Appendix II: Inconel 718 + Cold work

DISTRIBUTION A: Distribution approved for public release.



CRANFIELD UNIVERSITY

School of Water Energy and Environment

M.Sc. Advanced Mechanical Engineering

Academic Year: 2021-22

Effect of Peening and Heat Treatment processes on Inconel 718 (nickel alloy) manufactured by WAAM for creep resistant application

Author

Smaranika Tripathy

Supervisors

Dr. Supriyo Ganguly

Dr. Kuladeep Rajamudili

DISTRIBUTION A: Distribution approved for public release.

ABSTRACT

The wire arc additive manufacturing (WAAM) process offers significant potential of material saving and design flexibility to create complex functional components; however, as a layer-by-layer building process, a previously deposited layer is partially remelted and undergoes creep, viscous and plastic deformation from the thermal cycle of successive layer depositions. In as-deposited condition, this also resulted in epitaxial grain growth. In this study, a high strength precipitation hardening nickel alloy, IN718, was studied with an aim to understand the grain reformation by inter-layer robotic machine hammer peening which would induce cold straining in a deposited layer which would exhibit grain reformation from deposition of subsequent layers. The grain refinement from inter-layer peening treatment would lead to improvement in mechanical properties such as hardness, tensile strength & fatigue life.

To understand the impact of cold peening process, in this project, peened & non-peened Inconel 718 walls deposited by wire arc additive manufacturing (WAAM) process are compared using tensile and hardness testing and correlated with microstructural observations. Scanning electron microscopy and Energy dispersive spectroscopy were carried out to study the microstructural evolution due to peening. The impact of peening on breaking of dendritic and epitaxial grain structure and compositional homogenisation and subsequent improvement in aging response was also studied by comparing the age hardened performance in as-deposited and peened structures. The conventional thermal cycle, used for wrought alloy, was experimented to enhance diffusion of solute atoms in a WAAM built structure, characterised by segregation and dendritic grain structure with low angle grain boundaries, to observe the difference in the ageing response from different processing.

The future scope of the work is to conduct mechanical testing of Inconel 718 (nickel alloy) such as tensile testing, fracture toughness testing, creep testing, fatigue testing and Non-destructive testing for the wire-arc additive manufactured (WAAM). Further, accumulation of data consisting of evaluation of mechanical properties would lead to contribution and qualification of standarisation in the industry.

Keywords:

WAAM, Inconel 718, Peening, Ageing response

DISTRIBUTION A: Distribution approved for public release.

ACKNOWLEDGEMENTS

I would like to show my gratitude to the School of Water, Energy and Environment of the Cranfield University for offering me Cranfield Scholarship and for the entire support through the entire Cranfield journey. I would like to express my sincere appreciation towards my first supervisor, Dr. Supriyo Ganguly who accepted my request to conduct thesis under his supervision and for his continuance guidance for the successful completion of the individual thesis. In addition, I would to like to thank my other supervisor Dr. Kuladeep Rajamudili who guided me throughout the individual thesis and experimentation. The research experience within the Welding Engineering and Laser Processing Centre has been the most amazing part of my career journey. I am also very thankful to the Welding team and lab staff in different labs who have supported me throughout the experiments. Also, I express my gratefulness to the family who has supported me to fulfill the research and academic experience at Cranfield University. Above all, who has given me the opportunity and the will to complete this Masters of Science in Advanced Mechanical Engineering at Cranfield University and who has showed His mercy and love throughout my life, my deepest love to Almighty God in Jesus.

DISTRIBUTION A: Distribution approved for public release.

TABLE OF CONTENTS

ABSTRACT **2**
ACKNOWLEDGMENTS **3**
LIST OF FIGURES **6**
LIST OF TABLES **8**
LIST OF EQUATIONS **9**
LIST OF ABBREVIATIONS **10**
1. INTRODUCTION **11**
1.1 Research Background 11
1.2 Motivation 13
1.3 Aims and Objectives 14
2. LITERATURE REVIEW **16**
2.1 IN718 in detail 16
2.1.1 Nickel-base Superalloys 16
2.1.2 Nickel-base Superalloys Processing 16
2.1.3 Material Properties of Inconel 718 17
2.1.4 Crystal Structure of Inconel 718 18
2.1.5 Phase Diagram of Inconel 718 18
2.1.6 Solidification Behaviour of IN718 19
2.2 WAAM for IN718 21
2.2.1 Different AM Processes 21
2.2.2 Wire-arc additive manufacturing technique (WAAM) Process 22
2.2.3 Microstructural evolution for WAAM deposited parts 23
2.3 Strengthening Mechanisms 25
2.3.1 Different types of Strengthening mechanisms for WAAM 25
2.3.2 WAAM with peened treatment 26
2.3.3 WAAM with inter-layer machine-hammer peened treatment 27
2.3.4 Microstructural changes due to peening 27
2.3.5 Mechanical Properties improvement because of peening 29
2.4 Heat Treatment for WAAM parts 31
2.4.1 Heat Treatment Principle & Standards 31
2.4.2 Microstructural Characterisation for heat treated samples 32
2.4.3 Mechanical Properties for heat treated samples 34
2.5 Homogenisation Kinetics for IN718 35
3. METHODOLOGY **38**
3.1 Experimental Methodology 38

DISTRIBUTION A: Distribution approved for public release.

3.2 WAAM for IN718 with inter-layer peened treatment 38

3.3 Post-deposition Heat Treatment of samples from the WAAM IN718 walls 41

3.4 Metallographic Preparation for Microstructure 43

3.5 Microhardness Test 46

4. RESULTS & DISCUSSION 47

4.1 Microstructure using Optical Microscopy 47

4.1.1 Comparison between samples before heat treated (TT-P, TT-NP, BD-P, BD-NP, WA-P, WA-NP) and wire sample 47

4.1.2 Comparison for peened samples before and after heat treatment process 49

4.1.3 Comparison for non-peened samples before heat treatment and after modified heat treatment process 50

4.2 Microstructure using Scanning Electron Microscopy (SEM) and elemental composition in Energy dispersive X-ray spectroscopy (EDS) 51

4.2.1 Wire Sample Characterisation 51

4.2.2 Strengthening mechanism impact of peening for samples before Heat Treatment Microstructural Evolution 52

4.2.3 Different Heat Treatment Processes Microstructural Evolution 56

4.2.4 Rationale behind the homogenisation treatment change 59

4.3 Optical Macrostructure Study 59

4.4 Mechanical Property defined by Microhardness 62

4.4.1 Comparison between TT-P and TT-NP as-deposited before heat treatment 62

4.4.2 Comparison for peened samples before and after heat treatment process 63

4.4.3 Comparison for NP and P before HT and after modified HT 64

5. CONCLUSION 65

6. FUTURE WORK 65

7. REFERENCES 66

DISTRIBUTION A: Distribution approved for public release.

LIST OF FIGURES

Figure 1 Processing of Nickel-base Superalloys..... 17
Figure 2 TTT diagram for IN718 hot-forged and vacuum melted 19
Figure 3 Graph Solidification behaviour of IN718 20
Figure 4 Steps of Solidification for IN718 20
Figure 5 AM Process Flow chart 21
Figure 6 WAAM with Plasma arc welding 23
Figure 7 Deposition in WAAM 24
Figure 8 Surface post-treatments applied to additively manufactured metal parts 26
Figure 9 Ultrasonic impact peening, Laser shock peening and moving paths, where Fs (static load), A (vibration amplitude) 27
Figure 10 Machine hammer peened treatment on Ti64 WAAM walls 27
Figure 11 Depth of deformation 28
Figure 12 HAZ bands and melt depth 28
Figure 13 (a) Thermal field interacts with machine-hammer peening (b) β map (c) Pole figures in reconstructed β map..... 29
Figure 14 Microhardness values of machine hammer peened (MHP), thin & thick walls (as-deposited) for Ti-6Al-4V alloy 30
Figure 15 Tensile Properties of machine hammer peened (MHP) & thin walls (as-deposited) 30
Figure 16 Standard heat treatment for IN718 alloy, A.C is air cool 32
Figure 17 Solution + δ- phase aged treatment for IN718 alloy, W.Q is water quenching 32
Figure 18 (a) Before heat-treatment (b) Standard heat treatment (c) Solution + δ- phase aging treatment samples 33
Figure 19 (a) Longitudinal microhardness (b) Transverse microhardness 34
Figure 20 (a) Tensile, Yield strength and Elongation% (b) Engineering Stress vs Strain curves 35
Figure 21 (a) As-cast (b) 1hour at 1050°C (c) 3 hours at 1050°C (d) 9 hours at 1050°C (e) 3 hours at 1100°C (f) 3 hours at 1150°C 36
Figure 22 Laves phase vol % vs homogenisation time at different homogenisation temperatures 36
Figure 23 Avrami plots for the dissolution of Laves phase at different temperature 37
Figure 24 (a) Flowchart for Experimental methodology 38
Figure 24 (b) Schematic diagram of WAAM 39
Figure 25 Experimental Setup for WAAM with inter-layer peened treatment (BD is build direction, WA is weld axis and TT is throat thickness)..... 40
Figure 26 Standard Heat Treatment Cycle..... 41
Figure 27 Modified Heat Treatment Cycle 42
Figure 28 IN718 Wall WAAM deposited with inter-layer peened treatment up to 240 mm along WA 42
Figure 29 Metallographic Preparation for microstructure study of samples 43
Figure 30 Specimens named based on normal direction to the axis shown BD, WA and TT 44

DISTRIBUTION A: Distribution approved for public release.

Figure 31 WAAM with inter-layer peened treated and without inter-layer peened treated 44
Figure 32 Grinding of samples in machine shown 44
Figure 33 Etched Samples for microstructure study 45
Figure 34 Sample for microhardness test (Bottom to Top with increment of 0.5 mm) 46
Figure 35 Sample of IN718 wire from conventional manufacturing process 47
Figure 36 (a) BD-NP (Normal to Build direction non-peened) (b) TT-NP (Normal to Throat thickness at mid-plane non-peened) (c) WA-NP (Normal to weld axis non-Peened) 48
Figure 37 (a) BD-P (Normal to Build direction Peened) (b) TT-P (Normal to Throat thickness at mid-plane Peened) (c) WA-P (Normal to Weld axis Peened) 48
Figure 38 (a) TT-P before Heat Treatment (b) TT-P SH after Standard Heat Treatment (c) TT-P MH after Modified Heat Treatment 49
Figure 39 (a) TT-NP MH before Heat Treatment (b) TT-NP MH after modified Heat Treatment 50
Figure 40 Wire Sample 51
Figure 41 (a) TT-NP before Heat Treatment (b) TT-P before Heat Treatment 53
Figure 42 (a) TT-NP before Heat Treatment 54
Figure 42 (b) TT-P before heat treatment 55
Figure 43 (a) TT-P Standard Heat Treatment (b) TT-P Modified Heat Treatment 56
Figure 44 TT-P Standard Heat Treatment 57
Figure 45 TT-P Modified Heat Treatment 58
Figure 46 (a) TT-P Before Heat Treatment (b) TT-P Standard Heat Treatment (c) TT-P Modified Heat Treatment 59
Figure 47 Before Heat Treatment Peened and Non-peened Samples 61
Figure 48 (a) TT-NP Before Heat Treatment (b) TT-NP Modified Heat Treatment 62
Figure 49 Hardness values for peened and non-peened IN718 WAAM samples before heat treatmen 63
Figure 50 (a) Top layer MHP with peening line (b) Peening line for thin wall 64
Figure 51 Hardness values for peened IN718 WAAM samples before heat treatment, standard heat treated and modified heat treated 65
Figure 52 Hardness values for non-peened IN718 WAAM samples before heat treatment and modified heat treated 65

DISTRIBUTION A: Distribution approved for public release.

LIST OF TABLES

Table 1 Nickel-base Superalloy Chemical Composition 16
Table 2 Mechanical Properties of IN718 17
Table 3 Chemical Composition of IN718 17
Table 4 AMS 5662M for forged IN718, Standard Heat Treatment 32
Table 5 Diffusion coefficient parameters of Ti, Nb and Mo in Nickel 37
Table 6 WAAM wall build parameters 39
Table 7 Welding Settings for WAAM 40
Table 8 Machine-hammer Peening (MHP) Settings 40
Table 9 Temperature and Holding time during Standard heat treatment process 41
Table 10 Temperature and Holding time during modified heat treatment process 42
Table 11 Samples for microstructure study 43
Table 12 Parameters for Grinding and Polishing 45
Table 13 Samples for Vickers Hardness test 46
Table 14 Parameters of laser beam in SEM 52
Table 15 Elemental Composition in both spectrums as per Figure 40 52
Table 16 (a) Elemental Composition in both spectrums (TT-NP) before Heat Treatment 54
Table 16 (b) Elemental Composition in both spectrums (TT-P) before Heat Treatment 55
Table 17 Elemental Composition in both spectrums (TT-P) Standard Heat Treatment 57
Table 18 Elemental Composition in both spectrums (TT-P) Modified Heat Treatment 58

DISTRIBUTION A: Distribution approved for public release.

LIST OF EQUATIONS

Equation 1 35
Equation 2 35
Equation 3 37
Equation 4 37
Equation 5 37
Equation 6 37
Equation 7 53
Equation 8 53

DISTRIBUTION A: Distribution approved for public release.

LIST OF ABBREVIATIONS

WAAM	Wire-arc additive manufacturing
IN718	Inconel 718

DISTRIBUTION A: Distribution approved for public release.

1. INTRODUCTION

1.1 Research Background

Inconel 718 (IN718) is a nickel base superalloy that belongs to the family of Inconel alloys (Ni-Cr based superalloys). IN718 is precipitation hardened Ni-Cr alloy that is subjected to solution-annealing and offers unique mechanical properties such as high ultimate tensile strength, creep properties, excellent corrosion resistance, fatigue and oxidation prevention [1]. The high mechanical strength of IN718 alloy is because of the precipitation of Ni_3(NbAlTi) phase that leads to the strengthening effect. Also, IN718 alloy can resist the crack initiation and crack growth during welding process because the lower content of Al and Ti and addition of Nb in the base composition leads to delayed aging response [2]. Additionally, IN718 alloy has the capability to withstand at high temperatures and have structural & property stability even in high stress environment as has higher content of Ni and Co.

IN718 alloy offers combination of resistance to surface degradation and high temperature and high pressure due to superior mechanical properties for wide use in load bearing applications and specialised applications, gas turbines, diesel engine turbocharger casings, exhaust manifolds, nuclear reactors, liquid-fuelled rockets, rocket motors and cryogenic storage tanks [1]. It has a wide temperature range operating between -252° to 704°C. The IN718 alloy surface and its tribological properties could be improved by subjecting to different heat treatment techniques depending on the area of applications.

Additive Manufacturing (AM) processes have been widely used to fabricate hybrid components with cost-effectiveness and offers unique flexibility to manufacture complex parts. Some AM processes particularly, electron beam melting (EBM) utilises high energy consumption and selective laser melting (SLM) requires vacuum chamber environment, although, wire arc additive manufacturing (WAAM) has better advantages in terms of low cost for investment and high adaptability [4].

WAAM is a Direct Energy Deposition (DED) additive manufacturing process, and during WAAM successive depositions, a considerable amount of wire undergoes layer build process for complex geometries. The wire-arc additively manufactured part has some challenges such as residual stress, fluctuations in thermal distribution and heat conduction that lead to thermal gradients, distortion and low-grade microstructure [3].

DISTRIBUTION A: Distribution approved for public release.

However, there is Nb segregation phase during solidification and its extent depends on cooling rates. Further, there is dendritic grain growth with the formation of Nb, Mo, Ti austenitic dendrites leading into laves phase and stable phases, NbC and TiN [2]. Also, the microhardness of IN718 alloy is improved because of the formation of matrix interfacial layer and further refinement in TiC dendrites [1].

There are different strengthening mechanisms to improve mechanical properties of WAAM component such as interpass rolling & peening that generates plastic deformation in the interpass layers. The deformation leads to dislocation that plays as an obstacle to dislocation movements, precipitates and grain boundaries. Also, during multiple thermal cycles recrystallisation takes place followed by recovery process [5]. For a wrought alloy, there is a diffusion of solute atoms characterised by low angle grain boundaries, while, this diffusion can be enhanced by different heat treatment processes. The differences in aging response and selection of solutioning and aging temperature determines the size distribution of the formed precipitates and grain boundary morphology [5].

DISTRIBUTION A: Distribution approved for public release.

1.2 Motivation

The motivation is to conduct different heat treatment studies and mechanical tests for correlation between microstructural evolution and material properties on WAAM deposited IN718 alloy to contribute for the standardisation of WAAM deposited parts. Since, WAAM offers good geometrical accuracy of complex parts and is a cost-effective process. Also, through WAAM, the composition and phase fraction could be controlled and the research is done to control dilution for IN718 alloy.

There are strengthening mechanisms and heat treatment processes which would change the microstructure evolution and further improve mechanical properties such as rupture strength, tensile strength and hardness needs to be researched. Therefore, study is conducted for solution enhancement of WAAM IN718 alloy properties and comparison with the wrought alloys. The research focus is on the microstructural evolution of the WAAM as-deposited IN718 alloy parts with inter-layer peened treatment and without peened treatment.

Various techniques to control dilution of solute atoms is investigated by carrying different heat-treated WAAM IN718 alloy parts with inter-layer peened treatment and without peened treatment.

DISTRIBUTION A: Distribution approved for public release.

1.3 Aims and Objectives

The aim of this project is to study the grain reformation by inter-layer robotic machine hammer peening in WAAM deposited IN718 alloy walls and modify the heat treatment based on the strategies to control dilution in WAAM deposited IN718 alloy. The objective is to obtain the comparable strength and microstructural characterisation for IN718 wrought alloy and WAAM deposited IN718 alloy with inter-layer peened treatment and control on dilution with standard heat-treatment and modified heat treatment.

Underlying objectives for the project:

1. To analyse mechanical data from experiments based on hardness results for WAAM as-deposited, standard and modified heat-treated with inter-layer peened treatment and without inter-layer peened treatment.
2. To interpret the SEM results and EDS maps for WAAM as-deposited, standard and modified heat-treated with inter-layer peened treatment and without inter-layer peened treatment to understand the Nb segregation phase, dendritic grain growth and elemental composition in the dendrites and matrix.
3. Strategy to decide for modification of standard heat treatment cycle based on alloy% in the dendrites, dendritic spacing and precipitates formation.
4. To discuss optical microscopic results for observation of low angle grain boundaries for WAAM as-deposited, standard and modified heat-treated with inter-layer peened treatment and without inter-layer peened treatment.

In continuation to the Introduction chapter, the detailed effect of peening and heat treatment processes on IN 718 (nickel alloy) manufactured by wire-arc additive manufacturing technique for creep resistant application is mentioned in the following chapters of the project.

Chapter 2 describes the Literature review on IN718 alloy, WAAM process, strengthening mechanisms and heat treatment processes for IN718 alloy.

Chapter 3 outlines the experimental methodology for WAAM IN718 walls as-deposited, standardised heat-treated and modified heat-treated with inter-layer peened treatment.

DISTRIBUTION A: Distribution approved for public release.

Chapter 4 shows the results and discussion on hardness test, SEM results and optical microscopy images for WAAM IN718 walls as-deposited, standardised heat-treated and modified heat-treated with inter-layer peened treatment.

In the end, Chapter 5 briefly outline the conclusion of the entire project.

DISTRIBUTION A: Distribution approved for public release.

2. LITERATURE REVIEW

2.1 IN718 in detail

2.1.1 Nickel-base Superalloys

Inconel belongs to a family of austenite Ni-Cr base superalloys where Ni is the alloy base and special characteristic is the presence of high phase stability of FCC nickel matrix [3]. However, Al and Cr as alloying elements improve the surface stability of Ni, whereas, Re and Ru as alloying elements in new generation of superalloys achieve desired requirements but increase the overall cost [6]. The research on IN718 has been primarily centred on precipitation of δ-phase which deals with precipitation hardening and strengthen the grain boundaries [3]. There were some listing Ni-base superalloys mentioned in Table 1 [3]: -

Nickel-base Superalloy	Chemical Composition
Inconel Alloy 600	76 Ni-15Cr-8Fe
Nimonic Alloy 75	80/20 nickel-chromium alloy with additions of Ti & C
Inconel Alloy 601	Lower nickel (61%) content with Al & Ti
Inconel Alloy X750	Al & Ti additions for age hardening
Inconel Alloy X	48Ni-22Cr-18Fe-9Mo + W
Waspaloy	60Ni-19Cr-4Mo-3Ti-1.3Al
Nimonic 90	Ni 54% min Cr 18-21% Co 15-21% Ti 2-3% Al 1-2%
Rene N6	4Cr-12Co-1Mo-W6 -Ta7- Al5.8 - Hf 0.2 - Re5- BalNi
TMS 162	3Cr- 6Co-4Mo-6W-6Ta-6Al-5Re-6Ru-balance Ni
Udimet 720LI	Ni 57- Cr 16-Co 15- Mo 3-Ti 5- Al 2.5- C 0.1
Inconel 100	Ni 60-Cr 10- Co 15- Mo 3-Al 5.5- Ti 4.7-C 0.18- B 0.014-Zr 0.06
Inconel 825	Ni 37.1- Fe 32.2-Cr 22.8- Mo 3.24-Cu 2.07- Ti 0.859- C 0.0155
Haynes 282	Ni 57-Cr 20- Co 10- Mo 8.5-Ti 2.1-Al 1.5-Fe 1.5- Mn 0.3

Table 1 Nickel-base Superalloy Chemical Composition

2.1.2 Nickel-base Superalloys Processing

The Nickel-base superalloys processing starts with remelting the fabricated ingots, casted, accompanied by wrought processing and finally again remelting to get into powder [3]. The wide range of austenitic Ni-Cr superalloys were produced by fabrication of ingots that have undergone vacuum induction melting and melted in air/slag environments based on specific use of application [3] as shown in Figure 1.

The main processes of melting, solidification and control on alloying of elements (Ti, Nb, V etc.) determine the specific type of nickel base superalloy [8]. The near-final shape of IN718 processed parts which requires very less machining on the surface for better geometrical accuracy, reliability for high temperature application and reduced

DISTRIBUTION A: Distribution approved for public release.

buy-to fly ratios can also be used for space applications in the future [7]. The purification of alloy is essential for desirable performance and deoxidation is important because of carbon boil and gas evolution [7].

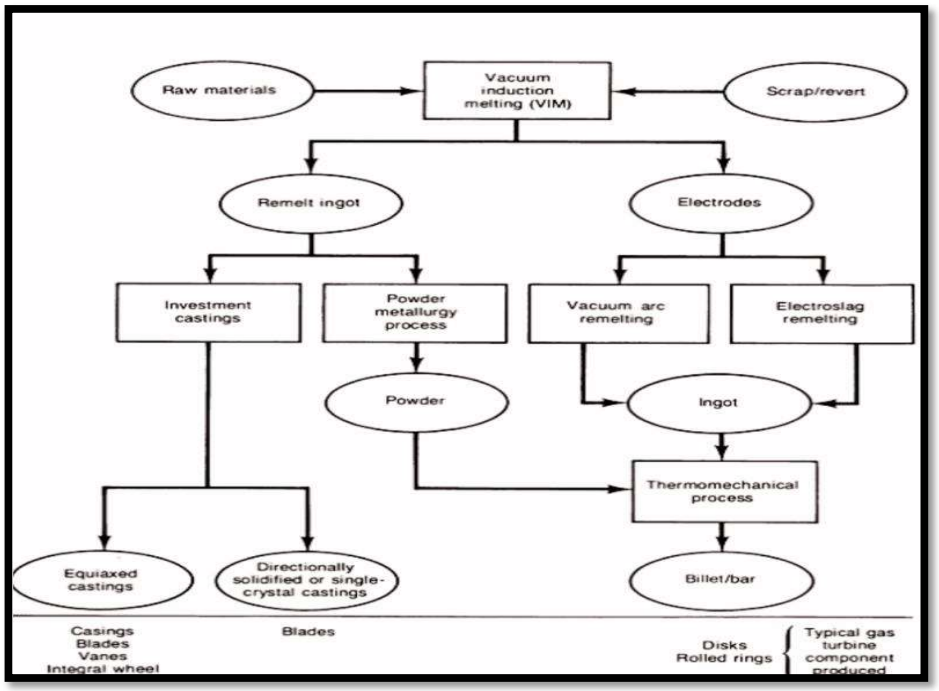


Figure 1 Processing of Nickel-base Superalloys [3]

2.1.3 Material Properties of Inconel 718

The material properties of In718 have been derived from the tensile data after the IN718 alloy has been rolled and conventionally manufactured and is shown in Table 2 [9].

Properties	Elongation (%)	Yield Strength (MPa)	Hardness Brinell	Tensile Strength (MPa)	Density (g/cm^3)	Modulus of elasticity (GPa)	Area Reduction
IN718 (Rolled)	8-15	1172	331	1407	8.19	199.9	8-15

Table 2 Mechanical Properties of IN718 [9]

The chemical composition of IN718 is described in the Table 3 [9],

Element	Ni	Cr	Nb	Mo	Ti	Co	Al	Fe
%	50-55	17-21	4.8-5.5	2.8-3	0.65-1.15	1	0.2-0.8	Bal

Table 3 Chemical Composition of IN718 [9]

DISTRIBUTION A: Distribution approved for public release.

2.1.4 Crystal Structure of Inconel 718

IN718 is a face centred cubic solid solution of nickel, chromium and iron with gamma γ as the matrix, gamma-prime γ' is Ni_3(AlTiNb) and has a face centred cubic structure with higher content of Al and gamma double-prime γ" is Ni_3V and has a body centred tetragonal crystal structure [2]. The IN718 microstructure contains topologically close-packed (TCP) phase which includes tetragonal σ CrFe phases, orthorhombic δ Ni_3(Nb,Ti), hexagonal laves $(Ni,Fe,Cr)_2(Nb,Mo,Ti)$ [9]. The gamma-prime γ' and gamma double-prime γ" were the metaphases in the matrix and the heat treatment processes were employed so that the % of these metaphases increase the strengthening effect in IN718 [9].

2.1.5 Phase-diagram of Inconel 718

The FCC solid solution of Ni, Cr, Fe in IN718 has a matrix phase γ and other secondary phases which include carbides such as sigma, laves, TiC, Nb(Ta)C and M_6C. There were different groups into which these intermetallic phases and divided into such as geometrically close-packed, primary & secondary carbides and topologically close-packed [10]. The most important parameters that affect the strength of IN718 were grain size, grain morphology, cold work, control of various phases through either solid-solution hardeners or precipitated phases. The main strengthening precipitate phases γ' and γ'' were metastable and at higher temperature range these change to δ phase [2]. However, the most detrimental phases that can lead to brittleness were σ, μ, laves, CrCo, FeCr and FeCrMo but if they were in trace amounts, they can be useful for creep properties [11]. The γ'' has a BCT ordered $D0_{22}$ structure and can be distinguished as disk-shaped coherent particles (thickness $50\text{-}90*10^{-10}$m, average diameter $600*10^{-10}$m) which occur on {100} planes and occupies a volume fraction of 16% after full heat treatment is done [10]. The γ' has an FCC ordered $L1_2$ structure and can be visible as spherical-shaped, cuboidal, globular because of changes in aluminium/titanium ratio, molybdenum content and it occupies a normal volume fraction of 4% after a full heat treatment [10]. Also, the strengthening from γ' depends on the size of particle and gets decreased around 0.6 times the melting temperature (T_m). The δ (orthorhombic Ni_3Nb) is formed as coarsened and elongated acicular shape particularly in the temperature range of 815 to 980℃ at low aging and high aging temperatures by cellular reaction and precipitation in intragranular regions [10]. The laves is hexagonal $(Fe,Ni,Cr)_2(Nb,Ti)$ which affects the size in the intermetallic with higher concentration

DISTRIBUTION A: Distribution approved for public release.

of Mo and Nb. Since, the laves phase is irregular shaped globules at exposure of higher temperature and elongated so, it must be solutionised and prolonged soaking for temperature range of 1065 -1080°C before processing as it can affect the ductility of material, fatigue, tensile and creep properties [11]. There is a role of the different alloying elements as Co can raise the solvus temperature of γ' and for hardening precipitation and intermetallic formation is done by Al, Ti, Nb. Further B,Ta improves creep, B, C, Hf, Zr leads to grain boundary refinement and Re leads to retardation in γ' coarsening [10]. The TTT-diagram for hot-forged and vacuum melted IN718 is shown in Figure 2.

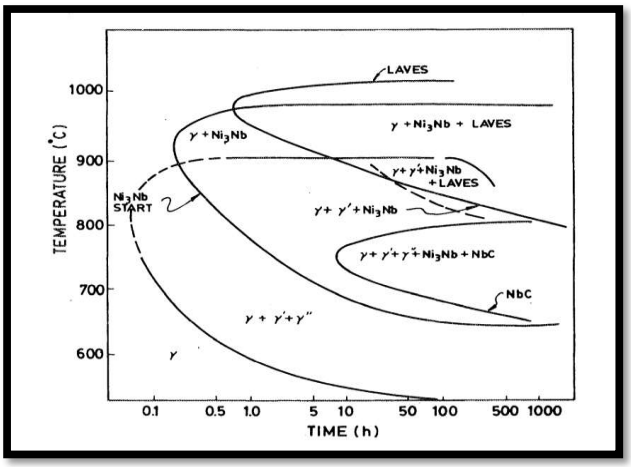


Figure 2 TTT diagram for IN718 hot-forged and vacuum melted [12]

2.1.6 Solidification Behaviour of IN718

The simplified pseudo binary solidification diagram shows the % of Nb as the variable for composition change as shown in Figure 3. The marked points 1 & 2 represent the solidus (1352 F) and liquidus (1395 F) temperatures with Nb weight % of 5.18 and solidus temperature is the inflection point between two local maxima as shown in Figure 3 [2]. The process of solidification starts with the primary dendrites formation which become depleted in Nb, C and liquid gets enriched in Nb, C. In the second step, there is a formation of γ/ NbC eutectic and when in the liquid, Nb, C is depleted as shown in Figure 4. When its composition is shifted back to γ phase then significantly more γ dendrites start to grow with the liquid enrichment in Nb only because the C led to the formation of γ/ NbC eutectic [2]. The ternary eutectic is formed during IN718 solidification which is formed on Ni-Nb-C ternary diagram as shown in Figure 3 [2].

DISTRIBUTION A: Distribution approved for public release.

In the next stages, the final solidification is finished with the formation of γ/Laves eutectic and the weight% of Nb is 19.1 at a temperature (1230 F) as shown in Figure 4. Further, marked points 5 & 6 represent weight% of Nb of about 9.3 in γ eutectic and 22.4 in eutectic Laves phase as shown in Figure 3 [2]. Hence, the formation of NbC from liquid is done isothermally at 1282 F and final composition in end solidification is a binary eutectic phase of γ + Laves. The eutectic γ/NbC is not formed isothermally at 1282 F and carbides were liquated below this temperature range at a temperature of about 1232F up to 1267F [2].

The final solidification constituent is three phase eutectic mixture of Laves, γ and NbC. Further research studies for the final solidification constituent has shown that the formation has extended the range of solidification, γ/Laves eutectic leads to further stability of the phases and alloying elements except Nb were required for formation of Laves phase [2]. Also, ternary and quaternary alloying when added to the Ni-Nb alloy system and behaviour of alloying elements for segregation can also lead to formation of Laves phase.

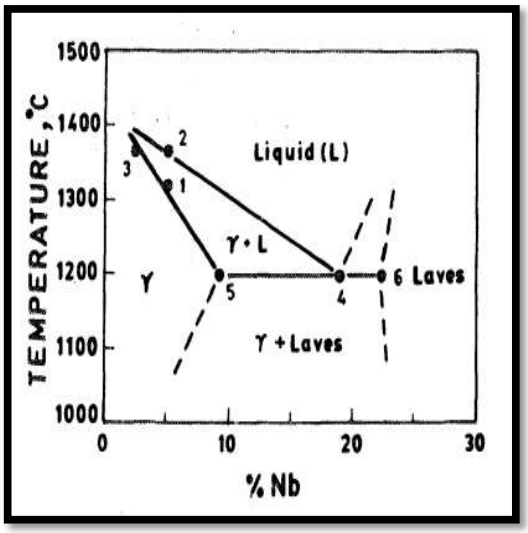


Figure 3 Graph Solidification behaviour of IN718 [2]

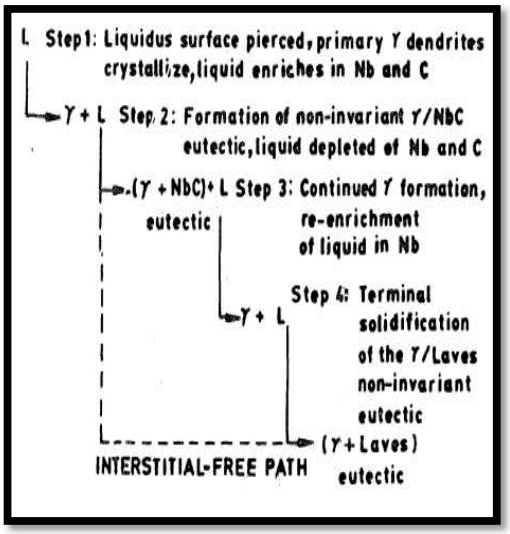


Figure 4 Steps of Solidification for IN718 [2]

DISTRIBUTION A: Distribution approved for public release.

2.2 WAAM for IN718

2.2.1 Different AM Processes

The additive manufacturing processes have been divided into main types powder, liquid, solid and filament. The broad additive manufacturing techniques such as direct energy deposition (DED), powder bed fusion, sheet lamination, binder jetting and material jetting [9]. For IN718 which is expensive, therefore the additive manufacturing techniques have to take into account the reduction of material loss, ease in design flexibility and manufacturing. The additive manufacturing technique starts with building a CAD model, converting it to STL file, transferring it to the machine, start by building the component, further post-processing and usage for specific application as shown in Figure 5 [9].

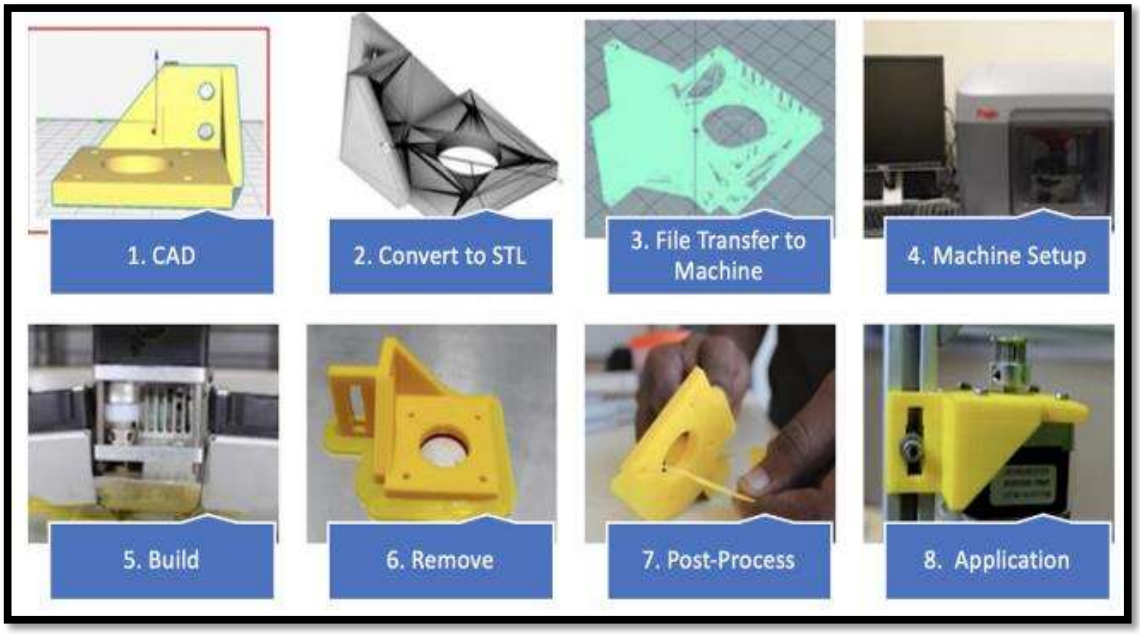


Figure 5 AM Process flow chart [9]

The numerous AM techniques that have been researched on for IN718 such as laser direct metal deposition process (DMD) and laser powder bed fusion (PBF) [9]. Also, solid layer based additive manufacturing techniques include sheet lamination process which is further divided into ultrasonic additive manufacturing (UAM) that binds by ultrasonic welding and laminated object manufacturing (LOM) that bonds material sheets with various adhesives [9]. For the laser-based processes, when the energy source melts the powder later it fuses with the powder bed forming build layers by re-

DISTRIBUTION A: Distribution approved for public release.

melting of the powder and for the direct energy deposition processes (DED), laser is used as a narrow-focused beam melts the material for deposition without the feed material available [9]. Though there were a lot of factors on which laser powder processes depends on porosity, process parameters and powder source, offering certain limitations on quantity of production build and components at large scale. One unique additive manufacturing technique (WAAM) which is under direct energy deposition process (DED) that offers to build large scale components with high deposition rate and electric arc (plasma torch) is the main heat source where the wire of the material such as IN718 is filled as feedstock [13].

2.2.2 Wire-arc additive manufacturing technique (WAAM) Process

WAAM offers unique flexibility to manufacture components at large scale mainly because buy-to-fly ratio is less, high rate of deposition, less material wastage and volume of the build is high [13]. It is advantageous technique because of design flexibility and allowing any welding equipment for AM purpose with platforms build to cater this technology as a part of industrial automation. WAAM is also referred to as cold metal transfer (CMT)-metal inert gas (MIG) process based on controlled delivery of beads with no spatter because of reduced thermal heat input [13]. There could be a phenomenon of arc wandering if the distance of torch from the layer is not maintained at constant distance and mostly occurs at the end of the layer deposition but by maintaining inert gas to shield the plasma arc [13]. Further the wire is filled as feedstock from same direction, the robotic mechanism path is complicated. Besides WAAM technique can lead to challenges of residual stresses due to cooling after shrinkage and distortion in the part produced because of the heat input from the plasma torch. Some important process parameters of WAAM plays a role in deposition quality such as wire feed speed (WFS), travel speed (TS), current, wire diameter and stand off distance.

The critical application of IN718 WAAM components require desired mechanical properties and there were factors in WAAM process which needs to be researched as the alloys were greatly affected by microstructure characterisation, strengthening mechanisms and various post-deposition after heat treatment processes. Adequate oxygen level certainly must be below 3 parts per million as WAAM builds layer by layer

DISTRIBUTION A: Distribution approved for public release.

and oxide can be accumulated which can lead to reduction in tensile ductility and surface finish, therefore requires adequate gas shielding [14]. There can be other reasons that leads to oxidation such as low rate of cooling and the thermal conductivity of IN718 (11.4 W/mK) is low as a result of which the deposited layer is exposed at higher temperatures to the environment [14]. The other important factors for WAAM were substrate, deposition method, heat input and weldability. Since, WAAM involves constant heat input but heat transfer process is non-linear as a result of which the heat absorption depends on material, time and environment [15]. The partial re-melting of the alternate layers deposited one on other leads in WAAM is based on feed rate which determines the penetration and fusion between these alternate layers as shown in Figure 6. The high heat input is beneficial for building components which need higher rate of deposition and fabrication process is carried out at higher melting point than its substrate as shown in Figure 6 [15].

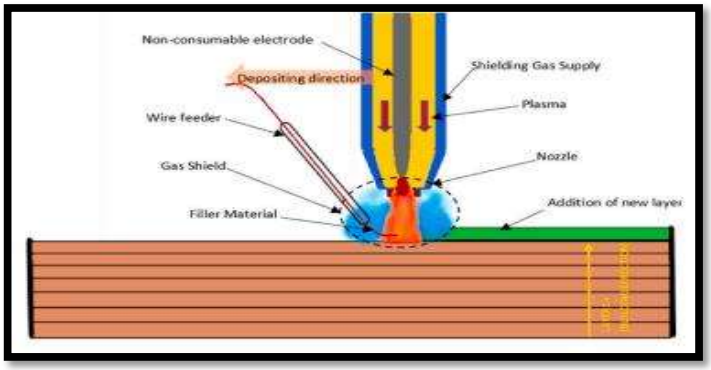


Figure 6 WAAM with Plasma arc welding [15]

2.2.3 Microstructural evolution for WAAM deposited parts

The transformation in the different phases and microstructural evolution depends on the input of heat supply, rate of deposition, material of the alloy and temperature changes [15]. During WAAM deposition, there were defects produced such as deformations, inclusions, porosity and cracks penetration on the surface of the WAAM deposited layer [15]. Further thermal cycling in WAAM process leads to formation of coarse grains in columnar direction that lead to microstructural changes and distribution of grains. WAAM process with hot deformation can lead to resistance to solidification cracking and controlled gas flow rate supply reduced the defects of porosity during WAAM deposition as shown in Figure 7.

DISTRIBUTION A: Distribution approved for public release.

In the WAAM deposition, alternate layers were deposited to form components of different scales though, when depositing a new layer over pre-deposited layer it is partially remelted. When there is a solidification of molten pool at the surface of the layer, nucleation originates resulting in fine grains but at the interface, there were segregation and changes in the size of the grains [5]. In the as-deposited wrought alloy of IN718, secondary dendrites can be observed in dendrite length of around 5μm within the grain and phases such as laves, carbide, TiN were segregated within the inter-dendritic boundaries [5]. Additionally, direct treatment does not lead to changes in these inter-dendritic boundaries, but aging temperature leads to precipitation in γ matrix as γ' and γ'' without dissolution of the laves phase within the inter-dendritic boundaries [5].

The inter-layer peened treatment leads to plastic deformation and grain size refinement by increased elongation of grains significantly strengthening the grain boundary and effect of work hardening [15]. This strengthening mechanism results in improved mechanical properties because of high-density dislocations such as yield strength and tensile strength of the alloys. The post-deposited after heat treatment processes leads to homogenisation in the microstructure as the precipitates were re-distributed which were unevenly distributed along the boundaries of the grain structure because of which anisotropy is reduced [15]. Also, recrystallisation occurs when the post-deposited alloy is heat treated in the homogenisation cycle across grains in the original state resulting in drastic improvement in tensile properties because of strengthening effect of precipitation [15].

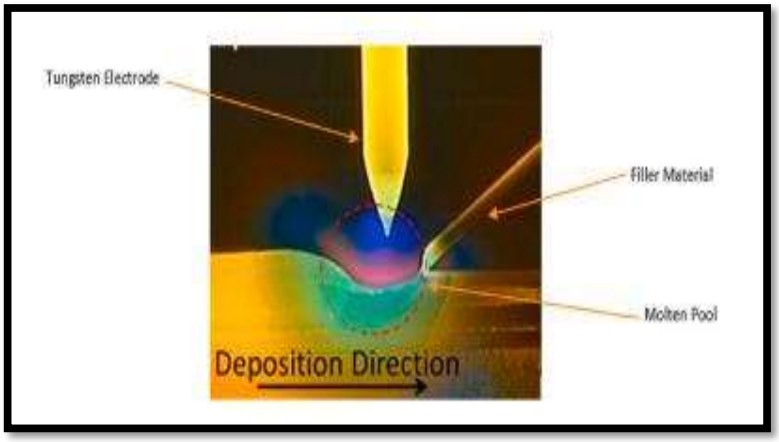


Figure 7 Deposition in WAAM [15]

DISTRIBUTION A: Distribution approved for public release.

2.3 Strengthening Mechanisms

2.3.1 Different types of Strengthening mechanisms for WAAM

There are number of different strengthening mechanisms such as inter-pass rolling, inter-pass cooling, hot forging, inter-layer hammering, ultrasonic needle peening and laser shock peening that improves the mechanical properties.

For in-process refinement of grains, inter-pass rolling technique plastically deforms causing plastic strain on the deposited layer. Further, heat from the process leads to formation of new and equiaxed β grains that were up to 100μm [16]. But the rolling is restricted as the loads can mostly be applied only in walls that straight hence, peening has been researched for applying load with complicated geometrical features. Machine-hammer peening enables indentation with oscillation leading to near-surface compressive stresses and hardening of the surface which can further increase the fatigue life of the WAAM part [15]. The new β grains orientation originates grain refinement by not growing in initial grain when the temperature is raised while depositing another alternate layer [17]. This enables to the strengthening of grain boundary and effect of work hardening leads to high-density dislocations. There is hot forging incorporated where with the help forging leads to reduction of contact area as a result of which stress is increased and solidification refinement of the microstructure takes place and deformation is increased [15]. Also, for inter pass cold rolling, the columnar growth of the coarser grains is weakened as a result of which recrystallisation takes place and the strain hardening effect is observed enhancing the microhardness and tensile properties [15]. The residual stresses and distortion can be alleviated in WAAM components with the help of these strengthening mechanisms as shown in Figure 8 [19].

The option of post-treatment on the surface is highly dependent on the geometrical features, properties of material, cost of treatment, process parameters effect and scale for the treatment [19]. The research on the strengthening mechanisms defines the desired mechanical properties based on customised surface treatment for specific additive manufacturing technique.

DISTRIBUTION A: Distribution approved for public release.

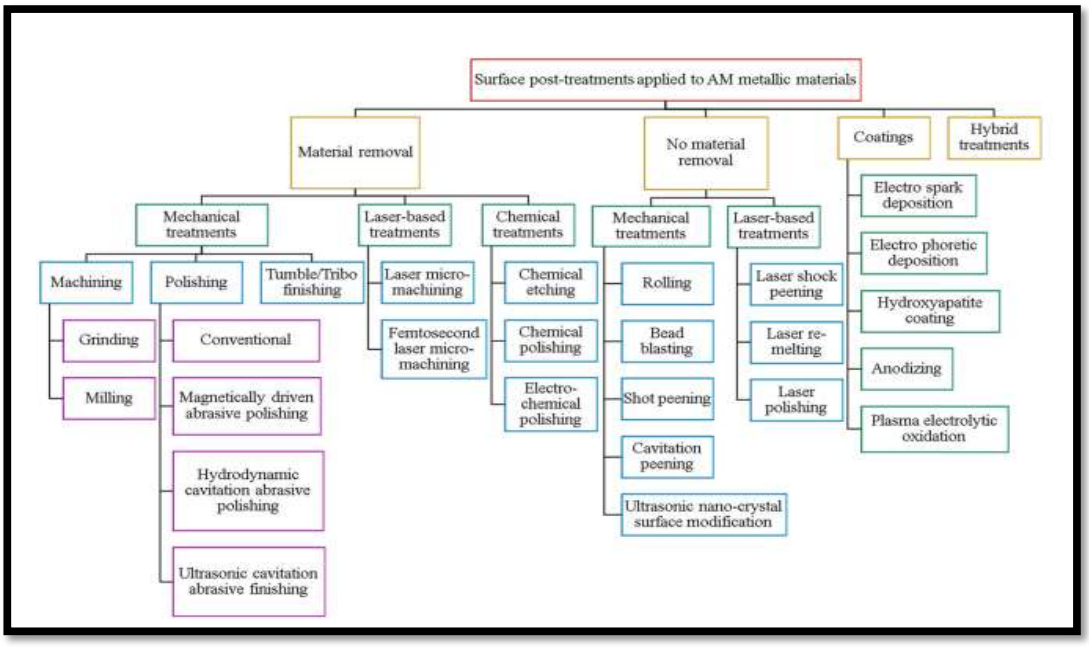


Figure 8 Surface post-treatments applied to additively manufactured metal parts [19]

2.3.2 WAAM with peened treatment

The robotic mechanism of inter-layer peened treatment along with WAAM deposition of alternate layers on the substrate develops the stress state at the surface as residual stress from tensile to compressive which refines the coarse grains as it can be observed for laser shock peening treatment that transmits the laser shock wave onto the surface of the WAAM part and the substrate as well [20]. There are other peening techniques such as ultrasonic needle peening applied with overlapping rate and scanning strategy which generates plastic strain by formation of dislocations on the part's surface. There is laser shock peening which is accompanied by high-pressure shock wave that can lead to dislocation, twinning slip of hexagonal close-packed α phase and redistribution of residual stress [15]. However, in ultrasonic needle peening, needle impacts with low pressure on the material surface but for a laser shock peening, high-pressure laser shock wave penetrating the stress flow in the material in short time scale as shown in Figure 9 [18].The shot-peening comes under the cold working process as a result of which surface roughness is controlled and high compressive residual stress on the deposited layers leading to improvement in surface morphology can be controlled by number of important process parameters [19].

DISTRIBUTION A: Distribution approved for public release.

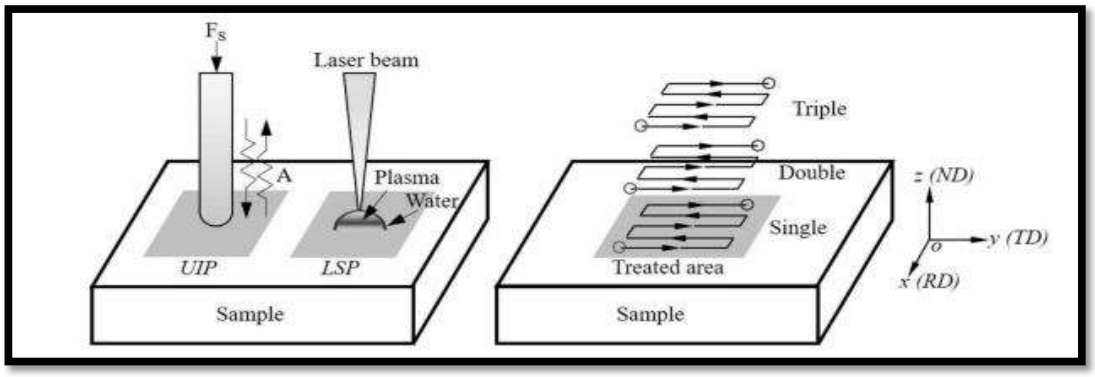


Figure 9 Ultrasonic impact peening, Laser shock peening and moving paths, where Fs (static load), A (vibration amplitude) [18]

2.3.3 WAAM with inter-layer machine-hammer peened treatment

The machine-hammer peened treatment is carried out with an impact distance of 0.2mm with given radius of the tool as 2mm and tool operates at 180Hz and maximum pressure of 6bar for the system as shown in Figure 10 [20]. The inter-layer peened treatment produces very high energy density with highest plastic deformation and when a next layer is deposited using WAAM, there is β re-growth as the previous layer is partially re-melted [20]. The twinning of β grains because of deformation from machine hammer peening and rapid thermal cycles leads to produce columnar structures and β grain refinement led to producing better isotropic properties [20].

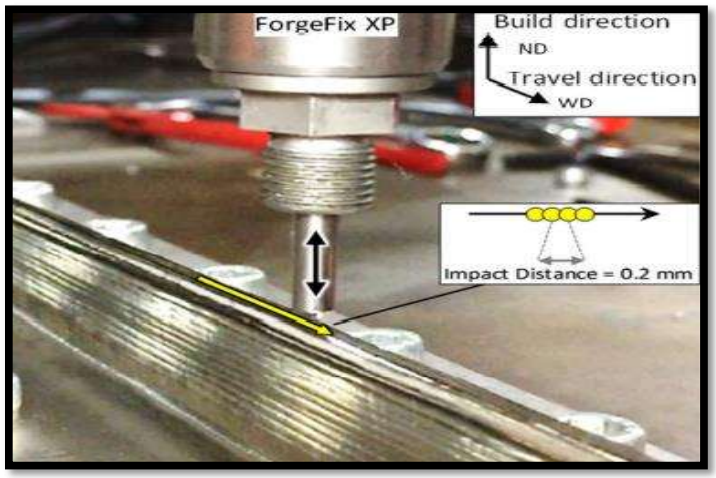


Figure 10 Machine hammer peened treatment on Ti64 WAAM walls [20]

2.3.4 Microstructural changes due to peening

The EBSD-LAM technique is used to study the strain distribution map that shows the clear deformation on the sub-surface area when a single indent of machine hammer peening treatment is done on WAAM deposited layer as shown in Figure 11 [20]. For

DISTRIBUTION A: Distribution approved for public release.

activation of β grain refinement, there is a strain limit above which it takes place and plastic strain is about 8 at a range of depth of 500-600 µm in Figure 11 [20].

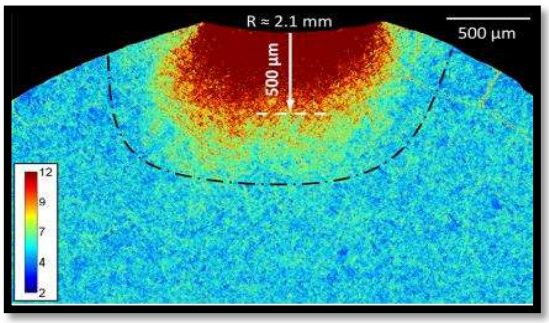


Figure 11 Depth of deformation [20]

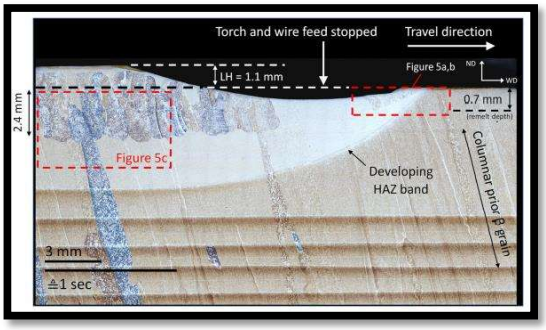


Figure 12 HAZ bands and melt depth [20]

However, when peening treatment is done after partial melting of deposited layer, there is no formation of β orientations of approximately 0.5 mm deep than the surface of the layer [20]. In Figure 12, it can be observed the depth of remelting is approximately of 0.7mm and generation of new β grain orientations because of strain is developed sufficiently but below these layers, there was less strain deformation [20].

In Figure 13 (a), it is seen that the thermal field is present in the moving melt pool heated above β transus, and β grain misorientations were generated as a result of sufficient deformation [20]. Fine β recrystallised grains is observed in EBSD map clearly indicating the refinement boundary, HAZ band and remelt depth as shown in Figure 13 (b) [20]. Additionally, the reconstructed β grains exist in deposited layers in Figure 13 (c), (1) presence of coarse grains under deformed depth from previous layer (non-peened) (2) presence of β recrystallised grains downwards growth ahead of melt pool (3) during solidification recrystallised grains up to melt pool shown in details in the pole figures.

The β grains at the fusion boundary because of the plasma torch movement leads to epitaxial re-growth specifically during solidification behind the melt pool and the directional growth leads to fine columnar grains [20]. Therefore, machine-hammer peening lead to plastically deforming the deposited layer material that remelted the previous deposited layers and new columnar grains were formed by the process of recrystallisation in solid state and finally forming the refinement boundary and HAZ band.

DISTRIBUTION A: Distribution approved for public release.

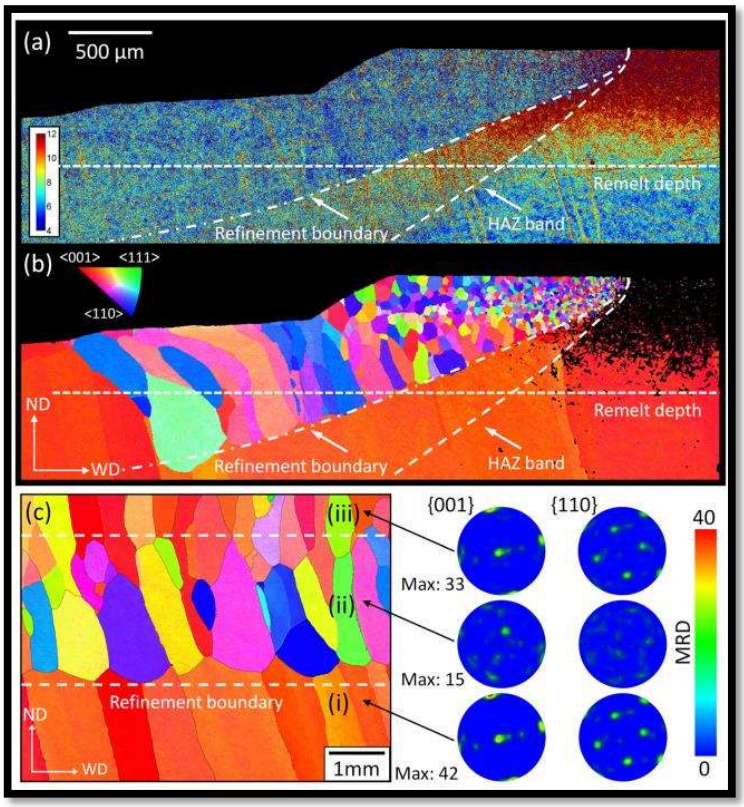


Figure 13 (a) Thermal field interacts with machine-hammer peening (b) β map (c) Pole figures in reconstructed β map [20]

2.3.5 Mechanical Properties improvement because of peening

The mechanical properties of machine hammer peened Ti-6Al-4V alloy which were additively manufacturing have been compared in terms of microhardness values, tensile properties and fatigue improvement [21]. The microhardness measurements were done as shown in Figure 14, performed in Vickers hardness test results. It was observed that impact on thick walls by machine hammer peened treatment was higher than thin walls by same treatment as a difference of 1mm at the depth of cold work as shown in Figure 14 because in higher thickness, the material is constrained laterally and goes into deeper depths [21]. The indentation for microhardness profile measurements increased the amount of cold work in thicker walls with machine-hammer peened treatment and led to increased effect of work hardening.

DISTRIBUTION A: Distribution approved for public release.

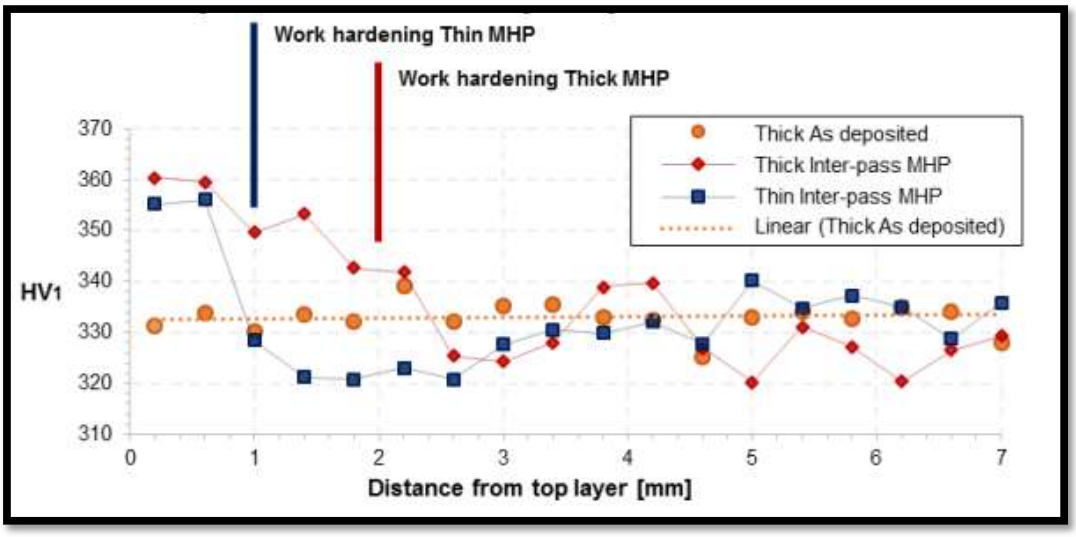


Figure 14 Microhardness values of machine hammer peened (MHP), thin & thick walls (as-deposited) for Ti-6Al-4V alloy [21]

The samples cut along the horizontal direction show higher strength than the samples cut along the vertical direction which show higher elongation because of β grain growth vertically [21]. It was observed that for samples cut along the vertical direction there wass elongation percentage decrease of about 8-9% but the yield strength and ultimate tensile increase for samples cut along both these directions [21]. When there was reduction in the strength for samples along vertical direction there was elongation in the preferential direction, isotropic properties were maintained and grain refinement took place for WAAM walls with inter-layer machine hammer-peened treatment as shown in Figure 15 [21].

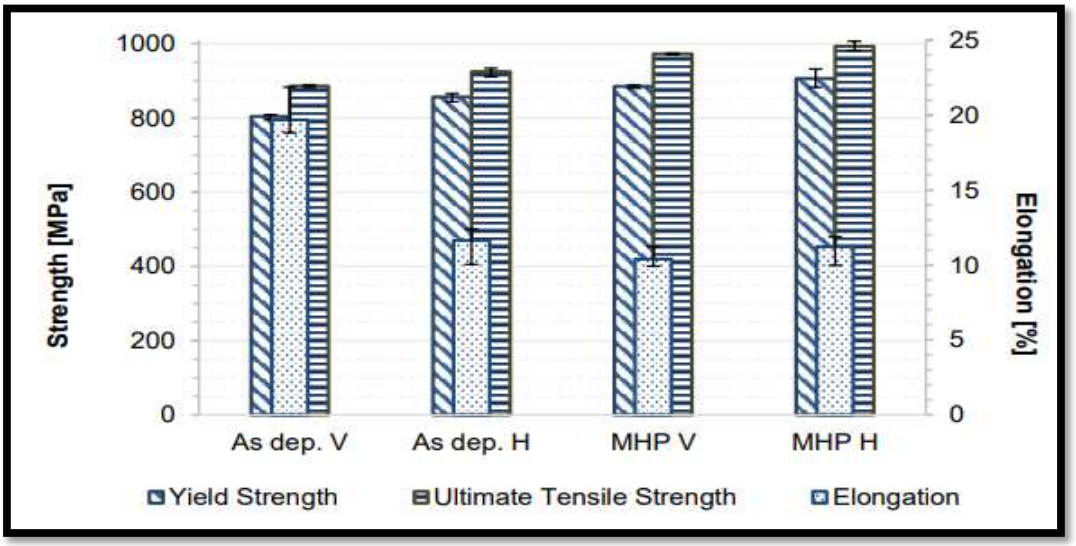


Figure 15 Tensile Properties of machine hammer peened (MHP) & thin walls (as-deposited) [21]

DISTRIBUTION A: Distribution approved for public release.

2.4 Heat Treatment for WAAM parts

2.4.1 Heat Treatment Principle & Standards

The purpose of heat treatment for WAAM parts for IN718 alloys is to redistribute the microstructure in terms of various phases precipitation strengthening the mechanical properties depending upon the specified application of use. The high strength that can be achieved in IN718 alloy grains because of secondary phases precipitation into the γ austenitic matrix at a temperature range of 590-815℃ [22]. However, the formation of secondary phases such as metal carbides, δ and laves phases were because of heat treatment, where the metal carbides strengthen the material by transformation of grain boundaries at the time of solidification but the laves phase leads to depletion of Nb and Mo in the Ni-Cr matrix of solid-solution IN718 alloy [23].

When the process of annealing takes place at a temperature of about 960-980℃ which leads to further recrystallisation of secondary phases by laves phase transformation and formation of δ phase at high temperature range exposed for longer time duration [22]. The δ phase decreases the ductility in the material but the overall hardness and strength of the IN718 heat treated alloy was increased [22].

The aging treatment on WAAM IN718 alloys can take place at different temperature range from 620-780℃ which leads to initiation and growth of precipitation of secondary phase specially in the inter-dendritic areas around grain boundaries and finally defined morphology grain orientation in secondary precipitates [23].

Therefore, the stress relief effect and dependence on time and temperature for recrystallisation process needs research on the heat treatment at different time cycle and temperatures. The IN718 before heat treatment shows large columnar grains along with the formation of laves phase which needs to be treated. The standard solution heat treatment has to have higher treatment temperature so that the laves phase could be dissolved and coarsening of the grains could also be reduced. The industrial standard based on (AMS-5662M for forged IN718) [24] where the sample rate was 5S/s as shown in the Table 4 [24]. In this treatment, all samples were degreased in acetone for 10 minutes in ultrasonic bath were cleansed and dried and thermocouple were attached to the sample and the readings in the oscilloscope were clearly observed [24].

DISTRIBUTION A: Distribution approved for public release.

Standard Heat Treatment Steps	Temperature	Time
Solution	970-980˚C	1 hour
Aging	718˚C	8 hours
Furnace cool	620˚ C	8 hours

Table 4 AMS 5662M for forged IN718, Standard Heat Treatment [24]

2.4.2 Microstructural Characterisation for heat treated samples

The IN718 samples were standard heat treated as shown in Figure 16 and solutionised and double aged treatment done as shown in Figure 17 following these heat-treatment cycles [25]. The two main strengthening precipitates of IN718 were γ' (face centred cubic Ni_3Al) and γ'' (metastable body centred tetragonal Ni_3Nb) so there must be redistribution of the grain size by recrystallisation and δ phase controls the grain size [25]. When the δ phase volume fraction was increased, assuming Nb/Al element as constant volume fraction as a result of which the volume fraction of γ'' precipitate was decreased [25]. Further δ phase, γ' and γ'' precipitates play a very important role in fatigue and creep property of the IN718 alloy.

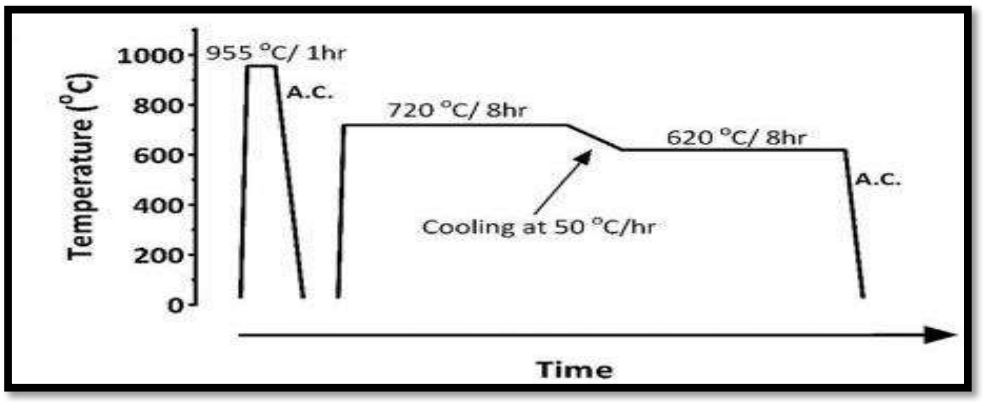


Figure 16 Standard heat treatment for IN718 alloy, A.C is air cool [25]

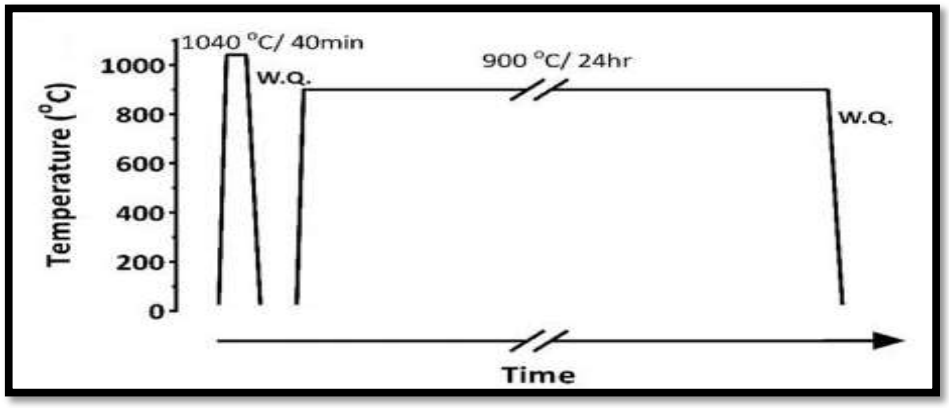


Figure 17 Solution + δ- phase aged treatment for IN718 alloy, W.Q is water quenching [25]

DISTRIBUTION A: Distribution approved for public release.

The SEM images of IN718 alloy microstructure were observed in three different conditions; before heat treatment, standard heat treatment and Solution + δ- phase aged treatment as shown in Figure 18 [25]. It can be observed that the before heat treated samples of IN718 alloy in Figure 18 (a) had average grain size of approximately 25μm and the grains have been shaped irregularly with dispersion of carbides and no δ phase [25]. When the samples undergone standard heat treatment in Figure 18 (b), the average grain size was about 12μm and some spherical δ- phases started to form on the boundaries of the grains based on the recrystallisation process [25]. Further when the IN718 alloy samples undergone solutionising and δ- phase aged treatment in Figure 18 (c), the grain size was increased to about 50 μm and δ- phases occurred with needle-shaped along with twins within the grains and grain boundaries of particular orientations [25].

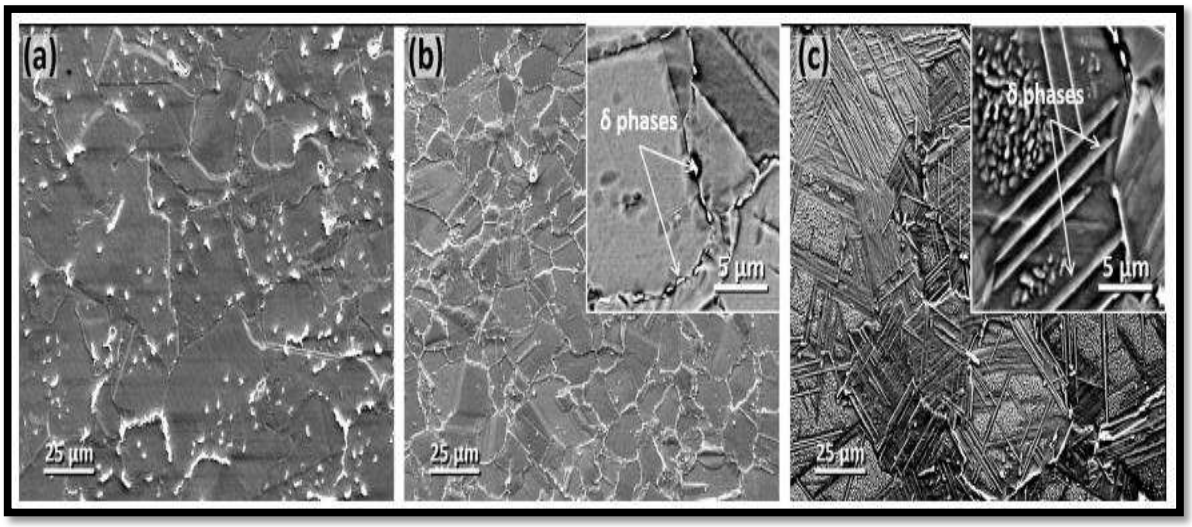


Figure 18 (a) Before heat-treatment (b) Standard heat treatment (c) Solution + δ- phase aging treatment samples

The aging of WAAM IN718 takes place properly when the aging elements such as Al, Ti, Nb are in solution and not precipitated, hence, homogenisation was done so that the segregation of elements was less and the undesired phases were dissolved [26]. In WAAM the thermal cycles lead to segregation of Nb and Mo and laves phase have been formed along the inter-dendrites [26]. Therefore, solutionising temperature must increase so that Nb get diffused and laves phase get dissolved and aging temperature lead to precipitation of strengthening phases γ' and γ'' in the austenitic γ matrix. Further, equiaxed grain structure are more desirable although WAAM forms columnar grain growth as it could be coarsened by increasing temperature and time for hold.

DISTRIBUTION A: Distribution approved for public release.

2.4.3 Mechanical Properties for heat treated samples

The IN625 WAAM samples were studied subjected to heat treatment solutioning at a temperature of 980˚C with holding time of 30 minutes, 1 hour and 2 hours followed by water quench method [27]. The IN625 WAAM parts undergone the microhardness measurement values along two directions; longitudinal (y-axis) and transverse (x-axis) [27]. In Figure 19, it can be clearly observed that the microhardness values range from 220-240 VHN and the values do not follow a particular pattern of increasing or decreasing for both the directions [27]. It was observed that as the heat-treatment holding time increased the average hardness values in standard deviation has decreased. Additionally, the heat treatment relieved the stress and increased the hardness values but later when the holding time increased, it dropped in both directions. Therefore, anisotropic microstructures are studied in detail so as to understand the behaviour.

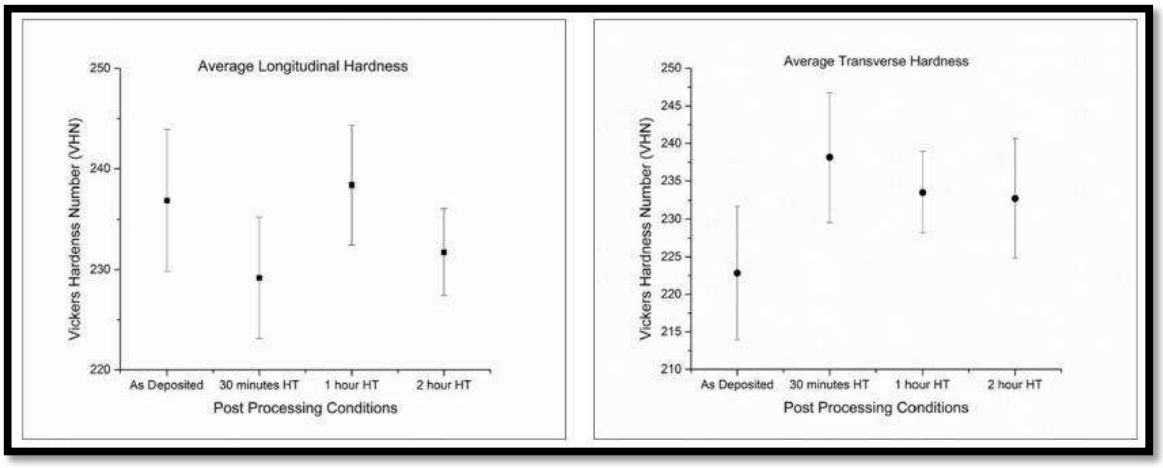


Figure 19 (a) Longitudinal microhardness (b) Transverse microhardness

The IN625 WAAM samples based on as-deposited and heat treatment in three different holding times, 30 minutes, 1 hour and 2 hours were prepared to undergo the tensile test, the engineering stress vs strain curves were plotted as shown in Figure 20 (b) and graph for tensile strength and elongation as shown in Figure 20 (a). It is clearly observed that the yield strength and elongation % has decreased for 30 minutes and 1 hour holding time from the as-deposited conditions but increased for 2 hour holding time in Figure 20 (a) [27]. However, the ductility was found to be decreased for IN625 WAAM samples which were heat treated and holding time was more than 30 minutes in Figure 20 (b) [27].

DISTRIBUTION A: Distribution approved for public release.

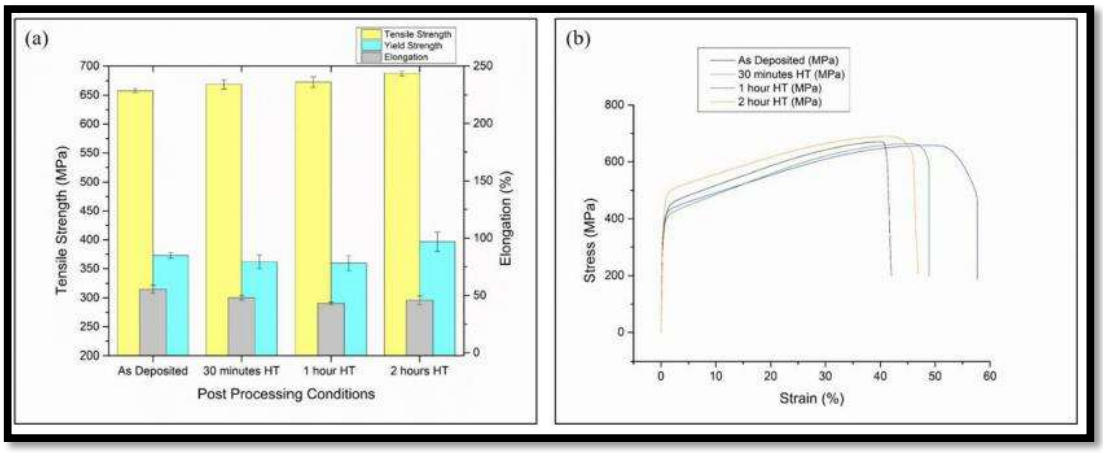


Figure 20 (a) Tensile, Yield strength and Elongation% (b) Engineering Stress vs Strain curves

2.5 Homogenisation Kinetics for IN718

The SEM micrographs in Figure 18 (a) before-heat treatment as-deposited samples showed the laves structure had about weight % of 20 for Nb and high amount of Mo as compared to the dendritic core and because of the segregation of Nb, Mo and Ti the homogenisation plays an important role. Therefore, when the IN718 samples were subjected to homogenisation temperature at 1050˚C and when the holding time increased then the dendritic structures and the weight % of the laves phase started to decrease as shown in Figure 21 [28]. Similarly, when the holding time was taken as constant for 3 hours then also the weight % of laves phase decreased when the homogenisation temperature increased at 1050˚C, 1100˚C and 1150˚C [28]. This has been concluded that the volume fraction % of laves phase which can be compared with area fraction % of laves phase in micrographs in Figure 21 [28] that the laves phase was dissolved when the homogenisation temperature was increased. The graph plotted in Figure 22 [28] discussed that laves phase was dissolved at a very faster rate at higher temperatures also described in Avrami kinetics of laves phase dissolution given by Johnson-Mehl-Avrami-Kolmogorov Equation 1 [JMAK] as shown below [28]:

$$X = 1 - \exp(-Kt^n) \quad [1]$$

Where n is defined as Avrami exponent, K is defined as temperature-dependent and X is defined as dissolute fraction and calculated by Equation 2 shown below [28]: -

$$X = \frac{fo-f}{fo} \quad [2]$$

DISTRIBUTION A: Distribution approved for public release.

Where f and f_o are current volume fraction of laves phase initial volume fraction (f_o = 0.0357) in microstructure respectively [28].

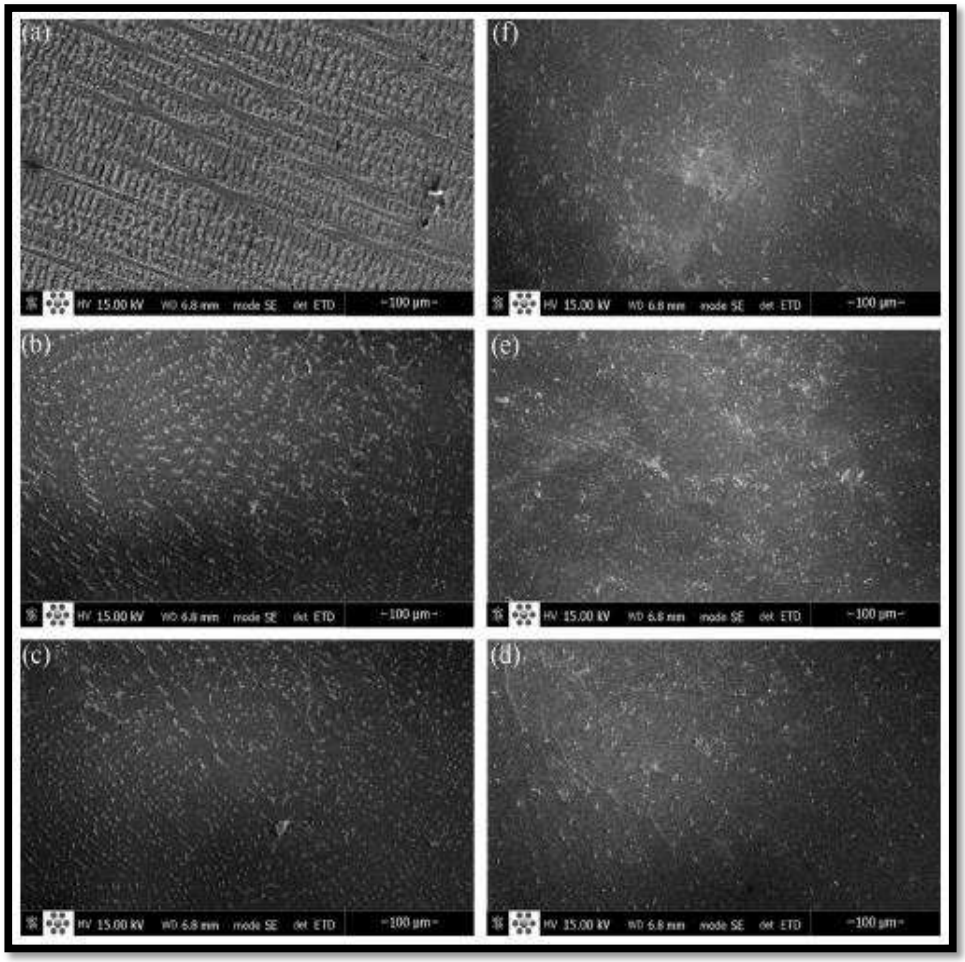


Figure 21 (a) As-cast (b) 1hour at 1050˚C (c) 3 hours at 1050˚C (d) 9 hours at 1050˚C (e) 3 hours at 1100˚C (f) 3 hours at 1150˚C [28]

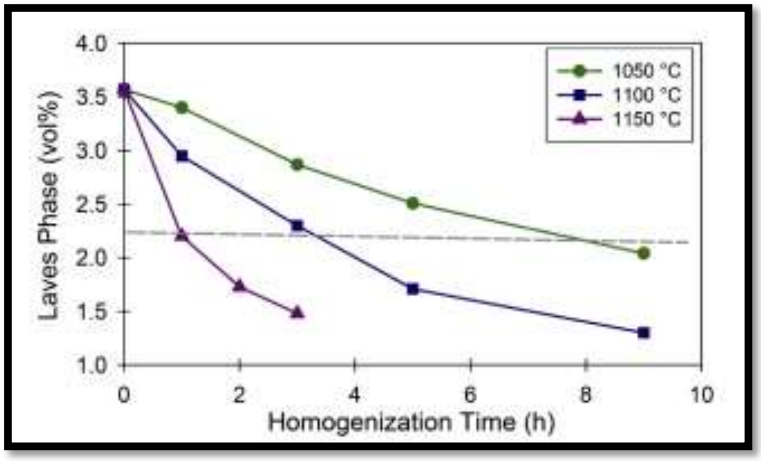


Figure 22 Laves phase vol % vs homogenisation time at different homogenisation temperatures [28]

DISTRIBUTION A: Distribution approved for public release.

The equations which are based on the temperature dependency of K shown in Equation 3, natural logarithm on the R.H.S and L.H.S of the equation in Equation 4 and plot for slope of lnK vs 1/T in Figure 23 showed the activation energy for dissolution of laves phase [28].

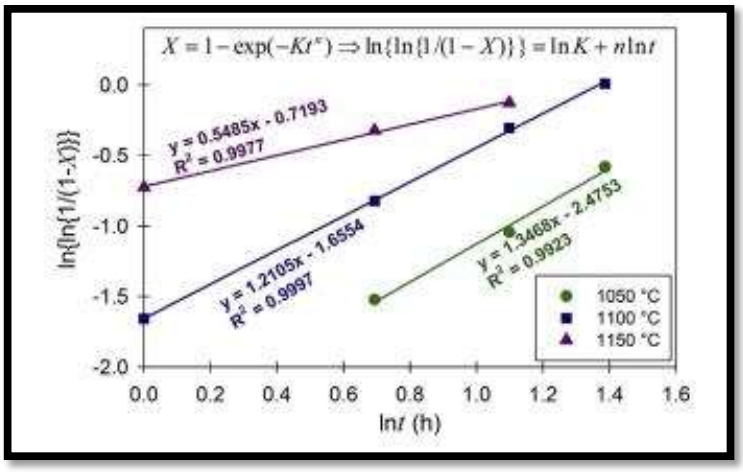


Figure 23 Avrami plots for the dissolution of Laves phase at different temperature [28]

$$K = Koexp(-\frac{Q}{RT}) \quad [3]$$

$$\ln(K) = \ln(Ko) + \left(-\frac{Q}{R}\right) * (\frac{1}{T}) \quad [4]$$

Since, laves phase consisted of Nb, Ti, and Mo which should be dissolved and the parameters of diffusion coefficient of the elements in Nickel are based on equation 5:

$$D = Doexp\ (-\frac{Q}{RT}) \quad [5]$$

Where D is the diffusion coefficient and various parameters of diffusion coefficients mentioned in Table 5 where Q is activation energy [28].

Elements	Q (kJ/mol)	Do(m^2/s)	$D_{1050°C}$ (m^2/s)	$D_{1100°C}$ (m^2/s)	$D_{1150°C}$ (m^2/s)
Ti	257	$86*10^{-6}$	$0.6*10^{-14}$	$1.4*10^{-14}$	$3.2*10^{-14}$
Nb	202	$1.04*10^{-6}$	$1.1*10^{-14}$	$2.1*10^{-14}$	$4.0*10^{-14}$
Mo	288	$300*10^{-6}$	$0.1*10^{-14}$	$0.3*10^{-14}$	$0.8*10^{-14}$

Table 5 Diffusion coefficient parameters of Ti, Nb and Mo in Nickel [28]

The diffusion distance based on equation 6 was responsible for dissolved laves phase

$$x = (Dt)^{0.5} \quad [6]$$

Therefore, the diffusion of Mo in Ni determines the dissolution of laves phase determined based on the diffusion equations where Q for diffusion of Mo in Ni (288kJ/mol).

DISTRIBUTION A: Distribution approved for public release.

3. METHODOLOGY

3.1 Experimental Methodology

The experiments were divided into main stages as described in the Figure 24 (a) explained in the detailed flowchart. The method of the experiments for WAAM deposited IN718 walls were heat treated based on standard and modified heat treatment cycles and conducted mechanical tests, metallography analysis using optical microscopy and scanning electron microscopy.

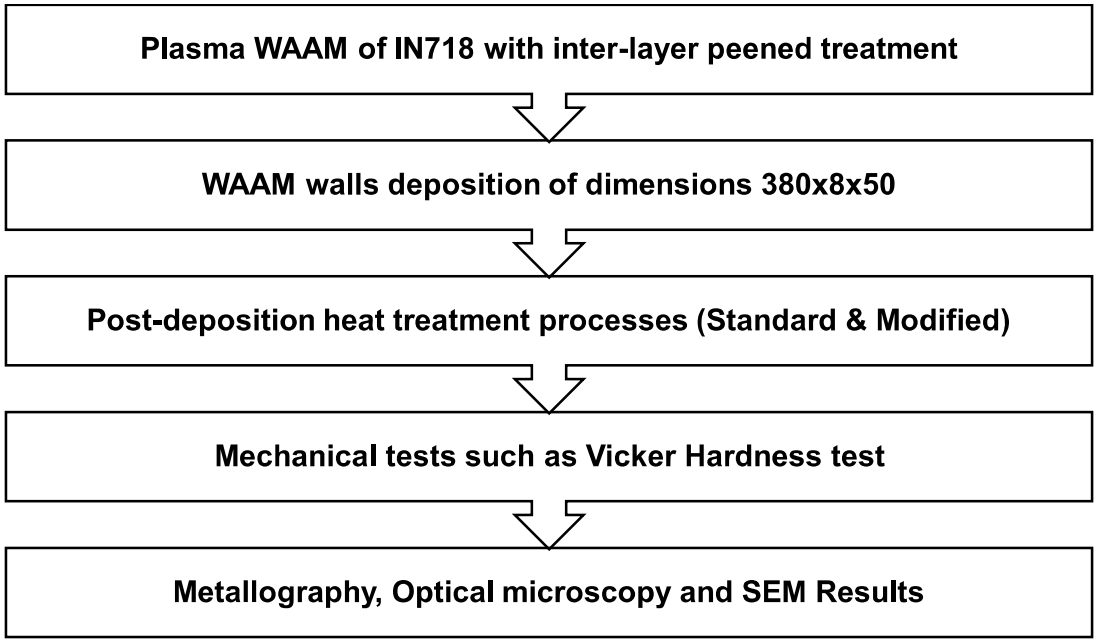


Figure 24 (a) Flowchart for Experimental methodology

3.2 WAAM for IN718 with inter-layer peened treatment

The wire arc additive manufacturing (WAAM) process build two Inconel 718 (IN718) walls with the help of the experimental setup in the Welding Engineering & Laser Processing Centre at Cranfield University.

The WAAM incorporated higher deposition rate and the effect of process parameters such as heat input, melt pool and arc stability on the deposited WAAM walls, microstructural phase segregation, residual stresses and solidification of IN718 walls. The schematic diagram of WAAM in Figure 24 (b) demonstrate the cold metal transfer driven WAAM process along with Argon shielding gas deposited on substrate. The experimental setup consisted of a power source, plasma torch (WAAM shield), wire feeder, peening tool and 6-axis robot which was programmed through software so that

DISTRIBUTION A: Distribution approved for public release.

the deposition path was controlled for laying first layer deposited up to 380mm on the substrate then peening was carried out up to 240mm along the weld axis (WA). The two WAAM walls were deposited with height 50mm along the build direction (BD) and throat thickness (TT) of the WAAM walls were 8mm as indicated in Figure 25. The experiment was performed by first setting the robotic programs on the WAAM deposition software and then setting the welding and WAAM parameters in Table 6 and checking the air flow and gas shielding with argon (~400ppm O_2).

The IN718 wire which was fed into the wire feeder and started deposition on the substrate with peened treatment as next stage up to 240mm and the plasma torch reversed depositing the next alternate layer on top of the previous deposited layer.

WAAM Parameters	**Values**
Stand-off distance	8mm
Wire diameter	1.14mm
Wire feed speed	2m/min
Travel speed	6mm/s
Current	180A

Table 6 WAAM wall build parameters

The inter-pass temperature was measured at three different points as A, B, C (start point of 1st deposition, middle point of WAAM deposited layer and end point of 1st deposition) after a standard time of 3 minutes and continued for all the deposited layers leaded up to a total of 84 layers roughly each layer up to 0.6mm and end temperature was measured after the peened treatment was done. Further the welding parameters for the WAAM setup and the Machine-hammer peening (MHP) machine parameters are mentioned in Table 7 and Table 8 respectively.

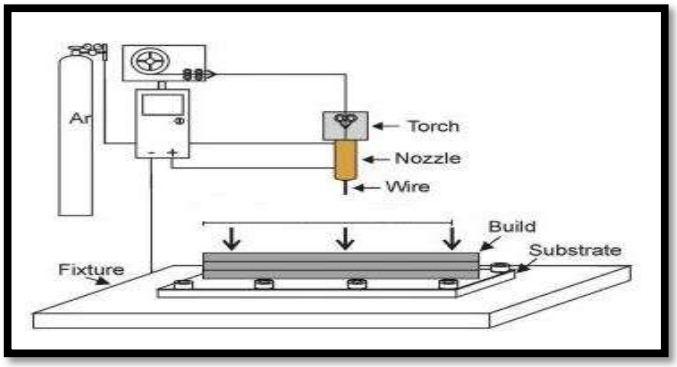


Figure 24 (b) Schematic diagram of WAAM

DISTRIBUTION A: Distribution approved for public release.

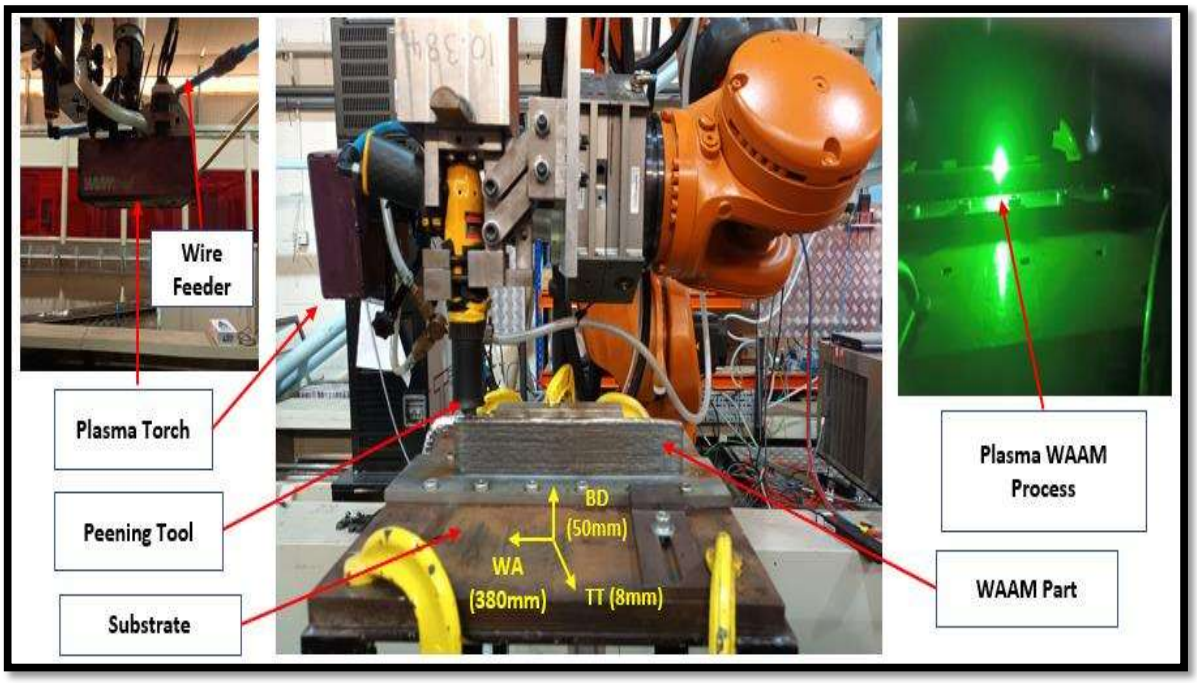


Figure 25 Experimental Setup for WAAM with inter-layer peened treatment (BD is build direction, WA is weld axis and TT is throat thickness)

WELDING SETTINGS	
Wire Diameter	1.14 mm
Plasma Gas	1 L/min
Shielding Gas	10 L/min
Trailing Gas	70 L/min
Torch Stand-off	8 mm
Wait Time b4 Peen	3 min

Table 7 Welding Settings for WAAM

MHP SETTINGS	
Supply Pressure	7 bar
Impact Freq.	36/s
Tip Radius	10 mm
Travel Speed	18 mm/s

Table 8 Machine-hammer Peening (MHP) Settings

The present project work covers the study of samples which were as-deposited, standard heat-treated and modified heat-treated extracted for hardness tests, optical microscopy and scanning electron microscopic analyses from two IN718 WAAM deposited walls with inter-layer peened treatment and without inter-layer peened treatment. However, in future the effect of peening and the modified heat treatment cycle would be also studied with the help of tensile test results and plotted engineering stress vs strain curves in continuation to the present project.

DISTRIBUTION A: Distribution approved for public release.

3.3 Post-deposition Heat Treatment of samples from the WAAM IN718 walls

The WAAM IN718 deposited walls with inter-layer peened treatment were subjected to standard heat treatment cycle in Figure 26 as per AMS 5596 specification described in Table 9 [26]. The peened sample was subjected to standard heat treatment and attached with the thermocouple as the data was recorded in the oscilloscope (Yokogawa DL750 ScopeCorder). The sample was subjected to cleaning in acetone and rinsed in clean water, dried and put in furnace.

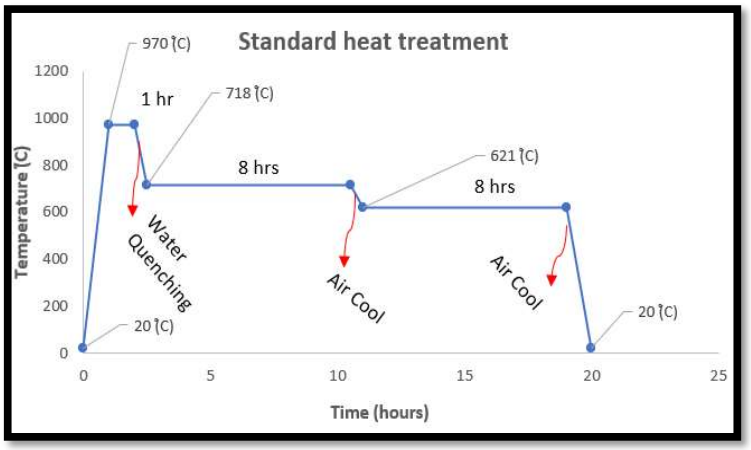


Figure 26 Standard Heat Treatment Cycle [26]

Steps	Temperature	Time
Solutionising	970˚C	1 hour
Aging 1	718˚C	8 hours
Aging 2	621˚C	8 hours

Table 9 Temperature and Holding time during Standard heat treatment process

The homogenisation temperature was increased by keeping the holding time of 1 hour constant as discussed in literature review in section 2.5 that the laves phase is dissolved as Mo in Ni is diffused. The homogenisation temperature was studied for temperatures 1050 ℃, 1100 ℃, 1150 ℃ and the laves phase dissolution was compared, the purpose of the project was to understand the microstructural changes which could affect the mechanical properties by considering the solutionising temperature as 1050 ℃ keeping the holding time for 1 hour. The future project could include the heat treatment of peened samples by increasing the temperatures up to 1100 ℃ and 1150 ℃ or increasing the holding time keeping the homogenisation temperatures constant.

DISTRIBUTION A: Distribution approved for public release.

Therefore, the standard heat treatment process was modified by only increasing the solutionising temperature by 1050˚C and following the same process as per AMS 5596 specification as shown in Figure 27.

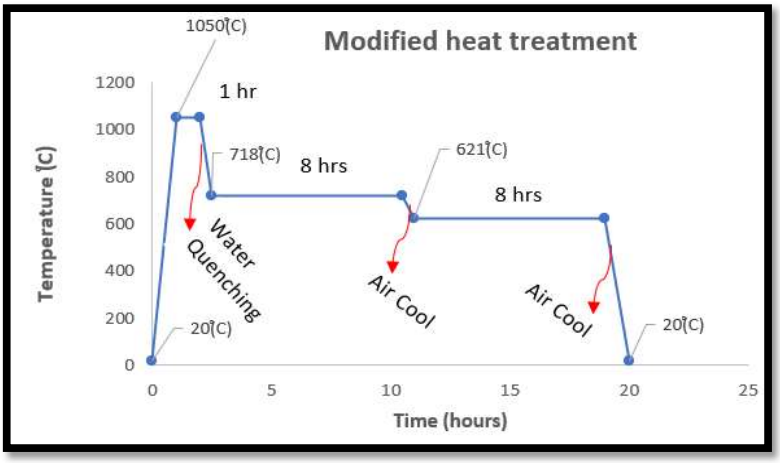


Figure 27 Modified Heat Treatment Cycle

The steps for the modified heat treatment cycle is mentioned in Table 10 which is treated for both peened and non-peened IN718 WAAM deposited wall samples.

Steps	Temperature	Time
Solutionising	1050˚C	1 hour
Aging 1	718˚C	8 hours
Aging 2	621˚C	8 hours

Table 10 Temperature and Holding time during modified heat treatment process

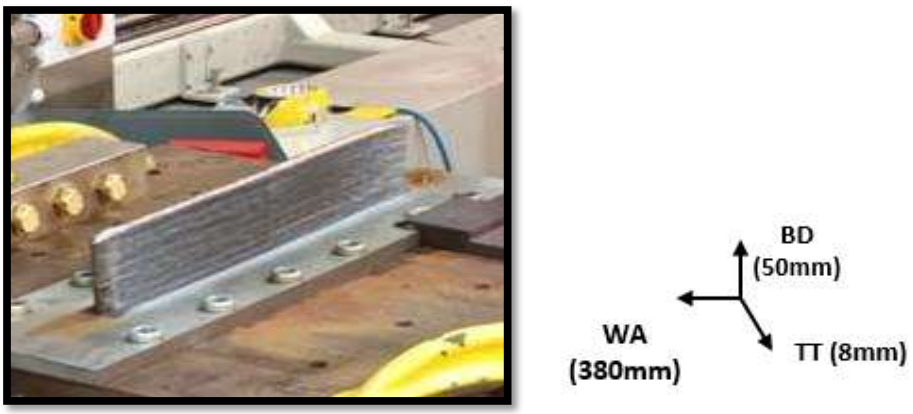


Figure 28 IN718 Wall WAAM deposited with inter-layer peened treatment up to 240 mm along WA

In Figure 28, the samples for standard & modified heat treatment were taken from the IN718 WAAM deposited wall of dimensions 380x8x50 mm (peened and non-peened).

DISTRIBUTION A: Distribution approved for public release.

3.4 Metallographic Preparation for Microstructure

The WAAM deposited wall with inter-layer peened treatment of IN718 alloy were cut for samples for microstructure study using scanning electron microscopy and optical microscopy. There is a standard procedure that must be undergone before the microstructure study as defined in following flowchart Figure 29.

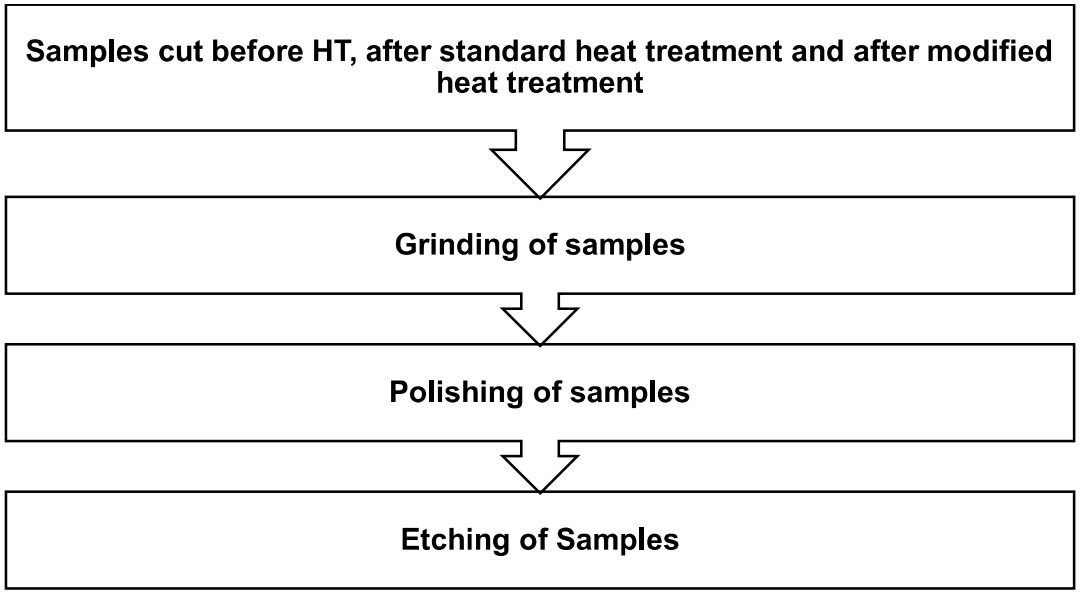


Figure 29 Metallographic Preparation for microstructure study of samples

There was total 10 samples that have been prepared for optical microscopy and there was total 5 samples for scanning electron microscopy as shown in Table 11.

Microstructure study	Samples
Optical Microscopy	BD-P, BD-NP, WA-P, WA-NP, TT-P, TT-NP, TT-P SH, TT-P MH, TT-NP MH, Wire Sample
Scanning Electron Microscopy	TT-P, TT-NP, TT-P SH, TT-P MH, Wire Sample

Table 11 Samples for microstructure study

In the first step, the samples were cut in three different directions i.e., normal to build direction (BD), normal to weld axis (WA) and normal to throat thickness (TT) at mid plane as shown in Figure 30 for either with inter-layer peened treated (P) or without inter-layer peened treated (NP) in Figure 31 which were cut before heat treatment, after standard heat treatment (SH) and after modified heat treatment (MH).

DISTRIBUTION A: Distribution approved for public release.

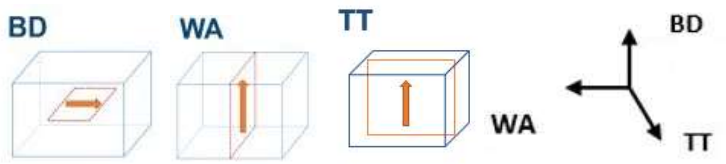


Figure 30 Specimens named based on normal direction to the axis shown BD, WA and TT

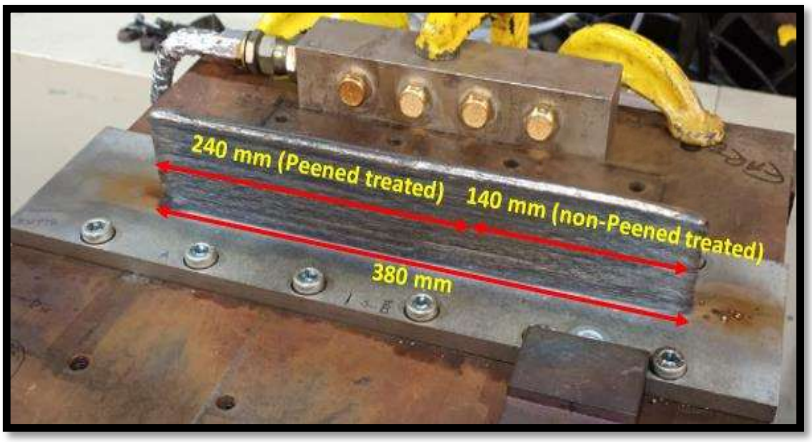


Figure 31 WAAM with inter-layer peened treated and without inter-layer peened treated

The next step is grinding of these samples as they were started with coarse grain size to refined grain size for which there were EU standard grit sizes from 120, 240, 1200 and 2400 grits as shown in Figure 32. The samples were further polished with the silicon carbide grids and diamond liquid for finish up to 3µm. The parameters for grinding and polishing were mentioned in Table 12.



Figure 32 Grinding of samples in machine shown

DISTRIBUTION A: Distribution approved for public release.

Process	Wheel speed	Direction	Grinding Pressure (lbf)	Grinding Time (min)
120 grit Grinding	200	Opposite	40	10
240 grit Grinding	200	Opposite	40	12
1200 grit Grinding	200	Opposite	40	8
2400 grit Grinding	200	Opposite	20	8
Polishing	200	Same	30	5

Table 12 Parameters for Grinding and Polishing

The final step is etching of the samples as shown in Figure 33 which were done by dipped solution of 8% oxalic acid in volume fraction using titanium wires after which they were cleaned in acetone solution and dried by electrical blow dryer and checked using optical microscope.

However, in the microstructure study using SEM and optical microscopy was helpful to understand the secondary phases, precipitates formation, grain boundaries and twinning of grains boundaries. Further EDS was done to determine the elemental composition in the dendrite's growth area and the matrix, the inter-dendritic spacing was measured so as to effectively understand the reduction of diffusion distance after modified heat treated IN718 WAAM samples with inter-layer peened treatment as compared to the standard heat treated IN718 WAAM samples with inter-layer peened treatment.

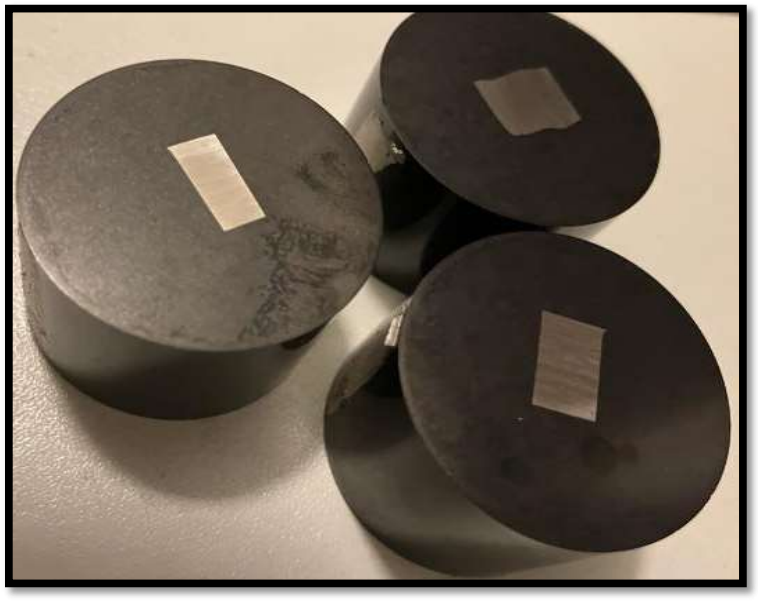


Figure 33 Etched Samples for microstructure study

DISTRIBUTION A: Distribution approved for public release.

Further, macrostructure study was done on the same 10 samples in Table 11 that were prepared for optical microscopy as well. This study helped to understand the columnar grain growth along the build direction (BD), remelting shape and recrystallised core. The magnification was in the range of 2mm for the macrostructure study.

3.5 Microhardness test

There was total 5 samples described that were prepared for microhardness test which is done in Vickers Hardness tester in Zwick/Roell hardness machine as the samples were subjected to indentations from bottom to top cut normal to weld axis in Figure 34 at an increment of 0.5 mm by a pyramidal diamond indenter of impact of about 500g for 15 seconds. These samples were Peened before heat treatment (P), Non-peened before heat treatment (NP), Peened after standard heat treatment (P-SH), Peened after modified heat treatment (P-MH) and non-peened after modified heat treatment (NP-MH) as described in Table 13. The centreline was considered at 4mm at which the indentation started at the mid-section of the width of the IN718 WAAM wall deposited.

Test	Samples
Vickers Hardness	P, NP, P-SH, P-MH, NP-MH

Table 13 Samples for Vickers Hardness test

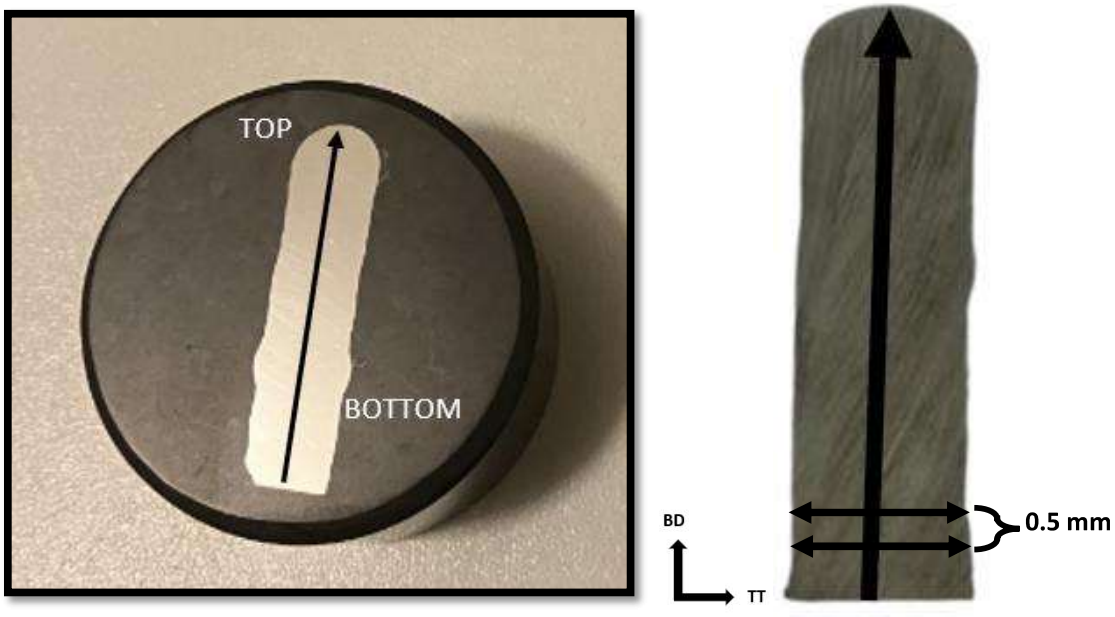


Figure 34 Sample for microhardness test (Bottom to Top with increment of 0.5 mm)

DISTRIBUTION A: Distribution approved for public release.

4. RESULTS AND DISCUSSION

4.1 Microstructure using Optical Microscopy

4.1.1 Comparison between samples before heat treated (TT-P, TT-NP, BD-P, BD-NP, WA-P, WA-NP) and wire-sample

The optical micrographs have been compared to understand the microstructure characterisation before heat treatment of IN718 WAAM deposited walls (with and without inter-layer peened treatment) compared with the wire sample. The optical micrograph of IN718 wire in Figure 35 indicated the face centred cubic matrix of γ and presence of strengthening carbides along with the metastable phases. The γ' and γ'' phases and hexagonal laves phase were present as observed in scale of 100μm. Therefore, the strengthening parameters such as γ' and γ'' are increased by various heat treatment processes so as to possess better mechanical properties.

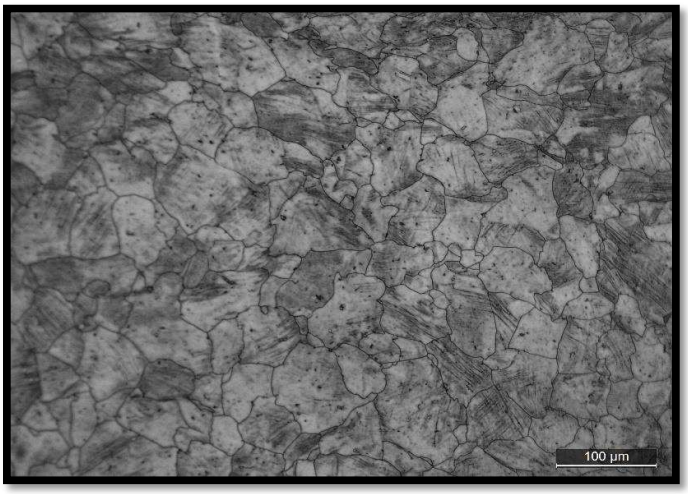


Figure 35 Sample of IN718 wire from conventional manufacturing process

The IN718 WAAM deposited walls without inter-layer peened treatment were cut in three directions, normal to BD, normal to WA and normal to throat thickness at mid-plane and taken for optical micrographs as shown in Figure 36. Before heat treatment, these non-peened samples showed dendritic structure all across the micrograph taken at a scale of 100μm in all the three samples (BD-NP, WA-NP and TT-NP). Also, these showed low-angle grain boundaries indicating the columnar grain growth. There could be a higher presence of laves phase in the non-peened 3 samples but it could be clearly observed in scanning electron microscopy (SEM) along with the elemental composition more clearly observed in Energy dispersive X-ray spectroscopy (EDS).

DISTRIBUTION A: Distribution approved for public release.

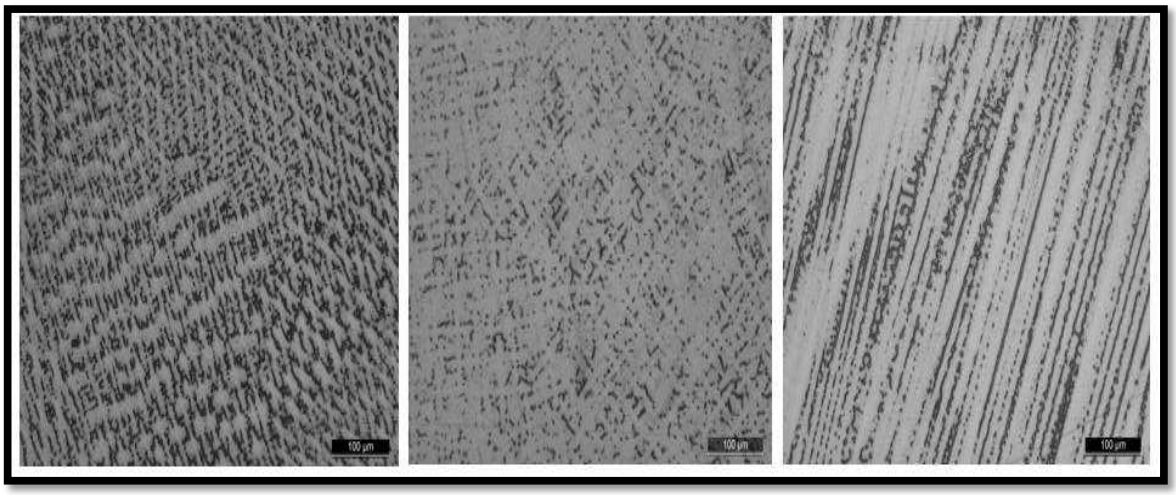


Figure 36

(a) BD-NP (Normal to Build direction Non-Peened) (b) TT-NP (Normal to Throat thickness at mid-plane Non-Peened) (c) WA-NP (Normal to Weld axis Non-Peened)

The IN718 WAAM deposited walls with inter-layer peened treatment were cut in three directions, normal to BD, normal to WA and normal to throat thickness at mid-plane and taken for optical micrographs in Figure 37. These micrographs indicated that the dendritic structure was less and the growth in dendritic direction is not closer to perpendicular angles to interlayer boundary as for non-peened samples but the growth in dendritic direction was more random. Further, peening as a strengthening mechanism lead to recrystallisation of the equiaxed grains and further grain refinement as observed in micrographs in Figure 37.

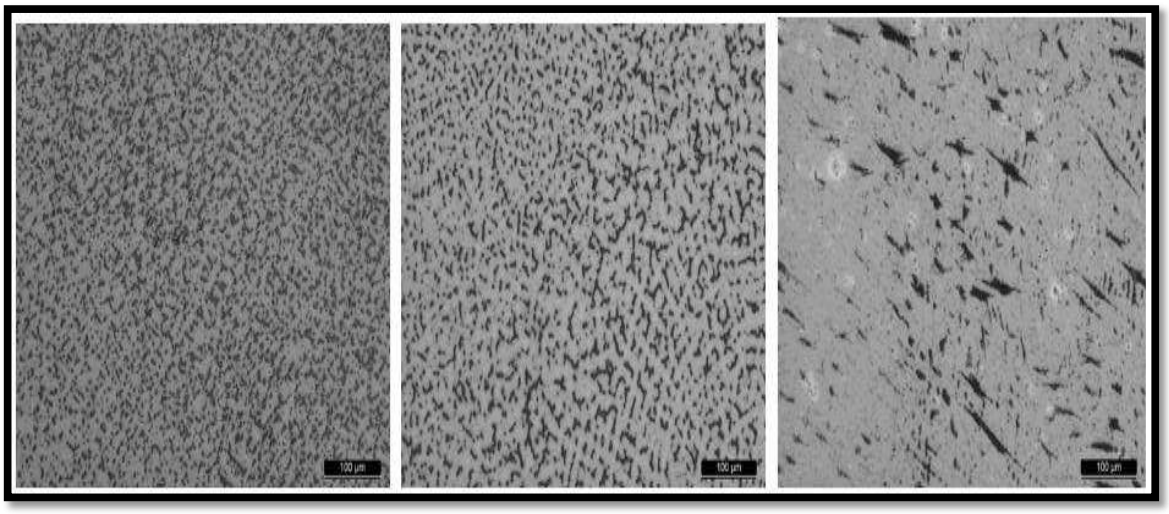


Figure 37

(a) BD-P (Normal to Build direction- Peened) (b) TT-P (Normal to Throat thickness at mid-plane- Peened) (c) WA-P (Normal to Weld axis- Peened)

DISTRIBUTION A: Distribution approved for public release.

4.1.2 Comparison for peened samples before and after heat treatment process

The IN718 WAAM wall samples with inter-layer peened treatment were cut in a direction normal to throat thickness at the mid plane (TT-P) of the WAAM wall and subjected to three conditions;

1. ***Before Heat Treatment: -***

The peened sample (TT-P) in optical micrographs in Figure 38 (a) showed the dendritic structure grown in random direction along with presence of laves phase better observed in Scanning electron microscopy results.

2. ***Standard Heat Treatment: -***

The peened sample (TT-P SH) after standard heat treatment process as per AMS-5562 (hot forged IN718 bar) in Figure 26 shown in optical micrographs in Figure 38 (b). The dendritic structure was less when samples were heat treated and also the area fraction of laves phase decreased with homogenisation temperature of 970˚C for 1 hour and further aging treatment for 718˚C for 8 hours and 621˚C for 8 hours.

3. ***Modified Heat Treatment: -***

The peened sample (TT-P MH) after modified heat treatment process in Figure 27 shown in optical micrographs in Figure 38 (c) lead to dissolution of laves phase and disappearance of dendrites because of increased homogenisation temperature of 1050˚C for 1 hour followed by aging treatment for 718˚C for 8 hours and 621˚C for 8 hours as grain boundaries have been clearly observed.

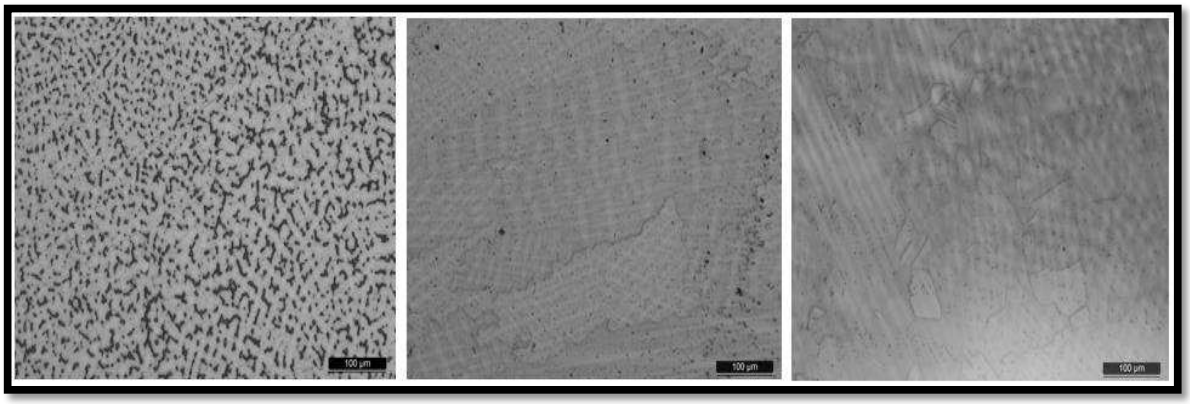


Figure 38

(a) TT-P before Heat Treatment (b) TT-P SH after standard Heat Treatment (c) TT-P MH after modified Heat Treatment

DISTRIBUTION A: Distribution approved for public release.

4.1.3 Comparison for non-peened samples before heat treatment and after modified heat treatment process

The two samples from IN718 WAAM deposited walls without inter-layer peened treatment were compared in optical micrographs as shown in Figure 39 (a) before heat treatment (b) after modified heat treatment. The optical microscopic study indicated that there was a presence of laves phase and dendritic microstructure more in the form of columnar grain growth before heat treatment. However, when the non-peened samples were subjected to modified heat treatment process, the laves phase is observed to be dissolved but there could be presence of the precipitates of Ti and Nb rich inclusions in form of δ phase more clearly observed in scanning electron microscopy (SEM) and elemental composition using Energy dispersive X-ray spectroscopy (EDS). Also, the grain size has grown during the modified heat treatment process which led to the formation of equiaxed grains instead of columnar grain growth as heat treatment led to diffusion of the Mo and other elements in Ni responsible for laves phase formation during WAAM deposition of IN718.

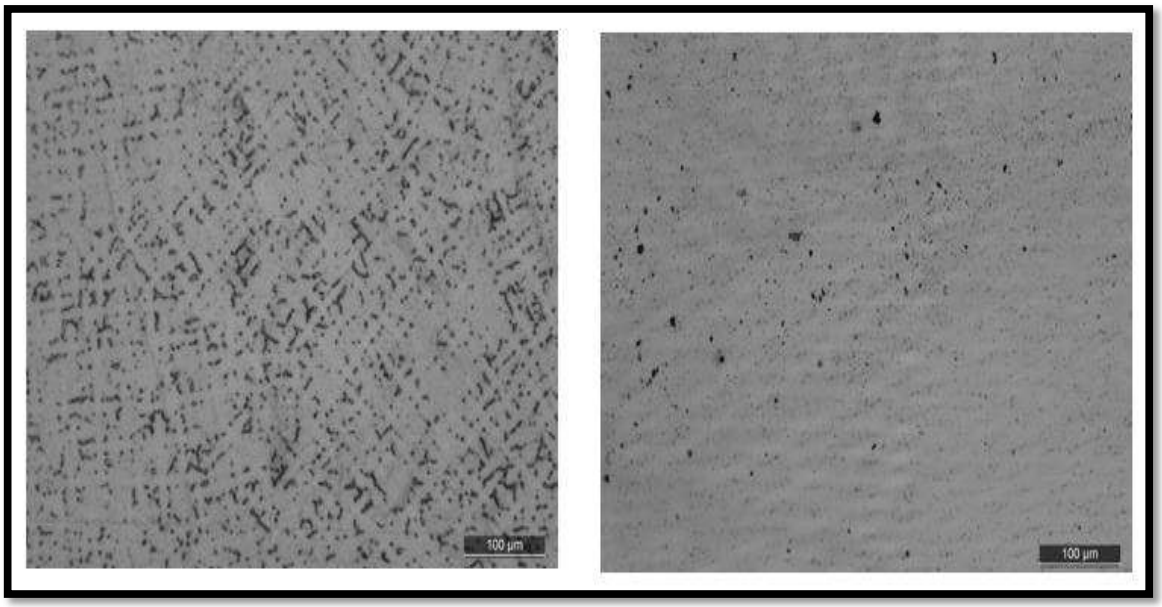


Figure 39

(a) TT-NP MH before Heat Treatment (b) TT-NP MH after modified Heat Treatment

DISTRIBUTION A: Distribution approved for public release.

4.2 Microstructure using Scanning Electron Microscopy (SEM) and elemental composition in Energy dispersive X-ray spectroscopy (EDS)

4.2.1 Wire Sample Characterisation

The filler metal wire of IN718 with specifications AWS A5.14 ASME SFA-5.14 undergone the scanning electron microscopy (SEM) as shown in Figure 40 set at a scale of 10µm. Further the laser beam settings for SEM were mentioned in Table 14. The grain boundaries were clearly observed in the wire sample along with the elemental segregation in very slight portion as shown in Figure 40. Further, the Energy dispersive X-ray spectroscopy (EDS) provided the elemental composition found in the wire cross section. In Table 15 and Figure 40, it had been observed that spectrum 11 showed the streaks aligned with wire axis (present during wire production) where Nb had been present richly as compared to the matrix. However, there is introduction of inert gas fusion elements such as C, O and small amounts of Si which had not been present in IN718 chemical composition shown previously in Table 3.

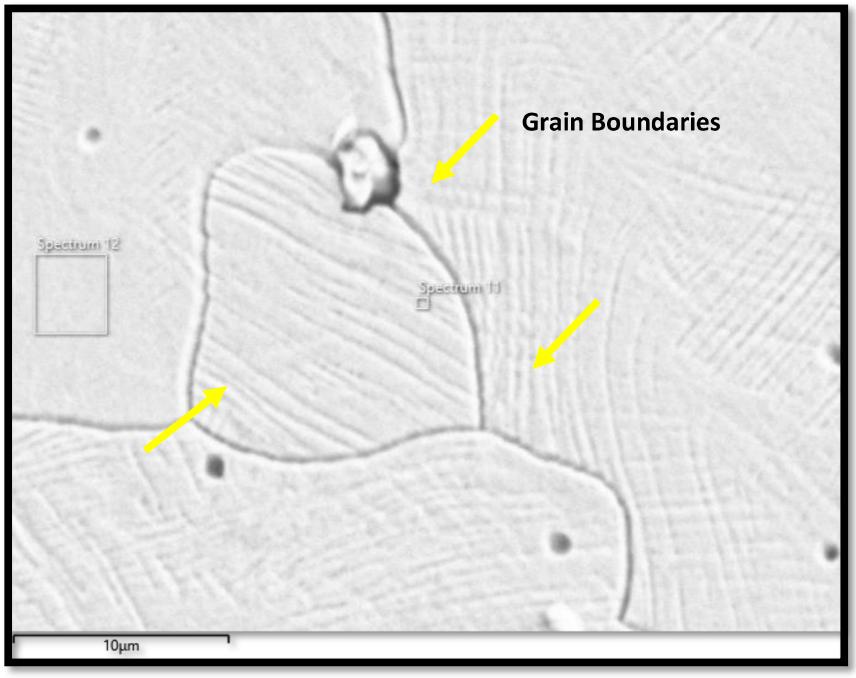


Figure 40 Wire Sample

The parameters of the laser beam for the wire sample the accelerating voltage of electrons, working distance, depth of focus of the laser beam and the spot size has been mentioned in Table 14.

DISTRIBUTION A: Distribution approved for public release.

Parameters	Values
Accelerating voltage (HV)	20keV
Working distance	5.02mm
Depth of focus	0.58 µm
Spot size	25nm

Table 14 Parameters of laser beam in SEM

The matrix of the IN718 wire sample has been defined in Spectrum 12 and as observed the weight % of the elements remain same with a slight weight % change in few elements such as Nb, Mo, Ti. The chemical composition has been found to be in the weight % range of elements as mentioned in Table 3 under Literature review section.

Spectrum Label	Spectrum 11 (Steaks)	Spectrum 12 (Matrix)
C	1.50	2.26
O	1.20	1.51
Al	0.53	0.51
Si	0.22	0.28
Ti	0.52	1.12
Cr	16.70	16.80
Fe	16.77	15.56
Ni	55.27	54.37
Nb	4.51	4.32
Mo	2.77	3.26
Total	100.00	100.00

Table 15 Elemental Composition in both spectrums as per Figure 40

4.2.2 Strengthening mechanism impact of peening for samples before Heat Treatment Microstructural Evolution

The IN718 WAAM deposited wall samples with inter-layer peened treatment and without inter-layer peened treatment before heat treatment were subjected to scanning electron microscopy (SEM) as shown in Figure 41 (a) and (b) respectively. The working distance of laser beam is 6mm and accelerating voltage of electrons is 20keV. The non-peened sample cut normal to throat thickness direction along mid plane out of IN718 WAAM wall indicated the presence of dendritic structure with less dendritic spacing up to 0.13 µm and numerous residual laves phase in Figure 42. The peened sample cut normal to throat thickness direction along mid plane out of IN718 WAAM indicated the presence of dendritic structure with higher dendritic spacing in the range of 0.1 to 0.47 µm. Additionally for the non-peened sample, the dendritic grain growth was perpendicular to the inter layer boundary but for peened sample, the dendritic grain growth was random and spacing increased between the dendrites as shown in Figure 41 (a) and (b).

DISTRIBUTION A: Distribution approved for public release.

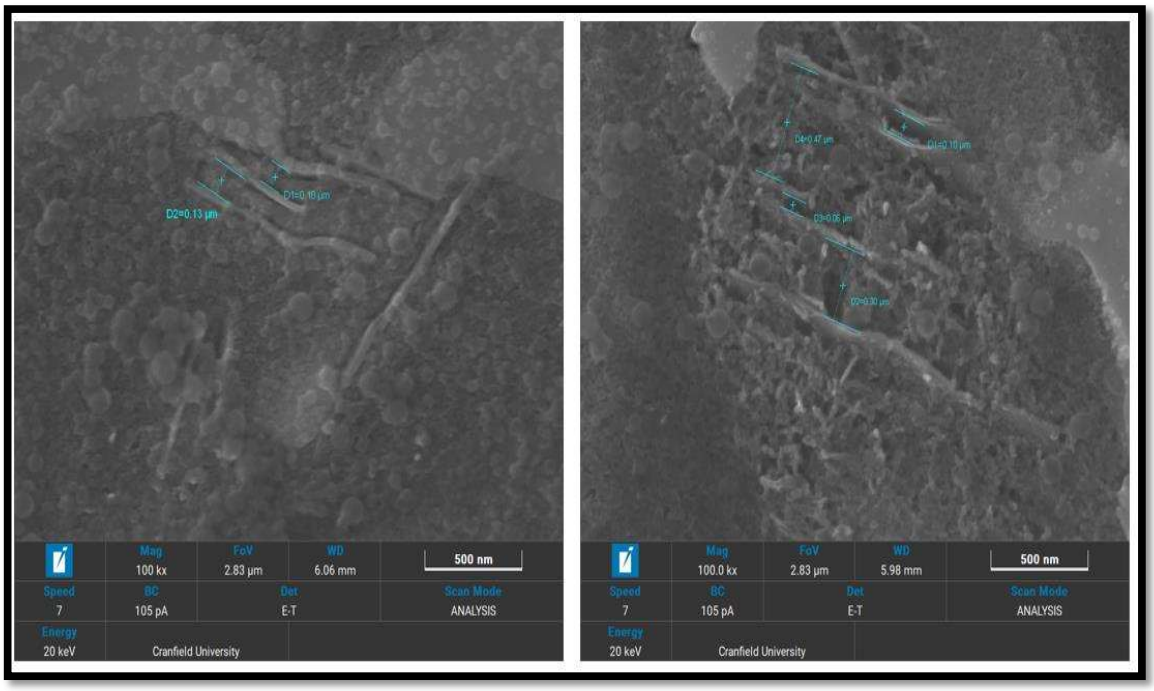


Figure 41 (a) TT-NP before Heat Treatment (b) TT-P before Heat Treatment

The laves and carbides have been distributed in non-peened sample before heat treatment process as shown in Figure 42 (a). Spectrum 7 has indicated that the laves phase consisted of higher weight% of Nb and alloying elements such as Al and Ti had been responsible for formation of γ' precipitation phase (AlTi). Also, the higher weight % of Nb, Al and Ti in the non-peened sample led to formation of hardening precipitates and intermetallic in the form of laves, NbC carbides and TiN nitrides. TiN precipitation has been occurred at temperature above the liquidus and NbC precipitation has been observed in temperature range of 1280-1265°C [22] in the Equation 7 as follows: -

$$L \rightarrow \gamma + NbC \quad [7]$$

The laves phase has been formed in the temperature range of 1160–1075 °C [22] as shown in Equation 8 as follows: -

$$L \rightarrow \gamma + Laves \quad [8]$$

In Figure 42, it has been shown that Spectrum 8 indicated the matrix with decrease in weight % of elements such as Nb, Ti and Al. The Table 16 (a) has described the elemental composition for Spectrum 7 and Spectrum 8 as per Figure 42 (a) in a scale of 10µm.

DISTRIBUTION A: Distribution approved for public release.

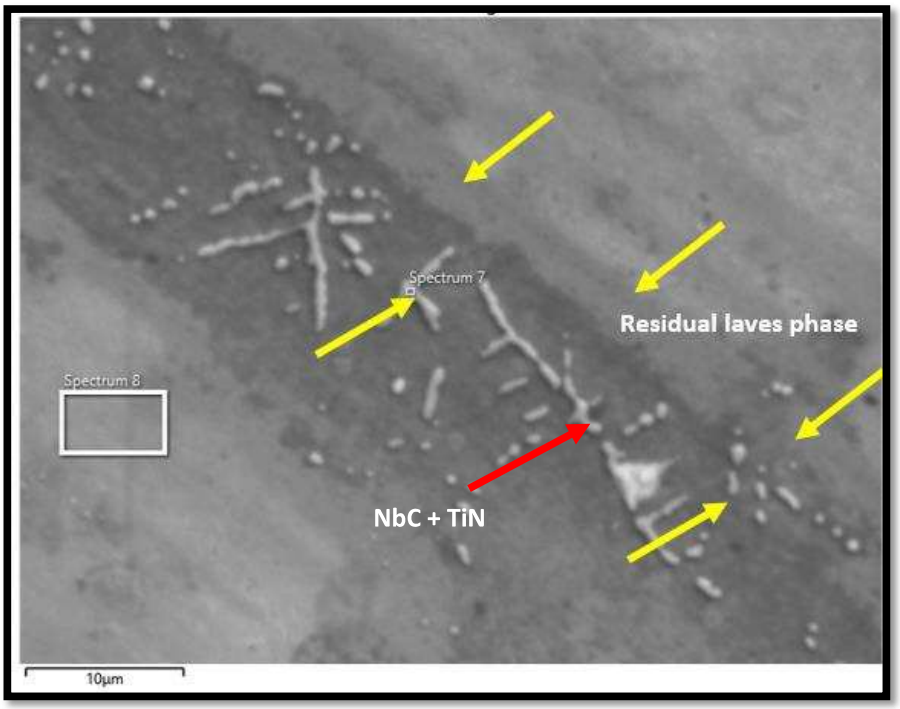


Figure 42 (a) TT-NP before Heat Treatment

Spectrum Label	Spectrum 7 (Dendrite)	Spectrum 8 (Matrix)
C	6.12	9.81
O	2.16	3.14
Al	0.49	0.44
Si	0.55	0.72
Ti	2.17	1.44
Cr	10.36	13.32
Fe	8.95	11.27
Ni	57.31	50.47
Nb	10.23	7.14
Mo	1.65	2.25
Total	100.00	100.00

Table 16 (a) Elemental Composition in both spectrums (TT-NP) before Heat Treatment

The scale of 1µm in Figure 42 (b) for the peened sample cut normal to the throat thickness direction at mid plane indicated the columnar dendrites grain growth. The fine equiaxed grains are shown in the remelted zone which has undergone large number of repetitive thermal cycles in between the WAAM deposited layers. The large columnar grains in Spectrum 22, 23 and 24 has indicated that there is less thermal cycling and the recrystallisation does not occur. But the peening mechanism had led to the recrystallisation within the repeated thermal cycles as a result of which the

DISTRIBUTION A: Distribution approved for public release.

anisotropic properties are decreased responsible for more isotropic mechanical properties for peened IN718 WAAM deposited wall sample.

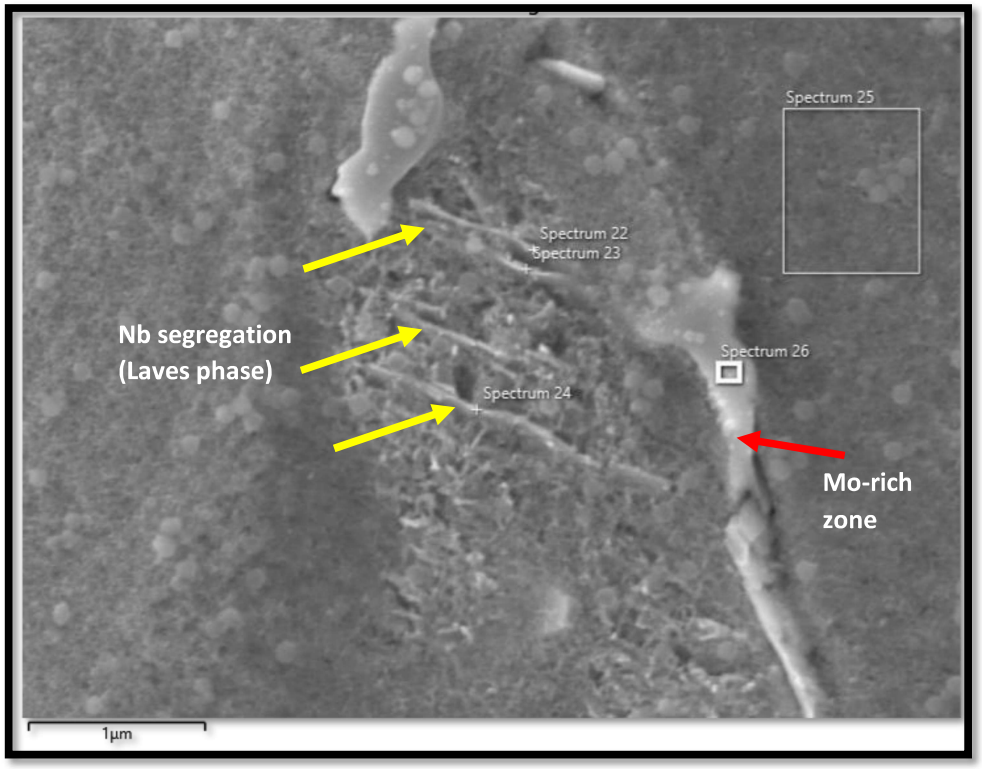


Figure 42 (b) TT-P before heat treatment

The Table 16 (b) has illustrated the elemental composition for different spectrums as per Figure 43 as the dendrites has shown increased weight % of Nb for spectrum 22, 23 and 24 shown Nb-rich zone and Mo rich zone in Spectrum 26 as compared to the elemental composition in Spectrum 25 for the matrix.

Spectrum Label	Spectrum 22 (Dendrite)	Spectrum 23 (Dendrite)	Spectrum 24 (Dendrite)	Spectrum 25 (Matrix)	Spectrum 26 (Mo-rich)
C	3.13	2.65	5.04	6.62	7.77
O	3.58	3.78	4.52	4.45	3.53
Al	0.29	0.28	0.38	0.49	0.47
Si	0.21	0.21	0.28	0.58	0.65
Ti	1.52	1.56	1.44	1.15	0.07
Cr	11.61	11.18	12.16	13.87	14.13
Fe	11.01	10.49	10.56	11.80	14.38
Ni	56.40	56.46	51.56	50.34	44.02
Nb	10.21	11.00	11.94	8.30	10.58
Mo	1.85	2.39	2.11	2.40	4.40
Total	100.00	100.00	100.00	100.00	100.00

Table 16 (b) Elemental Composition in both spectrums (TT-P) before Heat Treatment

DISTRIBUTION A: Distribution approved for public release.

The Nb segregation and formation of Nb-rich brittle laves phase at the interdendritic area as shown in Figure 43 has led to affect in mechanical properties and large columnar grains led to less strengthening of grain boundary.

4.2.3 Different Heat Treatment Processes Microstructural Evolution

The peened sample cut normal to throat thickness at the mid plane of IN718 WAAM wall undergone standard heat treatment process that led to the precipitation of δ phase which could be observed as needle like morphology along the grain boundaries as shown in Figure 43 (a). The dendritic spacing has been about 0.1 to 0.3 µm for the peened sample subjected to standard heat treatment. The peened sample cut normal to throat thickness at the mid plane of IN718 WAAM wall undergone modified heat treatment process showed no trace of laves phase in the microstructure as the homogenisation treatment with increased temperature up to 1050˚C with holding time of 1 hour clearly indicated in Figure 43 (b). Further the δ phase has not been observed in Figure 43 (b) and the dendrites have been dissolved as well.

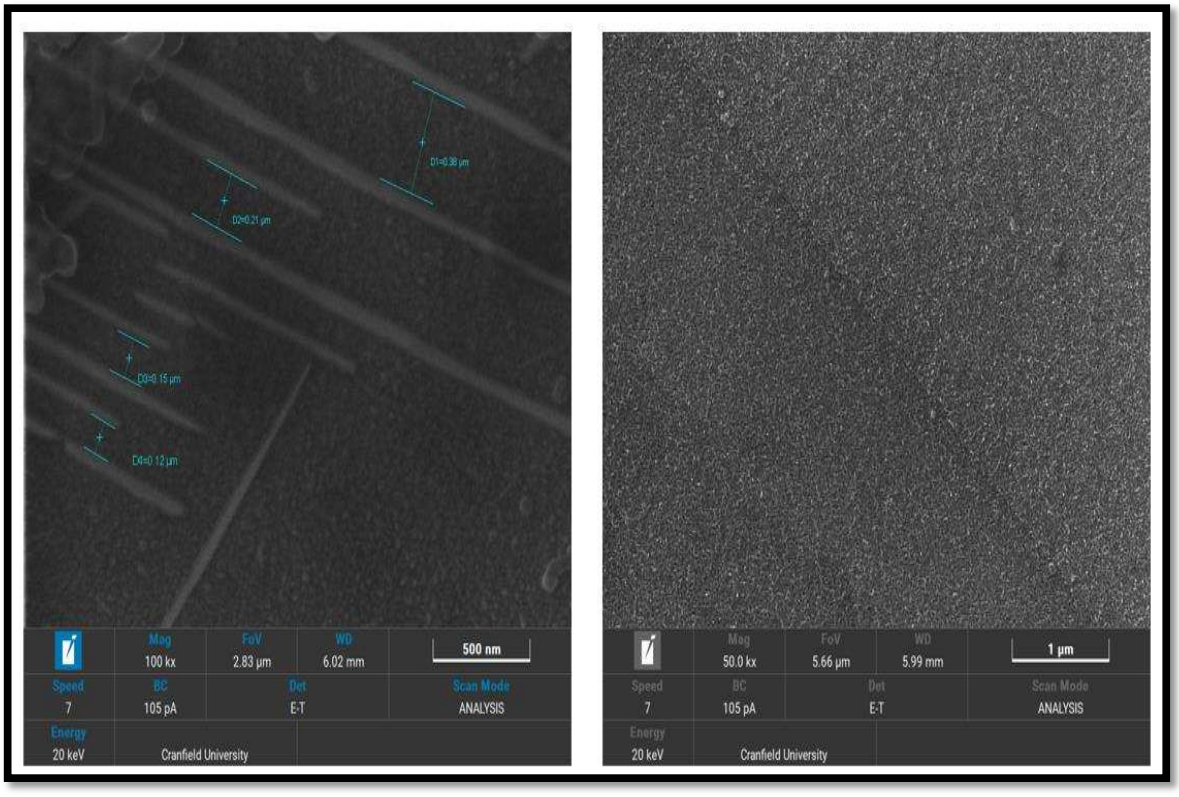


Figure 43 (a) TT-P Standard Heat Treatment (b) TT-P Modified Heat Treatment

DISTRIBUTION A: Distribution approved for public release.

The needle like morphology of δ phase as observed in Figure 44 has been easily distinguishable from the spherical γ' and elliptical γ''. Also, during the standard heat treatment process in the temperature range of 850 to 1000˚C, the precipitation of δ phase has taken place and as observed in Table 17 the Nb weight % was very high in dendrites about 3% higher as compared to the matrix. Also, the region of partial dissolved laves phase has been indicated in Figure 44. The increased % of C in Spectrum 9,10 and 11 as compared to the matrix in Spectrum 12 observed the presence of carbides in form of NbC as shown in Table 17.

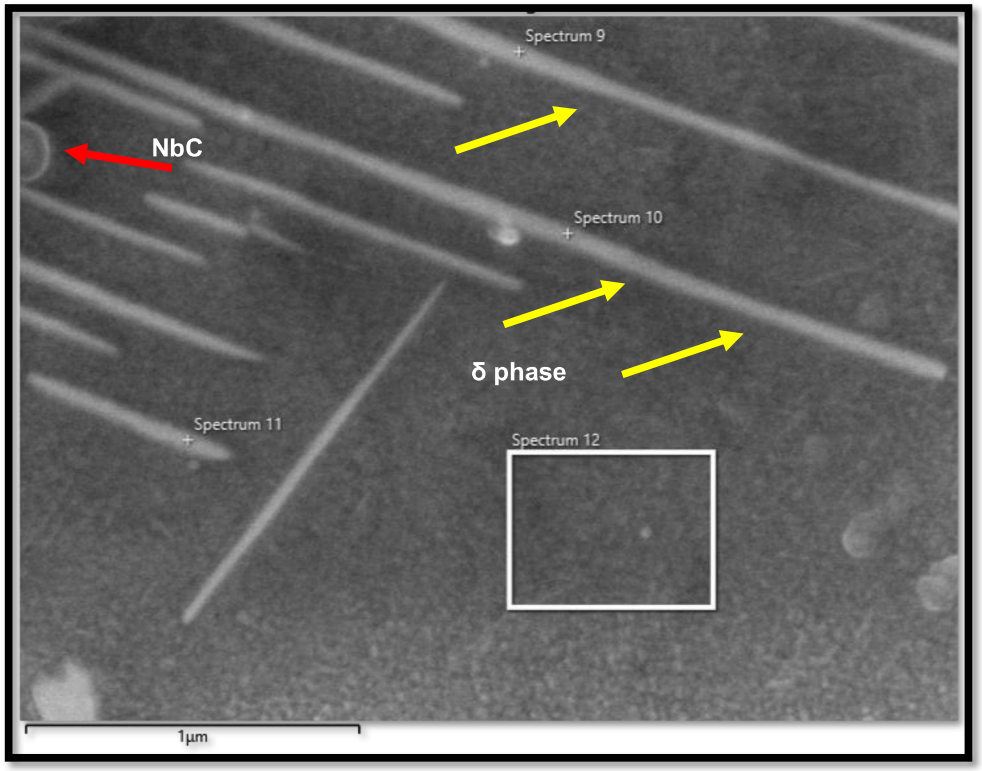


Figure 44 TT-P Standard Heat Treatment

Spectrum Label	Spectrum 9 (Dendrite)	Spectrum 10 (Dendrite)	Spectrum 11 (Dendrite)	Spectrum 12 (Matrix)
C	23.35	26.42	22.26	12.75
Al	0.36	0.37	0.41	0.56
Si	0.13	0.13	0.13	
Ti	1.30	1.13	0.87	
Cr	10.48	10.60	12.06	15.62
Fe	8.74	9.20	10.46	14.55
Ni	45.51	42.38	45.60	50.31
Nb	8.12	7.72	6.32	3.77
Mo	2.01	2.05	1.89	2.44
Total	100.00	100.00	100.00	100.00

Table 17 Elemental Composition in both spectrums (TT-P) Standard Heat Treatment

DISTRIBUTION A: Distribution approved for public release.

The homogenisation temperature of 1050˚C in the modified heat treatment process showed that the laves phase was dissolved as shown in Figure 45. The Nb and Mo rich areas has been dissolved in Spectrum 1,2,3 regions of dendrites as shown in Table 18. The elemental composition of Nb and C in terms of weight% have been evenly distributed in Spectrum 4 in the matrix and is the same for all the spectrums (dendrites and matrix) observed in a scale of 500nm.

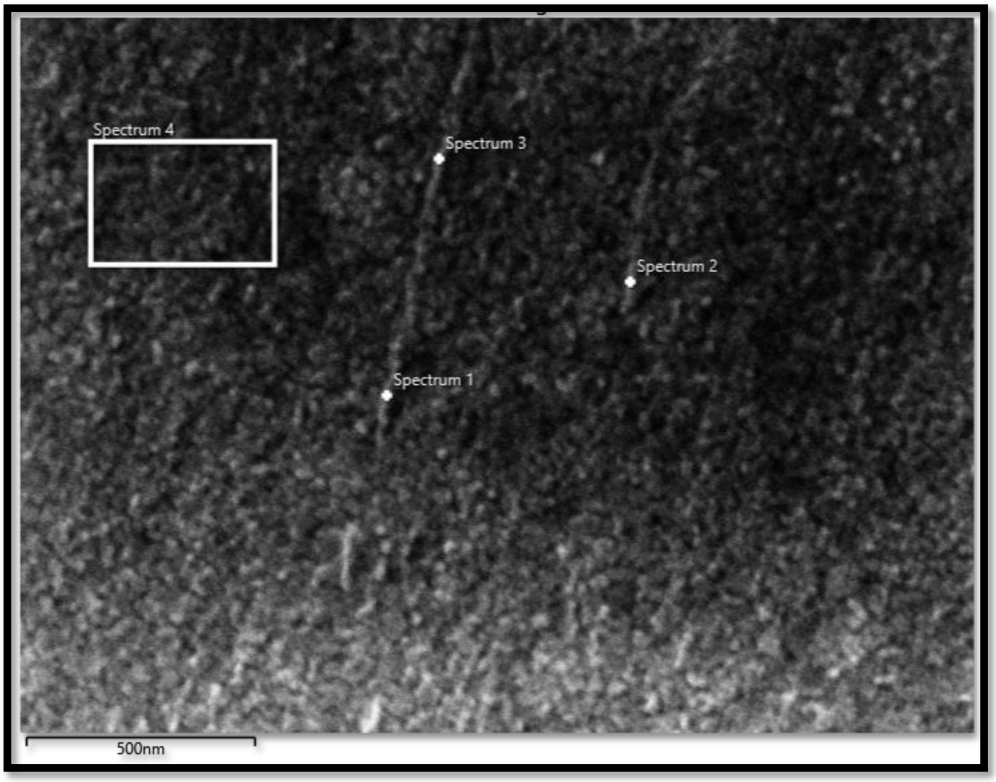


Figure 45 TT-P Modified Heat Treatment

Spectrum Label	Spectrum 1 (Dendrite)	Spectrum 2 (Dendrite)	Spectrum 3 (Dendrite)	Spectrum 4 (Matrix)
C	5.41	5.62	6.04	6.89
O	1.15			1.10
Al	0.54	0.60	0.52	0.52
Si	0.08	0.11	0.03	0.08
S	0.13			
Ti	0.96	1.07	0.93	1.00
Cr	16.07	16.00	15.84	16.09
Fe	15.35	15.46	15.16	15.01
Ni	53.64	54.33	54.70	52.21
Nb	4.66	4.47	4.35	4.61
Mo	2.01	2.33	2.44	2.49
Total	100.00	100.00	100.00	100.00

Table 18 Elemental Composition in both spectrums (TT-P) Modified Heat Treatment

DISTRIBUTION A: Distribution approved for public release.

4.2.4 Rationale behind the homogenisation treatment change

This modified heat treatment cycle has been designed based on the Laves phase eutectic temperature at 1185 ˚C and has been experimented by following the homogenisation temperature of 1150˚C for peened and non-peened sample of IN718 WAAM deposited wall with holding time of 1 hour as shown in Figure 27.

4.3 Optical Macrostructure Study

The optical microstructure study has been done at a scale of 1mm for peened samples cut normal to throat thickness direction from IN718 WAAM deposited wall for before heat treatment and after standard heat treatment cycle to 2mm for peened samples after modified heat treatment as shown in Figure 46. For the TT-P samples in all three conditions indicated the inter-layer boundary because of deposited layer alternate to one another by dotted red lines in Figure 46 (a), (b) and (c). The band represented between these inter-layer boundaries showed the concentration of Nb and Mo in laves phase at melt boundaries, carbide such as NbC and δ phase that formed the γ matrix for peened samples before heat treatment and subjected to standard heat treatment. Further, the modified heat-treated peened sample showed only the eutectic rich region that mainly consisted of the precipitates of γ' and γ'' and free of the γ matrix with dissolution of laves phase, carbides and δ phase subjected to homogenisation temperature of 1050˚C with holding time for 1 hour.

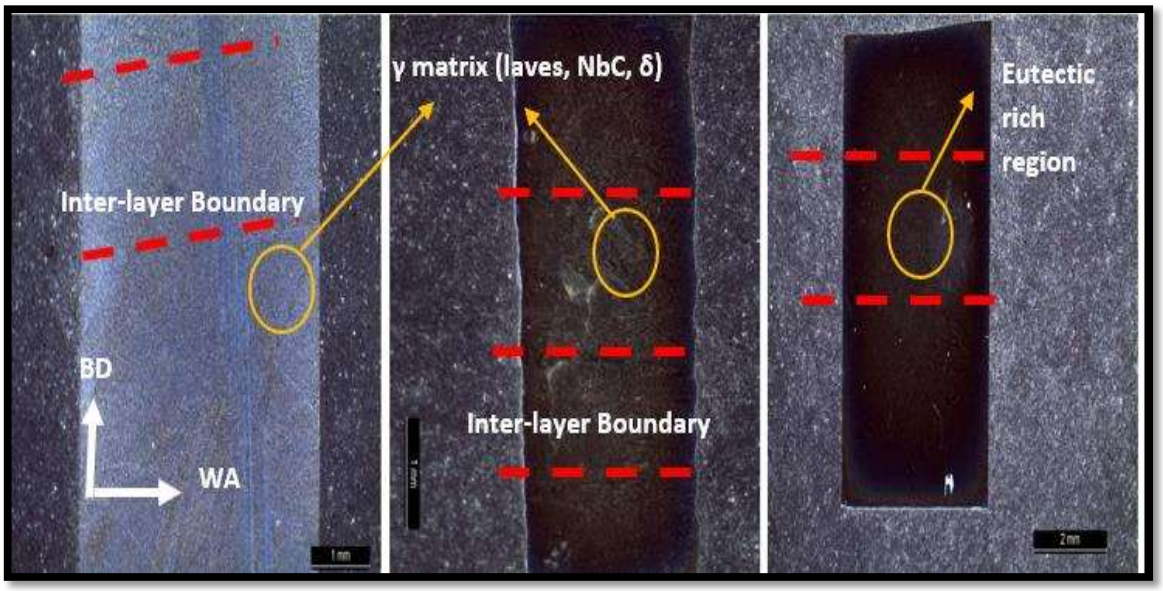


Figure 46 (a) TT-P Before Heat Treatment (b) TT-P Standard Heat Treatment (c) TT-P Modified Heat Treatment

DISTRIBUTION A: Distribution approved for public release.

The Figure 47 has showed non-peened and peened samples before heat treatment and the dendritic grain growth mainly along the columnar grain direction in Figure 47 (c) and (d) has been clearly observed. Also, for the peened sample the refinement boundary in Figure 47 (b) was formed apart from the inter-layer boundary whereas for the non-peened sample only the inter-layer boundary has been seen in Figure 47 (a).

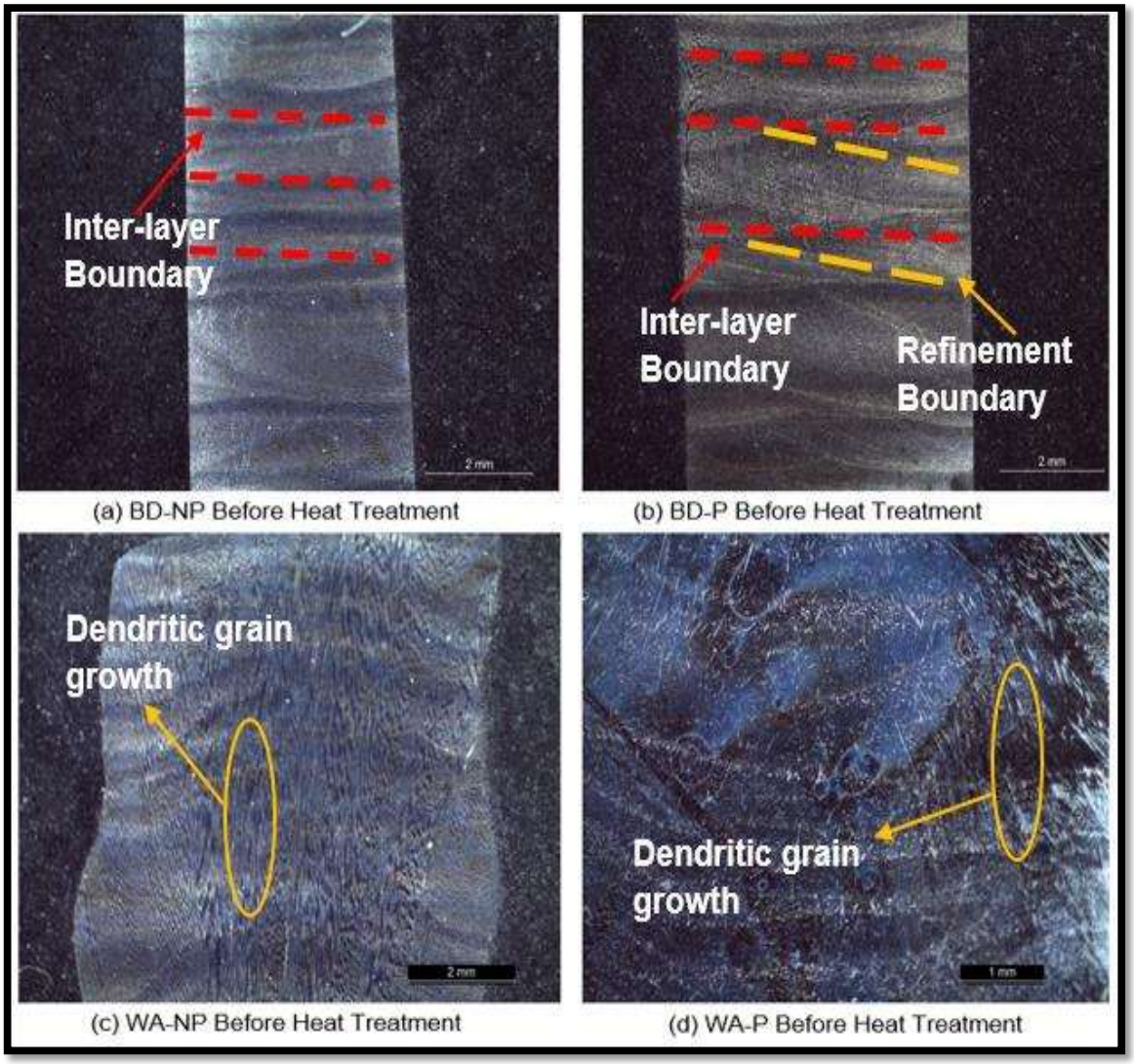


Figure 47 Before Heat Treatment Peened and Non-peened Samples

The refinement boundary (β transus temperature) has indicated the recrystallised β grains that melted back from the melt pool had been nucleated during solidification process after peened layer treatment. The survived β grains along with the inter layer boundary form the fusion boundary along with fine columnar grains directional growth from bottom to top.

DISTRIBUTION A: Distribution approved for public release.

The Figure 48 in the optical macroscopy study has shown that the columnar grain growth was observed in non-peened sample before heat treatment and after the homogenisation and double aging cycle had been applied to the same non-peened sample the columnar grains disappeared and equiaxial grains existed with dissolution of the dendrites. Further the solidification of the WAAM deposited layer does not grow from same grains rather new β grains has to be nucleated in every thermal cycle of WAAM deposition of alternate deposited layers as a result of which the columnar grain structure has been formed which has been dissolved when subjected to modified heat treatment.

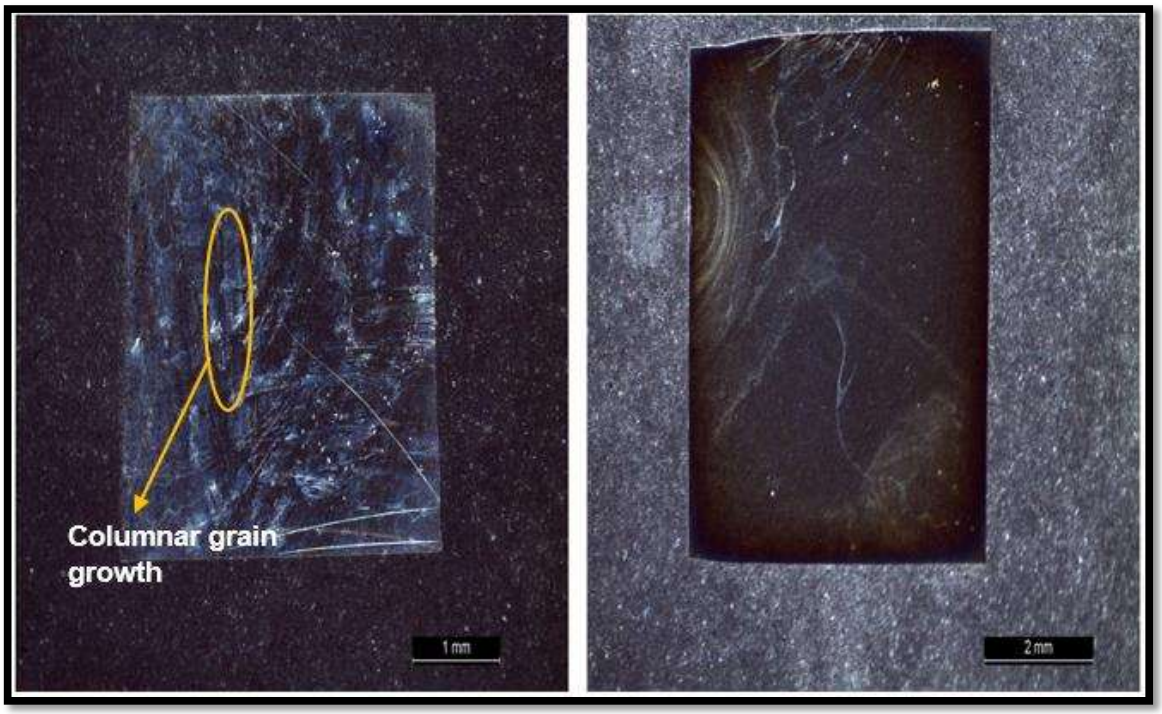


Figure 48 (a) TT-NP Before Heat Treatment (b) TT-NP Modified Heat Treatment

DISTRIBUTION A: Distribution approved for public release.

4.4 Mechanical Property defined by Microhardness

4.4.1 Comparison between TT-P and TT-NP as-deposited before heat treatment

The samples cut normal to the throat thickness direction at the mid plane from the IN718 deposited walls subjected to inter- layer peened treatment (TT-P) and without inter-layer peened treatment (TT-NP) in as-deposited state before heat treatment were undergone microhardness test in Zwick/Roell hardness machine with a total of 61 points indentations with increments of 0.5mm starting from the bottom portion of the prepared sample to the top along the central axis of the BD-TT plane as shown in Figure 34. The microhardness results shown indicate that the IN718 wall samples with inter-layer peened treatment has 18% higher HRV value as compared to the one without inter-layer peened treatment as shown in Figure 49. The hardening has occurred more predominantly at the top surface and reached a peak value of 576 HRV at a distance of 30.5 mm from the bottom portion along the centreline. However, higher the load higher is the microhardness value at the same depth is observed. The strengthening mechanism of peening produced hardening layer because of severe plastic deformation that leads to compressive residual stresses from the impact of machine-hammer peening on the deposited WAAM layer subjected to yield stress to generate the overlap of these indents on the peened line and crystal refinement occurs throughout the surface leading to increased yield strength of the WAAM deposited surface layer of IN718 top wall with inter-layer peened treatment.

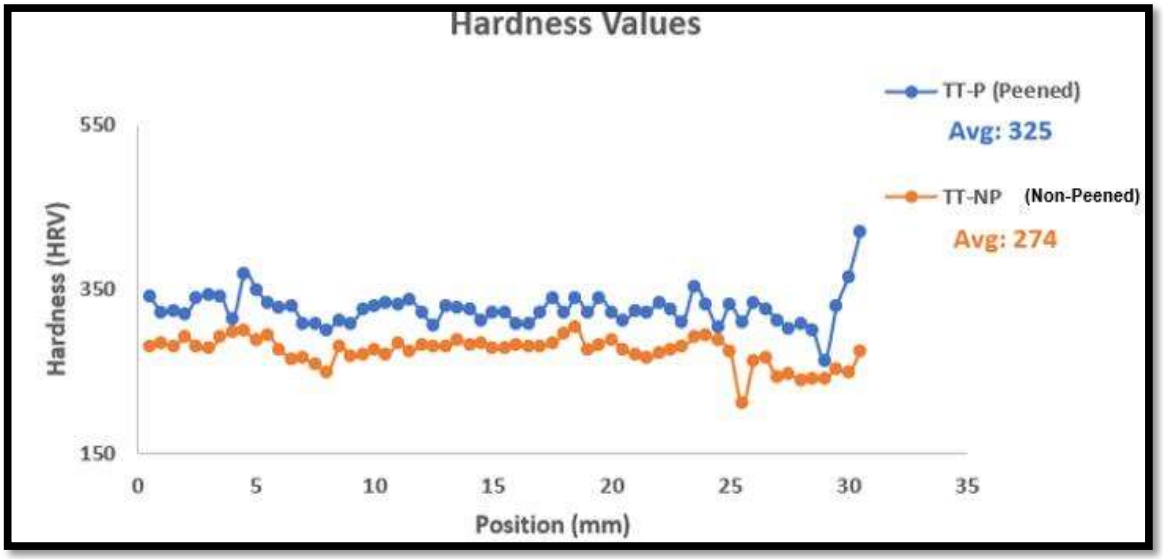


Figure 49 Hardness values for peened and non-peened IN718 WAAM samples before heat treatment

DISTRIBUTION A: Distribution approved for public release.

In Figure 50, the overlap of indents in peened line leads to a compressive layer of residual stresses which further increases the microhardness values on the surface of the top wall layer.

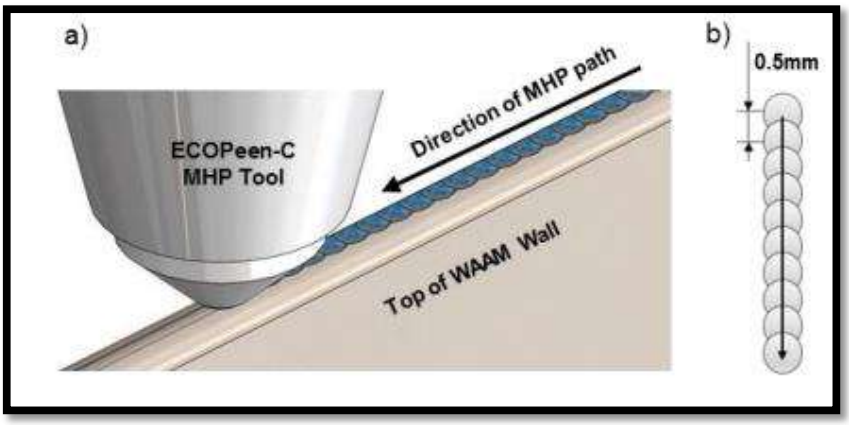


Figure 50 (a) Top layer MHP with peening line (b) Peening line for thin wall [21]

4.4.2 Comparison for peened samples before and after heat treatment process

The peened sample of IN718 WAAM deposited wall after subjected to standard heat treatment process has achieved average hardness value of 465 HRV which is approximately 43% higher than the average hardness value for the peened sample before heat treatment. Further when the microhardness test had been performed for peened sample of IN718 WAAM deposited wall subjected to modified heat treatment process the average hardness value was 527 HRV approximately 62% higher than the average hardness value for the peened sample before heat treatment as shown in the graph in Figure 51.

The Vickers hardness test has given the material response to the aging treatment and it has been found that hardening effect has been because of the precipitation of γ'' in the matrix. Further for the standard and modified heat-treated samples the precipitation of δ phase, dissolution of laves phase has improved the material response to aging. The indents started from 0.5mm position from the bottom surface of the sample with 0.5 mm increments up to 31.5 mm at the centreline which showed 4mm mid line of the throat thickness of peened sample.

DISTRIBUTION A: Distribution approved for public release.

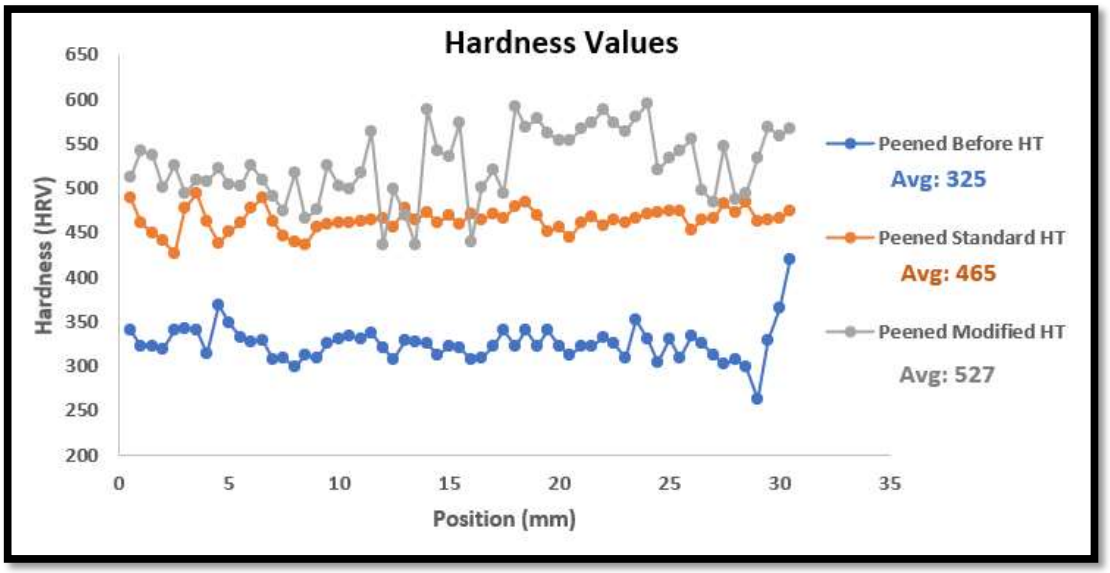


Figure 51 Hardness values for peened IN718 WAAM samples before heat treatment, standard heat treated and modified heat treated

4.4.3 Comparison for NP and P before HT and after modified HT

In Figure 52, the non-peened sample before heat treatment achieved average hardness value of 275 HRV and after modified heat treatment the hardness value increased to 87%. The heat treatment cycle increased the hardness values through precipitation hardening due to γ' and γ'' by dissolution of laves, δ phase due to less concentration of Nb.

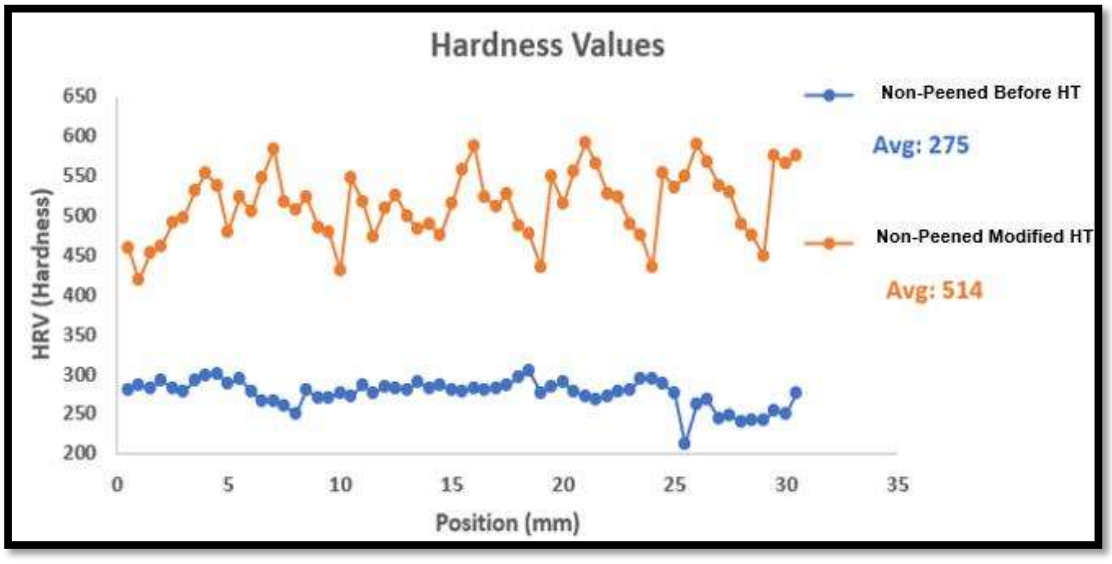


Figure 52 Hardness values for non-peened IN718 WAAM samples before heat treatment and modified heat treated

DISTRIBUTION A: Distribution approved for public release.

5. CONCLUSION

The WAAM deposited IN718 walls with inter-layer peened treatment and without inter-layer peened treatment samples under different heat treatment conditions brought to some important summarisation as follows: -

(a) The as-deposited WAAM IN718 parts have dendritic grains that contain laves phase which is because of segregation of Ti and Nb.
(b) The peening mechanism has led to the improvement in mechanical properties particularly in microhardness value because of new recrystallised β grains and further grain refinement.
(c) The standard heat treatment process led to dissolution of laves phase but the acicular δ phase has precipitated at the grain boundaries and the microhardness value is increased.
(d) The modified heat treatment based on the laves phase eutectic temperature led to further dissolution of laves phase and dendrites containing Nb and Ti rich inclusions that led to further increase of microhardness value as compared to the standard heat treatment process.

The microstructural study using SEM and optical microscopy correlated with the mechanical property performed in the form of Vickers hardness test. The WAAM processes based on the process parameters such as deposition rate affected by the feed rate and heat input led to repeated thermal cycles which can lead to residual stresses and distortion of the WAAM deposited wall. Therefore, strengthening mechanism such as peening and different heat treatment processes are required to achieve the desired mechanical properties.

6. FUTURE WORK

The future scope of this project is to conduct the tensile test for the WAAM deposited IN718 walls with inter-layer peened treatment and without inter-layer peened treatment samples and observe the significant changes in engineering stress vs strain curves and values in yield strength, ultimate tensile strength and elongation. Also, the modified heat treatment processes could be improved based on the specific application of environment based on which numerical models could be utilized based on parametric analysis for consideration of the heat treatments.

DISTRIBUTION A: Distribution approved for public release.

7. REFERENCES

1. Yilbas, B.S., Ali, H., Al-Aqeeli, N. and Karatas, C.İ.H.A.N., 2016. Laser treatment of Inconel 718 alloy and surface characteristics. *Optics & Laser Technology*, *78*, pp.153-158.

2. Muralidharan, B.G., Shankar, V. and Gill, T.P., 1996. Weldability of Inconel 718-A review.

3. Akca, E. and Gürsel, A., 2015. A review on superalloys and IN718 nickel-based INCONEL superalloy. *Periodicals of Engineering and Natural Sciences (PEN)*, *3*(1).

4. Dharmendra, C., Shakerin, S. and Mohammadi, M., 2021. Metallurgical Assessment of Additive Manufactured Nickel Aluminum Bronze-316L Stainless Steel Bimetallic Structure: Effect of Deposit Geometry on the Interfacial Characteristics and Cracking. *Journal of Materials Engineering and Performance*, *30*(12), pp.8746-8762.

5. Qi, H., Azer, M. and Ritter, A., 2009. Studies of standard heat treatment effects on microstructure and mechanical properties of laser net shape manufactured Inconel 718. *Metallurgical and Materials Transactions A*, *40*(10), pp.2410-2422.

6. Kawalkar, R., Dubey, H.K. and Lokhande, S.P., 2022. A review for advancements in standardization for additive manufacturing. *Materials Today: Proceedings*, *50*, pp.1983-1990.

7. Godec, M., Malej, S., Feizpour, D., Donik, Č., Balažic, M., Klobčar, D., Pambaguian, L., Conradi, M. and Kocijan, A., 2021. Hybrid additive manufacturing of Inconel 718 for future space applications. *Materials Characterization*, *172*, p.110842.

8. Weber, J.H., 2011. Nickel-based superalloys: alloying methods and thermomechanical processing. *Encyclopedia of Materials: Science and Technology*, pp.6149-6153.

9. Kumar, S.P., Elangovan, S., Mohanraj, R. and Ramakrishna, J.R., 2021. A review on properties of Inconel 625 and Inconel 718 fabricated using direct energy deposition. *Materials Today: Proceedings*, *46*, pp.7892-7906.

10. Belan, J., 2016. GCP and TCP phases presented in nickel-base superalloys. *Materials Today: Proceedings*, *3*(4), pp.936-941.

11. Anderson, M., Thielin, A.L., Bridier, F., Bocher, P. and Savoie, J., 2017. δ Phase precipitation in Inconel 718 and associated mechanical properties. *Materials Science and Engineering: A*, *679*, pp.48-55.

12. Adams, B.L., 2004. ASM Handbook of Metalography and Micorestructures. ASM International, Estados Unidos de América.

13. Williams, S.W. and Martina, F., 2015. Wire+ air additive manufacture. *Mater Sci & Tech, IoM, DOI*.

14. Xu, X., Ding, J., Ganguly, S., Diao, C. and Williams, S., 2018. Oxide accumulation effects on wire+ arc layer-by-layer additive manufacture process. *Journal of Materials Processing Technology*, *252*, pp.739-750.

DISTRIBUTION A: Distribution approved for public release.

15. Kumar, N., Bhavsar, H., Mahesh, P.V.S., Srivastava, A.K., Bora, B.J., Saxena, A. and Dixit, A.R., 2022. Wire Arc Additive Manufacturing–A revolutionary method in additive manufacturing. *Materials Chemistry and Physics*, p.126144.

16. Chi, J., Cai, Z., Wan, Z., Zhang, H., Chen, Z., Li, L., Li, Y., Peng, P. and Guo, W., 2020. Effects of heat treatment combined with laser shock peening on wire and arc additive manufactured Ti17 titanium alloy: Microstructures, residual stress and mechanical properties. *Surface and Coatings Technology*, *396*, p.125908.

17. Hönnige, J.R., Colegrove, P. and Williams, S., 2017. Improvement of microstructure and mechanical properties in wire+ arc additively manufactured Ti-6Al-4V with machine hammer peening. *Procedia engineering*, *216*, pp.8-17.

18. Wang, Z.D., Sun, G.F., Lu, Y., Chen, M.Z., Bi, K.D. and Ni, Z.H., 2020. Microstructural characterization and mechanical behavior of ultrasonic impact peened and laser shock peened AISI 316L stainless steel. *Surface and Coatings Technology*, *385*, p.125403.

19. Maleki, E., Bagherifard, S., Bandini, M. and Guagliano, M., 2021. Surface post-treatments for metal additive manufacturing: Progress, challenges, and opportunities. *Additive Manufacturing*, *37*, p.101619.

20. Hönnige, J.R., Davis, A.E., Ho, A., Kennedy, J.R., Neto, L., Prangnell, P. and Williams, S., 2020. The effectiveness of grain refinement by machine hammer peening in high deposition rate wire-arc AM Ti-6Al-4V. *Metallurgical and Materials Transactions A*, *51*(7), pp.3692-3703.

21. Neto, L., Williams, S., Ding, J., Hönnige, J. and Martina, F., 2019, September. Mechanical properties enhancement of additive manufactured Ti-6Al-4V by machine hammer peening. In *International Conference on Advanced Surface Enhancement* (pp. 121-132). Springer, Singapore.

22. Kindermann, R.M., Roy, M.J., Morana, R. and Prangnell, P.B., 2020. Process response of Inconel 718 to wire+ arc additive manufacturing with cold metal transfer. *Materials & Design*, *195*, p.109031.

23. Picasso, A.C., Lanz, C.A., Lissarrague, M.S. and Garófoli, A.D., 2016. Microstructure Evolution of a Nickel-Base Alloy Resistant to High Temperature during Aging. *Journal of Minerals and Materials Characterization and Engineering*, *4*(1), pp.48-61.

24. Xu, X., Ganguly, S., Ding, J., Seow, C.E. and Williams, S., 2018. Enhancing mechanical properties of wire+ arc additively manufactured INCONEL 718 superalloy through in-process thermomechanical processing. *Materials & Design*, *160*, pp.1042-1051.

25. Xu, J., Huang, Z. and Jiang, L., 2017. Effect of heat treatment on low cycle fatigue of IN718 superalloy at the elevated temperatures. *Materials Science and Engineering: A*, *690*, pp.137-145.

DISTRIBUTION A: Distribution approved for public release.

26. Rao, G.A., Srinivas, M. and Sarma, D.S., 2004. Effect of solution treatment temperature on microstructure and mechanical properties of hot isostatically pressed superalloy Inconel* 718. Materials science and technology, 20(9), pp.1161-1170.

27. Tanvir, A.N.M., Ahsan, M.D., Seo, G., Kim, J.D., Ji, C., Bates, B., Lee, Y. and Kim, D.B., 2020. Heat treatment effects on Inconel 625 components fabricated by wire+ arc additively manufacturing (WAAM)—part 2: mechanical properties. *The International Journal of Advanced Manufacturing Technology*, *110*(7), pp.1709-1721.

28. Rafiei, M., Mirzadeh, H., Malekan, M. and Sohrabi, M.J., 2019. Homogenization kinetics of a typical nickel-based superalloy. *Journal of Alloys and Compounds*, *793*, pp.277-282.

29. Seow, W. and Inconel, A.A.M., 718: Effect of post-deposition heat treatments on microstructure and tensile properties. *Mater. Des*, (183).

DISTRIBUTION A: Distribution approved for public release.

Appendix IV: Impact of solutionising temperature on hardness response of as-deposited of Rene 41

DISTRIBUTION A: Distribution approved for public release.



MUHAMMET AKYUZ

ADDITIVE MANUFACTURING OF A HEAT RESISTANT NICKEL-BASED SUPERALLOY

SCHOOL OF AEROSPACE, TRANSPORT AND MANUFACTURING
Aerospace Manufacturing

MSc
Academic Year: 2021 - 2022

Supervisor: SUPRIYO GANGULY
Associate Supervisor: KULADEEP RAJAMUDILI
August 2022

DISTRIBUTION A: Distribution approved for public release.

DISTRIBUTION A: Distribution approved for public release.



SCHOOL OF AEROSPACE, TRANSPORT AND MANUFACTURING
Aerospace Manufacturing

MSc

Academic Year 2021 - 2022

MUHAMMET AKYUZ

Additive Manufacturing of a Heat Resistant Nickel-Based Superalloy

Supervisor: SUPRIYO GANGULY
Associate Supervisor: KULADEEP RAJAMUDILI
August 2022

This thesis is submitted in partial fulfilment of the requirements for the degree of Master of Science

© Cranfield University 2022. All rights reserved. No part of this publication may be reproduced without the written permission of the copyright owner.

DISTRIBUTION A: Distribution approved for public release.

DISTRIBUTION A: Distribution approved for public release.

ABSTRACT

Nickel-based superalloy Rene 41, which can be precipitation hardened by heat treatment, was produced with Plasma Arc Welding (PAW) Based WAAM. In order to improve the mechanical properties after WAAM deposition, it was aimed to observe the effects of heat treatments: These are, Standard Heat treatment for Rene 41 wrought alloys 1065 °C which is sub solvus temperature of γ′ and Modified Heat treatment for Rene 41, 1200 °C which is super-solvus temperature of γ′. After solutionising heat treatments, the material was held for 16 hours in order to increase the strength of the material by forming precipitates at 760 °C. In order to examine the effects of applied heat treatments on microstructure and mechanical properties, Vickers hardness test and LOM, SEM and EDS analyses were performed on the cross-sectional areas in 3 different axes, which are Build Direction, Wall Axis and Through Thickness. In the as deposited wall sample, it was observed that the columnar dendritic structures grew epitaxially along the building direction. Mo and Ti alloying elements showed segregation behaviour in the microstructure. Contrary to the as-deposited wall, discreted carbide distribution was observed at the grain boundaries and interdendritic region after heat treatments. In the hardness values, an increase of 9% in standard heat treatment and 4% in the recommended modified heat treatment was observed compared to the as deposited wall.

Keywords:

AM, WAAM, Plasma Arc Welding, DED, Superalloy, Rene 41, Heat Treatment,

DISTRIBUTION A: Distribution approved for public release.

DISTRIBUTION A: Distribution approved for public release.

ACKNOWLEDGEMENTS

First of all, I would like to acknowledge and deepest thanks to my supervisors Dr Supriyo Ganguly and Dr Kuladeep Rajamudili who made this project possible. Their guidance, support and insightful comments have always motivated me in that experience.

I would like to thank Cranfield University in that journey. I would also like to my warmest thanks to Emma German, Nisar Shah, Steve Pop, Tracey Roberts, Kristopher Bramley, Christine Chalk, Caghan Tuncer, and all WELPC staff for their supports in completing this project.

I would like to express my warmest thanks to my family and friends who always believe me. It is impossible to extend enough thanks to them who gave me the support on toughest time.

Finally, I would like to express my deepest gratitude and respect to the Republic of Türkiye and the Ministry of National Education for giving me the opportunity and funding to study this education.

DISTRIBUTION A: Distribution approved for public release.

DISTRIBUTION A: Distribution approved for public release.

TABLE OF CONTENTS

ABSTRACT i
ACKNOWLEDGEMENTS iii
LIST OF FIGURES vi
LIST OF TABLES viii
LIST OF EQUATIONS ix
LIST OF ABBREVIATIONS x
1 INTRODUCTION 1
1.1 Background 1
1.2 Aim and Objectives 2
2 LITERATURE REVIEW 3
2.1 Additive Manufacturing (AM) 3
2.2 Wire Arc Additive Manufacturing (WAAM) 5
2.3 Material 6
2.3.1 Nickel-Based Superalloys 6
2.3.2 Rene 41 8
2.3.3 Issues of Rene 41 9
2.4 Heat Treatment 10
2.4.1 Proposed for Modified Heat Treatment 12
3 METHODOLOGY 15
3.1 WAAM of Rene 41 15
3.2 Post Deposition Heat Treatment 19
3.3 Metallographic Preparation and Analyses 21
3.4 Microhardness Test 22
4 Results and Discussion 25
4.1 As-Deposited Microstructure 25
4.2 Characterisation of Wire Sample 29
4.3 Segregations of Rene41's alloying element in WAAM 30
4.4 Effect of Post Deposition Heat Treatments for Rene 41 WAAM 33
4.4.1 Standard Heat Treatment Effect 33
4.4.2 Modified Heat Treatment Effect 35
4.5 Hardness Results 37
5 Conclusions 43
6 Future Work 45
REFERENCES 47
APPENDICES 51

DISTRIBUTION A: Distribution approved for public release.

LIST OF FIGURES

Figure 1 Additive Manufacturing Market Size (2014-2017) 3

Figure 2 Weldability Assessment of Nickel-Based Superalloys..... 10

Figure 3 Schematic Diagram of Precipitation Hardening..... 11

Figure 4 Experimental Setup of WAAM..... 16

Figure 5 Schematic Diagram of Deposition..... 17

Figure 6 Plasma WAAM Deposition 18

Figure 7 Deposited Wall of Rene 41..... 18

Figure 8 Height of Deposited Wall..... 19

Figure 9 Standard Heat Treatment Cycle for Rene 41 20

Figure 10 Modified Heat Treatment Cycle for Rene 41 21

Figure 11 Hardness Test Direction..... 23

Figure 12 Microstructures of As-deposited Wall: (a) TT cross-section, (b) WA cross-section 25

Figure 13 LOM Image of BD Cross-section..... 26

Figure 14 Sem Images of As Deposited Wall: (a) TT Cross-Section, (b) WA Cross-Section..... 27

Figure 15 SEM Image of As-Deposited Wall, BD Cross-Section..... 28

Figure 16 Micro Images of Wire: (a) LOM Image, (b) SEM Image 29

Figure 17 SEM Image of Wire Sample..... 30

Figure 18 K Factor Constant Values 32

Figure 19 SEM Image After Standard Heat Treatment: (a) EDS Analysis, (b) Map Spectrum 33

Figure 20 EDS Mapping After Standard Heat Treatment: (a) General, (b) Mo, (c) Ti, (d) C..... 35

Figure 21 SEM Image After Modified Heat Treatment: (a) EDS Analysis, (b) Map Spectrum 36

Figure 22 EDS Mapping After Modified Heat Treatment: (a) General, (b) Mo, (c) Ti, (d) C..... 37

Figure 23 Hardness Results of As-deposited Wall on WA Cross-Section (from bottom to top layers)..... 38

DISTRIBUTION A: Distribution approved for public release.

Figure 24 Comparison of Hardness Test Results for 3 Conditions on WA Cross Section (from bottom to top layers)..... 39

Figure 25 Comparison of Hardness Test Results for 3 Conditions on BD Cross Section..... 40

DISTRIBUTION A: Distribution approved for public release.

LIST OF TABLES

Table 1 Additive Manufacturing Methods 4

Table 2 DED Methods Comparison 6

Table 3 Phases Observed in Nickel-Based Superalloys 7

Table 4 Composition of Rene 41 (wt.%) [16] 8

Table 5 Activation Energy, Diffusion Coefficient of Mo and Ti in Ni, Atomic Radiuses 13

Table 6 Welding Parameters for Deposition 15

Table 7 Vickers Hardness Test Parameters for Rene 41 22

Table 8 EDS Analysis of As Deposited Wall 28

Table 9 EDS Analysis of Rene 41 Wire 30

Table 10 Comparison of EDS Analysis 31

Table 11 Compositions Ratio of Inter-dendritic Areas to Wire 32

Table 12 EDS Results After Standard Heat Treatment 34

Table 13 EDS Results After Modified Heat Treatment 36

DISTRIBUTION A: Distribution approved for public release.

LIST OF EQUATIONS

$\boldsymbol{D = D0\exp(-QRT)}$ Equation 1 13

$\boldsymbol{x = Dt}$ Equation 2 13

DISTRIBUTION A: Distribution approved for public release.

LIST OF ABBREVIATIONS

IT	Information Technology

DISTRIBUTION A: Distribution approved for public release.

1 INTRODUCTION

1.1 Background

Additive Manufacturing (AM) occupies an important place in the manufacturing industry as it offers advantages such as easier production of complex geometries, design flexibility, less waste material, and faster production times. In addition, it provides a great deal of savings and advantages in the industry due to lower costs and less energy consumption. In other words, it is a cost-effective approach. Among the additive manufacturing methods, Wire Arc Additive Manufacturing (WAAM) allows the production of parts in larger sizes and near net shapes compared to other manufacturing methods. During wire arc additive manufacturing, parts in the desired geometry are deposited layer by layer by melting the fed wire on a substrate under an electric arc. This deposition process is controlled by industrial robots or Computer Numerical Control (CNC) systems. With the advantages of a high deposition rate and lower equipment costs, its usage area in the industry is increasing day by day.

Besides, WAAM has different welding technologies, which are Gas Metal Arc Welding (GMAW), Gas Tungsten Arc Welding (GTAW) and Plasma Arc Welding (PAW). Among them, PAW enables more efficient and higher precision production because it has the highest arc density, and the heat input is more controllable. Therefore, in this study, the production of superalloys with PAW technology by wire arc additive manufacturing method was chosen. Superalloys are also used in aviation, marine and petroleum industries, as they show high mechanical properties and strength against the loads, they are exposed to at high service temperatures. In this study, Rene 41 was chosen because of its material strength under load at high temperatures. Rene 41 has high oxidation resistance under high temperatures as well as high strength and creep-rupture resistance. Because of these properties, Rene 41 is a superalloy used in turbine blades, especially in aircraft engines. In such areas where Rene 41 alloy should be used, it obtains its high mechanical properties as a result of precipitation hardening application.

DISTRIBUTION A: Distribution approved for public release.

1.2 Aim and Objectives

The main aim of this research is to examine the effects of WAAM on Rene 41 and to increase the mechanical properties of the wall deposited with the WAAM method by applying post-deposition heat treatment. It is aimed to determine the conditions of the heat treatment applied after deposition by the Rene 41 material structure to improve the material strength with the desired properties. To obtain this aim, the following objectives were determined to examine the effects of WAAM on Rene 41 and evaluate the material properties obtained as a result of heat treatment application and expected to be improved.

- It was aimed to observe the effects of 3 different parameters, which are as-deposited, standard heat treatment and modified heat treatment, on microstructure and mechanical properties.
- It is aimed to compare the effects of the microstructural analysis and mechanical test results to be obtained under post-deposition heat treatments and as deposited conditions on three different axes: Build Direction (BD), Wall Axis (WA) and Through Thickness (TT).

DISTRIBUTION A: Distribution approved for public release.

2 LITERATURE REVIEW

2.1 Additive Manufacturing (AM)

Additive manufacturing, unlike traditional production processes, offers numerous conveniences in producing the part in the desired geometry. Due to the advantages, it provides, such as the production of complex parts, low cost and less material waste, the rate of use in the industry is increasing. [1] In addition, Additive manufacturing technology can reduce the cost of alloy parts, which are expensive to produce for industries such as aerospace and marine, by up to 50%. Therefore, it provides significant savings in the production of very large-scale parts. Production is achieved by solidifying each layer after depositing on the previous layer and repeating this process until the desired geometry is reached. This way, net shape parts can be produced without needing another process. [2]

Due to the advantages, it provides in the production of parts, unlike subtractive manufacturing, the importance of Metal additive manufacturing is increasing. The market share of Metal additive manufacturing is increasing day by day, not only in aerospace but also in various advanced industries such as automotive, medical, oil and gas, due to features such as the production of lighter products and advanced production capability. [3] Figure 1 shows the Additive Manufacturing market size between 2014 and 2027. [4]

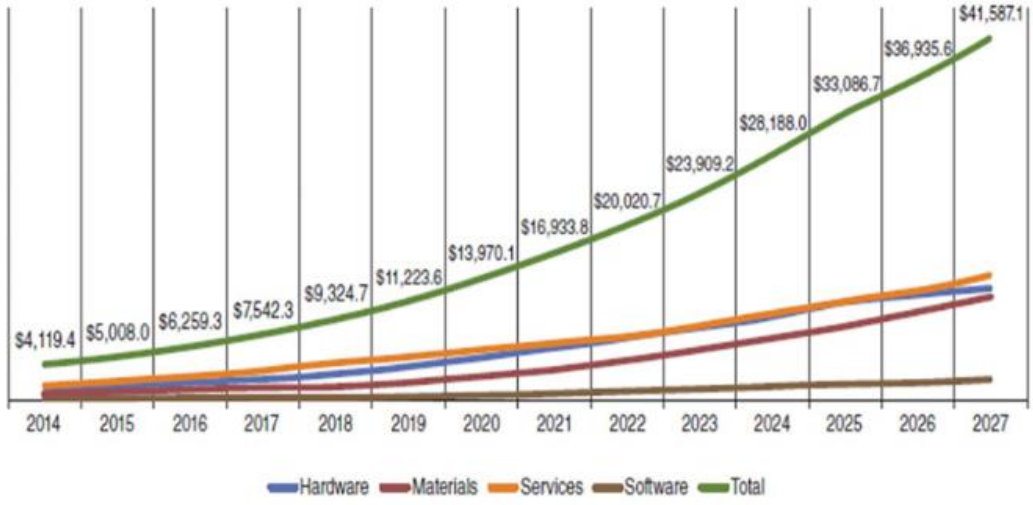


Figure 1 Additive Manufacturing Market Size (2014-2017)

DISTRIBUTION A: Distribution approved for public release.

Additive Manufacturing has more than one production method in the industry. These can be examined under seven main headings: directed energy deposition, binder jetting, material extrusion, material jetting, powder bed fusion, sheet lamination and vat photo-polymerization. A detailed explanation of this is given in Table 1. Parts can be produced on a larger scale with the Directed Energy Deposition production method, one of these production techniques. This production technique is a production method that is formed by melting the material using thermal energy, first on a substrate, and then by depositing the layers on top of each other with heat energy. [5]

Table 1 Additive Manufacturing Methods

Binder Jetting	A liquid bonding agent is deposited to join Powder materials.
Directed Energy Deposition	Thermal energy is used to fuse materials by melting as deposited.
Material Extrusion	Material is selectively dispensed through a nozzle or orifice.
Material Jetting	Droplets of build material are selectively deposited.
Powder Bed Fusion	Thermal energy selectively fuses regions of a powder bed.
Sheet Lamination	Sheets of material are bonded to form an object.
Vat Photo-Polymerization	Liquid photopolymer is cured by light-activated polymerization.

In Directed Energy Deposition, a laser, electron beam or electrical arc is used as an energy source. With this energy, the powder material or the fed wire is melted, and the deposition process is carried out. In contrast to other AM processes, the DED production method is easier to produce more complex shapes. On the other hand, parts produced with WAAM realized with electrical or plasma arc can be built on a larger scale compared to other DED energy sources. [6]

DISTRIBUTION A: Distribution approved for public release.

2.2 Wire Arc Additive Manufacturing (WAAM)

The WAAM mechanism is used to produce 3D parts by melting the wire fed from the wire spool with the thermal energy generated by the plasma arc. This method was first used in 1920. This method provides a significant advantage compared to other production methods, as equipment costs and waste materials are low. Depending on the geometrical shape of the part to be produced, molten metal drops, which are formed by melting the wire, are obtained by depositing on a continuous layer below. This method provides numerous advantages over other methods due to high-speed production, no material waste, low cost, and more effective fusion between layers. However, in addition to these, deformations caused by the effect of heat during the production of the part, the surface quality of the final product not being as good as in traditional methods and the residual stress formed in part are the main problems of the WAAM process. It is also important to choose the necessary process parameters such as heat input, consumables, path shape and post-deposition heat treatment for deposition to minimize defects. [7,8]

In addition, with the developing technology, the effective use of capital, resources and time in production comes to the fore. Additive manufacturing is one of the most useful production methods for creating 3D structures in recent years. No moulds or additional tools are required to produce structures formed by depositing layers on each other. In addition, there is no need for processes such as assembly since complex parts are produced as a whole in one piece. In this sense, in the WAAM method, more controllable microstructures can be obtained more quickly and efficiently than in other production methods. The comparison of WAAM with other DED methods is also indicated in

Table 2. [9]

DISTRIBUTION A: Distribution approved for public release.

Table 2 DED Methods Comparison

Parameter	Laser Beam	Electron Beam	Welding Arc
Energy Source	Photon	Electron	Metallic Ion
Heat Source	Electromagnetic Wave	Kinetic Energy	Electric Arc
Energy Density	10^6 W/mm^2	10^8 W/mm^2	10^6-10^8 W/mm^2
Energy Efficiency	Least	Intermediate	Excellent
Deposition Rate	150-200 gm/hr	600-800 gm/hr	2-4 kg/hr
Vacuum	Not Required	Required	Not Required

2.3 Material

2.3.1 Nickel-Based Superalloys

Nickel-based superalloys have excellent mechanical properties, high corrosion and oxidation resistance, and high resistance to yielding and fatigue when subjected to high-temperature loading. Because of these properties, it is used in jet engines and gas turbines. [10] Nickel-based Superalloys get their mechanical properties from a heat treatment called precipitation hardening. In precipitation hardening, the gamma prime (γ′) phase is precipitated in the microstructure to increase the material strength. [11] In addition, the carbide distribution formed in the microstructure is vital for material strength. Carbides in the form of $M_{23}C_6$ play an active role in improving the creep strength as well as increasing the tensile strength at high temperatures. Besides, coarse MC-type carbides dispersed in some matrix may cause brittleness in the material structure. For all these reasons, it is imperative to control the carbide distribution and morphology in the microstructure. This shows that the optimization of the heat treatments to be applied should be done correctly. [12]

DISTRIBUTION A: Distribution approved for public release.

Nickel-based superalloys have a wide variety of microstructures, intermetallic phases, and morphologies because they contain high proportions of multiple alloying elements. Table 3 indicates the phase structures formed by the alloying elements in superalloys. [13]

Table 3 Phases Observed in Nickel-Based Superalloys

Matrix Phase		
γ (FCC)		
Solid Solution Strengtheners		
Co, Cr, Mo, W, (Fe, Ru, Re)		
Precipitate Phases		
γ′ - $Ni_3(Al,Ti)$ ($L1_2$)	**γ″ - Ni_3Nb (BCT)**	
Al, Ti	*Nb*	
Carbides		
MC	**$M_{23}C_6$**	**M_6C**
W, Mo, Ti, Ta, Nb, Hf	*W, Mo, Cr*	*Mo, W, Nb*

The microstructure of superalloys is γ matrix with face-centered cubic lattice structure with secondary phases. In addition, due to the high solubility of nickel, the matrix phase contains large proportions of alloying elements. Cr, Co, Mo, W, Fe, Ru, and Re alloying elements help to strengthen the matrix's solid solution by dissolving them in the matrix phase. [13] When aluminium and titanium compositions in the microstructure reach saturation in the matrix phase, they form γ′ precipitates due to their similar lattice structures. γ′ precipitates can be found in the structure of spherical, cubic and cuboidal morphologies. These shapes and dimensions are the main factors determining the material's strength. Heat treatments can change the precipitates' sizes, distribution, and morphological structures. [14]

DISTRIBUTION A: Distribution approved for public release.

Another structure that increases the strength of superalloys is carbide formations. Various carbide structures can be observed according to the superalloy's composition, solidification rate and production method. The most common carbide structures are mainly MC and $M_{23}C_6$ carbide types. Here, the letter M represents metal atoms such as Mo, Ti, Cr, W, Nb, Ta, and Hf. Due to the separation of C during the solidification process of superalloys, MC-type carbide formation in the liquid phase was observed in the interdendritic region. [15]

2.3.2 Rene 41

The heat-resistant super alloy Rene 41 was developed in the 1950's to show high strength at high temperatures. Table 4 shows the composition of Rene 41. Due to its high tensile strength, creep-rupture resistance, and excellent oxidation resistance between temperatures of 650-900 °C, it is frequently used in aircraft engines where high strength is required for high-temperature services. Rene 41 takes these properties due to precipitation hardening heat treatment. Increasing strength with this heat treatment depends on the morphology of the phases in the microstructure, the segregation state and the carbides deposited at the grain boundaries. [16]

Table 4 Composition of Rene 41 (wt.%) [16]

Ni	Cr	Co	Mo	Fe	Ti	Al	Si	Mn	C
Bal.	18-20	10-12	9-10.5	≤5	3-3.5	1.4-1.8	≤0.5	≤0.5	0.06-0.12

As major alloying elements, Rene 41 contains Mo, Cr, Co, Fe, Ti, and Al. Of these alloying elements, Mo, Cr, Co, Fe and Ni are present in the structure as solid solutions and provide material strength by forming lattice strain. Al and Ti form the γ′ precipitate phase. In addition, Cobalt promotes γ′ precipitate formation by lowering the solubility of Al and Ti in Nickel. [17]

DISTRIBUTION A: Distribution approved for public release.

2.3.3 Issues of Rene 41

The two main problems of WAAM are residual stress after deposition and undesired microstructure. While residual stress causes deformation and structural defects in the part, the microstructure formed after deposition prevents the material's mechanical properties gained by the standard heat treatments applied for wrought alloys. Furthermore, the WAAM process causes columnar grain growth and anisotropy in grain structure. Designed heat treatments can eliminate this undesirable microstructure. [18,19]

Although the γ′ phase in the microstructure increases the material strength, Rene 41 has fair weldability due to the aluminium and titanium elements in the composition. [11] The weldability assessment of nickel-based superalloys is shown in Figure 2 Weldability Assessment of Nickel-Based Superalloys. During welding, strain crack formation is observed in the heat-affected zone and base metal due to the content of this alloy. For this reason, Rene 41 manufacturing with new production methods is significant to overcome these problems. [20] Due to its strength under high temperature, the production of Rene 41 alloy has been evaluated with Laser Melting Deposition and Laser Powder Bed Fusion, additive manufacturing methods. The recommended standard heat treatment was applied for the wrought alloy of Rene 41 to eliminate post-production errors. The effects of Post Deposition Heat Treatments were investigated. However, it was determined that the standard heat treatment did not eliminate the observed errors as desired. [16,20] For this reason, it is desired to see the effect of the Standard Heat treatment and the recommended Modified Heat Treatment on WAAM. It is aimed to eliminate microstructural defects such as segregation after WAAM, dendrite arm spacing distance and coarsening in γ′ precipitates after PDHTs are applied.

DISTRIBUTION A: Distribution approved for public release.

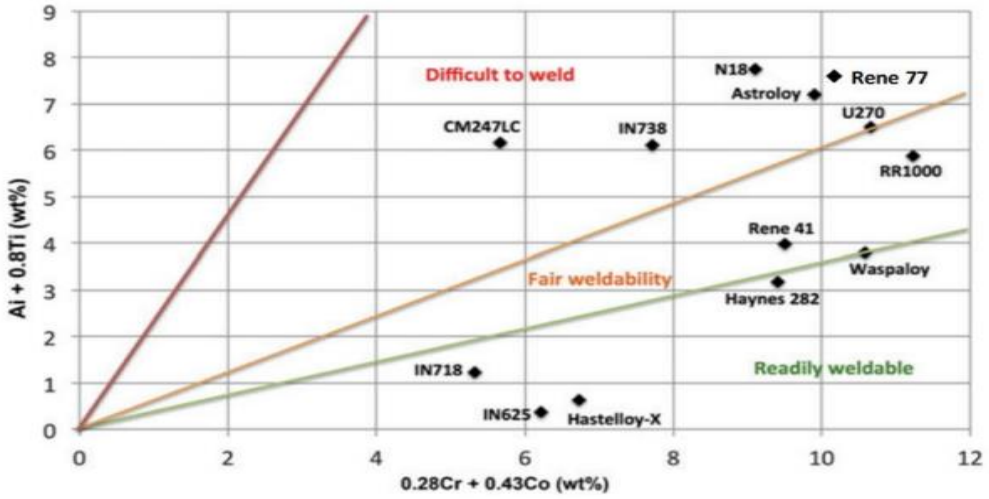


Figure 2 Weldability Assessment of Nickel-Based Superalloys

2.4 Heat Treatment

Nickel-based superalloys have multiple strengthening methods. In general, grain boundaries, dislocation, solid solution, and precipitation strengthening are used to increase the strength of precipitation-hardenable alloys.

Heat treatments are a series of heating and cooling processes applied to improve the strength of materials. The strength and mechanical properties of metallic materials that can be subjected to precipitation hardening heat treatment can be improved by this method. Rene 41 alloy is a precipitation hardening alloy. It is heat treated to obtain γ′ and carbide precipitates at grain boundaries in the matrix. This heat treatment process consists of two stages: solution annealing and precipitation hardening. This process is shown in Figure 3 Schematic Diagram of Precipitation Hardening. Solution annealing is applied to the material by heating it to a temperature where the segregations in the structure can be removed, and a homogeneous structure is obtained. Then, the temperature at which precipitation can form is determined according to the alloying elements in the material, and a second heating and cooling process is applied to obtain the precipitates in the structure [21]

DISTRIBUTION A: Distribution approved for public release.

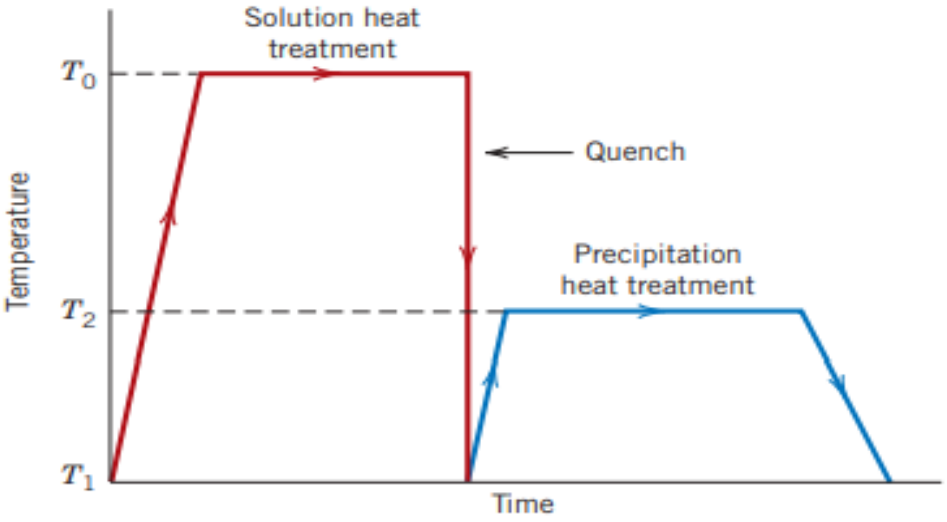


Figure 3 Schematic Diagram of Precipitation Hardening

Rene alloys are used at high service temperatures and have a face-centered cubic crystal structure. Its microstructure consists of the γ matrix, the γ′ phase precipitated in the γ matrix, and carbides deposited predominantly at the grain boundaries. The most critical effect in increasing the mechanical properties is the precipitation of the γ′ phase in the microstructure at the correct rate and size. The reason Rene alloys have good high-temperature resistance and good mechanical properties in the material structure depends on the volume fraction of the γ′ phase in the microstructure, the precipitate size, and its distribution in the structure. γ′ precipitates of up to 70% greatly support the improvement of the mechanical properties of nickel-based superalloys. In addition, sufficient carbon elements in the chemical composition ensure carbide formation. The proper distribution of carbides in the structure and grain boundaries is prominent in increasing the high-temperature resistance. In some cases, carbide formation can also cause crack formation. The effect of carbides on material properties depends on their geometric shape, size, and distribution. [22]

DISTRIBUTION A: Distribution approved for public release.

Rene 41's heat treatment cycle applied for wrought alloys, 4 hours waiting at 1065 °C and air cooling, then 16 hours at 760 °C for precipitation hardening, then air cooling process has been tested on two different Additive manufacturing methods, Laser melting deposition (LMD) and Laser powder bed fusion (LPBF). [20,22] As a result of the LMD process of Rene 41, it was observed that the gamma prime phase was aligned and combined, causing a decrease in material strength. [16] In the LBPF process, it was determined that undissolved carbides and gamma prime precipitates accumulated in the grain boundaries after standard heat treatment and prevented recrystallization. [20]

The heat treatment cycles must be chosen correctly to obtain the residual stresses, morphology, and desired mechanical properties after production. Generally, homogenisation, solutionizing and ageing heat treatments are applied to change the microstructure of the materials. Homogenization heat treatment is applied to reduce segregations in the microstructure and to make the microfiber more homogeneous. In order to apply precipitation hardening, as indicated in Figure 3 Schematic Diagram of Precipitation Hardening, the material is first heated to 1040-1230 °C to remove the precipitates formed during solidification. The material must then be rapidly cooled to prevent the formation of new precipitates. The material is then aged below the γ′ solvus temperature (1071-1082 °C) to form the γ′ precipitate phase required to increase its strength. [23]

2.4.1 Proposed for Modified Heat Treatment

The main phases that increase the strength in superalloys are gamma prime, which has a face-centred cubic lattice structure, and double gamma prime, which has a body-centred tetragonal lattice structure. Molybdenum, a refractory element in both phases, increases the strength of the solid solution in superalloys. It also affects diffusivity in both phases, increases yield strength and prevents precipitate coarsening. Therefore, molybdenum is a very crucial element in Rene 41, with an atomic mass of 95.95 u and an Atomic Radius of 1.45 Å, the composition of molybdenum in Rene 41 is between 9-10.5 %wt. In contrast, Nickel's Atomic Radius is 1.35 Å. [24] Due to the considerable atomic weight and

DISTRIBUTION A: Distribution approved for public release.

the significant difference between the atomic radius and nickel in the superalloy, it was deemed appropriate to determine the heat treatment parameters of the Molybdenum element according to the diffusion values in the microstructure. In Table 5 Activation Energy, Diffusion Coefficient of Mo and Ti in Ni, Atomic Radiuses, Activation Energy, Diffusion Coefficient of Molybdenum and Titanium in Nickel, and Atomic Radiuses of Mo and Ti are shown.

Table 5 Activation Energy, Diffusion Coefficient of Mo and Ti in Ni, Atomic Radiuses

Element	Q *(kj/mol)*	D_0 *(m^2/s)*	Atomic Radius *(Å)*
Mo	288.15	300 x 10^6	1.45
Ti	257	86 x 10^6	1.40

Considering the solvus temperature of the gamma prime phase (1071-1082 °C) and the calculation made according to the diffusivity equation specified in Equation 1 and diffusion distance showed in Equation 2, the solutionizing temperature of the precipitation hardening heat treatment was determined as 1200 °C. To compare the results with the standard heat treatment data applied for Rene 41's wrought alloys, the holding time was not changed and was applied as 4 hours. Accordingly, after deposition, the material applied for Rene 41's wrought alloys was kept at 1065 °C, the sub solvus of gamma prime temperature, for 4 hours, and then air cooling was performed. In addition, the material, which was determined as the temperature of the super solvus of gamma prime phase for the modified temperature, was held at 1200 °C for 4 hours and air cooling was applied.

$$\boldsymbol{D = D_0 \exp(-\frac{Q}{RT})} \qquad \textbf{Equation 1}$$

$$\boldsymbol{x = \sqrt{Dt}} \qquad \textbf{Equation 2}$$

DISTRIBUTION A: Distribution approved for public release.

DISTRIBUTION A: Distribution approved for public release.

3 METHODOLOGY

3.1 WAAM of Rene 41

In the WAAM Process of Rene 41, FANUC's 6-axis ARC Mate 120iB robot was used for the deposition. A plasma water-cooled welding torch, wire feeder, a rotating rotor for double side deposition and a water-cooled TPS brand welding camera for observing the process is connected to the robot for production. The composition of Rene 41 wire is shown in Table 4. Deposition commercially available 1 mm diameter Rene 41 wire filler was carried out on Inconel 718 substrate under an argon atmosphere, in an inert indoor environment with less than 700 ppm oxygen. The oxygen ratio was observed during the experiment with an oxygen analyzer device. The experimental setup is shown in detail in Figure 4. The dimensions of the wall produced as double side and oscillation path were deposited on both sides as 250 mm in length, 55 mm in height, and 16 mm in thickness. A schematic diagram of the process is shown in figure u. Welding parameters of the process are indicated in Table 6.

Table 6 Welding Parameters for Deposition

Parameters	Values
Wire Ø	1 mm
Wire Feed Speed	2 m/min
Travel Speed	6 mm/sec
Current	180 A
Stand of Distance	8 mm

DISTRIBUTION A: Distribution approved for public release.

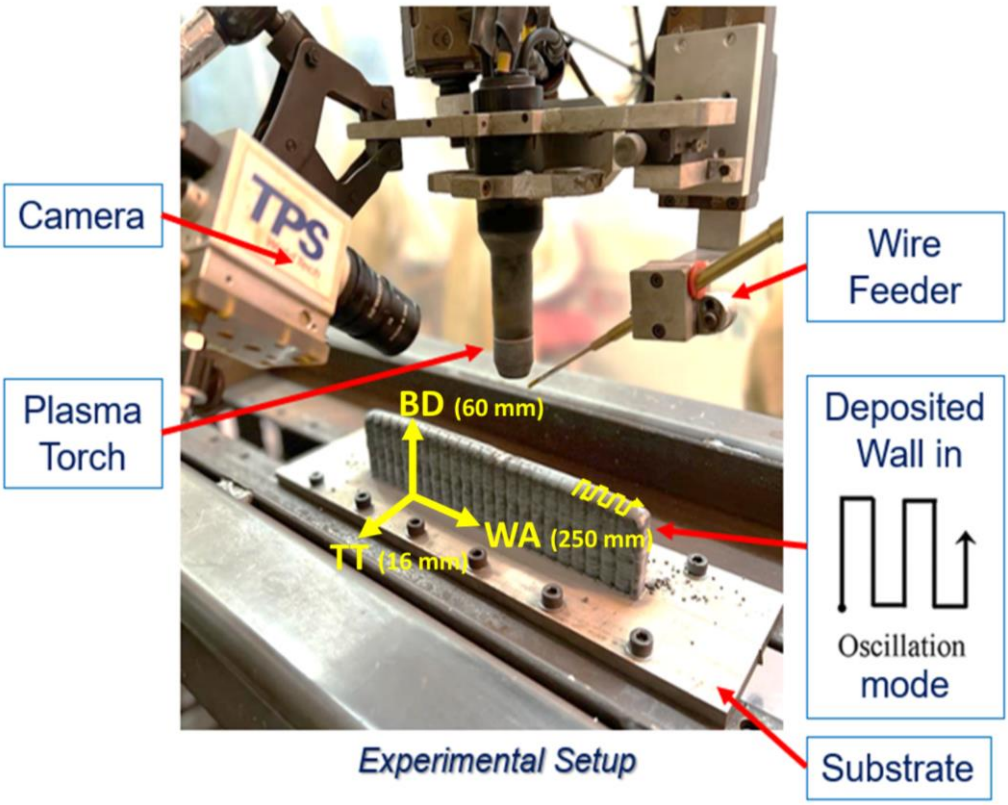


Figure 4 Experimental Setup of WAAM

Rene 41 wire melted to weld pool with PAW, and after the first layer was deposited on the substrate, the next layers were deposited on the pre-deposited layers. The direction of deposition was in the opposite direction of the previous layer deposition. After the layer deposition for Side A, the welding table is turned and deposited for Side B. Welding table rotates again, and deposition is made for side A in the opposite direction of the previous layer. A dwell time of 60 seconds was set after each layer deposition. In Figure 5, schematic diagram of deposition is shown.

DISTRIBUTION A: Distribution approved for public release.

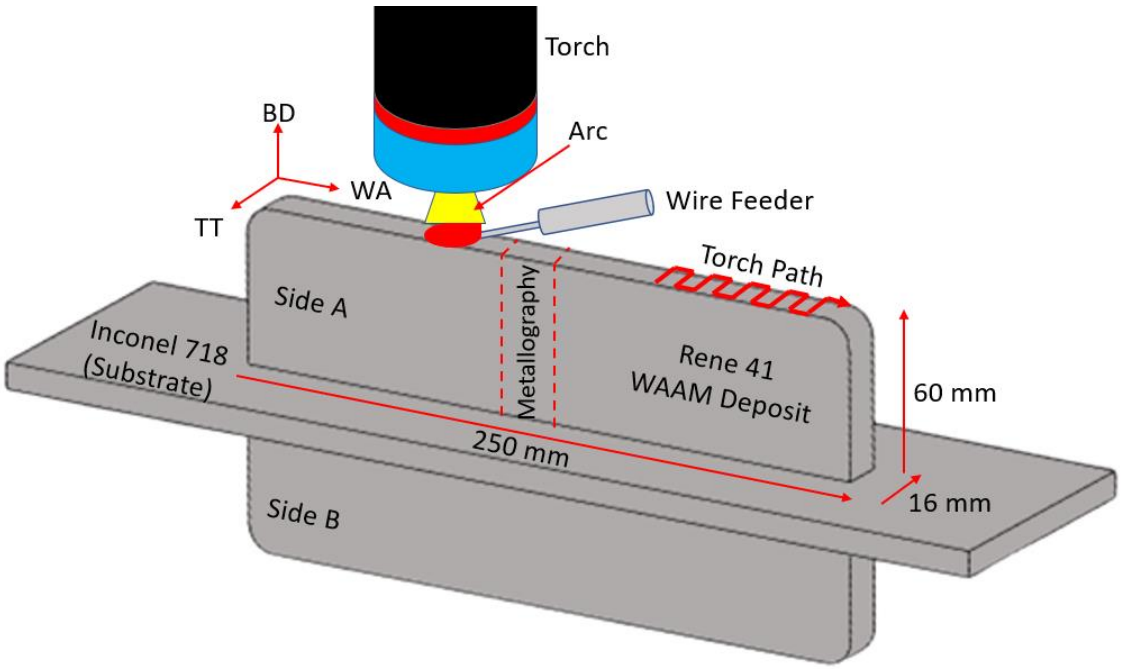


Figure 5 Schematic Diagram of Deposition

WAAM deposition parameters were determined according to [25]. Therefore, the Contact tip to work Distance has been defined as 8 mm. The current was applied as 180 A, and the Voltage was observed as 24 volts during deposition. Torch travel speed was determined as 3 mm/s for the first layer and 4 mm/s for the second layer to make the lower layers of the deposition more durable. The torch travel speed was determined as 6 mm/s for the deposition of all subsequent layers. A total of 62 layers were deposited on both sides. (argon information will be added) Plasma WAAM deposition is shown in figure Figure 6.

DISTRIBUTION A: Distribution approved for public release.

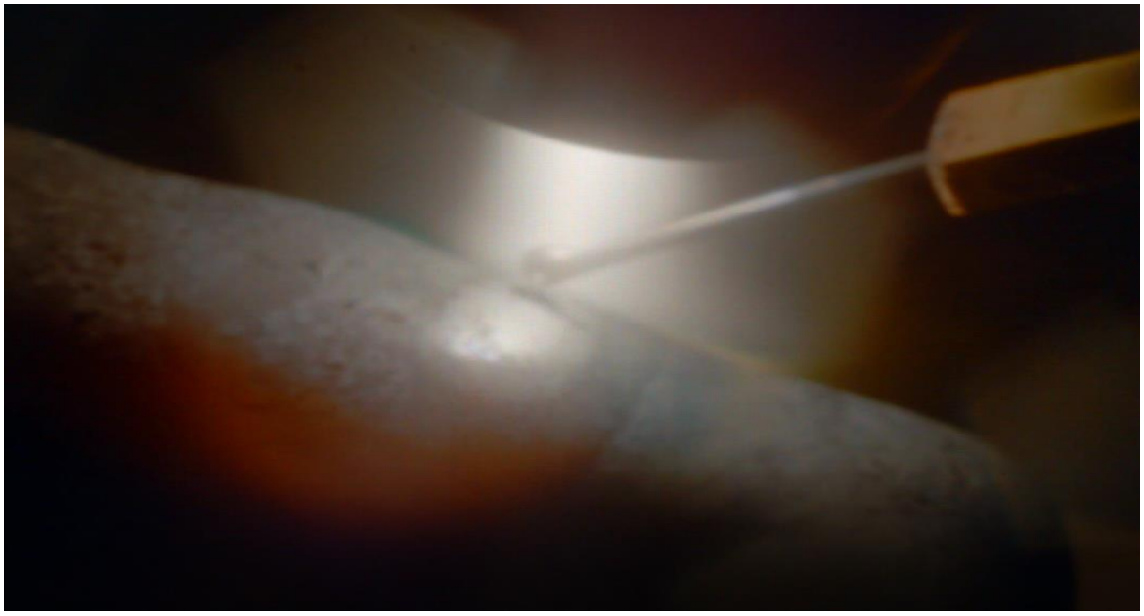


Figure 6 Plasma WAAM Deposition

Deposited wall of Rene 41 is shown in Figure 7. After deposition of 62 layers on both sides, the wall height was measured as 55 mm on average, as shown in Figure 8. While the wall is being deposited, some repair processes have been applied to eliminate the height difference in the corners. The reason for this may be the low droplet transfer and size at the wall edges at the time of layer deposition.



Figure 7 Deposited Wall of Rene 41

DISTRIBUTION A: Distribution approved for public release.



Figure 8 Height of Deposited Wall

3.2 Post Deposition Heat Treatment

The heat treatments were carried out using the Carbolite RHF 1400 model furnace shown in figure k. The heat elements in the furnace are covered with tough alumina, and the maximum temperature supported by the oven is 1200 °C. It is planned to perform heat treatment under two different conditions. Each heat treatment consists of 2 stages. Accordingly, as shown in figure c, the pieces cut for metallography from the middle of both deposited walls were first heated to 1065 °C with a heating rate of 10 °C /min for the standard heat treatment process, kept at this temperature for 4 hours to remove segregations, and cooled in air. The heat treatment cycle is shown in Figure 9.

DISTRIBUTION A: Distribution approved for public release.

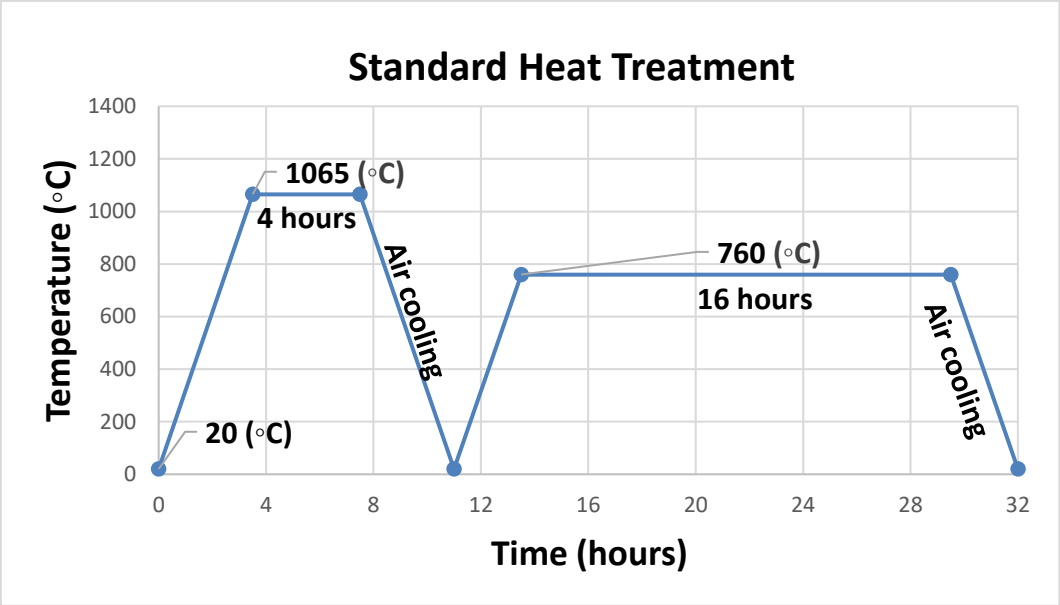


Figure 9 Standard Heat Treatment Cycle for Rene 41

The other piece cut for modified heat treatment was heated to 1200 °C with a heating rate of 10 °C/min and held at this temperature for 4 hours to dissolve the rough gamma prime phase formed during deposition and shorten the dendrite arm spacing distance, then cooled in air. [20] The heat treatment cycle is shown in Figure 10. These two materials were then heated to 760 °C to form precipitates in the structure and increase the strength of the material. They were held at this temperature for 16 hours for the formation of stable precipitates, and the material was cooled in the air to prevent excessive ageing.

DISTRIBUTION A: Distribution approved for public release.

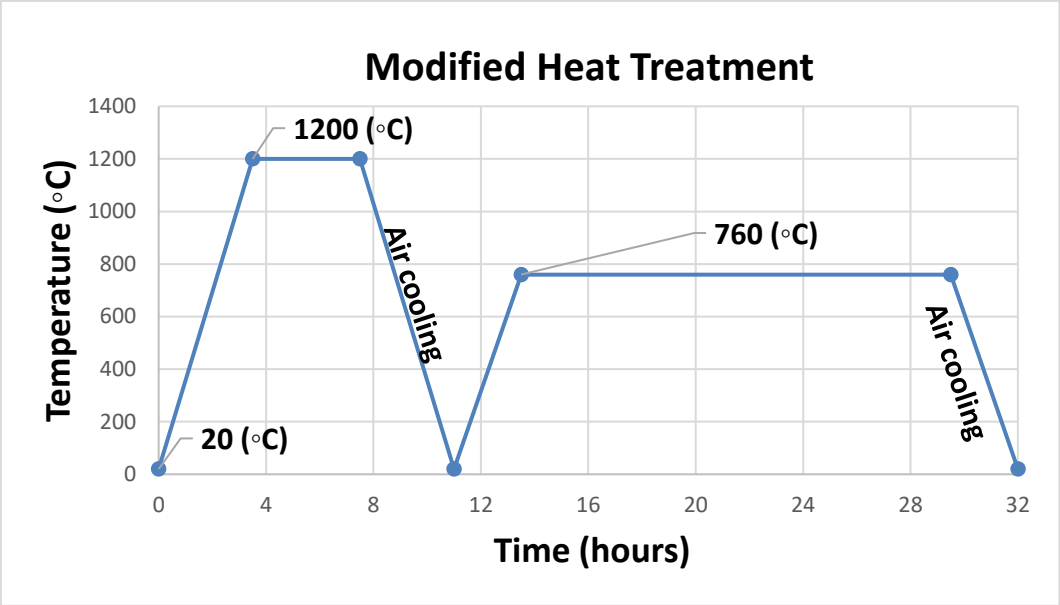


Figure 10 Modified Heat Treatment Cycle for Rene 41

3.3 Metallographic Preparation and Analyses

Metallographic samples were cut from the middle of both walls in 20 cm thicknesses, as seen in the Figure 5. After the two middle pieces were cut, the samples were cut to the required dimensions after the heat treatment to see the microstructure and mechanical strength differences of the BD, WA, and TT axes. Samples were prepared on three axes from 3 conditions: As deposited- Standard Heat Treatment and Modified Heat Treatment. In addition, the wire sample used in deposition was cut in suitable sizes for mounted for SEM and EDS analysis. Samples were then cold mounted into the resin. After cold mounted, the samples were ground with coarse P240g, fine P1200g, and finer P2500g silicon carbide abrasive sheets, respectively. After grinding, the samples were first polished with 3 µm diamond abrasive suspensions using textile cloth and then cleaned using 1 µm OP-s colloidal silica suspension. A chemical solution called Aqua regia with 75% Hydrochloric Acid (HCl) and 25% Concentrated Nitric Acid (HNO_3) was used

DISTRIBUTION A: Distribution approved for public release.

for etching. The etched samples were examined under the Leica DM 2700M model Light Optical Microscope. In addition, the microstructure was also analyzed with the high-resolution TESCAN S8000 SEM device. BSE and SE images were obtained. In addition, Oxford Instruments X-Max model Energy Dispersive Spectrometry detector, which is connected to the SEM device, was used for composition analysis of the material. Here, it is aimed to examine the segregation behavior of (Mo, Cr and Co alloying elements) in the microstructure.

3.4 Microhardness Test

In order to compare the mechanical properties of the deposited wall with as deposited and different heat treatment conditions, the Vickers Hardness test was applied to the samples with a Zwick/Roell hardness machine. To see the effects of 3 different axes in each of the three conditions, the hardness test was applied in the horizontal and vertical directions. In addition, for the as-deposited sample, a sample was cut along the height and tested in the BD direction to observe the difference in hardness between the layers. For the Vickers Hardness test as shown in Table 7, a 0.5 kg load was applied every 1 mm on the material, and a holding time of 15 sec was determined. The directions of the hardness tests applied are shown in Figure 11.

Table 7 Vickers Hardness Test Parameters for Rene 41

Distance	1 mm
Time	15 sec
Load	0.5 kg

DISTRIBUTION A: Distribution approved for public release.

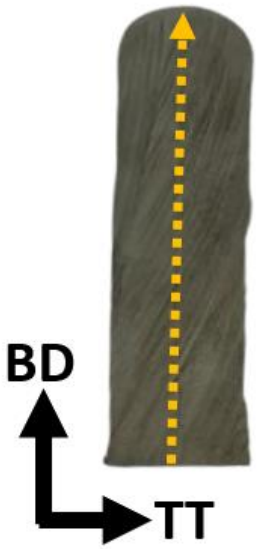


Figure 11 Hardness Test Direction

DISTRIBUTION A: Distribution approved for public release.

DISTRIBUTION A: Distribution approved for public release.

4 Results and Discussion

During the deposition of Rene 41 with WAAM, its microstructure and phase changes depend on the solidification process. In order to solidify, constitutional undercooling is used because the actual temperature gradient is lower than the slope of liquidus. In fact, differences in the temperature gradient and cooling rate can produce different microstructures and phase transformations, such as variations in dendrite morphology, and interdendritic distance.

4.1 As-Deposited Microstructure

After Rene 41's WAAM deposition, the microstructure of as deposition condition was investigated in LOM and SEM along 3 different axes: BD, WA and TT. It has been observed that columnar dendritic structures grow epitaxially along the Build Direction in the microstructure of the As-deposited wall. The samples were cut in both the WA direction and the TT direction for examination in the BD direction. It was observed that both faces showed similar columnar dendritic structures in the BD direction. LOM images are shown in Figure 12.

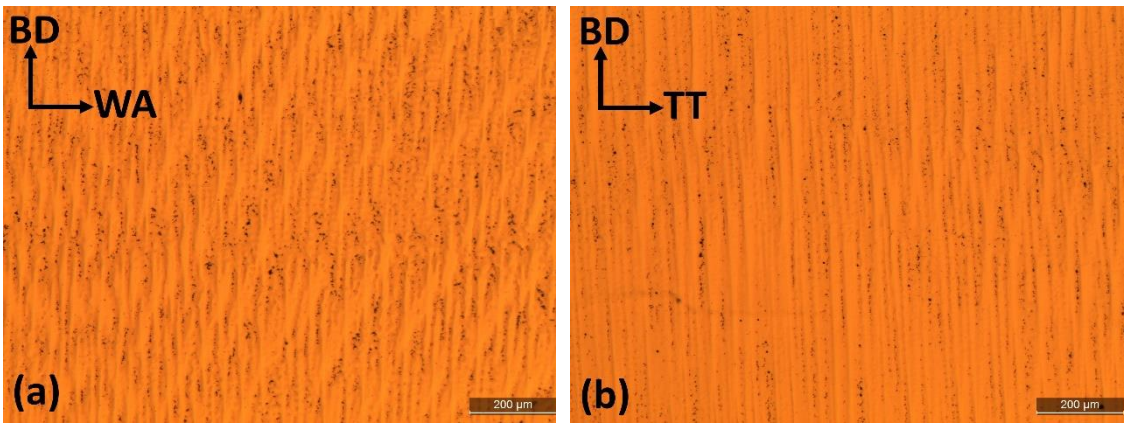


Figure 12 Microstructures of As-deposited Wall:
(a) TT cross-section, (b) WA cross-section

DISTRIBUTION A: Distribution approved for public release.

In addition, the density of dendritic structures was observed when the sample prepared in the direction of BD was examined to understand the microstructure from the top along the Build Direction. The microstructure image of BD cross-section is given in Figure 13.

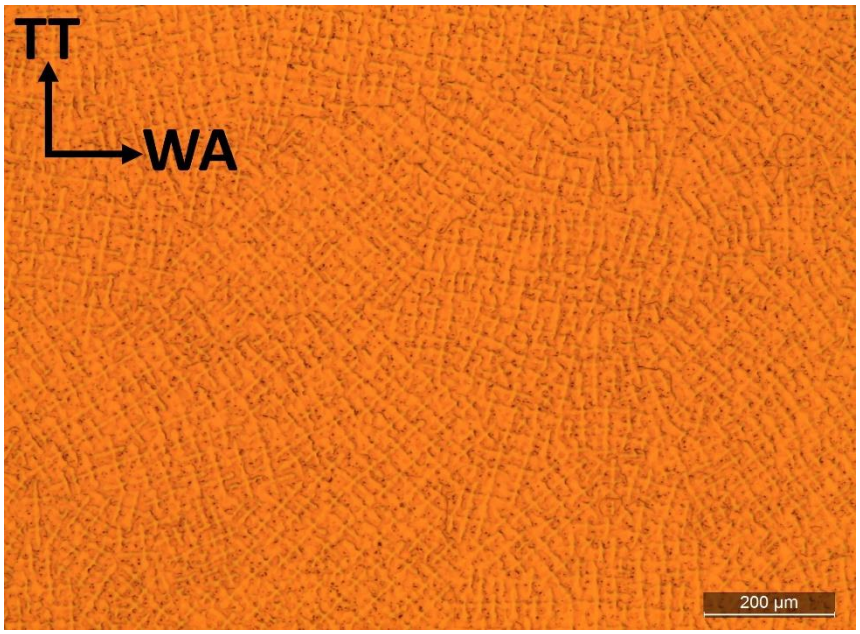


Figure 13 LOM Image of BD Cross-section

In the SEM examinations, 3 different regions were determined for as-deposited conditions. Darker areas represent the Dendrites, Gray areas represent the interdendritic space, and bright white particles represent carbides. The growth of the columnar dendrites is attributed to the epitaxial growth of the primary dendrites from the previously deposited layer that has partially remelted and may serve as nucleation particles. [cgn24] In addition, SEM images taken from the TT cross-section and WA cross-section shown in Figure 14 clearly show that the dendrites grow parallel to the Build Direction. The columnar grain growth is a result of directional thermal gradient in the Build Direction.

DISTRIBUTION A: Distribution approved for public release.

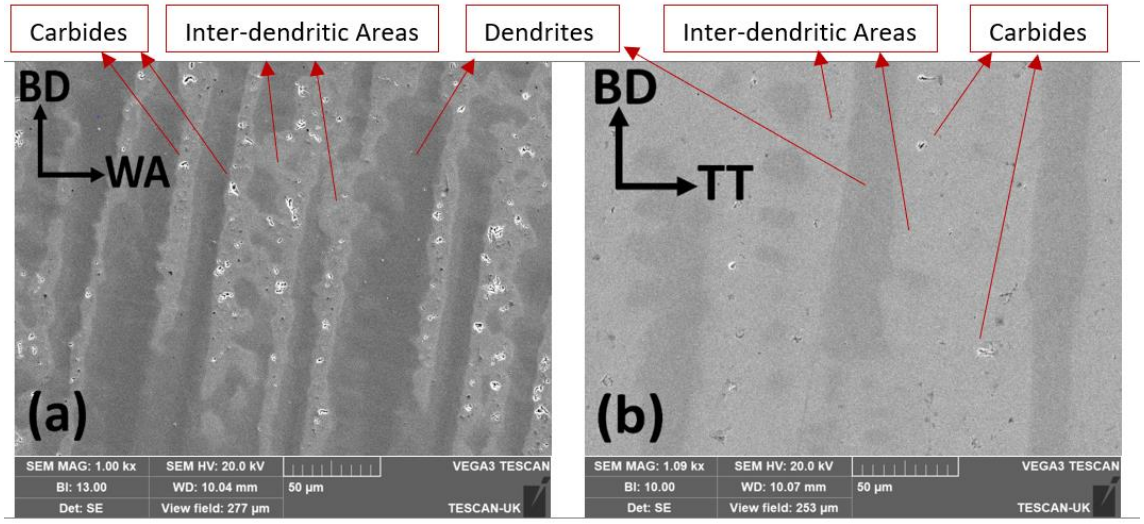


Figure 14 Sem Images of As Deposited Wall:
(a) TT Cross-Section, (b) WA Cross-Section

As a result of the EDS analysis made to the BSE image obtained from the SEM analysis, the element composition in the matrix, dendrites, inter-dendritic regions and carbides were obtained. According to this analysis, it was determined that the ratio of titanium and molybdenum was higher in the inter-dendritic region. In addition, it was determined that the molybdenum ratio in the carbide particles in the 22nd spectrum shown in figure 4 was higher than in matrix and dendritic regions. In the microstructure clearly grey and dark regions can be seen and they are based on proportion of high atomic number elements partitioning between the two regions. In addition that, In figure 15, Sem image of build direction cross-section area, all phases can be observe clearly. Thus, Eds analyses made on that image, according to Table 8, Interdendritic areas including more segregation than dendrites.

DISTRIBUTION A: Distribution approved for public release.

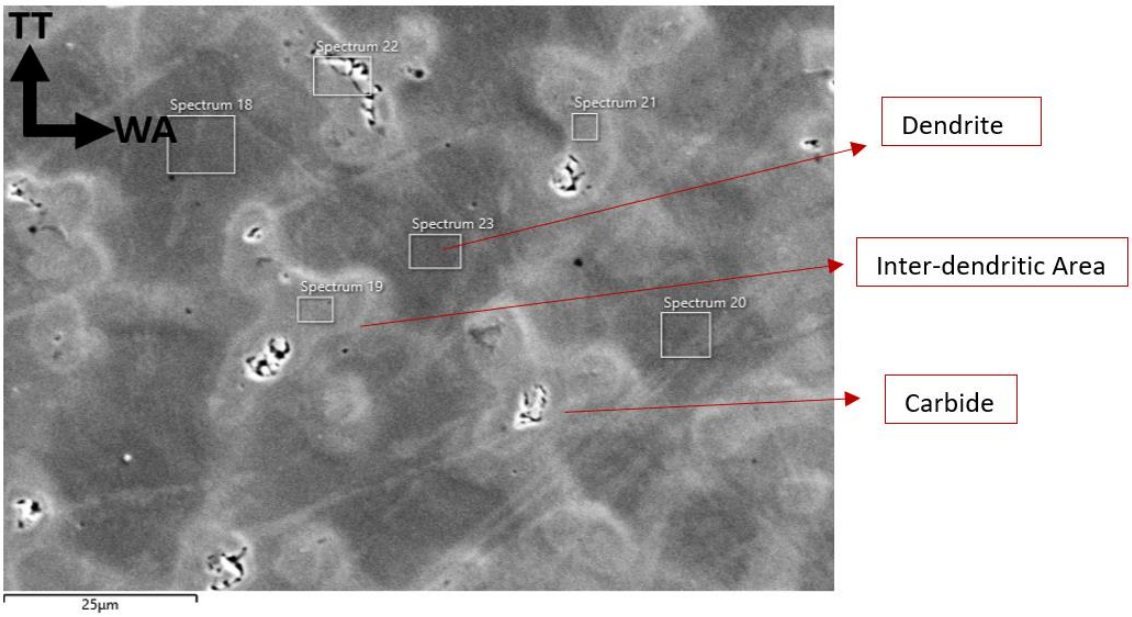


Figure 15 SEM Image of As-Deposited Wall, BD Cross-Section

Table 8 EDS Analysis of As Deposited Wall

Spectrum Label	Spectrum 18	Spectrum 19	Spectrum 20	Spectrum 21	Spectrum 22	Spectrum 23
Al	1.50	1.39	1.47	1.41	0.97	1.48
Ti	2.04	4.16	2.05	4.25	3.62	1.97
Cr	19.11	18.65	19.21	18.56	21.46	19.16
Fe	4.29	3.40	4.26	3.40	3.29	4.33
Co	10.10	8.91	9.93	8.78	8.81	10.08
Ni	53.67	49.55	53.46	50.04	40.53	53.68
Nb	-	0.52	-	0.73	0.72	-
Mo	7.63	11.47	7.84	10.79	18.31	7.68

DISTRIBUTION A: Distribution approved for public release.

4.2 Characterisation of Wire Sample

LOM and SEM images were taken, and EDS analysis was applied to examine the composition and microstructure of the 1 mm diameter wire sample used in deposition. The composition ratio is given in Table 1Table 4. In order to reduce the error rate, samples from different sections of the wire were analyzed. To compare the segregations and phase morphologies, sizes, distances, and shapes of the deposited Rene 41 Wall, it was decided to choose the fed wire sample as a reference. The LOM and SEM images of the wire sample are given in Figure 16. Grain boundaries are clearly visible in both images.

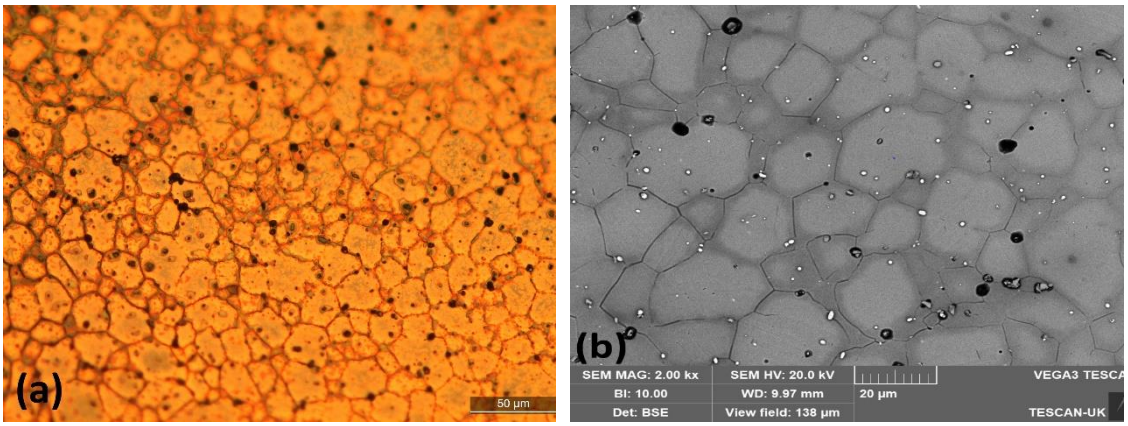


Figure 16 Micro Images of Wire: (a) LOM Image, (b) SEM Image

In the EDS examination performed on the Wire Sample, it was observed that there was a more homogeneous distribution. In addition, approximately 10% Oxygen and 1% Chlorine were found in the analysis. This is because the wire sample is electrolytically etched with 8% Oxalic Acid, which is an etching solution different from the wall samples. According to EDS analysis of Figure 17, the average composition of the wire sample is given in Table 9.

DISTRIBUTION A: Distribution approved for public release.

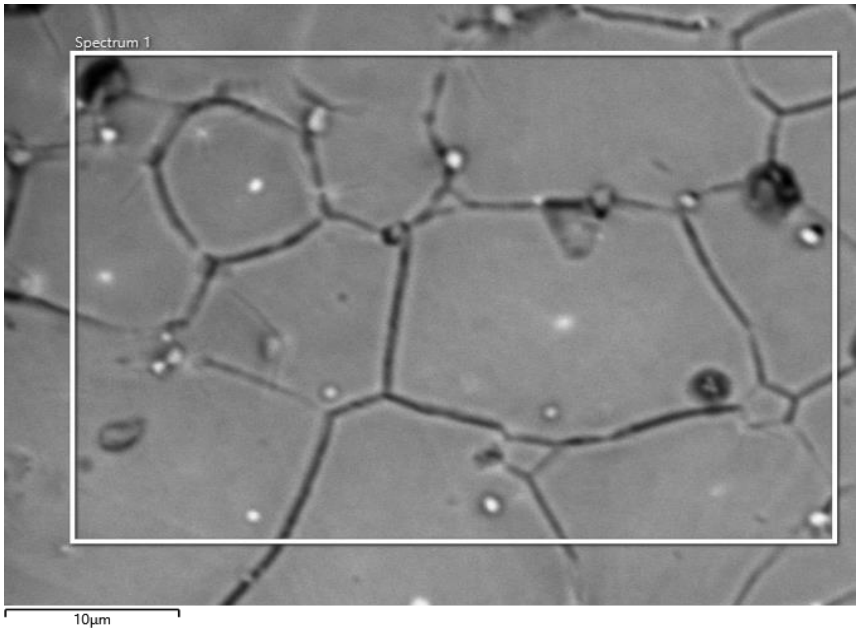


Figure 17 SEM Image of Wire Sample

Table 9 EDS Analysis of Rene 41 Wire

Elements	O	Al	Cl	Ti	Cr	Fe	Co	Ni	Mo
Alloying Compositions (wt.%)	11.00	1.90	1.29	3.77	16.66	2.48	8.53	45.87	8.48

4.3 Segregations of Rene41's alloying element in WAAM

As shown in the EDS analysis, elemental composition was calculated by analyzes taken from regions such as dendritic and interdendritic precipitates. When the results obtained were compared with Wire sample EDS analysis, it was observed that there was segregation.

DISTRIBUTION A: Distribution approved for public release.

Table 10 Comparison of EDS Analysis

Elements	Wire Sample	Dendrite	Inter-Dendritic Region	Carbide
Al	1.90	1.50	1.39	0.97
Ti	3.77	2.04	4.16	3.62
Cr	16.66	19.11	18.65	21.46
Fe	2.48	4.29	3.40	3.29
Co	8.53	10.10	8.91	8.81
Ni	45.87	53.67	49.55	40.53
Mo	8.48	7.63	11.47	18.31

The K Factor constant calculated in Table Figure 18, it shows that Fe, Co and Ni compositions with K greater than 1 are predominantly in the dendritic structure, but Ti and Mo compositions with K less than 1 are mostly found in the indertendritic region.

Spectrum Label	Spectrum 18 C Solid (Dendritic Core)	Spectrum 19 C Liquid (Inter-Dendritic)	Spectrum 20 C Solid (Dendritic Core)	Spectrum 21 C Liquid (Inter-Dendritic)
Al	1.50	1.39	1.47	1.41
Ti	2.04	4.16	2.05	4.25
Cr	19.11	18.65	19.21	18.56
Fe	4.29	3.40	4.26	3.40
Co	10.10	8.91	9.93	8.78
Ni	53.67	49.55	53.46	50.04
Mo	7.63	11.47	7.84	10.79
K Factor Constant (C Solid / C Liquid)				
Al	1.08		1.04	

DISTRIBUTION A: Distribution approved for public release.

Ti	0.49	0.48
Cr	1.02	1.04
Fe	1.26	1.25
Co	1.13	1.13
Ni	1.08	1.07
Mo	0.67	0.73

Figure 18 K Factor Constant Values

In Table g, when the Elemental compositional of the Interdendritic regions and Wire sample is compared, it has been observed that especially the titanium in the Wire composition is not homogeneously distributed in inter-dendritic areas.

Table 11 Compositions Ratio of Inter-dendritic Areas to Wire

Elements	Spectrum 19 / Wire	Spectrum 21 / Wire
Al	0.73	0.74
Ti	1.12	1.13
Cr	1.12	1.11
Fe	1.37	1.37
Co	1.05	1.03
Ni	1.08	1.09
Mo	1.35	1.27

DISTRIBUTION A: Distribution approved for public release.

4.4 Effect of Post Deposition Heat Treatments for Rene 41 WAAM

4.4.1 Standard Heat Treatment Effect

In order to examine the WAAM effects of the heat treatment cycle applied for Rene 41 wrought alloys, the standard heat treatment applied for wrought alloys after deposition. When the as-deposited samples were examined, it was observed that the carbides in the structure diffused randomly. But after heat treatment carbides are aligned and coalesced in boundaries. SEM image after standard heat treatment is given in Figure 19. In addition, the components of carbides accumulated in the borders are shown on the EDS Map in Figure 20. According to EDS results in Table 12, it was determined that the Molybdenum ratio in the carbides was high (%27, %32), also Carbides ratio increased in the microstructure.

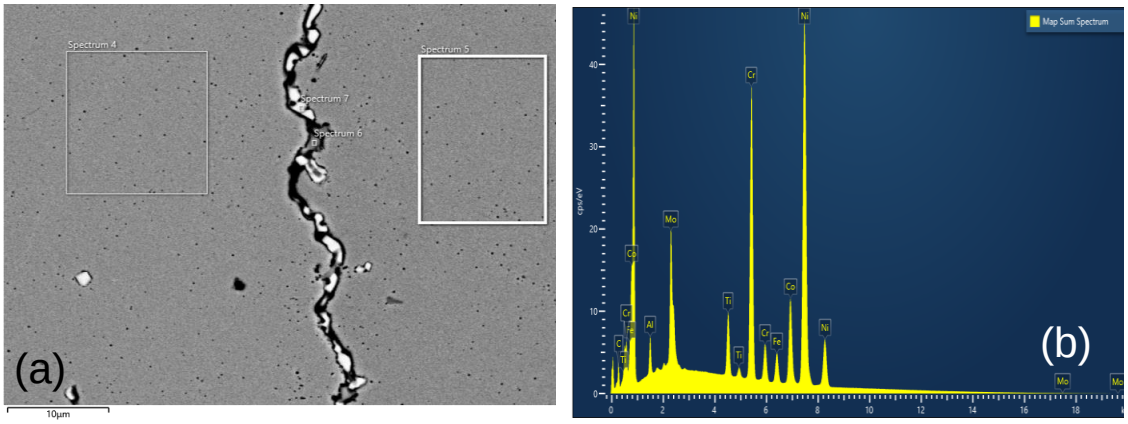


Figure 19 SEM Image After Standard Heat Treatment:
(a) EDS Analysis, (b) Map Spectrum

DISTRIBUTION A: Distribution approved for public release.

Table 12 EDS Results After Standard Heat Treatment

Spectrum Label	Spectrum 4	Spectrum 5	Spectrum 6	Spectrum 7
C	-	-	20.17	9.03
Al	1.65	1.65	0.19	0.61
Ti	3.18	2.92	33.91	3.48
Cr	19.65	19.66	5.15	17.53
Fe	2.76	2.90	-	1.58
Co	10.55	10.76	1.70	7.65
Ni	53.19	53.52	7.44	27.20
Nb	-	-	4.36	-
Mo	8.89	8.60	27.04	32.69

DISTRIBUTION A: Distribution approved for public release.

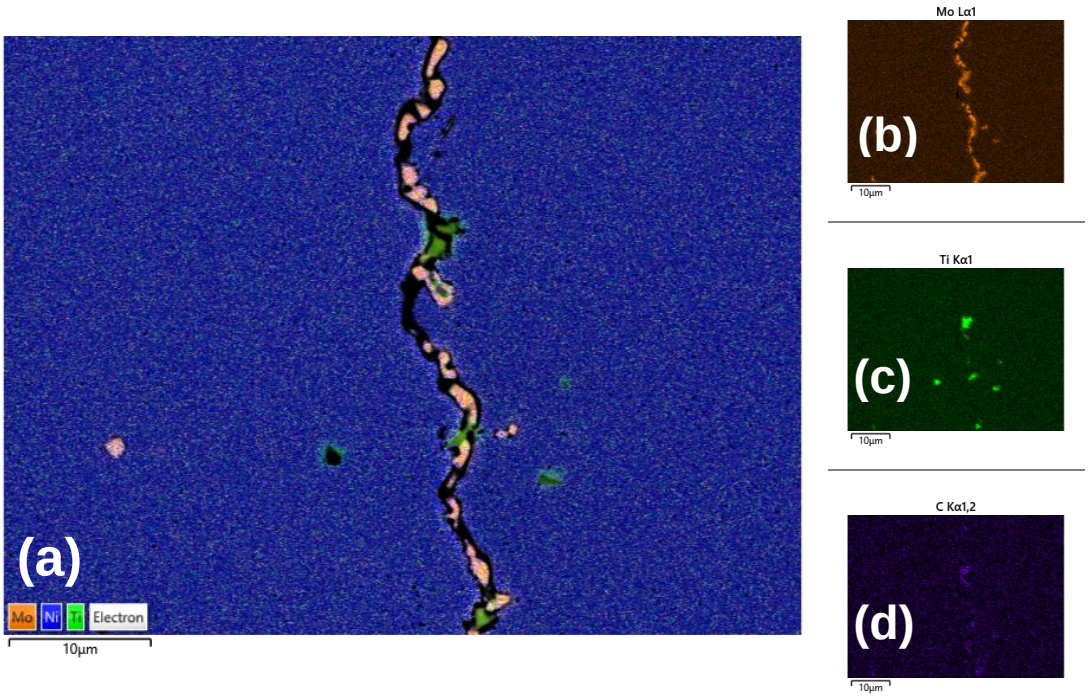


Figure 20 EDS Mapping After Standard Heat Treatment:
(a) General, (b) Mo, (c) Ti, (d) C

4.4.2 Modified Heat Treatment Effect

After Modified Heat Treatment, it was aimed to achieve single phase in microstructure on 1200 °C. As a result of the analysis performed after the modified post deposition heat treatment recommended after WAAM, it was observed that the formation of carbide rich in the Molybdenum and Titanium ratio increased at the grain boundaries in the microstructure. figure where the formed carbides are aligned. After modified heat treatment SEM image is shown in the Figure 21. As shown in Table 13, It was observed that the percentages of titanium (%29, %30) in the structure of carbides increased. It was also observed that there was a significant decrease in the carbide ratio in the structure. This prevented the hardness values in the material from reaching the desired levels.

DISTRIBUTION A: Distribution approved for public release.

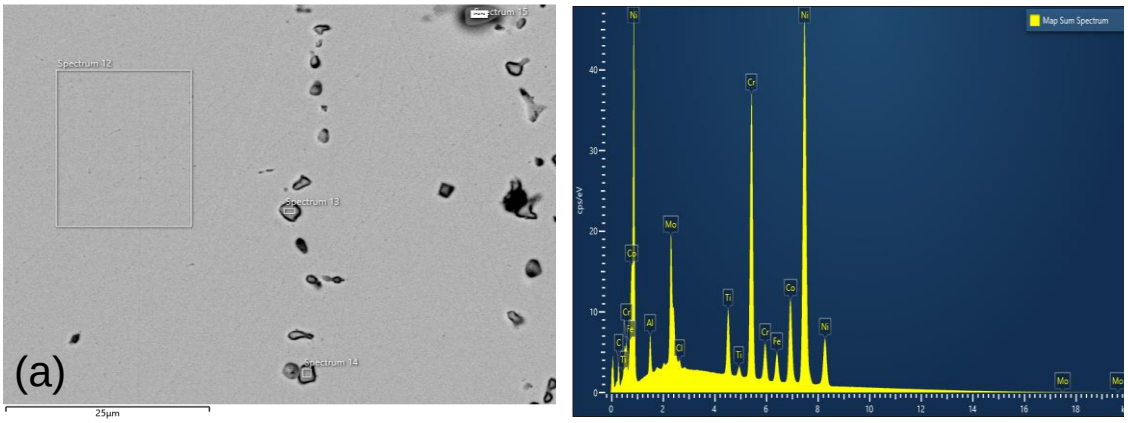


Figure 21 SEM Image After Modified Heat Treatment: (a) EDS Analysis, (b) Map Spectrum

Table 13 EDS Results After Modified Heat Treatment

Spectrum Label	Spectrum 12	Spectrum 13	Spectrum 14	Spectrum 15
C	-	19.23	18.38	-
Al	1.69	0.31	0.21	1.62
Ti	3.15	29.25	30.05	2.92
V	0.15	0.40	0.38	0.15
Cr	19.22	7.01	7.47	18.57
Fe	2.72	0.65	0.74	2.63
Co	10.42	2.53	2.56	10.26
Ni	53.35	11.71	12.50	50.49
Nb	-	3.27	3.41	-
Mo	9.05	25.63	24.29	8.86

DISTRIBUTION A: Distribution approved for public release.

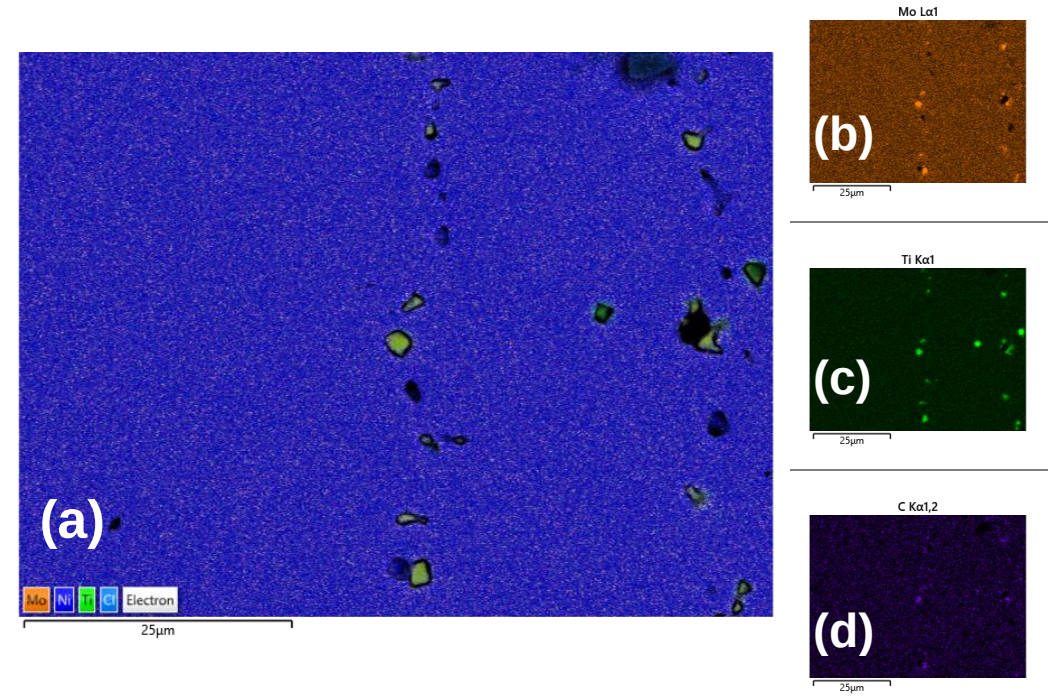


Figure 22 EDS Mapping After Modified Heat Treatment:
(a) General, (b) Mo, (c) Ti, (d) C

4.5 Hardness Results

As a result of Vickers hardness tests on the build direction cross-section, the hardness differences between the layers were examined. The average hardness was determined to be 434 Vickers. It is seen on the trendline in Figure 23 that the hardness values decrease from the lower layers to the upper layers. In addition, very inconsistent fluctuating hardness values are observed between 372 HV and 465 HV in as-deposited.

DISTRIBUTION A: Distribution approved for public release.

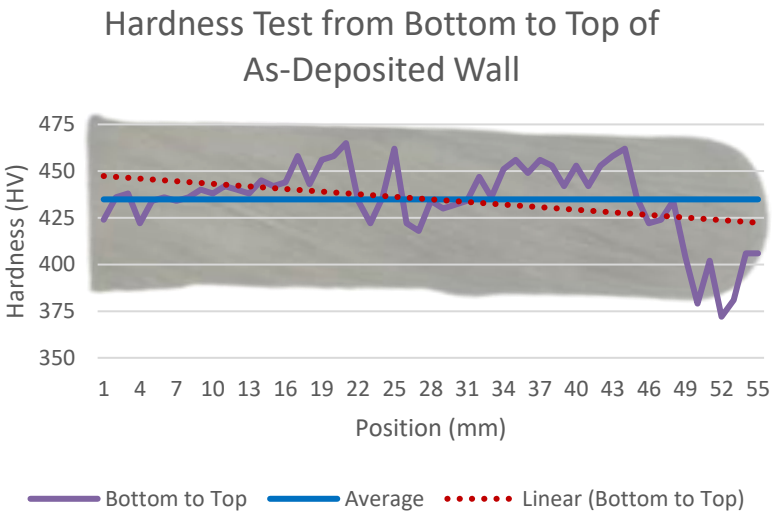


Figure 23 Hardness Results of As-deposited Wall on WA Cross-Section (from bottom to top layers)

The hardness test results applied to see the change in the mechanical values in the Build direction of the material after heat treatment are shown in Figure 24. Accordingly, it was observed that the best hardness values were obtained after standard heat treatment. It was observed that the average hardness value after standard heat treatment was 466, while this value was 449 after modified heat treatment and 434 after as deposited.

DISTRIBUTION A: Distribution approved for public release.

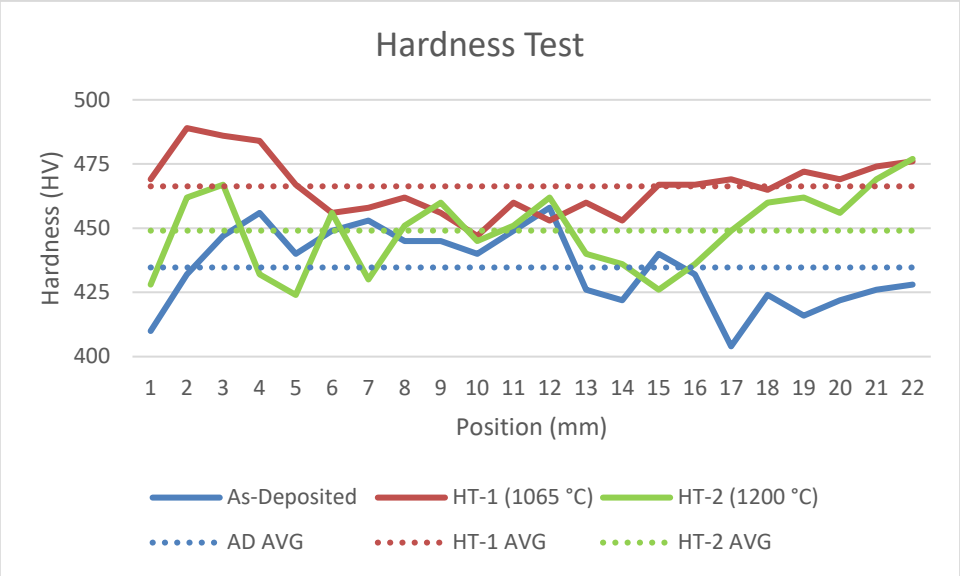


Figure 24 Comparison of Hardness Test Results for 3 Conditions on WA Cross Section (from bottom to top layers)

In order to observe the hardness values in different axes, the hardness test was carried out in the BD cross-sectional area, and the results are given in Figure 25. It has been observed that the results give similar results to the hardness test performed in the direction of BD. Accordingly, the highest hardness value was observed to be 462 HV after standard heat treatment, 444 HV after modified heat treatment, and 424 HV after as-deposited. It was reported in the literature [20] that the precipitates and carbides are scattered randomly in the as deposited samples. On the other hand, the heat treatment results in coalescence of carbides and precipitates along the grain boundaries. This phenomenon can affect material hardness positively.

DISTRIBUTION A: Distribution approved for public release.

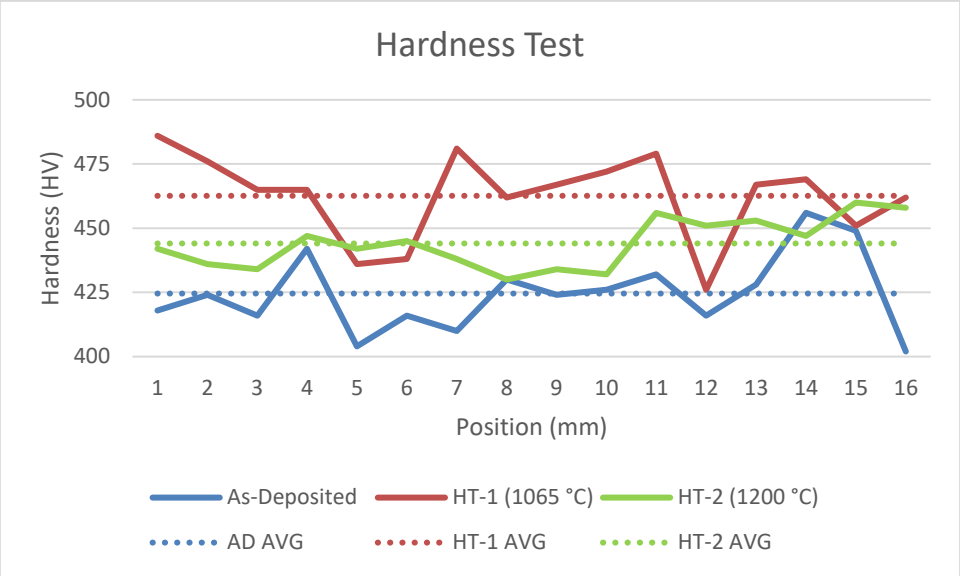


Figure 25 Comparison of Hardness Test Results for 3 Conditions on BD Cross Section

According to the hardness test results, an increase of approximately 9% was observed in the hardness values compared to the as-deposited sample for standard heat treatment. However, for modified heat treatment, this rate only improved by about 4%. The hardness values acquired after the ageing process can be explained by the carbide and gamma prime precipitates accumulating at the grain boundaries. After standard heat treatment, carbides arranged in a certain alignment in the microstructure are the most important factors in increasing the hardness. However, the presence of carbides in modified heat treatment did not have a sufficient effect on the increase in hardness.

As a result of the hardness tests performed on the samples, it was observed that the values were not uniform. It was observed that the hardness values of the As-deposited wall after WAAM were similar to that of the as deposited material in the LMD process of Rene 41, which was performed previously (427). In the ordinary heat treatment applied after the LMD treatment, only 448 HV could be reached. This value was measured as approximately 400 HV after the standard heat treatment applied to the wrought alloys of Rene 41. [16]

DISTRIBUTION A: Distribution approved for public release.

DISTRIBUTION A: Distribution approved for public release.

DISTRIBUTION A: Distribution approved for public release.

5 Conclusions

This project studied different heat treatment scenarios after the WAAM deposition of Rene 41. The main concluding remarks are listed as follows.

- Optical microscopy and SEM analysis was conducted on the additively manufactured samples. Columnar dendrites were clearly observed in the images. Also, it was observed that columnar dendrites structures are growth epitaxially along the Build Direction for as-deposited wall.

- According to the K factor constant made by EDS analysis, it was observed that the ratio of Molybdenum and Titanium was high in the interdendritic areas.

- An increase was observed in the hardness values of the material after the precipitates and carbides formed at 760 degrees after the heat treatments applied for both heat cycles. For both heat treatment cycles, it was observed that discrete carbide distribution on grain boundaries and inter-dendritic zones, refractory elements like Mo strongly segregate while Ni and Cr deplete in these areas.

- According to the results of EDS Mapping analysis, it was observed that Molybdenum and Titanium were intense in Carbid compositions. Also, After both heat treatments, it was observed that the molybdenum in the matrix was distributed more homogeneously than the as-deposited wall. This was similar to the homogeneously dispersed molybdenum percentage in the Wire sample.

- To see the difference in the hardness values between the layers after deposition, as a result of the hardness test, a slight decrease was observed in the hardness of the upper layers compared to the lower layers.

- It was observed carbides are scattered randomly in the as deposited samples. On the other hand, the heat treatment results in coalescence of carbides along the grain boundaries. This phenomenon can affect material hardness positively.

- In the hardness tests applied to different cross-sectional areas after heat treatments, an increase of 4% for modified heat treatment and 9% for standard heat treatment was observed, according to the as-deposited condition, the desired mechanical values could not be obtained.

DISTRIBUTION A: Distribution approved for public release.

DISTRIBUTION A: Distribution approved for public release.

6 Future Work

The following recommendations have been proposed to achieve better results and improve the project in the next phases.

- To obtain more information about the mechanical properties of the material, the tensile test can be applied at room temperature and at high temperatures where the material is operating.
- Parameters can be changed to see the effects of different heat treatment cycles on the material. Solutionising holding time can be extended. After hardening, the material can be water quenched.
- After precipitation hardening heat treatment is applied, TEM analysis should be done to see the morphology, size and shape of the precipitates formed in the microstructure.
- DSC analysis can be done to determine the heat capacity of the material after WAAM, so that the amount of heat required for phase changes can be more accurately determined and a new heat treatment can be recommended.

DISTRIBUTION A: Distribution approved for public release.

DISTRIBUTION A: Distribution approved for public release.

REFERENCES

1. Yang L., Hsu K., Baughman B., Godfrey D., Medina F., Menon M., et al. Additive Manufacturing of Metals: The Technology, Materials, Design and Production Springer Series in Advanced Manufacturing. Available at: http://www.springer.com/series/7113

2. Dhinakaran V., Ajith J., Fathima Yasin Fahmidha A., Jagadeesha T., Sathish T., Stalin B. Wire Arc Additive Manufacturing (WAAM) process of nickel based superalloys-A review. Materials Today: Proceedings. Elsevier Ltd; 2020; 21: 920–925. Available at: DOI:10.1016/J.MATPR.2019.08.159 (Accessed: 16 June 2022)

3. Dababneh F., Taheri H. Investigation of the influence of process interruption on mechanical properties of metal additive manufacturing parts. CIRP Journal of Manufacturing Science and Technology. August 2022; 38: 706–716. Available at: DOI:10.1016/J.CIRPJ.2022.06.008 (Accessed: 16 August 2022)

4. Shrinivas Mahale R., Shamanth V., Hemanth K., Nithin SK., Sharath PC., Shashanka R., et al. Processes and applications of metal additive manufacturing. Materials Today: Proceedings. Elsevier Ltd; 1 January 2022; 54: 228–233. Available at: DOI:10.1016/J.MATPR.2021.08.298 (Accessed: 16 August 2022)

5. Shah P., Racasan R., Bills P. Comparison of different additive manufacturing methods using computed tomography. Case Studies in Nondestructive Testing and Evaluation. Elsevier Ltd; 1 November 2016; 6: 69–78. Available at: DOI:10.1016/J.CSNDT.2016.05.008 (Accessed: 16 August 2022)

6. Blakey-Milner B., Gradl P., Snedden G., Brooks M., Pitot J., Lopez E., et al. Metal additive manufacturing in aerospace: A review. Materials and Design. Elsevier Ltd; 1 November 2021; 209. Available at: DOI:10.1016/J.MATDES.2021.110008 (Accessed: 16 August 2022)

DISTRIBUTION A: Distribution approved for public release.

7. Singh SR., Khanna P. Wire arc additive manufacturing (WAAM): A new process to shape engineering materials. Materials Today: Proceedings. Elsevier Ltd; 2021; 44: 118–128. Available at: DOI:10.1016/J.MATPR.2020.08.030 (Accessed: 16 August 2022)

8. Durai Murugan P., Vijayananth S., Natarajan MP., Jayabalakrishnan D., Arul K., Jayaseelan V., et al. A current state of metal additive manufacturing methods: A review. Materials Today: Proceedings. Elsevier Ltd; 1 January 2022; 59: 1277–1283. Available at: DOI:10.1016/J.MATPR.2021.11.503 (Accessed: 16 August 2022)

9. Tomar B., Shiva S., Nath T. A review on wire arc additive manufacturing: Processing parameters, defects, quality improvement and recent advances. Materials Today Communications. Elsevier Ltd; 1 June 2022; 31. Available at: DOI:10.1016/J.MTCOMM.2022.103739 (Accessed: 16 August 2022)

10. Li J., Wang HM. Microstructure and mechanical properties of rapid directionally solidified Ni-base superalloy Rene'41 by laser melting deposition manufacturing. Materials Science and Engineering A. July 2010; 527(18–19): 4823–4829. Available at: DOI:10.1016/J.MSEA.2010.04.062 (Accessed: 16 August 2022)

11. Atabay SE., Sanchez-Mata O., Muñiz-Lerma JA., Gauvin R., Brochu M. Microstructure and mechanical properties of rene 41 alloy manufactured by laser powder bed fusion. Materials Science and Engineering A. Elsevier Ltd; 31 January 2020; 773. Available at: DOI:10.1016/J.MSEA.2019.138849 (Accessed: 16 August 2022)

12. Zhang H., Wang Y., de Vecchis RR., Xiong W. Evolution of carbide precipitates in Haynes® 282 superalloy processed by wire arc additive manufacturing. Journal of Materials Processing Technology. Elsevier Ltd; 1 July 2022; 305. Available at: DOI:10.1016/J.JMATPROTEC.2022.117597 (Accessed: 17 August 2022)

DISTRIBUTION A: Distribution approved for public release.

13. Reed RC (Roger C. The superalloys : fundamentals and applications. Cambridge University Press; 2006. 372 p.

14. Carter LN. SELECTIVE LASER MELTING OF NICKEL SUPERALLOYS FOR HIGH TEMPERATURE APPLICATIONS. 2013.

15. Singh Handa S. DEGREE PROJECT FOR MASTER OF SCIENCE WITH SPECIALIZATION IN MANUFACTURING Precipitation of Carbides in a Ni-based Superalloy. Available at: www.hv.se

16. Li J., Wang HM., Tang HB. Effect of heat treatment on microstructure and mechanical properties of laser melting deposited Ni-base superalloy Rene'41. Materials Science and Engineering A. 30 July 2012; 550: 97–102. Available at: DOI:10.1016/j.msea.2012.04.037

17. Crump S., London B. Discontinuous Grain Boundaries of Forged René 41.

18. Hönnige J., Seow CE., Ganguly S., Xu X., Cabeza S., Coules H., et al. Study of residual stress and microstructural evolution in as-deposited and inter-pass rolled wire plus arc additively manufactured Inconel 718 alloy after ageing treatment. Materials Science and Engineering A. Elsevier Ltd; 13 January 2021; 801. Available at: DOI:10.1016/J.MSEA.2020.140368 (Accessed: 16 June 2022)

19. Seow CE., Coules HE., Wu G., Khan RHU., Xu X., Williams S. Wire + Arc Additively Manufactured Inconel 718: Effect of post-deposition heat treatments on microstructure and tensile properties. Materials and Design. Elsevier Ltd; 5 December 2019; 183. Available at: DOI:10.1016/j.matdes.2019.108157

20. Atabay SE., Sanchez-Mata O., Muñiz-Lerma JA., Brochu M. Effect of heat treatment on the microstructure and elevated temperature tensile properties of Rene 41 alloy produced by laser powder bed fusion. Journal of Alloys and Compounds. Elsevier Ltd; 25 March 2021; 858. Available at: DOI:10.1016/j.jallcom.2020.157645

21. Callister WD., Rethwisch DG. Materials Science and Engineering.

DISTRIBUTION A: Distribution approved for public release.

22. Yang C., Xu Y., Nie H., Xiao X., Jia G., Shen Z. Effects of heat treatments on the microstructure and mechanical properties of Rene 80. Materials and Design. 2013; 43: 66–73. Available at: DOI:10.1016/J.MATDES.2012.06.039 (Accessed: 17 August 2022)

23. Kim HT., Chun SS., Yao XX., Fang Y., Choi J. Gamma prime () precipitating and ageing behaviours in two newly developed nickel-base superalloys. JOURNAL OF MATE RIALS SCIENCE. 1997.

24. Swalin RA., Martin A., Olson R. Diffusion of Magnesium, Silicon, And Molybdenum in Nickel.

25. Xu X., Ganguly S., Ding J., Seow CE., Williams S. Enhancing mechanical properties of wire + arc additively manufactured INCONEL 718 superalloy through in-process thermomechanical processing. Materials and Design. Elsevier Ltd; 15 December 2018; 160: 1042–1051. Available at: DOI:10.1016/j.matdes.2018.10.038

DISTRIBUTION A: Distribution approved for public release.

APPENDICES

DISTRIBUTION A: Distribution approved for public release.

Appendix V: Impact of solutionising temperature on hardness response of as-deposited Co based H188

DISTRIBUTION A: Distribution approved for public release.

CRANFIELD UNIVERSITY

School of Aerospace, Transport, and Manufacturing
Metal Additive Manufacturing and Welding Engineering

MSc Individual Research Project

Academic Year 2021 - 22

Veeramanikandan Selvakumar

Additive Manufacture of a heat-resistant Cobalt-based superalloy

Supervisor: Dr. Supriyo Ganguly
Associate Supervisor: Dr. Kuladeep Rajamudili
August 2022

This thesis is submitted in partial fulfillment of the requirements for the degree of MSc

© Cranfield University 2022. All rights reserved. No part of this publication may be reproduced without the written permission of the copyright owner.

DISTRIBUTION A: Distribution approved for public release.

ABSTRACT

Cobalt-based superalloys are exclusively used in the field of aerospace, which requires high creep-resistant components. Additive manufacturing helps in reducing material waste as well as lead time. In this report, the fabrication and post-processing of Haynes 188 walls using plasma-WAAM technology were done. And the thermo-mechanical properties of the fabricated walls were studied. Both the walls of dimension 250x16x50 mm were deposited simultaneously using a turn table mechanism wherein the substrate is fixed with the part rotator. The entire fabrication took place in a globalized shielding environment and used an oscillatory bi-directional deposition strategy to build a stable wall. The deposited walls were machined and removed from the substrate to carry out post-processing. Standard heat treatment and modified heat treatment were done in post-processing. The modified solutionizing heat treatment cycle was designed using the data collected from the SEM and EDS results of the deposited material to homogenize the deposited wall. Using Fick's second law of diffusivity, these data were then used to calculate the time required for soaking during the solutionizing process. These three sets of samples were moulded, polished, and etched to carry out the hardness, SEM, and EDS tests. The test results were used to compare the differences in thermo-mechanical properties of as-deposited, standard heat-treated, and modified heat-treated samples. From the SEM and EDS analysis, it was clear that the heat treatment had a great effect on homogenizing the samples. This was observed by the fact that the precipitated particles during solidification were segregated throughout in an irregular pattern with the dendrite's formation post standard heat-treatment, precipitated particles were aligned along the grain boundary. With modified heat-treated samples, the precipitates were in a semi-dissolved state and spaced equidistance to each other in the solvus base. The samples were tested for their mechanical properties using the Vickers hardness test. The average hardness value of as-deposited, standard heat-treated, and modified heat-treated samples across the cross-section are 266HV, 242HV, and 255HV respectively. The hardness value of as-deposited samples is slightly higher than that of heat-treated samples, which was an expected outcome of the solutionizing heat treatment.

Keywords:

WAAM, Plasma Arc Additive Manufacturing, H188, Oscillating strategy, Homogenisation, Diffusivity, Precipitation, Fick's law, solutionizing.

DISTRIBUTION A: Distribution approved for public release.

ACKNOWLEDGEMENTS

I would like to express our gratitude to my supervisors Dr. Supriyo Ganguly and Dr. Kuladeep Rajamudili for their consistent support and guidance throughout this project. I would also like to thank all the technicians working in the Welding and Additive Manufacturing center of Cranfield University. I'm grateful to Emma German who helped me during the initial stages of the project with the setup, lab bookings, and meetings. I would like to thank William James for sharing his hardness test data for my comparison study. Many thanks to Christine Kimpton, Diane Johnson, Steve Pope, and Tracey Roberts who helped me with the Material characterization. I would also like to thank Tim Pryor, who helped to carry out the heat treatment.

DISTRIBUTION A: Distribution approved for public release.

TABLE OF CONTENTS

ABSTRACT i
ACKNOWLEDGEMENTS ii
LIST OF FIGURES iv
LIST OF TABLES v
LIST OF EQUATIONS vi
LIST OF ABBREVIATIONS vii
1. Introduction 1
2. Literature review 3
2.1. Plasma Arc WAAM technology 4
2.2. Necessity of Shielding 4
2.3. Deposition Strategies 5
2.4. Heat treatment process 6
3. Materials and Experimental Methods 7
3.1. Materials 7
3.2. Experimental Setup 8
3.3. Experimental methodology 8
3.4. Sample preparations 10
3.5. Heat treatment calculations 10
4. Results & Discussion 11
4.1. Depositing characteristics 11
4.1.1. Discussion 12
4.2. Heat treatment 13
4.2.1. Results 13
4.2.2. Discussion 13
4.3. Microstructure characteristics 13
4.3.1. Optical microscopic analysis 13
4.3.2. Scanning Electron Microscopy (SEM) with Energy Dispersive Spectroscopy (EDS) analysis 15
4.4. Microhardness 17
4.4.1. Results 17

DISTRIBUTION A: Distribution approved for public release.

4.4.2. Discussion 18
5. Conclusion 19
6. Future works 21
7. References 22

LIST OF FIGURES

Figure 1 Different deposition strategies (a) single pass (b) overlapping pass (c) oscillatory pass [12,13] 5
Figure 2 (a) Bi-directional layer deposition (b) unidirectional layer deposition[16] 6
Figure 3 Plasma-WAAM Experimental setup[21] 8
Figure 4 Side-view diagram of the deposited wall 9
Figure 5 Double side deposited H188 wall with its cross-sectional machines surface. 12
Figure 6 Optical microscopic images of Haynes 188 as-deposited samples at magnifications (a) 5x, (b) 10x, (c) 20x, (d) 50x; standard heat-treated samples at magnifications (1) 5x, (2) 10x, (3) 20x, (4) 50x; Modified heat-treated samples at magnifications (i) 5x, (ii) 10x, (iii) 20x, (iv) 50x. 14
Figure 7 BSE images of (a) as-deposited (b) Standard heat-treated (c) modified heat-treated samples 15
Figure 8 EDS results of segregated particles. 16
Figure 9 Microhardness values along the transverse and longitudinal axis of the deposited wall before and after heat treatment 18

DISTRIBUTION A: Distribution approved for public release.

LIST OF TABLES

Table 1 Chemical Composition of the Haynes 188 wire[8] 7
Table 2 Deposition parameters 10
Table 3 EDS results of H188 wire, as deposited, standard heat-treated, modified heat-treated 16
Table 4 Mean and standard deviation values of the hardness for the deposited samples 18

DISTRIBUTION A: Distribution approved for public release.

LIST OF EQUATIONS

(3-1)..... 10

(3-2)..... 11

(3-3)..... 11

(3-4)..... 11

DISTRIBUTION A: Distribution approved for public release.

LIST OF ABBREVIATIONS

AM	Additive Manufacturing
BSE	Back Scatter Electrons
CTWD	Contact to work distance
CW	Cold Wire
CWFS	Cold Wire Feed Speed
DED	Direct Energy Deposition
EDS	Energy Dispersive X-ray Spectroscopy
GMAW	Gas Metal Arc Welding
GTAW	Gas Tungsten Arc Welding
HT	Heat Treatment
HV	Hardness Value
MAM	Metal Additive Manufacturing
PAW	Plasma Arc Welding
PBF	Powder Bed Fusion
SEM	Scanning Electron Microscopy
TS	Travel Speed
WAAM	Wire Arc Additive Manufacturing
WFS	Wire Feed Speed

DISTRIBUTION A: Distribution approved for public release.

1. Introduction

Additive manufacturing (AM) is a cutting-edge development for over the past three decades, as the name suggests it is a layer-by-layer process until the final component is built. These final parts can be net-shape which could directly be utilized for application or near-net-shape which would require machining for support structure removal and surface finishing. Although this technology was founded for polymers, later due to its process necessity and reliability gained momentum in metal based additive manufacturing. Metal AM impact over the aerospace industries is higher compared to the other industries since reduced cost mainly by efficient use of the material and eliminating the tool and fixture requirement and decreased buy to fly ratio[1]. Mostly these materials are exotic and show enhanced properties such as creep and corrosion resistance, strength, and fatigue life. These are mostly seen in superalloys like Inconel – 625, Rene – 41, Inconel – 718, etc[2]. One such Cobalt-based superalloy is Haynes 188 (H188) which is discussed in detail further. Metal Additive Manufacturing (MAM) is categorized into two types based on process, Powder Bed Fusion (PBF) and Direct Energy Deposition (DED). Further DED is classified based on its feedstock, powder, or wire. Here, since superalloys are used for aerospace applications that requires large parts, wire-based DED process called Wire and Arc Additive Manufacturing (WAAM) technology can be utilized in producing large structure application parts, that are near-net shape which require only surface finishing in most cases[3]. WAAM uses a basic setup of automatic welding technology like Plasma Arc Welding (PAW), Gas Tungsten Arc Welding (GTAW), and Gas Metal Arc Welding (GMAW). To trace the component's path related with layer-by-layer approach, a manipulator was used. Most used manipulators are robots or Computer Numerical Control (CNC) gantries. To have a controlled and compulsively constricted metal droplet transfer, here plasma arc was used for deposition fitted with the Fanuc robot manipulator[1].

In addition to nickel (Ni) based superalloys, some of the Cobalt (Co) based superalloys are used in aerospace applications due to its capacity to withstand high temperature and excellent creep resistance. Haynes 188 is generally used for different turbine engine parts such as combustion chamber, liquid oxygen injection tubes, etc..,.

DISTRIBUTION A: Distribution approved for public release.

Here with WAAM process the deposited H188, have reduced cracking despite alleviated gamma-prime phase due to the segregation of low-level solutes[4].

There are different deposition strategies depending upon the requirements and applications which requires and needs the higher and optimised deposition rate. Overlapping and oscillating deposition strategies are commonly utilised in the WAAM processes. Since the productivity and more material deposition could be found in oscillating strategy, H188 was deposited in oscillated pattern layer by layer until reaches the height of 50mm. Moreover, employing this strategy helps us in faster cooling rate in a globalised shielding environment[5].

To prevent materials from oxidising during deposition wherein the molten metal gets solidified in the available atmosphere, which could absorb oxygen, hence every WAAM process requires shielding gas that could prevent the alloys from oxidising once it gets deposited. Although the supplying shielding gas along with the torch only provide shielding for the molten metal but this wouldn't be sufficient as the molten material wouldn't have solidified completely, hence the technique of globalised shielding was used. In which the whole deposition process takes place in oxygen less environment by pumping in the shielding gas such as pure Argon (Ar) gas or Helium-Argon (He-Ar) mixture and removing the existing oxygen content pumping out[6].

Many different commercially available Ni-based superalloys are mostly solid solution strengthened, also that are designed for AM applications. In the latest development of Co-Ni superalloys, such as H188 it is likely to recognize and increasing solid solution strengthening elements like in this case is the tungsten element. And moreover, this material strengthening by means of gamma prime (γ') precipitation[7]. Therefore, H188 undergoes heat-treatment after forming to homogeneous the material for strengthening. In traditional manufacturing process, H188 is heat treated at 1175^0C for one hour, which is considered as standard heat-treatment, whereas to determine the heat treatment cycle for Wire-Arc Additive Manufactured H188 material is done using Fick's second law of diffusivity, which gives the time required to homogeneous the material[8,9].

This report mainly concentrates on the additive manufacture of Haynes 188 superalloy using wire feed stock and its effect of strengthening techniques on mechanical and material properties. The progress was initiated with the deposition of

DISTRIBUTION A: Distribution approved for public release.

wall using plasma arc WAAM technology by oscillating depositing strategy in a global shielding environment. After which the wall geometry and hardness was tested. Later, heat treatment cycle was designed using the data and images procured from the Scanning Electron Microscope (SEM) and Energy Dispersive Spectroscopy (EDS) analysis. Segment two discusses about assessing the works done on H188 material and analysis various information results obtained by other AM technologies in producing the same material. Also, about the different heat treatments carried out on this element. Segment three extensively focuses on the material composition and characteristics. Also, about experimental setup and procedure. Segment four and five discusses about the acquires data and interpreting with the results. In final segment, the summation of the report and stating important findings from the experiments are presented.

The aim of this project is to additive manufacture Haynes 188 superalloy using WAAM technology and to study the strengthening effects caused by the various heat treatments. Manufacture of samples using an oscillated, plasma WAAM process and post-deposition heat-treatment of WAAM samples. Metallographic observations to understand the material structure and SEM observations using EDS to understand the composition of any observed intermetallic phases. And to develop critical understanding the strengthening response of H188 in directed energy deposition using wire plus arc manufacturing, as well as critical understanding of the microstructure produced and its suitability in generating the strength of the alloy under different thermal treatments. Mechanical testing at room temperature, in here the mechanical test was hardness testing.

2. Literature review

Producing aerospace application parts using additive manufacturing technologies has been done extensively. These studies were mainly done in superalloys such Inconel – 718, Inconel – 625, Rene-41 and so on which are mostly Ni-based, some studies were carried on Cobalt based superalloys such as Haynes-188 and Haynes-25[2]. There are attempts to produce H188 using AM technology that use powder as feedstock and have studied their postprocessing strengthening techniques as well[4]. In this segment, the findings have been classified into different outputs such as Plasma

DISTRIBUTION A: Distribution approved for public release.

Arc WAAM technology, necessity of shielding, deposition strategies, and heat-treatment process.

2.1. Plasma Arc WAAM technology

WAAM is one of the recently developing additive manufacturing technology in the sector of aerospace industries since ability to produce large parts with high buy-to-fly ratio that uses advance welding technology setup adapted to its application. WAAM works on the principle of melting the metal wire into molten metal droplets using ignited arc. The ignited arc from the type of power source determines the WAAM technology. Commonly used WAAM technologies are Gas Metal Arc Welding (GMAW), Gas Tungsten Arc Welding (GTAW) and Plasma Arc Welding (PAW). Plasma Wire Deposition (PWD) is a technique by which the arc is created between the non-consumable tungsten which acts as the cathode while the copper built within the torch acts as the anode. These arcs are generally constricted by means of medium of inert gas (typically argon) dispersed between the cathode and anode. Hence this provides more arc stability, high energy density and low contamination levels since its very controlled process compared to that of the GTAW process. The plasma torch nozzle and the cold wire feeder are attached to the manipulator. Generally, manipulators are used to the trace the path of the material deposition along the sliced layer. These paths are designed in effective and high deposition strategy mechanism. There are three different types of deposition strategies. They are, single pass, overlapping pass and oscillatory pass[10–13]. Under deposition strategies section these deposition strategy mechanisms are discussed in detail.

2.2. Necessity of Shielding

The flow of inert gas between the cathode and anode provides a medium for arc to constrict and form higher energy accumulation, which helps the metallic wire to melt and for liquid metal state to get transferred to the substrate in droplets form. These transferred molten metals are vulnerable to get oxidised, hence a separate vent or a localised gas shielding device is fitted along with the nozzle. To eliminate any risk of getting oxidation in materials like superalloys due to low solidification rate, it usually preferred to carry out the deposition in globalised shielding environment, where the complete setup is set inside the tent of shielding gas atmosphere by which the oxygen inside the tent pumped out while the inert gas (usually argon) is pumped in. For

DISTRIBUTION A: Distribution approved for public release.

superalloys such as H188 can maintain the oxygen level below 600ppm inside the tent environment[6,14,15].

2.3. Deposition Strategies

The main objective of additive manufacturing is to get the parts in net or near-net shape and reduce the lead time of the process with less wastage. Hence, to obtain the part faster and with good clarity, a deposition strategy in single pass or in oscillating pattern or in overlapping pattern also known as parallel pattern is established as shown in Figure 1. These deposition strategies will have effect in the microstructure formation and in mechanical properties. Also, to avoid any slope formation and reduce dwell time while building a high component or a high wall these deposition strategies can used with bi-directional unlike usually in the unidirectional. Figure 2 depicts the schematic difference between unidirectional and bi-directional deposition.

In oscillating strategy, material input is higher in a single layer volume whereas in single layer pass it requires more addition of layer, this could be compensated by the productivity rate as the average cooling rate is lower due to the higher heat input compared to the other strategy. Also, with respect to deposition strategy, the material microstructure and mechanical properties change due to different thermal cycles undergone during different strategy mechanisms[5,12,13,16].

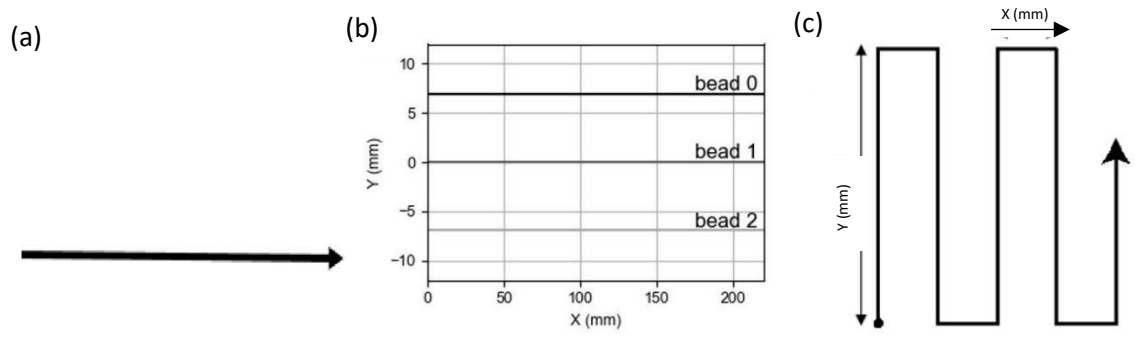


Figure 1 Different deposition strategies (a) single pass (b) overlapping pass (c) oscillatory pass [12,13]

DISTRIBUTION A: Distribution approved for public release.

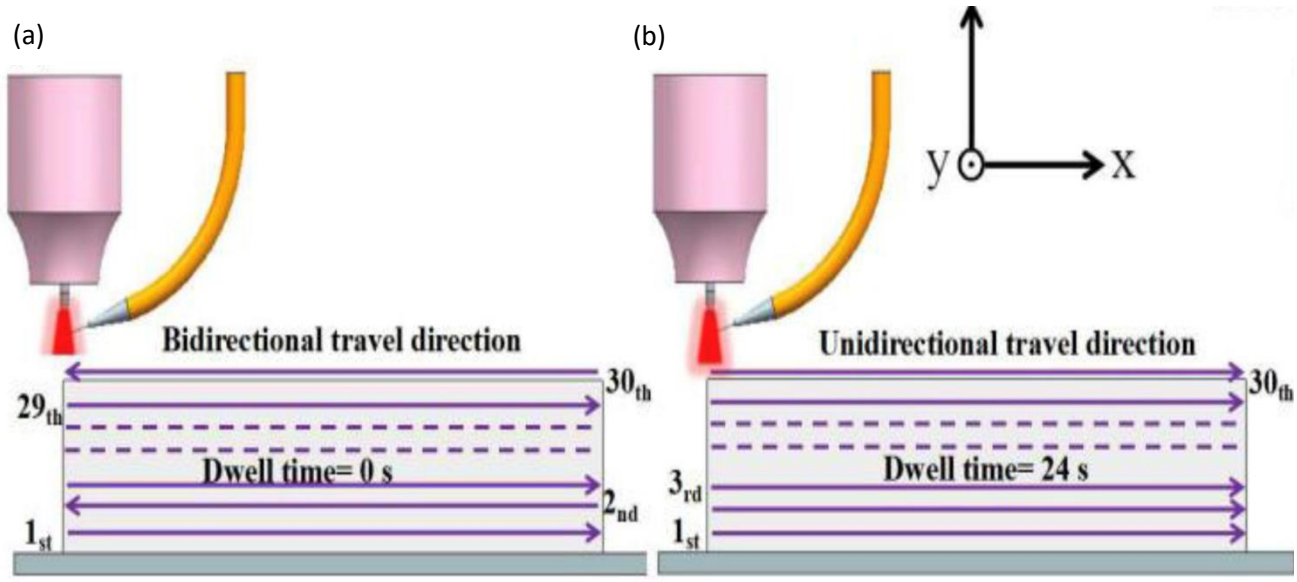


Figure 2 (a) Bi-directional layer deposition (b) unidirectional layer deposition[16]

After reviewing various deposition strategies, for different materials, it is good to go with bi-directional oscillating strategy for deposition, which could give continuous productivity due to higher energy build up in the process and helps in construct thin and rigid wall formation.

2.4. Heat treatment process

Haynes - 188 is a Co-based superalloy that requires solid solution strengthening as part of its strengthening technique post deposition. Haynes alloys are designed to be solution hardened due inclusion of elements like tungsten or molybdenum in its composition. These alloys segregates particles like M_6C carbides when solution hardened which forms the Face-Centred Cubic (FCC) matrix structure[17].

After deposition, the liquid metal droplets are solidified and forms γ' precipitate, these precipitates post heat treatment forms M_6C carbides which leaves the presence of strengthening element tungsten element and thus forming tungsten carbides after solution hardening. In here, solution strengthening is carried out by solutionizing process, where the specimen is heat treated in a furnace at solutionizing temperature and the shoot down to room temperature by quenching by cooled air or water. The H188 alloy doesn't require aging hardening as it is solution strengthened alloy. The heat treatment for this alloy is generally done at 1175^0C for one hour, which is consider as standard heat treatment cycle. This standard heat treatment is generally carried out, when the alloy is built in the traditional technology. To determine the heat

DISTRIBUTION A: Distribution approved for public release.

treatment cycle for WAAM deposited H188 is done by solving Fick's second law of diffusivity to obtain the time required (soaking time) to achieve homogenise material[4,8,9,18–20].

3. Materials and Experimental Methods

3.1. Materials

Table 1 Chemical Composition of the Haynes 188 wire[8]

Chemistry	Co 22Cr 22Ni
Element	**Weight (%)**
Cobalt	39 (Bal.)
Nickel	22
Chromium	22
Tungsten	14
Iron	3
Manganese	1.25
Silicon	0.35
Carbon	0.10
Lanthanum	0.03
Boron	0.015

Haynes international's Haynes-188 (H188) alloy wire of diameter 1.14mm was used as cold wire feeder for the experiments using plasma-WAAM technology. From Table 1 provides the composition data of alloying elements in the Haynes 188 alloy. The substrate used for the experiment was Inconel 718 plate of dimension 400x12x50mm and was clamped along the turntable axis as shown in Figure 3 such that the wall is deposited on the 50mm wide face of the plate. This phase was preferred as the turn table deposition happens on either side of the substrate and to have uniform heat distribution after each layer gradually dissipating. This phase ideal for

DISTRIBUTION A: Distribution approved for public release.

depositing in oscillating pattern and thus the heat gets accumulated and helps in melting the cold wire fed into the plasma arc and melt pool. On either side of the substrate phase 10 holes were drilled to clamp it firm with the turn tables so that it doesn't get detached from the turntable due to the induced residual stress. The shielding gas used in the experiments was pure argon (Ar) (99.999%)

3.2. Experimental Setup

As represented in the Figure 3, the Plasma torch and the Cold wire nozzle were attached to the manipulator which is a six axis Fanuc robot in this case for depositing the wall on the substrate. The wall of dimension 250x16x50mm was deposited in oscillating pattern using a program that was drafted and uploaded to the robot to carry out the automatic deposition of walls till completion.

The program drafted for wall deposition, linked the plasma power source integrated program with the robot movements. The program continues until the wall height reaches 50mm, which the robot determines by means of initial input given based on the bead-on-plate measurements. The plasma arc process was monitored by the voltage readings from the EWM PC300 program. The wire droplet transfer mode, work distance and weld pool were observed using a TPS process camera that was fitted with the plasma torch by the side of cold wire feeder nozzle.

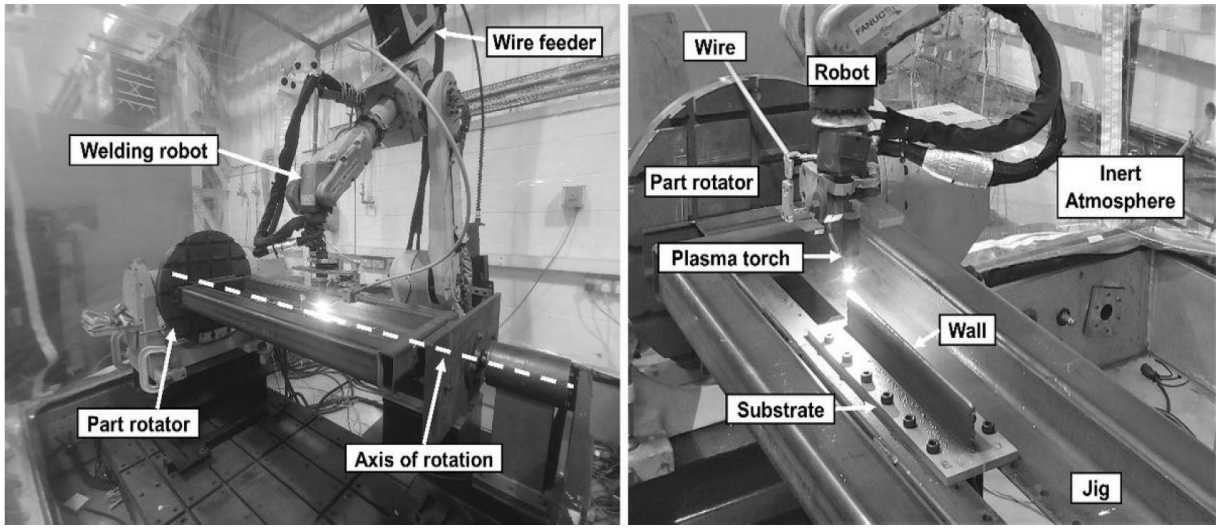


Figure 3 Plasma-WAAM Experimental setup[21]

3.3. Experimental methodology

The main objective of this project is to additive manufacture of H188 alloy, considering that the plasma WAAM process used EWM T552 tetrix plasma series heat

DISTRIBUTION A: Distribution approved for public release.

source for depositing a wall of 250 mm x 16 mm x 50mm as a sample for testing. The wall was deposited with the good operating parameters. The cold wire feed speed was controlled from the heat source software program that controls the oscillating parameters through which the heat input to the plasma generation controlled. To maintain and update the layer height in the program, the height of the wall is measured using vernier calliper after each layer to determine the height of the layer. Measuring this height is essential while building a near-net shape components.

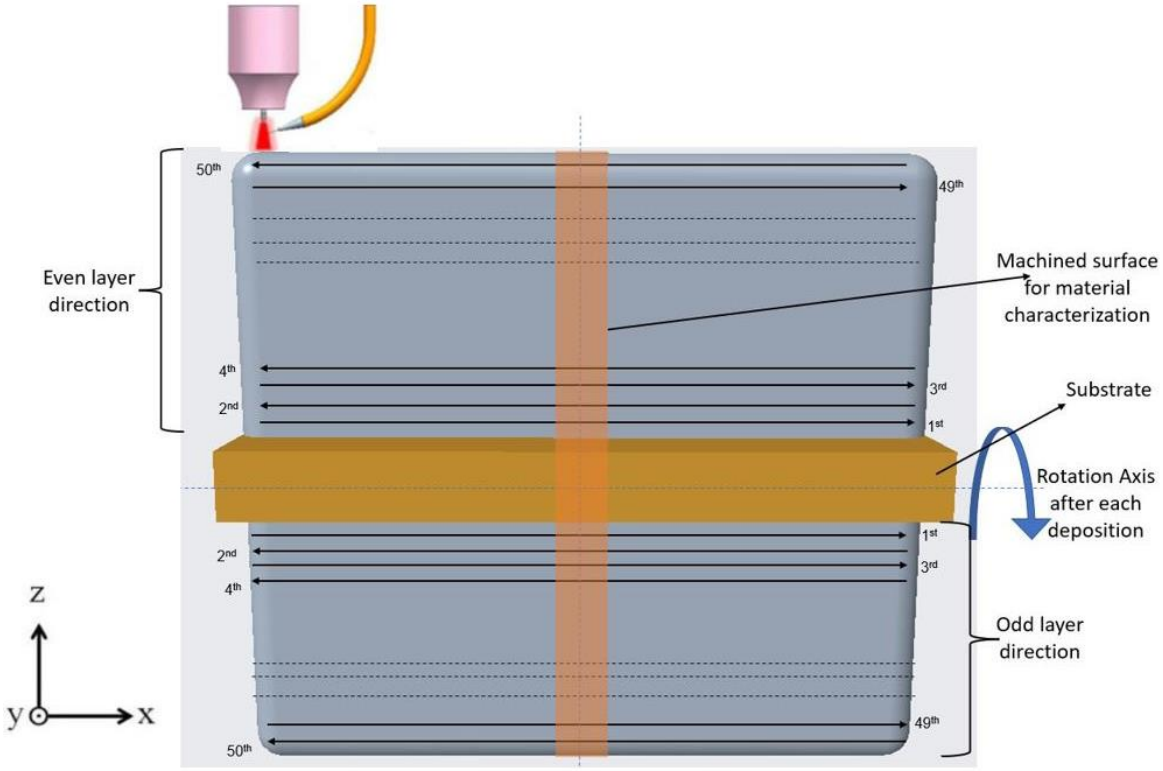


Figure 4 Side-view diagram of the deposited wall

In this project, an additive manufactured cobalt-based superalloy wall was built using turn table mechanism as shown Figure 4. The walls were built in either side of the substrate while the odd layers are built one direction, the even layers start depositing from end position of odd layer and finishes at start of odd layer. The interpass temperature of this process was maintained as process was taking place continuously, since the deposition was happening at regular interval due to layers were deposited on either side of the substrate. Table 2 provides the deposition parameters under which plasma-WAAM wall was built.

DISTRIBUTION A: Distribution approved for public release.

Table 2 Deposition parameters

Wire feed speed (m/min)	Travel Speed (mm/s)	Avg. Voltage (v)	Avg. Current (A)
2.1	6	25	177.5

3.4. Sample preparations

The oscillating pattern double side deposited walls were cut at the centre to collect a 10mm wide specimen for microscopic examination. These test samples were hot mounted with Bakelite, grinded from 250 grit till 2500 grit and then polished under Mol cloth 3nm with diamond suspension solution and final finish using Chem cloth with colloidal silica. These prepared samples were then etched using 95ml of HCl with 5g of oxalic acid. Then the samples were analysed under SEM to obtain Back Scattered Electron (BSE) images and Computerised EDS was used to acquire elemental composition in the material. The BSE images and EDS results were obtained using TESCAN VEGA3 apparatus. The microstructures of these samples were acquired using the optical microscope. Finally, the microhardness was measured using Vickers hardness tester at 200g force. The test was carried out at every 2mm interval from the base till the top on all the samples.

3.5. Heat treatment calculations

As mentioned before, this material requires solid solution strengthening to achieve the desired microstructures and mechanical properties. To homogenous the matrix structure of the deposited material, a standard heat treatment as well as calculated heat treatment cycles were carried out. These heat-treated samples characteristics were studied and analysed to that of as deposited samples. Calculated or modified heat treatment cycle was obtained from deriving the Fick's second law of equation.

$$\frac{\partial C}{\partial t} = D\frac{\partial^2 C}{\partial x^2} \quad (3\text{-}1)$$

DISTRIBUTION A: Distribution approved for public release.

By solving the above equation to a practical environment under the semi-infinite solid gives the solution to the Fick's second law,

$\frac{C_x - C_0}{C_S - C_0} = 1 - \mathrm{erf}\left(\frac{x}{2\sqrt{Dt}}\right)$	(3-2)
Applying the boundary condition, here are the surface concentrations of the initial (C_0), final (C_s)and required (C_x) determined from the EDS analysis. And erf(x/2√Dt) is a Gaussian error function which is a constant and be denoted as "z". [9]	
$z = \frac{x}{2\sqrt{Dt}}$ erf(z) can be obtained from the gaussian error tabulation if the value is not available, it could be obtained by means of interpolation method[9]	(3-3)
Diffusion Coefficient (D) determines the diffusivity of the particular in the solute solvus state at a heat-treating temperature.	
$D = D_0\, exp\left(-\frac{Q}{RT}\right)$ D = Diffusion Coefficient (m^2/s) D_0 = Maximal Diffusion Coefficient of tungsten in fcc cobalt ($5.1x10^{-6}\ m^2/s$)[22] Q_W= the activation energy for diffusion of tungsten (261480 J/mol)[22] R = universal gas constant (8.314 J/ (mol· K)) T = the absolute temperature (1448K) $D_{at\ 1448K} = 1.88x10^{-15}\ m^2/s$	(3-4)

The diffusion coefficient of tungsten in FCC structure Cobalt at 1175^0C is found from the diffuse coefficient research paper by Naghavi S, Hegde V, Wolverton C[22]. With Z value determined from equation (3-2), from data collected using EDS analysis and the value of x can be determined from finding the inter-dendritic spacing from the BSE images. After calculating these unknowns, it could be substituted in the equation (3-3) and solved to determine the amount of time (t) required to homogeneous the tungsten carbide particles in the fcc cobalt matrix at 1175^0C.

4. Results & Discussion

4.1. Depositing characteristics

Figure 5 depicts the H188 wall deposited using plasma WAAM technology. The figure shows that the H188 oscillating wall deposited using plasma power source was rigid and well-constructed without any collapse and with minimal spattering during the deposition. The good finish with even waviness of the deposited wall is due to controlled plasma power supply. This efficient and controlled process that evenly conducts the heat input to the wire supplied with the cold wire feeder, is programmed

DISTRIBUTION A: Distribution approved for public release.

to feed when the arc is on, and the droplet transfer is monitored using a high-speed camera that is mounted with the plasma torch. The cold wire nozzle is attached with an adjuster, that could help move the cold wire to move vertically, to maintain the droplet transfer to be smooth as possible[10]. Since oscillating deposition strategy was used the heat accumulation after each layer helps in continuing the deposition and maintaining the interpass temperature[5]. And thus, the productivity of this deposition is higher. Since the process is double sided deposition using turn table, heat accumulated during single layer deposition gets dissipated gradually until the deposition is completed on the other side of the substrate, this slight heat dissipation helps in avoid any collapsing due to higher heat accumulation. Also, along the wall's metallographic cross-section views from Figure 5, no visual defects were found. All these characteristics sums up that the Plasma WAAM process is effective for depositing Haynes 188 material.



Figure 5 Double side deposited H188 wall with its cross-sectional machines surface.

4.1.1. Discussion

The alloys go through liquid, Gamma (γ), M_6C and $M_{23}C_6$ phases during its deposition until it gets solidified. H188 alloys gets solidification between the temperature 1260-1405^{0}C with its usual alloying composition[23]. During the deposition the alloy is in liquid phase and hence it is transferred to substrate as a droplet. The immediate next phase is γ-phase as the solidification begins. As the temperature drops below 1278^{0}C, tungsten and chromium rich carbides (M_6C) phase is obtained. Further decrease in temperature leads to precipitation of chromium rich ($M_{23}C_6$) carbide phase[24].

DISTRIBUTION A: Distribution approved for public release.

4.2. Heat treatment

4.2.1. Results

As mentioned in the heat treatment calculations section, the from SEM analysis the value of x and various surface concentrations of solute particles were determined from EDS analysis. The average inter-dendritic spacing is 30 microns.

$x=1.55x10^{-5}m$ $C_0=14$, $C_x=16$ & $C_s=33.2$ Therefore, z=1.15 (derived from solving the equation (3-2))
Now, Solving equation (3-3) gives the time for the material to homogeneous at 1175^0C, t=6.5hrs.

4.2.2. Discussion

The standard heat treatment process carried out for this material provided by the proprietor was solid solution strengthening for 1hour at 1175^0C. Whereas, solving the Fick's equation for the same temperature gave us the modified heat treatment for 6.5 hours. Further the microstructure characteristics and hardness of these samples are discussed in detail[4,8,20,25].

4.3. Microstructure characteristics

4.3.1. Optical microscopic analysis

4.3.1.1. Results

The polished and etched samples show microstructures under optical microscope. In Figure 6, shows the microstructures of as-deposited samples, standard heat-treated samples and modified heat-treated samples of the samples at different magnifications.

From the images it clearly shows that inter-dendritic spacing has not been seen and the heavy solute particles (M_6C carbides) are slightly dissolved in standard heat-treated samples. Whereas in the modified heat-treated samples these particles have tried to dissolve in the solution base. And moreover, these particles are forming equivalent distant stripes texture, that holds a uniformity after both heat treatment cycles. Globalised shielding with pure argon gas has protected the samples from oxidising as the alloying element burnout is low or nil.

DISTRIBUTION A: Distribution approved for public release.

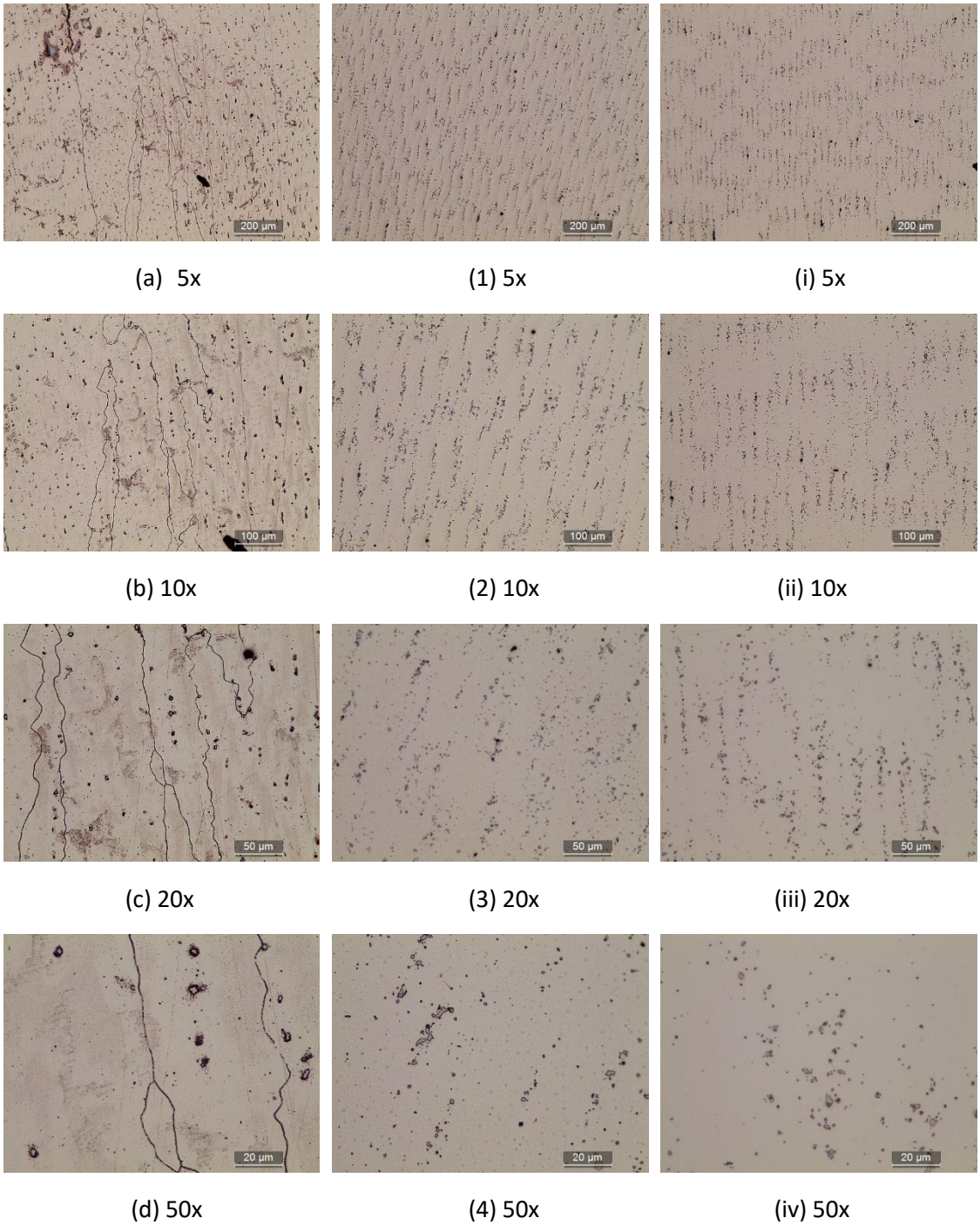


Figure 6 Optical microscopic images of Haynes 188 as-deposited samples at magnifications (a) 5x, (b) 10x, (c) 20x, (d) 50x; standard heat-treated samples at magnifications (1) 5x, (2) 10x, (3) 20x, (4) 50x; Modified heat-treated samples at magnifications (i) 5x, (ii) 10x, (iii) 20x, (iv) 50x.

4.3.1.2. Discussion

From figure 6 (a), as deposited samples exhibit columnar dendritic structures, which was discussed by Chun Guo [7] in study about microstructures in WAAM deposited superalloys. But in Yang Liu's microstructure study on powder bed fusion technology, non-heat treated and heat-treated samples microstructures from laser

DISTRIBUTION A: Distribution approved for public release.

powder bed fusion process (LPBF process) are completely different to that of the WAAM process[4]. In LPBF process, heat treated samples produced equiaxed grain morphology whereas in WAAM process, heat treated samples shows stripes of the semi-dissolved M_6C carbides into the Co base[26]. Further the grain boundaries and dendritic structure of as deposited and heat-treated samples are discussed in SEM analysis.

4.3.2. Scanning Electron Microscopy (SEM) with Energy Dispersive Spectroscopy (EDS) analysis

4.3.2.1. Results

The microstructure study gave a brief detail of the material structure on as built and heat-treated samples. For further understanding of the material microstructure properties and precipitate determination, Back Scatter Electron (BSE) imaging and EDS mapping using SEM. From Figure 7 shows the BSE images of as-deposited, standard heat-treated and modified heat-treated samples. The as-deposited samples show columnar dendritic structures that are scattered irregularly throughout the Co-base. In standard heat-treatment it could be seen that the carbides have diffused to grain boundaries and formed an equidistant dendritic structure. After carrying out the modified heat treatment cycle, signs of dendritic structures have been eliminated. The carbides have broken down and distributed throughout the spectrum surface.

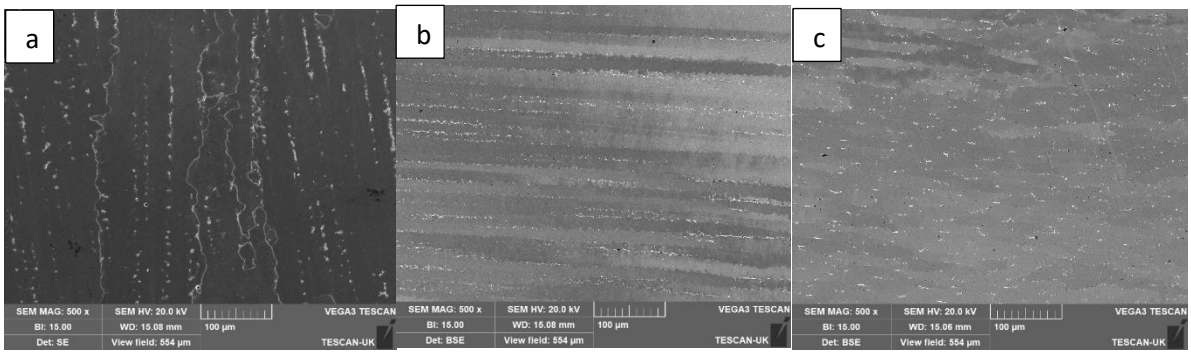


Figure 7 BSE images of (a) as-deposited (b) Standard heat-treated (c) modified heat-treated samples

DISTRIBUTION A: Distribution approved for public release.

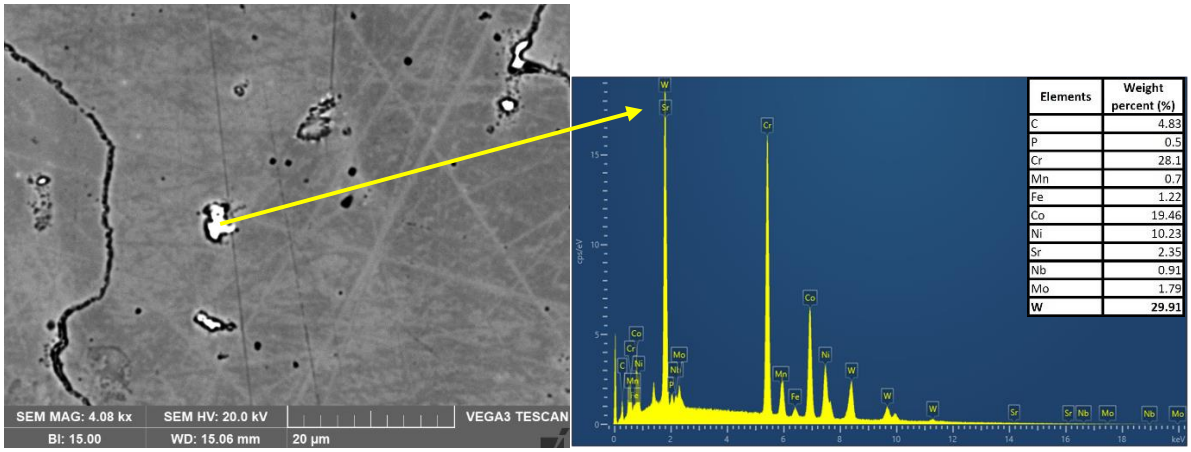


Figure 8 EDS results of segregated particles.

Table 3 EDS results of H188 wire, as deposited, standard heat-treated, modified heat-treated

Elements	Wire (%)	As deposited (%)	Standard Heat-treated (%)	Modified Heat-treated (%)
C	2.55	2.07	3.2	2.25
P	0	0	0.17	0.09
S	0	0.21	0	0
Cl	0.02	0.15	0	0
Cr	22.52	23.2	22.4	22.38
Mn	0.92	0.98	0.8	0.9
Fe	2.34	2.39	2.29	2.41
Co	35.35	34.34	34.98	35.42
Ni	22.06	21.67	22.16	22.21
Mo	0.5	0.5	0.42	0.57
W	13.74	14.49	13.58	13.77

Figure 8 shows the EDS results obtained from deposited samples. The white coloured particles are the segregated from solidification process, from EDS analysis the particle is found to be tungsten-rich particle. Table 3 suggests the chemical composition of wire, as-deposited, standard heat-treated and modified heat-treated samples.

4.3.2.2. Discussion

Post standard heat treatment, the particles have slightly diffused to form regularly spaced dendritic structures. As the diffusion happens, its counterpart to diffuse in the opposite directions effects the dendritic formation. The diffusion of tungsten-rich particles in the cobalt-rich surfaces formed the dendritic structures along the grain boundaries and counter diffusion slightly withheld the depth of valley

DISTRIBUTION A: Distribution approved for public release.

formation in the dendrites. With help of the Fick's second law, the time to homogenise the tungsten-rich particles in the Cobalt base was determined for the same temperature as of the standard process and the solutionizing time was increased from one hour to 6.5 hours[9]. This evidently showed the change in microstructure as well as in dendritic structure. The dendritic structures formed during the solidification process has been completely dissolved and an irregular scatter of carbide particles could be seen in the Figure 7, which is commonly seen in homogenized surface, these findings were similarly seen by A.K. Bhargava with Cu-Ni alloy[27].

These BSE images and TESCAN software helped in measuring the distance between the dendritic structure that helped in determining the value of x (distance) and solving the equation (3-3), which was used to find the time required for homogenization of deposited material.

The EDS analysis the deposited wall samples gave the data for the designing of modified heat treatment cycle by obtaining the maximum concentration (C_s) of the segregated particles (M_6C) i.e., tungsten carbide in this case for Haynes 188 which could be seen Figure 8. The value was used in solving the (3-2) equation and thus arrived at the error correction value (erf(z)) which was interpolated from the tabulated values to find the value z. The segregated particles are the solid solution strengtheners such as tungsten rich particles. Hence, these particles were diffused to grain boundaries to help in homogenisation and strengthening after solutionizing technique[20,28–32].

4.4. Microhardness

4.4.1. Results

After solutionizing at 1175^0C for one hour in one sample and 6.5 hours for another sample have similar hardness value. But as-deposited samples have slightly higher hardness value. This could be seen in Figure 9. The hardness was measured from bottom to top with interval 2mm distance between each indentation with force of 200g. Vickers hardness tester was used to determine the hardness value. Table 4 shows the values that oscillatory pass heat-treated samples hardness values are slightly lower than that of the single pass heat-treated sample. The test points were carried out in transverse axis to the substrate i.e., along the wall height and another set of tests were carried along build direction i.e., longitudinally. The microhardness

DISTRIBUTION A: Distribution approved for public release.

value along the transverse axis was between 222 and 292 HV and along the longitudinal axis ranges between 231 and 279 HV. The average hardness value of as-deposited, standard HT, modified HT samples along longitudinal and transverse axis were 266HV, 242HV, 255HV and 274HV, 263HV, 255HV respectively.

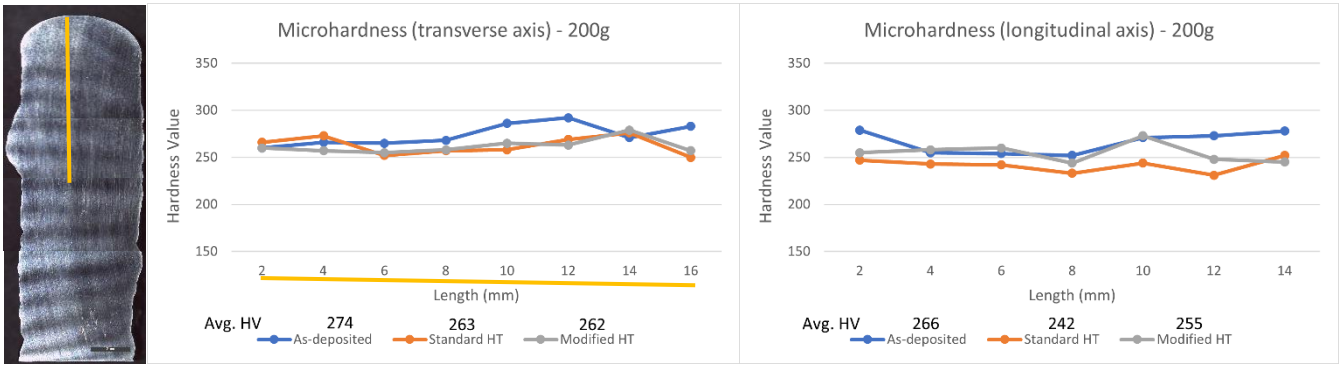


Figure 9 Microhardness values along the transverse and longitudinal axis of the deposited wall before and after heat treatment

Table 4 Mean and standard deviation values of the hardness for the deposited samples

Sample	Average (Mean) Hardness Value (HV)	Standard deviation
Single pass as deposited	277	10
Single pass heat-treated	280	10
Oscillatory as deposited	274	11
Oscillatory standard heat-treated	263	10
Oscillatory Modified heat-treated	262	8

4.4.2. Discussion

From the figure 9 and microhardness results shows the mechanical properties of as-deposited, Standard heat-treated and modified heat-treated samples. Post solutionizing the hardness of the material has slightly decreased. Solutionizing softening is a usual reaction happens during the solid solution strengthening process. Due to the solidification process, deposited material has high dislocation density. Hence, when the as-deposited material undergoes heat treatment process, it creates vacancies and owing the dislocated atoms to fill the gap, thus reducing the dislocation density[7,24,32,33].

According to Yang Liu and his team of researchers, occurrence of dislocation of the atoms in the matrix reflects on the material strength. The WAAM samples are

DISTRIBUTION A: Distribution approved for public release.

formed by the re-melting of previous layer and cooling down during dwell time (rapid temperature). This is repeated as heat and cold cycle, due to which the large number of residual stresses are inflicted in the deposited material, this stress makes the atoms to dislocate. Once the dislocation at a point happens, formulate, and creates a vacuum position in the matrix that leads subsequent dislocations of atoms which results in the dislocation of the walls. During the post processing heat treatment, the high temperature creates a vacuum in the matrix that helps the nearby particles to fill the gap and form the complete surface[4]. Therefore, less dislocations leads to less strength and that causes low hardness value after annealing.

According to Chun Guo, sometimes these slight fluctuations in the hardness value can be due the sample microstructure formation itself. Although that could be since the WAAM process comprises of sample built by many layers in multi-pass deposition direction. The various thermal cycles effects in one single layer caused by initial deposition later remelting and depositing another layer forms an in-between heat affected zone[7]. Hence, these different zones exhibited different grain size, precipitated particles, dendritic structures, etc. (microstructures).

All these reasoning effected the difference in the hardness values, before and after heat treatment process.

5. Conclusion

The research project focused on the fabrication and post-processing of the Cobalt-based superalloy (Haynes 188) using WAAM technology. Various metallographic observations changes were recognised in pre and post heat-treated samples. Some of the important accomplishments and findings from the project are stated below:

- Two walls of dimension 250 x 16 x 50 mm were deposited in oscillating strategy using Plasma – WAAM technology. Both the walls were erected simultaneously using a turn table. And to eliminate the slope formation at one and to have an evenly distributed heat accumulation, depositions were carried out in bi-directional.
- Post deposition the walls were machined down to sample size, and mould was formed for each sample. Some of the samples were retained to carry out the standard and modified heat treatment.

DISTRIBUTION A: Distribution approved for public release.

- Using Fick's second law and the values obtained from BSE images and EDS results helped in designing the solution heat treatment cycle for WAAM deposited samples to homogenise the material. After which the standard heat treatment of one hour and modified heat treatment of 6.5 hours at 1175^0C were carried in furnace and then immediately water quenched.
- After all the samples were moulded, polished, and etched, it was sent to the SEM analysis to get BSE image at varies higher magnifications of each sample and EDS results with chemical composition concentration of each alloying elements were also acquired.
- Then the microstructure study of these samples was carried out using optical microscope to analyse the grain boundary conditions and change in the dendritic structures with effect to the different heat treatments were analysed. The as-deposited samples exhibit irregular precipitation of particles in the solvus medium with dendritic structures. Whereas after standard heat treatment process the samples showed no sign of dendritic structures but the particles found to form a stripe at an equidistance to each other precipitated particles. The particles were in semi-dissolved state and have diffused to equal distance each other segregated particles in solvus base after carrying the modified heat treatment.
- From SEM analysis, it was much clearer and with higher magnification BSE images of the samples were obtained. These images gave a clear sketch of the grain refinement with each progress. As-deposited sample's BSE image gave initial particles precipitated position and size due to solidification process as well as inter-dendritic distance. In standard heat-treated samples, the precipitated particles are well aligned and found along the grain boundaries. Modified heat-treated samples showed the particles have disbursed evenly in the solvus base.
- The EDS results depicts the precipitated particles and solid solution strengtherners are rich in tungsten. These particles are formed during solidification process; hence these carbides could be seen from the as-deposited samples. Using the EDS point elemental analysis determining the particle composition provided the elements concentrations. These concentration values were later used in the Fick's equation to determine the

DISTRIBUTION A: Distribution approved for public release.

required time to diffuse the particle for required distance. Also, from EDS analysis wire, as-deposited, standard heat-treated and modified heat-treated samples elemental composition are determined and compared.

- The microhardness of the samples was tested using Vickers hardness tester, which was carried out to evaluate the mechanical property of the deposited material. The microhardness was tested along transverse and longitudinal axis of the wall on the as-deposited, standard heat-treated and modified heat-treated samples at force of 200g. The as-deposited samples show slightly higher hardness value compared to the heat-treated samples, which was similar values in both the axis.
- Plasma-WAAM process for cobalt-based superalloy seems like highly potential technology for producing large parts for aerospace industry. Hence, further developing this process for application-based part development would be ideal.

6. Future works

The fabrication of Haynes 188 wall using plasma-WAAM and developed a heat treatment cycle to homogenise the material has been done successfully. Since, it's a superalloy, the material mainly used in aerospace industries and requires better understanding of its thermo-mechanical properties. Here are some future works to develop this process viable alternative to the existing processes,

- In the aspect of mechanical properties only microhardness of the samples was tested, to determine furthermore mechanical properties such as strength and ductility of the material, it is highly suggested to carry out the tensile testing of this deposited material for better understanding of the material. Based on the literature survey of this material suggested that the elongation property is higher in heat-treated samples unlike the hardness value which is vice-verse. This could impact in the material mechanical property and its application of use could be widen.
- Transmission Electron Microscope (TEM) imaging is one of the furthermore studies on microstructure analysis, the gamma-prime precipitates formed during the solidification in nano scale can be subjected to findings with this analysis. Although the SEM analysis provided with the required data in micro-

DISTRIBUTION A: Distribution approved for public release.

scale, for better understanding of the material in atomic level and its change with respect to the different heat treatments could be defined.

- One of the important properties of H188 is that it has very high creep resistance, which is commonly seen in superalloys. But this material since it is cobalt-based superalloy, its creep resistance quite higher than that of the other superalloys, therefore testing the additively manufactured H188 alloy for creep resistance is highly required to determine the material property to the application based.
- In this project, Fick's equation was solved and formulated in a excel sheet to design the modified heat treatment. The experiment carried out here was only at 1175^0C for 6.5 hours to homogenise the material, therefore increasing the temperature will affect in the time to decrease subsequently. It is highly suggested to carry out the heat treatment cycle at different temperatures and arriving at an optimized heat cycle that could provide with better property of the material than the as-deposited samples.
- In the alternative technique to design the heat treatment cycle for the deposited material can be obtained using a software knowns Thermo-Calc. It is a tool, that simulates the material behaviour based on the process and predicting the possible outcomes. Hence, this tool could be useful in deciding a heat treatment to homogeneous material.

7. References

1. Williams SW., Martina F., Addison AC., Ding J., Pardal G., Colegrove P. Wire + Arc additive manufacturing. Materials Science and Technology (United Kingdom). Taylor and Francis Ltd.; 21 June 2016; 32(7): 641–647. Available at: DOI:10.1179/1743284715Y.0000000073

2. Horn TJ., Harrysson OLA. Overview of current additive manufacturing technologies and selected applications. Science Progress. September 2012; 95(3): 255–282. Available at: DOI:10.3184/003685012X13420984463047

3. Lewandowski JJ., Seifi M. Metal Additive Manufacturing: A Review of Mechanical Properties. Annual Review of Materials Research. Annual Reviews Inc.; 2016. pp. 151–186. Available at: DOI:10.1146/annurev-matsci-070115-032024

4. Liu Y., Huang Z., Zhang C., Lu J., Ouyang N., Shen Q., et al. Hierarchical microstructure and strengthening mechanism of Haynes 188 alloy 2 manufactured by laser powder bed fusion.

5. Aldalur E., Veiga F., Suárez A., Bilbao J., Lamikiz A. High deposition wire arc additive manufacturing of mild steel: Strategies and heat input effect on microstructure and mechanical properties. Journal of Manufacturing Processes. Elsevier Ltd; 1 October 2020; 58: 615–626. Available at: DOI:10.1016/j.jmapro.2020.08.060

DISTRIBUTION A: Distribution approved for public release.

6. Zhou S., Zhang J., Wang J., Yang G., Wu K., Qin L. Effect of Oxygen Levels in Tent Shielding Atmosphere on Microstructural and Mechanical Properties of Ti-6Al-4V Fabricated by Wire Arc Additive Manufacturing. Journal of Materials Engineering and Performance. Springer; 1 July 2022; Available at: DOI:10.1007/s11665-022-06684-w

7. Guo C., Ying M., Dang H., Hu R., Chen F. Microstructural and intergranular corrosion properties of Inconel 625 superalloys fabricated using wire arc additive manufacturing. Materials Research Express. IOP Publishing Ltd; 1 March 2021; 8(3). Available at: DOI:10.1088/2053-1591/abe977

8. HAYNES ® 188 alloy. 2018.

9. William D. Callister., David G. Rethwisch. Materials_Science_and_Engineering. John Wiley & Sons. 2010; (8): 122–137.

10. Martina F., Mehnen J., Williams SW., Colegrove P., Wang F. Investigation of the benefits of plasma deposition for the additive layer manufacture of Ti-6Al-4V. Journal of Materials Processing Technology. June 2012; 212(6): 1377–1386. Available at: DOI:10.1016/j.jmatprotec.2012.02.002

11. Liu W., Jia C., Guo M., Gao J., Wu C. Compulsively constricted WAAM with arc plasma and droplets ejected from a narrow space. Additive Manufacturing. Elsevier B.V.; 1 May 2019; 27: 109–117. Available at: DOI:10.1016/j.addma.2019.03.003

12. Dirisu P., Ganguly S., Mehmanparast A., Martina F., Williams S. Analysis of fracture toughness properties of wire + arc additive manufactured high strength low alloy structural steel components. Materials Science and Engineering A. Elsevier Ltd; 23 September 2019; 765. Available at: DOI:10.1016/j.msea.2019.138285

13. Aldalur E., Veiga F., Suárez A., Bilbao J., Lamikiz A. Analysis of the wall geometry with different strategies for high deposition wire arc additive manufacturing of mild steel. Metals. MDPI AG; 1 July 2020; 10(7): 1–19. Available at: DOI:10.3390/met10070892

14. Levi TP., Stevens KJ. Oxidation behaviour of LM 6000 gas turbine engine substrate cobalt-base alloy 188. Materials at High Temperatures. 2007; 24(3): 173–185. Available at: DOI:10.3184/096034007X265198

15. Hou R., Evans DM., Mcclure JC., Nunes AC., Garcia G. Sponsored by the American Welding Society and the Welding Research Council Shielding Gas and Heat Transfer Effeciency in Plasma Arc Welding. 1996.

16. Wang J., Lin X., Li J., Hu Y., Zhou Y., Wang C., et al. Effects of deposition strategies on macro/microstructure and mechanical properties of wire and arc additive manufactured Ti–6Al–4V. Materials Science and Engineering A. Elsevier Ltd; 29 April 2019; 754: 735–749. Available at: DOI:10.1016/j.msea.2019.03.001

17. Klarstrom DL. Wrought Cobalt-Base Superalloys. JMEPEG. 1993.

18. Bhanu K., Rao S., Castelli MG., Allen GP., Ellis JR. A Critical Assessment of the Mechanistic Aspects in HAYNES 188 during Low-Cycle Fatigue in the Range 25 C to 1000 C. 1997.

19. Castelli MG., Rao KBS. Cyclic Deformation of Haynes 188 Superalloy Under Isothermal and Thermomechanical Loadings. The Minerals, Metals and Materials Society; 2012. pp. 375–382. Available at: DOI:10.7449/1996/superalloys_1996_375_382

DISTRIBUTION A: Distribution approved for public release.

20. Murray SP., Pusch KM., Polonsky AT., Torbet CJ., Seward GGE., Zhou N., et al. A defect-resistant Co–Ni superalloy for 3D printing. Nature Communications. Nature Research; 1 December 2020; 11(1). Available at: DOI:10.1038/s41467-020-18775-0

21. James WS., Ganguly S., Pardal G. Selection and Performance of AM Superalloys for High-Speed Flight Environments. 2022; Available at: DOI:10.21203/rs.3.rs-1666707/v1

22. Naghavi SS., Hegde VI., Wolverton C. Diffusion coefficients of transition metals in fcc cobalt. Acta Materialia. Elsevier Ltd; 15 June 2017; 132: 467–478. Available at: DOI:10.1016/j.actamat.2017.04.060

23. Wei HL., Mazumder J., DebRoy T. Evolution of solidification texture during additive manufacturing. Scientific Reports. Nature Publishing Group; 10 November 2015; 5. Available at: DOI:10.1038/srep16446

24. Halford GR., Saltsman JF., Kalluri S. HIGH TEMPERA_I_E FATIGUE BEHAVIOR OF HAYNES 188. 1988. Available at: https://ntrs.nasa.gov/search.jsp?R=19900019326

25. Herchenroeder RB. 'HAYNES' ALLOY NO. 188 AGING CHARACTERISTICS.

26. Homepage J., Arab SM., Haghighi A., Khajepour M., Jalalizadeh Y., Tavallayi MM. Iranian Journal of Materials Forming Conjoint Influence of Heat Treatment, Hot Deformation and Cold Working on the Microstructure and Mechanical Response of a Co-Based Superalloy. Iranian Journal of Materials Forming. 2021; 8(3): 34–45. Available at: DOI:10.22099/ijmf.2021.40550.1182

27. Bhargava AK., Banerjee MK. 2.14 Heat-Treating Copper and Nickel Alloys. In: Hashmi MSJ (ed.) Comprehensive Materials Finishing. Oxford: Elsevier; 2017. pp. 398–420. Available at: DOI:https://doi.org/10.1016/B978-0-12-803581-8.09196-7

28. Kalluri S., Halford GR. NASA Technical Memorandum 105381. 1991. Available at: https://ntrs.nasa.gov/search.jsp?R=19920015742

29. Wang Y., Chen X. Investigation on the microstructure and corrosion properties of Inconel 625 alloy fabricated by wire arc additive manufacturing. Materials Research Express. Institute of Physics Publishing; 21 August 2019; 6(10). Available at: DOI:10.1088/2053-1591/ab39f6

30. Siefert JA., Shingledecker JP., DuPont JN., David SA. Weldability and weld performance of candidate nickel based superalloys for advanced ultrasupercritical fossil power plants Part II: weldability and cross-weld creep performance. Science and Technology of Welding and Joining. Taylor and Francis Ltd.; 2016. pp. 397–427. Available at: DOI:10.1080/13621718.2016.1143708

31. Alexis J., Graneix J., Balcaen Y. Effect of Laser Welding Parameters on the Microstructure and Mechanical Properties of Dissimilar Hastelloy X/Haynes 188 Joints. Metallurgical and Materials Transactions A: Physical Metallurgy and Materials Science. Springer; 1 November 2021; 52(11): 5055–5065. Available at: DOI:10.1007/s11661-021-06452-w

32. Lee SY., Lu YL., Liaw PK., Choo H., Thompson SA., Blust JW., et al. High-temperature tensile-hold crack-growth behavior of HASTELLOY ® X alloy compared to HAYNES® 188 and HAYNES ® 230® alloys. Mechanics of Time-Dependent Materials. March 2008; 12(1): 31–44. Available at: DOI:10.1007/s11043-008-9049-6

DISTRIBUTION A: Distribution approved for public release.

33. Yang L., Hsu K., Baughman B., Godfrey D., Medina F., Menon M., et al. Microstructure, Mechanical Properties, and Design Considerations for Additive Manufacturing. 2017. pp. 45–61. Available at: DOI:10.1007/978-3-319-55128-9_3

DISTRIBUTION A: Distribution approved for public release.